Department of Biological Sciences and Pathobiology
University of Veterinary Medicine

Institute of Physiology, Pathophysiology and Biophysics
(Head: Univ.-Prof. Dr. Janina Burk-Luibl, MSc.)

The Role of the Solute Carrier 25 Proteins in Fatty Acid and 2,4-Dinitrophenol-Mediated Proton Transport

PhD thesis submitted for the fulfilment of the requirements for the degree of

DOCTOR OF PHILOSOPHY (PhD)

submitted by

Kristina Žuna, MSc.

Vienna, 05/2024

Acknowledgments

First and foremost, I want to thank my supervisor prof. Elena E. Pohl for giving me the opportunity to join her research group and pursue my PhD. Under her mentorship, I've learned various scientific techniques, attended congresses, pursued internships, and engaged in collaborations, all of which have shaped my scientific perspective. Prof. Pohl's guidance and encouragement have made me feel valued and respected since day one, an experience for which I'll be forever thankful.

I also want to express my appreciation to my second supervisor, Mario Vazdar, whose constant support and insightful discussions have been irreplaceable. Our collaboration resulted in many joint scientific publications, which is something I will always cherish.

Furthermore, I am thankful to Jürgen Kreiter, Olga Jovanović, and Alina Pashkovskaya for introducing me to the world of electrophysiology, and their continuous support and friendship since then. Special thanks go to Sarah Bardakji for her expertise in protein science, and for teaching me everything she knows with a confident kindness and patience. Many thanks go to Deniz Hofbauer and Tatyana Tyschuk for working with me on protein production and functional assays, and for being great students of mine. To my colleagues and the entire Institute for Physiology, Pathophysiology, and Biophysics, I extend heartfelt thanks. The supportive and friendly atmosphere you've cultivated has been essential in my growth, and many of you have become lifelong friends.

Beyond academia, I´m thankful for my family´s support, especially my mom and grandparents, who always inspired me to pursue my education, and to be strong-minded, independent, and curious. Even through many hardships in their own lives, they found the strength and resilience to shape me into the successful woman I am today. Furthermore, I'm also grateful to my husband's family for their love and acceptance.

Lastly, I want to thank my husband Marijo who has been a constant pillar of support, love and understanding throughout my entire education journey. Ten years ago, when we started our story, we were only kids who dreamed of big things. Ever since then, Marijo motivated me to strive for greatness. When it wasn´t easy on that path, he offered loving guidance and objectiveness, never doubting my abilities. This thesis is a testament to his love and support.

PhD committee

First supervisor:

Univ.-Prof. Dr. med. Elena E. Pohl
Department of Biological Sciences and Pathobiology
University of Veterinary Medicine, Vienna
Veterinärplatz 1
1210 Vienna, Austria

Second supervisor:

Mario Vazdar, PhD
Assistant Professor
Department of Mathematics, Informatics, and Cybernetics
University of Chemistry and Technology
Technická 5, 16628, Praha 6 - Dejvice
Prague, Czech Republic

List of publications

Publications included in the thesis:

Žuna, K, Tyschuk T, Beikbaghban T, Sternberg F, Kreiter J, Pohl EE. The 2-oxoglutarate/malate carrier extends the family of mitochondrial carriers capable of fatty acid and 2,4-dinitrophenol-activated proton transport. Acta Physiol (Oxf). 2024 Apr 5:e14143. doi: 10.1111/apha.14143.
Impact factor: 6.30

Žuna K, Jovanović O, Khailova LS, Škulj S, Brkljača Z, Kreiter J, Kotova EA, Vazdar M, Antonenko YN, Pohl EE. Mitochondrial Uncoupling Proteins (UCP1-UCP3) and Adenine Nucleotide Translocase (ANT1) Enhance the Protonophoric Action of 2,4-Dinitrophenol in Mitochondria and Planar Bilayer Membranes. (2021) *Biomolecules* 11(8):1178. doi: 10.3390/biom11081178.
Impact factor: 5.05

Jovanović O, Chekashkina K, Škulj S, **Žuna K**, Vazdar M, Bashkirov PV, Pohl EE. Membrane Lipid Reshaping Underlies Oxidative Stress Sensing by the Mitochondrial Proteins UCP1 and ANT1. (2022) *Antioxidants (Basel)* 11:2314. doi.org/10.3390/antiox11122314
Impact factor: 7.00

Kreiter J, Rupprecht A, Škulj S, Brkljača Z, **Žuna K**, Knyazev DG, Bardakji S, Vazdar M, Pohl EE. (2021) ANT1 Activation and Inhibition Patterns Support the Fatty Acid Cycling Mechanism for Proton Transport. *International Journal of Molecular Sciences* 22, 2490. doi.org/10.3390/ijms22052490
Impact factor: 5.60

Author´s contribution

Žuna, K, Tyschuk T, Beikbaghban T, Sternberg F, Kreiter J, Pohl EE. The 2-oxoglutarate/malate carrier extends the family of mitochondrial carriers capable of fatty acid and 2,4-dinitrophenol-activated proton transport. Acta Physiol (Oxf). 2024 Apr 5:e14143. doi: 10.1111/apha.14143.

- **Žuna, K.** – investigation, writing – original draft, Tyschuk, T. - investigation, writing – review & editing, Beikbaghban, T. - investigation, writing – review & editing, Sternberg, F. - investigation, writing – review & editing, Kreiter, J. - writing – review & editing, Pohl. E.E. – conceptualization, funding acquisition, project administration, resources, supervision, writing – original draft, writing – review & editing.

Žuna K, Jovanović O, Khailova LS, Škulj S, Brkljača Z, Kreiter J, Kotova EA, Vazdar M, Antonenko YN, Pohl EE. Mitochondrial Uncoupling Proteins (UCP1-UCP3) and Adenine Nucleotide Translocase (ANT1) Enhance the Protonophoric Action of 2,4-Dinitrophenol in Mitochondria and Planar Bilayer Membranes. (2021) *Biomolecules* 11(8):1178. doi: 10.3390/biom11081178.

- **Žuna, K.** – investigation, writing—original draft, writing—review and editing, Jovanović, O. – investigation, writing—review and editing, Khailova, L.S. – investigation, writing—review and editing, Škulj, S. – investigation, writing—review and editing, Brkljača, Z. – investigation, writing—review and editing, Kreiter, J. – investigation, writing—review and editing, Kotova, E.A. - writing—original draft, writing—review and editing, Vazdar, M. – investigation, funding acquisition, resources, supervision, writing—original draft, writing—review and editing, Antonenko, Y.N. – conceptualization, funding acquisition, resources, supervision, writing—original draft, writing—review and editing, Pohl, E.E. – conceptualization, funding acquisition, project administration, resources, supervision, writing – original draft, writing – review and editing.

Jovanović O, Chekashkina K, Škulj S, **Žuna K**, Vazdar M, Bashkirov PV, Pohl EE. Membrane Lipid Reshaping Underlies Oxidative Stress Sensing by the Mitochondrial Proteins UCP1 and ANT1. (2022) *Antioxidants (Basel)* 11:2314. doi.org/10.3390/antiox11122314

- Jovanović, O. – conceptualization, investigation, writing—original draft preparation, writing—review and editing, visualization, Chekashkina, K. – investigation, Škulj, S. – investigation, **Žuna, K.** – investigation, Vazdar, M. – investigation, resources, writing—review and editing, supervision, project administration, funding acquisition, Bashkirov, P.V. – investigation, resources, writing—review and editing, project administration visualization, supervision, funding acquisition, Pohl, E.E. – conceptualization, resources, writing—original draft preparation, writing—review and editing, supervision, project administration, funding acquisition

Kreiter J, Rupprecht A, Škulj S, Brkljača Z, **Žuna K**, Knyazev DG, Bardakji S, Vazdar M, Pohl EE. (2021) ANT1 Activation and Inhibition Patterns Support the Fatty Acid Cycling Mechanism for Proton Transport. *International Journal of Molecular Sciences* 22, 2490. doi.org/10.3390/ijms22052490

- Kreiter, J. – conceptualization, investigation, writing—original draft, writing—review and editing, Rupprecht, A. – conceptualization, writing—review and editing, Škulj, S. – investigation, writing—review and editing, Brkljača, Z. – investigation, writing—review and editing, **Žuna, K.** – investigation, writing—review and editing, Knyazev, D.G. – investigation, writing—review and editing, Bardakji, S. – investigation, writing—review and editing, Vazdar, M. – conceptualization, funding acquisition, investigation, resources, supervision, writing—original draft, writing—review and editing, Pohl, E.E. – conceptualization, funding acquisition, project administration, resources, supervision, writing—original draft, writing—review and editing

Declaration

I hereby declare that I have followed the rules of Good Scientific Practice in all aspects.

K. Zuna

Kristina Žuna
Vienna, 02.05.2024

Summary

By enhancing metabolic efficiency and counteracting harmful reactive oxygen species, uncoupling is a promising strategy for preventing and treating metabolic diseases such as obesity and type II diabetes. It involves the dissipation of mitochondrial membrane potential (MMP) through proton transport, independent of ATP production. Physiologically, uncoupling is facilitated by free fatty acids (FAs) and enhanced by various members of the solute carrier 25 (SLC25) protein family. Chemically synthesized uncoupling agents like 2,4-dinitrophenol (DNP) also exhibit potent protonophoric effects, demonstrating efficacy in weight loss and inhibition of cancer cell proliferation. Nonetheless, the intricate interaction between protonophores and proteins remains poorly understood, particularly regarding the uncoupling potential of individual SLC25 family members. Among these proteins is the 2-oxoglutarate/malate carrier (OGC), a pivotal component in mitochondrial energy creation.

To test how natural and chemical uncouplers affect proteins, we produced several SLC25 family members and incorporated them into proteoliposomes. By measuring the conductance, we demonstrated that adenine nucleotide translocase (ANT1) and uncoupling proteins 1-3 (UCP1-3) significantly enhance the protonophoric effect of DNP. Notably, we provide novel evidence confirming the involvement of the 2-oxoglutarate/malate carrier (OGC) in uncoupling, similar to ANT1 and UCPs, in the presence of FAs and DNP. Furthermore, we found that ANT1's uncoupling pattern points to the FA cycling model and that reactive alkenals, products of oxidative damage, reshape membrane lipids and indirectly increase uncoupling mediated by SLC25 carriers.

Based on our results, we propose that during high-energy demand, mitochondrial carriers support ATP production by transporting substrates in and out of the mitochondrial matrix. Conversely, under low energy demand or oxidative stress, they facilitate proton transport through an increased concentration of FAs. The synergistic effect of SLC25 family transporters can result in a beneficial and transient decrease in MMP. Understanding the uncoupling mechanisms of these proteins can help selectively design new or enhance existing chemical uncouplers. This targeted approach can be used to induce desired physiological changes in specific tissues, providing a potential therapeutic strategy against various diseases.

Table of Contents

1. Introduction

1.1. Energy production in mitochondria

1.1.1. Mitochondrial origin and structure

Mitochondria are vital organelles responsible for energy production in all eukaryotic cells. Beyond their energy-supplying function, mitochondria are involved in a myriad of other processes, such as ion homeostasis, lipid and nucleic acid metabolism, production and consumption of reactive oxygen species (ROS), apoptosis, and various biosynthetic pathways (Cooper 2000). A ground-breaking theory emerged in 1960 by the botanist Lynn Margulis, proposing the evolutionary origin of mitochondria from a symbiotic relationship between an early eukaryotic cell devoid of mitochondria and an aerobic prokaryote, likely a proteobacterium (Sagan 1968). The notion gains support from the shared characteristics between mitochondria and bacteria, including a double-membrane structure, autonomous ribosomes, and circular DNA. This symbiotic concept is further reinforced by extensive phylogenetic analysis of mitochondrial genes and proteins, establishing a clear link to archeproteobacteria, thereby confirming a common bacterial ancestor for mitochondria (Gray et al. 2001).

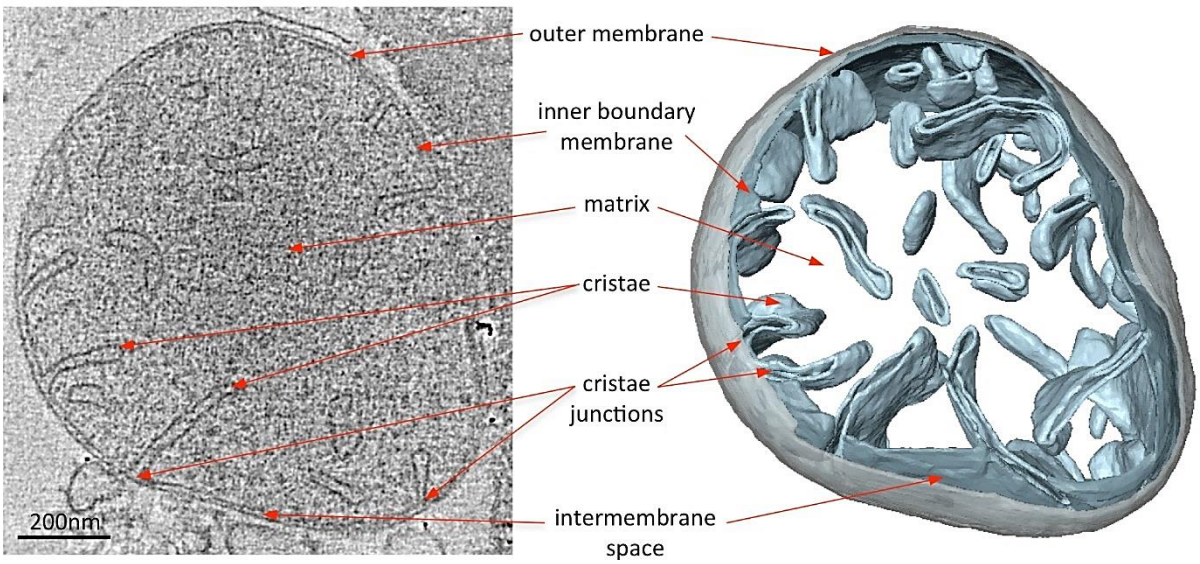

Figure 1. Central slice through of a tomographic volume of a wildtype *S. cerevisiae* mitochondrion (left) and corresponding surface-rendered volume (right). Various mitochondrial segments are depicted with red arrows. Adapted from Davies et al. 2014 with permission from JoVE.

Over billions of years, mitochondria evolved from endosymbiont bacteria to integrated cellular organelles. This process entailed losing unnecessary and redundant genes, as well as transferring a part of the genome to the nucleus (Nass 1969). Furthermore, orchestrated connections formed between mitochondrial membranes, cytoskeleton, and cell machinery. The inner (IMM) and the outer mitochondrial membrane (OMM) are important features of mitochondria inherited from the pre-existing forms of bacteria (Fig. 1) (Schwartz & Dayhoff 1978). The OMM divides the mitochondria from the cytosol, while still allowing for passive transport of charged molecules through pore-forming proteins, thereby establishing the intermembrane´s space with a similar composition to that of the cytosol. Conversely, the IMM is impermeable to charged molecules and requires various mitochondrial transporters to carry solutes across the IMM into the mitochondrial matrix. Within the matrix, the IMM folds into specialized compartments called cristae (Daems & Wisse 1966), augmenting the available surface area to accommodate large amounts of electron transport chain (ETC) enzymes (Mannella et al. 2008, Liesa & Shiriha, 2013). This spatial organization helps localize proton gradients and concentrate metabolites, fostering optimal conditions for efficient energy production.

1.1.2. Synthesis of adenosine triphosphate

Adenosine triphosphate (ATP) is a molecule that serves as the cell´s main source of energy, and it is mainly synthesized during aerobic respiration by the mitochondrial ETC complex. The cell can use different food sources for energy production, but the main ones are glucose and fatty acids. Glucose is broken down to pyruvate in the cytosolic process of glycolysis, while fatty acids go through the process of β-oxidation in mitochondria. Ultimately, both substrates are broken down to acetyl-CoA, which is either transported to or remains in mitochondria. Acetyl-CoA then goes through the citric acid cycle where its binding energy is transferred to the energy-carrying molecules nicotinamide adenine dinucleotide (NADH) and flavin adenine dinucleotide ($FADH_2$). The energy stored in NADH and FADH2 is utilized by the ETC complexes (I, III and IV) to pump protons from the matrix into the intermembrane space. ATP-synthase uses the created proton gradient to pump protons back into the matrix. The energy stored in the proton gradient is used to phosphorylate adenine diphosphate (ADP) to adenine triphosphate (ATP) (Fig. 2, left). Ideally, the transport of four protons back to the matrix is coupled to the synthesis of one molecule of ATP.

ATP can be also generated without the involvement of mitochondria during the lactic fermentation. However, these processes result in a lower number of ATP molecules synthesized in comparison to oxidative phosphorylation. Once synthesized, ATP can be used as an energy currency in a variety of cell processes, such as active transport, intracellular signaling, DNA/RNA synthesis, and neurotransmission.

1.2. Energy dissipation in mitochondria

1.2.1. Uncoupled respiration and basal proton leak

Not every proton transported from the mitochondrial intermembrane space to the matrix will be used to produce ATP. In other words, the transport of some protons through the IMM remains not coupled to oxidative phosphorylation (Fig. 2, right). This "proton leak" or "uncoupling" is present in all eukaryotic cells and its amount depends on the cell type. It can be thought of as the sum of the unregulated basal proton leak and the proton transport mediated by the proteins of the IMM (Rolfe & Brand 1997, Stuart et al. 2001).

Basal proton conductance is any free and non-regulated proton diffusion across the IMM. It increases with the increase in mitochondrial membrane potential (MMP) in a non-ohmic manner (Nicholls 1974). It is thought that protons translocate across natural membranes through "water wires", and the magnitude of the proton conductance might depend on the fatty acyl composition of the bilayer phospholipids (Porter et al, 1996, Fontaine et al, 1996, Brand et al, 2003) and the presence of free fatty acids (FAs) (Lardy & Pressman 1956, Grav & Blix 1979, Skulachev 1991). The unregulated proton leak accounts for 30-50% of the resting cellular metabolic rate of rat liver, heart, and skeletal mitochondria (for review see Rolfe & Brand 1997).

However, the basal proton leak accounts for only 5% of the total proton leak (Brand et al. 2005), which indicates that the regulated proton conductance plays a larger role in mitochondrial metabolism.

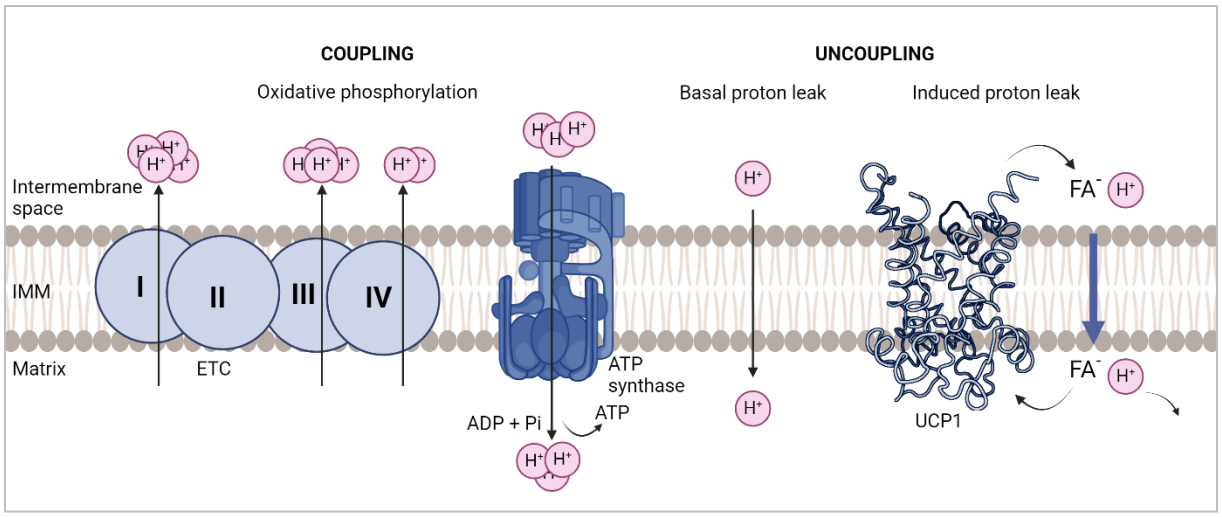

Figure 2. A simplified view of proton transport across the IMM. Coupled respiration implies proton transport by the complexes of the ETC, which are returned to the matrix by the ATP synthase and used to phosphorylate ADP to ATP (left). Proton transport uncoupled from ATP production can be divided into the basal proton leak and the free fatty acid (FA) proton transport induced by mitochondrial membrane proteins like the uncoupling protein 1 (UCP1) (right). Image created with BioRender.

1.2.2. Induced proton leak and the SLC25 protein family

The inducible part of the proton leak (protein-mediated proton transport) is potentiated and regulated by a number of mitochondrial anion carriers belonging to the solute carrier 25 (SLC25) family, which currently encompasses 53 members (For review, see Palmieri 2013 and Ruprecht & Kunji 2020). Predominantly, the primary role of the SLC25 proteins is to facilitate the transport of negatively charged substrates across the IMM, thereby contributing to the generation of ATP. Nonetheless, a subset of these carriers induces proton leak upon activation or potentiation by free fatty acids (FAs), N-acyl amino acids, reactive alkenals, or chemically synthesized protonophores.

The first protein discovered for its role in proton transport was the uncoupling protein 1 (UCP1) (For reviews see Cannon & Nedergaard 2004, Ricquier 2017, Nichols 2021). As the predominant protein in the mitochondria of the brown adipose tissue (BAT), it diverges from the substrate transport function like most of the SLC25 proteins. By enhancing the proton leak and supporting non-shivering thermogenesis, UCP1 serves as protection against cold conditions in small rodents, hibernating animals, and infants. The subfamily of uncoupling proteins comprises a total of six members. UCP2 and UCP3 were identified in 1997 (Fleury et al. 1997, Gimeno et al. 1997, Boss et al. 1997, Vidal-Puig et al. 1997), and their proton transport function

has been shown in various (mostly artificial) systems (For review, see Pohl et al 2019). UCP4 and UCP5 were discovered in 1999 (Mao et al. 1999) and 1998 (only at the gene level) (Sanchis et al. 1998), and UCP6 in 2005 (Haguenauer et al. 2005), but their physiological roles, tissue expression, and involvement in uncoupling are still under debate (Hoang et al. 2012, Hoang et al. 2015, Smorodchenko et al. 2017).

Another subfamily of the SLC25 family that potentiates uncoupling are the adenine nucleotide translocases 1-4 (ANT). Even though their main role is to transport the cytosolic ADP for the matrix ATP in a 1:1 manner, ANTs increase proton conductance in the presence of FAs (Andreyev et al. 1989, Brustovetsky & Klingenberg 1994, Bertholet et al. 2019 Kreiter et al. 2021, Kreiter et al. 2023). They are the most abundant proteins of the IMM, whose isoforms are widely expressed amongst all bodily tissues (Kagawa & Ohta 1990, Dolce et al. 2005). While it was initially hypothesized that ANTs and UCP1 also enhance the basal proton leak by their mere presence in live cells and mitochondria, this was not confirmed in isolated systems (Urbánková et al. 2003, Fedorenko et al. 2012, Bertholet et al. 2019, Kreiter et al. 2021). Notably, the uncoupling effect is present exclusively when these proteins are in the presence of FAs. Other members of the SLC25 family that were found to enhance the FA-mediated proton transport are the phosphate carrier (PiC) (Zácková et al. 2000, Engstová et al. 2001), aspartate/glutamate carrier (AGC) (Samartsev et al. 1997, Samartsev & Mokhova 1997), the dicarboxylate carrier (DIC) (Wieckowski & Wojtczak 1997), and the 2-oxoglutarate/malate carrier (OGC) (Žuna et al. 2024).

Protein-mediated proton transport can be inhibited by purine nucleotides (Modrianský et al. 1997, Andreyev et al. 1989, Hoang et al. 2012, Macher et al. 2017, Bertholet et al. 2019), or protein-specific inhibitors, such as carboxyatractyloside and bongkrekic acid (BA) for ANT1 (Andreyev et al. 1988, Andreyev et al. 1989, Brustovetsky et al. 1990, Brustovetsky and Klingenberg 1994, Bertholet et al. 2019, Kreiter et al. 2021) and genipine for UCPs (Kreiter et al. 2019).

1.2.3. Natural uncoupling

Protein-mediated proton transport is naturally enhanced by endogenous agents such as FAs and N-acyl amino acids (Long et al. 2016, Gao et al. 2022) and intensified by reactive alkenals (Pohl & Jovanovic 2019).

FAs serve as natural weak-acid protonophores, enabling membrane proton transport through individual “flip-flop” events or via protein-mediated activation. Their hydrophobic nature and integration into phospholipid membranes, like the IMM, facilitates passive diffusion in their neutral form (Hamilton 1999). Since the passive transport of FA anions back to the intermembrane space is slow, the overall process results in proton leakage and the decrease of MMP (Pohl et al. 2000). Notably, proton conductance increases with an increase in chain length and the number of unsaturated bonds in FAs (Beck et al. 2007, Rupprecht et al. 2010), as well as in the presence of mitochondrial carriers. How exactly proteins and FAs interact is still highly debated (See Chapter 2.3.4).

N-acyl amino acids (NAAAs) are another group of naturally present lipid protonophores (Long et al. 2016). Only medium-chain length NAAAs with neutral carboxylate-containing head groups exhibit protonophoric activity, but they mostly show lower uncoupling potency in comparison with their FA counterparts. Their action has so far not been tested in an isolated system with recombinant proteins, but experiments performed in mitochondria indicate that NAAAs interact with and directly activate ANT1 and UCP1 (Gao et al. 2022), with some adverse effects in adipocytes (Herrnhold et al. 2023).

Reactive alkenals (Ras) are peroxidation products created upon the reaction of n-6 or n-6 polyunsaturated fatty acids with the superoxide anion $O_2^{\bullet-}$ (Schauenstein & Esterbauer 1978). Some of the most known reactive alkenals are 4-hydroxy-2-nonenal, 4-oxo-2-nonenal, and 4-hydroxy-2-hexenal. Ras are not protonophores, but it was shown that they covalently modify phosphatidylethanolamine resulting in the formation of membrane-active adducts (Jovanovic et al. 2020). This exerted a direct influence on protein function, exemplified by a significant increase in UCP1 activity (Pohl & Jovanovic 2019).

Certain natural compounds can induce uncoupling through signaling pathways or upregulation of specific genes. Notably, secondary plant metabolites like resveratrol and capsaicin, alongside hormones such as adrenaline, noradrenaline, leptin, and the thyroid hormone T3, fall within this category (For review see Shrestha et al. 2021). While these molecules do not engage in proton transport, they affect the transcription and translation of proteins through a myriad of signalling cascades, ending in decreased MMP and increased proton transport.

1.2.4. Artificial uncoupling

Uncoupling can also be enhanced through the utilization of chemically synthesized protonophores. They can be sorted into categories such as phenols, aromatic amines, benzimidazoles, N-phenylanthranilates, phenylhydrazones, salicylic acids, and their derivatives. Classic chemical protonophores consist of a lipophilic moiety that interacts with lipids of the IMM and a weak carboxylic group with a pKa value between 3 and 8 (Terada 1981). They uncouple the MMP by translocating protons over the IMM.

Aromatic amines derivatives such as carbonyl cyanide p-trifluoro-methoxyphenyl hydrazone (FCCP) and carbonylcyanide-3-chlorophenylhydrazone (CCCP) are the most frequently used protonophores in research. They are potent uncoupling agents that can induce both plasma and mitochondrial membrane depolarization by facilitating H^+ currents (Hollenbeck et al. 1985, Par et al. 2002). FCCP, as a CCCP derivate, is almost exclusively used in mitochondrial oxygen consumption experiments where it leads to a complete collapse of MMP and shows the respiratory capacity of the measured system (Kane et al. 2017). However, the mechanism behind FCCP/CCCP-mediated uncoupling does not seem to revolve only around proton transport and is more complex than for conventional weak acids like FAs. FCCP and CCCP most likely react unspecifically with sulfhydryl groups of different proteins, and are not mitochondria-specific (Hollenbeck et al. 1985).

There has been a surge of recently synthesized chemical uncouplers, such as weak C-H acids. Among these is *o*-carborane, which can transverse both mitochondrial and artificial lipid membranes in neutral and anionic form. Notably, the rates of proton shuttling by *o*-carborane were comparable to conventional protonophores. Together with its resistance to catabolism, this makes *o*-carborane another target of interest in pharmacological research (Rokitskaya et al. 2016). Another recently discovered chemical uncoupler is ((2-fluorophenyl)6-[(2-fluorophenyl)amino](1,2,5-oxadiazolo[3,4-e]pyrazin-5-yl)amine) or BAM15, that is mitochondria-specific and less toxic than FCCP/CCCP (Kenwood et al. 2014), already known for its potent effects of killing breast cancer cells *in vitro* (Zunica et al. 2021, Xiong et al. 2019).

Other novel uncouplers are MitoFluo (Antonenko et al. 2016, Denisov et al. 2014), dodecyl triphenylphosphonium (C12TPP) (Severin et al. 2010), rhodamine 19 butyl ester C4R1 (Khailova et al. 2014), modified butyl triphenylphosphonium cations (Rokitskaya et al. 2023), and the bromoalkyl ester of a hydroquinone derivative, named FR58P1 (Urra et al. 2018). The number of newly discovered uncouplers and their derivatives is growing (For review, see

Shrestha et al. 2021), while their medically relevant properties are being improved through numerous tested derivatives every day. The pharmacological use of chemical uncouplers is a promising ally in the fight against metabolic diseases, cancer, and aging. Chemical protonophores are more potent than naturally present FAs, specifically because their molecular structure and dosage can be predetermined.

1.3. Regulation of the substrate transport by the SLC25 protein family

1.3.1. Categorization of the SLC25 protein family

The SLC25 family is the largest solute carrier family that spans over 53 identified members with genes widespread among eukaryotic organisms. Members of this family are nuclear-encoded and mostly present in mitochondria (Fig. 3), with some expressed in peroxisomes, chloroplasts and mitosomes. Mitochondrial carriers (MC) are expressed in the IMM in small amounts (~20 pmol per mg of total protein) (Palmieri 2013). Exceptions are ANT1, which is the most abundant protein in the IMMs of heart mitochondria, and UCP1, which is highly abundant in brown fat mitochondria (Palmieri 2013) and under cold-acclimating conditions (Rupprecht et al. 2012). The expression of other MCs varies greatly, where some are widely expressed among tissues (dicarboxylate carrier), and some are specifically expressed in specific organs or tissues (e.g., UCP1 in BAT). Several MCs have two or more isoforms (e.g. ANT1-4), which are expressed in different parts of an organism (Palmieri 2014).

Even though some MC members are still considered “orphans” because of their unidentified roles, others can be divided by the substrates they transport. Most of the carriers transport nucleotides/dinucleotides, carboxylates, or amino acids. Additionally, phosphate ions are transported by PiC, carnitine, and acylcarnitine by the carnitine/acylcarnitine transporter (CACT). Uncoupling proteins are sorted in a separate group because of the high homology between their sequences, but it is not clear whether they all transport FA anions or protons, or some other metabolites. UCP2 and UCP3 transport carboxylates in addition to protons/FAs (Vozza et al. 2014, Kreiter et al. 2023, De Leonardis et al. 2024), while UCP5 and UCP6 may transport sulfur oxyanions, phosphate and dicarboxylates (Gorgoglione et al. 2019). Despite UCP4 and UCP5 having the highest homology to each other; UCP4 presumably potentiates uncoupling of the MMP by mediating proton transport (Ho et al. 2012, Ramsden et al. 2012).

Moreover, it was proposed that UCPs transport chloride, bromide, nitrate (Huang & Klingenberg 1996, Hoang et al. 2015), and alkyl sulfonates (Rial et al. 2004).

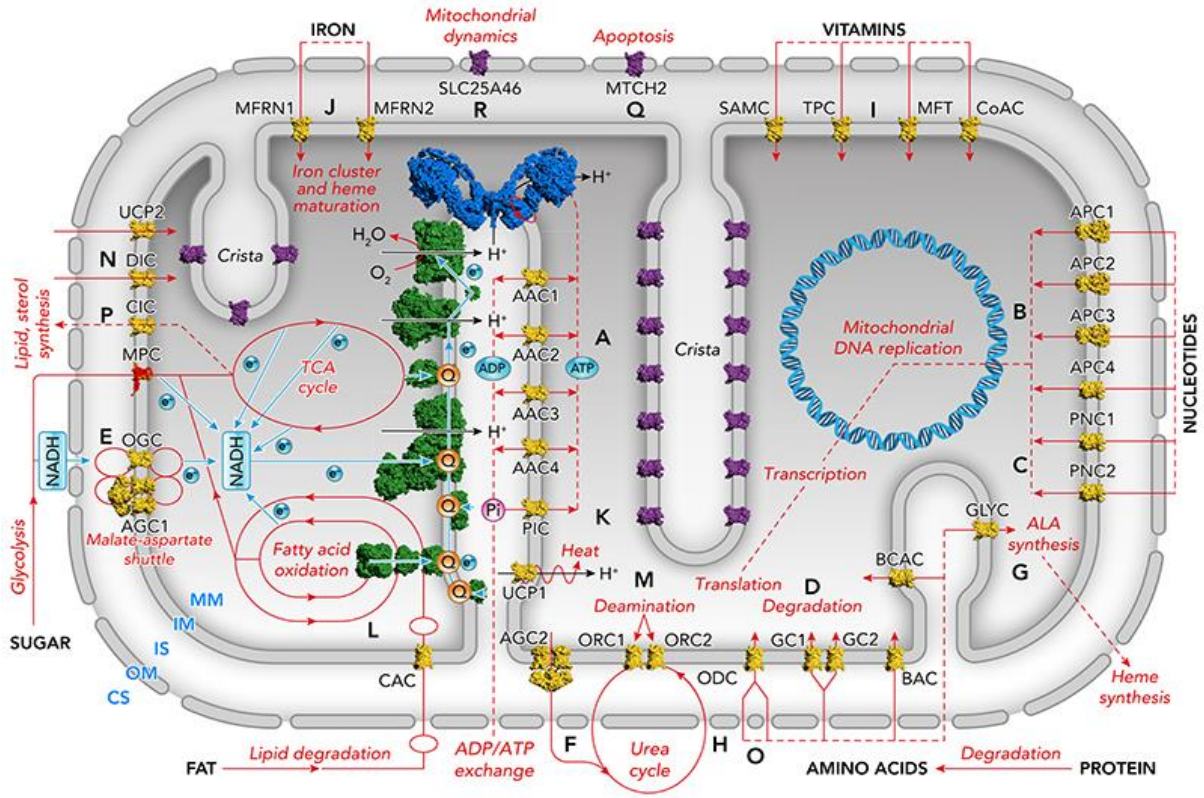

Figure 3. Schematic representation of the mitochondrion and the role of the SLC25 protein carrier family. Proteins of the electron transport chain are shown in green, ATP synthase in blue and others are: MPC, mitochondrial pyruvate carrier heterodimers; AAC1–4, ADP/ATP carriers; AGC1–2, aspartate/glutamate carriers; APC1–4, ATP-Mg/Pi carriers; BAC, basic amino acid carrier; CAC, carnitine-acylcarnitine carrier; CIC, citrate carrier; DIC, dicarboxylate carrier; GC1–2, glutamate carriers; GLYC, glycine carrier; MTFRN1–2, mitoferrins; ODC, oxoadipate carrier; OGC, 2-oxoglutarate/malate carrier; ORC1–2, ornithine carriers; PIC, phosphate carrier; SAMC, S-adenosylmethionine carrier; TPC, thiamine pyrophosphate carrier; UCP1, uncoupling protein; UCP2, uncoupling-like protein 2. Modified from Kunji et al. 2020 with permission from PubMed Central.

Much like UCPs serving multiple functions, several MCs such as ANT1, OGC, DIC, PiC, and AGC are primarily involved in transporting nucleotides/dinucleotides or carboxylates, enhance proton transport in the presence of FAs (Section 1.2.2). This suggests that SLC25 carriers likely possess more than one function initially identified or linked to their names. While the specific conditions required for their function remain largely unknown, it is evident that a comprehensive examination of each MC independently is essential to uncover their potential roles.

1.3.2. The structure of the SLC25 protein family

Current members of the SLC25 protein family were first classified and sorted according to their function and sequence similarity. Common features of these nuclear-encoded proteins include a similar size, about 300 amino acids in length, which is organized in three tandemly repeated homologous domains that span over the IMM (For review see Robinson & Kunji 2019 and Kunji et al. 2020). Each domain contains an odd-numbered transmembrane α-helix (H1, H3, or H5), a short loop matrix α-helix (h_{12}, h_{34}, or h_{56}), and an even-numbered transmembrane α-helix (H2, H4, or H6) (Fig. 4). Each domain has a mitochondrial carrier´s signature motif PX[D/E]XX[K/R]X[K/R] located at the C-terminus of the odd-numbered α-helix and the motif [D/E]GXXXX[W/Y/F][R/K]G located at the N-terminus of the even-numbered α-helix. The six α-helices create a barrel-shaped structure, where α-helices are about 45° tilted toward the membrane plane and where both termini are oriented toward the intermembrane space. Carriers are stabilized with intra-helical salt bridges that are interchangeable and leave the possibility of the protein´s cavity being open to the cytosol (c-state) or the matrix (m-state). Other key elements of SLC25 family proteins are the substrate binding site, and πGπxπG and πxxxπ motifs. These elements, together with the mitochondrial carrier´s signature motifs, slightly differ among the carriers.

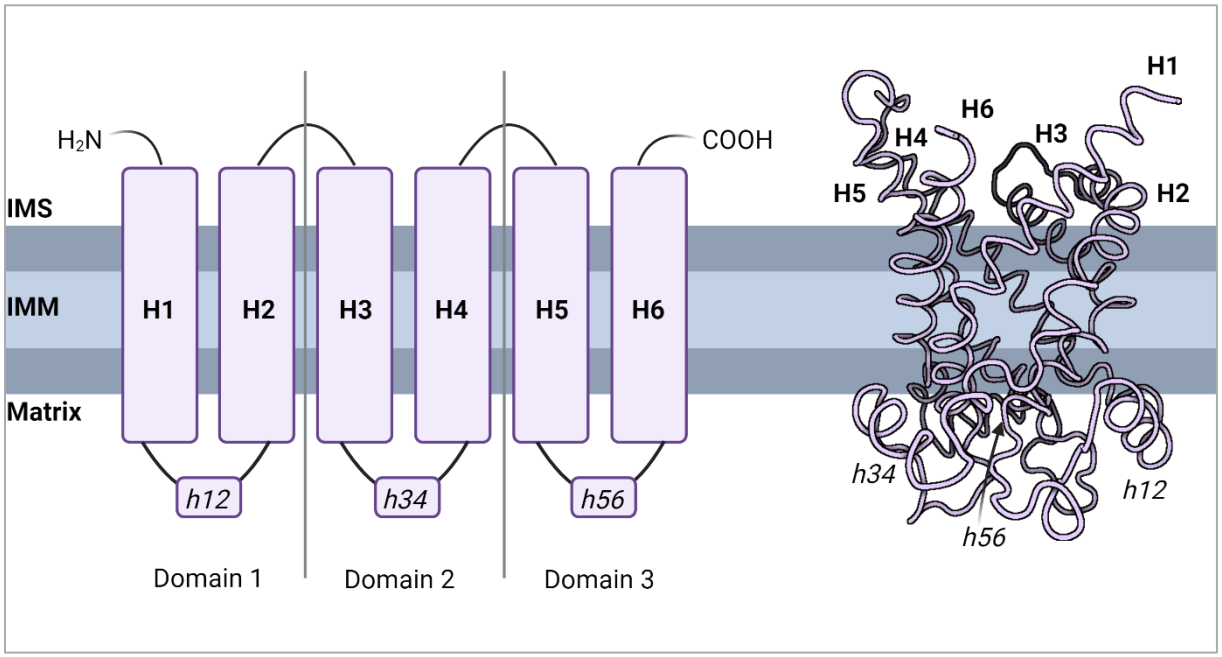

Figure 4. Topological model of SLC25 family proteins (left). The protein is divided into three similar domains, each containing two α-helices connected by shorter cytosolic and longer matrix loops. A lateral view of the 3D structure of ANT1 (PDB: 1OKC) shows six α-helices tilted by 45° relative to the membrane plane (right). Image created with BioRender. Modified from Huang & Klingenberg 1999 with permission from Elsevier.

Most of the structural and functional information on the SLC25 family came from ANT1, which was the first identified protein of this family. The crystallographic structure of ANT1 in complex with its inhibitor carboxyatractyloside (CATR), where the protein is in c-state, was resolved in 2003 at the 2.2 Å resolution (Pebay-Peyroula et al. 2003). ANT1's 3D structure made it possible to visualize the overall shape of the protein, explain experimental results that used site-directed mutagenesis, and align and extrapolate structures of other SLC25 carriers. In addition, important salt-bridges and on the cytoplasmic and matrix sides of the protein (Ruprecht et al. 2014), and the stabilizing roles of conserved glycines and kink-inducing prolines have been identified. The crucial role of cardiolipin was confirmed by identifying three cardiolipin molecules tightly bound to the matrix side of the protein by hydrogen bonds and electrostatic interactions with helix dipoles (Beyer & Klingenberg 1985, Pebay-Peyroula et al. 2003, Ruprecht et al. 2014). Furthermore, ANT1's crystal structure has shed light on what appears to be a conserved binding site among the whole carrier family (Kunji & Robinson 2006) which consists of one contact point found on each of the three even-numbered helices in the middle of the membrane.

For a long time, the structure of ANT1 in complex with CATR remained the only one resolved out of the entire SLC25 family. An attempt at the nuclear magnetic resonance (NMR) structure of UCP2 (Berardi et al. 2011) was highly criticized for the detergent choice, and the obtained structure was found leaky and unstable (Skulj et al. 2021). ANT1 was later resolved in complex with BA where the protein is in an m-state (Ruprecht et al. 2019), but the protein's structure in its free state has yet to be resolved. After twenty years of ANT1 being the only structurally resolved carrier of the family, the discovery and use of nanobodies and synthetic antibodies (sybodies) resulted in several 3D structures of UCP1, published in early 2023 (Kang & Chen 2023, Jones et al. 2023). Additionally, UCP1 was shown in a complex with DNP and ATP, and overall, the structures aligned well with the crystallographic ANT1 structure. Currently, ANT1 and UCP1 stand out as the only two proteins within the family with a resolved crystallographic structure. This unique feature makes them particularly important for studying not only the mechanism of substrate transport but also the intricacies of how proteins participate in FAs-activated proton transport.

1.3.3. Preserved substrate transport mechanism

Proteins of the SLC25 family have one substrate-binding site, and they can expose it to the cytosol or the matrix. When a substrate binds from the matrix to the protein in the m-state, it triggers a reaction that restructures the protein to the c-state, where the substrate is released to the cytosol. This process is called the altering access mechanism (Jardetzky 1966, Ruprecht et al. 2014, Drew & Boudker 2016).

Several carrier domains are responsible for transporting substrates. Cytoplasmic and matrix salt-bridge networks, as well as the cytoplasmic tyrosine brace ([YF][DE]xx[KR]) and matrix glutamine brace (Px[DE]xx[KR]xxxQ), form gates that open and close the carrier´s cavity on opposite sides during substrate translocation and expose the substrate binding site (Ruprecht et al 2019). Among the carriers, matrix salt bridges are rarely changed (Kunji & Robinson 2006, Cappello et al 2007,), while there is more variety across the cytoplasmic residues and salt bridges (Robinson et al. 2008, Miniero et al. 2011). The gates are approximately 15 Å thick, which prevents unregulated proton leak through the protein´s cavity (Ruprecht et al. 2020).

The substrate-binding site lies at the bottom of the water-filled cavity of the carrier, and its three contact points are universally conserved among the SLC25 family (Robinson & Kunji 2006). Analysis of the contact points among carriers discovered that contact point I (located on helix 2) distinguishes between different substrates within the same class, while contact point II (on helix 4) discriminates between different classes of substrates. Contact point III (on helix 6) is usually a positively charged amino acid that does not play a role in substrate binding specificity (Robinson & Kunji 2006 a, Robinson & Kunji 2006 b). The position and identity of contact points in each of the carriers depend on the size, shape, and chemical composition of the substrates they transport. Several conserved glycine and proline residues lie close to the substrate-binding site and act as hinges that help open the matrix or cytosolic gate (Ruprecht et al. 2019). These complex reactions come together to control the binding of substrates and their translocation to the corresponding binding site.

At the physiological level, substrate transport is regulated through allosteric interactions with activators or inhibitors, changes in local substrate and counter-substrate concentrations, and changes in the transcriptional and translational level of the carrier induced by extra- and intracellular signaling (For review see Kunji et al. 2020).

1.4. 2,4-dinitrophenol is a potent chemical protonophore

1.4.1. The physiological significance of 2,4-dinitrophenol

Phenols and phenol derivatives are another large group of synthetic uncouplers of pharmacological importance. The most famous among phenolic uncouplers is 2,4-dinitrophenol (DNP), originally registered by the pharmacological industry as a weight-loss drug in the United States in the mid-1930s (Cutting et al. 1933). Because of severe toxicity and lethal side effects, it was banned from use soon afterward (Colman 2007). However, DNP can still be illegally purchased online with relative ease and is mostly used by bodybuilders who are looking to shred excess fat tissue while maintaining their muscle mass. The number of deaths following its use is steadily increasing and calls for the development of a still missing antidote (Petróczi et al. 2015).

The interest in DNP does not only lie in the need for a cure, but in its efficacy and potency because it remains one of the most efficient weight-loss drugs ever used. As a weak acid, DNP holds an anionic form at the physiological pH and slowly crosses over the membranes. However, when DNP gets protonated, it quickly crosses the membranes and increases the proton transporting rate. In the case of IMM, this creates a significant drop in MMP, preventing ATP production and increasing the basal metabolic rate. As the rate of ATP production continues to drop, the demand for nutrients increases, causing a decrease in fat deposits and a rapid loss of weight (Rognstad & Katz 1969, Goldgof et al. 2014).

The uncoupling role DNP plays in mitochondrial physiology was proven multiple times in pure lipid bilayers (Bielawski et al. 1966, Lea & Croghan 1969, Finkelstein 1970, LeBlanc Jr. 1971, McLaughlin 1972) and isolated mitochondria (Chappell & Greville 1959, Carafoli & Rossi 1967, Yu et al. 1988, Lou et al. 2007). Besides acting on the lipid bilayer itself, DNP interacts with mitochondrial proteins, specifically those from the SLC25 family (Žuna et al. 2021, Bertholet et al. 2022). However, the molecular mechanism behind DNP's uncoupling was not described in detail yet (See section 1.4.). This prevents any future therapeutic use and hinders the development of drugs against obesity and other metabolic disorders.

1.4.2. The mechanism of DNP-mediated proton transport

First experiments demonstrating DNP-mediated proton transport were done on model membranes (Bielawski et al. 1966, Lea & Croghan 1969, Finkelstein 1970, LeBlanc Jr. 1971, McLaughlin 1972). Several mechanisms explaining how DNP exerts its electrical effects on lipid bilayers were proposed, starting from Finkelstein (Finkelstein 1970), who proposed that DNP is transported over the membrane as a carrier complex HA_2^- created from one neutralized form (HA) and one anionic form of the molecule (A^-). This hypothesis was confirmed experimentally by Lea and Croghan (Lea & Croghan 1969), who showed that the conductance increases exponentially with an increase in DNP concentration. However, experimental results by Bielawski et al. (Bielawski et al. 1966) and Liberman et al. (Liberman et al. 1970) showed that the conductance did not depend on the square root of DNP concentration, contradicting the carrier model. Hopfer et al. (Hopfer et al. 1970) proposed that if the carrier model is correct, the conductance maxima of DNP should be near the pH values of its pK, which is around 4 in water. Their experimental values did not confirm this hypothesis, but they neglected the fact that the pKa values of DNP in water and lipid bilayer are not the same. Finally, McLaughlin (McLaughlin 1972) emphasized the importance of lipid membrane composition on the transport mechanism of DNP and noted that DNP adsorbs to neutral lipids and creates a substantial negative surface potential. His experimental results denied the carrier complex transport model and the mechanism of DNP´s transport across lipid bilayers remains unknown.

After decades of research on DNP and hints coming from mitochondrial experiments, it was recently shown that DNP does not mediate proton transport only through lipid membranes, but also through activation of mitochondrial carriers (Žuna et al. 2021, Bertholet et al. 2022, Kang & Chen 2023). These two processes seem to be closely intertwined and dependent on DNP concentration, where the involvement of mitochondrial proteins is more noticeable at lower DNP concentrations. It was experimentally shown that DNP interacts with ANT1 and UCP1 at the same binding site, arginine 79, similar to FAs (Kang & Chen 2023, Kreiter et al. 2023). In addition to the homolog of arginine 79 (arginine 83), UCP1´s 3D structure showed that the phenyl ring of DNP interacts with tryptophan 280 through π–π interactions and the hydroxyl group interacts with arginine 276. The two-nitro groups interact with asparagine 281, leucine 277, arginine 91, glutamine 84, and arginine 83. It was then confirmed that the mutations of arginine 83 and glutamine 84 to alanine significantly decreased the ability of DNP to activate UCP1, proving they are involved in binding and/or transport (Kang & Chen 2023).

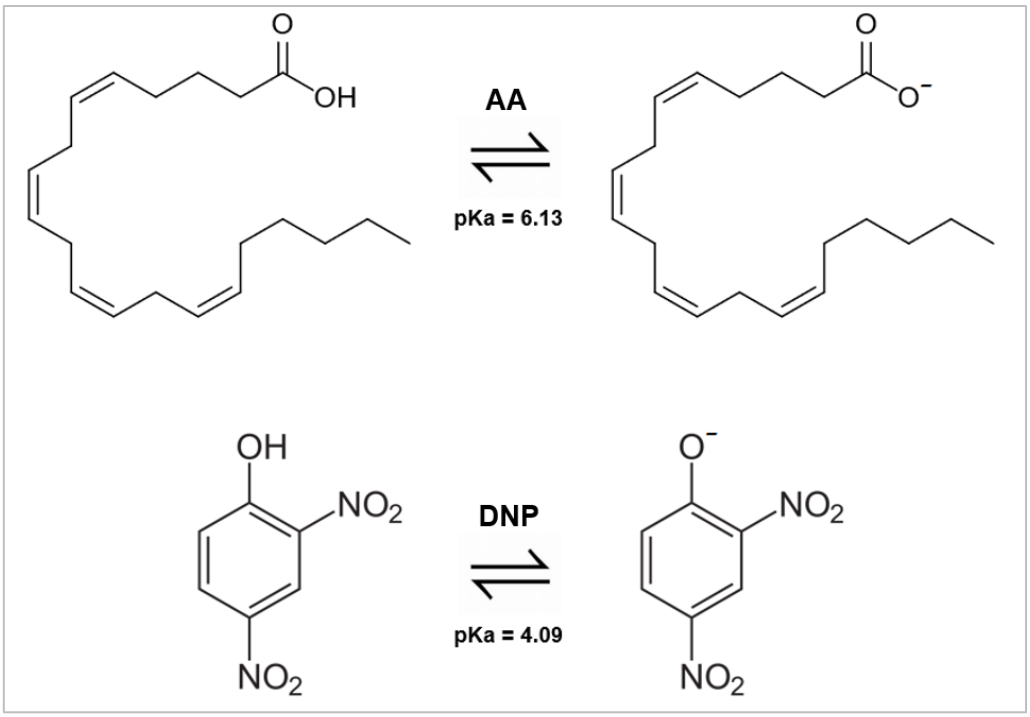

Figure 5. Chemical structures of arachidonic acid (AA) and 2,4-dinitrophenol (DNP). The pKa value of AA is 6.13 as determined in a DOPC bilayer (Pashkovskaya et al. 2018), and the pKa value of DNP is 4.09 as determined in water (Pearce & Simkins 1968).

As a weak acid, DNP appears to interact with mitochondrial carriers in a similar manner to FAs. Even though this might be true because they are both negatively charged at the physiological pH, they differ significantly in chemical structure (Fig. 5). The reaction mechanism of DNP and each chemical protonophore needs to be studied independently of FA-mediated uncoupling.

1.5. The mitochondrial 2-oxoglutarate/malate carrier

1.5.1. Discovery

The mitochondrial 2-oxoglutarate/malate carrier (OGC), also known as the α-ketoglutarate/malate antiporter, is a member of the SLC25 family. The main function of OGC is to transport one molecule of 2-oxoglutarate for one molecule of L-malate, or succinate, oxaloacetate, malonate, maleate, D-malate, or 2-oxoadipate, in decreasing order of affinity (for review, see Monne et al. 2013).

The existence of a mitochondrial carrier for 2-oxoglutarate was first proposed in the 1960s based on mitochondrial swelling experiments (Chappell 1968) and demonstrated multiple times later in isolated rat hearts (Sluse et al. 1973, Sluse & Liébecq 1973), rat liver (Palmieri et al.

1972), and plant mitochondria (Fonyó et al. 1976, Genchi et al. 1991). Finally, the carrier for 2-oxoglutarate was purified from pig and bovine heart mitochondria in the presence of detergent and cardiolipin (Bisaccia et al. 1985, Indiveri et al. 1987). After initial purifications in detergent, OGC was reconstituted in phospholipid vesicles, which enabled precise studies on carrier transport kinetics (Indiveri et al. 1987).

Once the cDNA sequence of OGC was published, it became possible to engineer a recombinant protein-expressing system in simple organisms and significantly multiply the yield, which was rather hard to obtain in larger amounts just by purification. That is how OGC became the first eukaryotic membrane protein that was recombinantly expressed in *E. coli* and reconstituted in liposomes (Fiermonte et al. 1993). This opened up the possibility to study the function of mitochondrial carriers in more detail, especially by applying site-directed mutagenesis. After OGC, many other carriers like ANT1 and UCP1 were purified and reconstituted from *E. coli* expression systems, enabling the discovery of the common substrate-binding site of the SLC25 family (For review, see Palmieri 2012).

1.5.2. Structure and substrate specificity

As soon as the cDNA sequence of OGC became known, it was clear that it belongs to the SLC25 family (Runswick et al. 1990). The sequence similarity between OGC, ANT and UCP1 implies that OGC shares their structure (Tab. 1), which was confirmed by artificial intelligence structure modelling (UniProt entry: Q02978).

OGC´s structure was initially characterized by using thiol reagents, which exposed cysteines 221 and 224 as open towards the cytoplasmic side and functionally relevant (Zara & Palmieri 1988). The third cysteine, C184, was found as a potential cross-linker responsible for OGC-dimerization (Bisaccia et al. 1996). Even though the dimerization process was later questioned, C184 also reacted to sulfhydryl reagents while transporting substrates, underlying its functional relevance. Many positively charged residues, such as lysines and arginines, were discovered as crucial for substrate transport through a series of experiments that used amino-acid-specific inhibitors, such as pyridoxal 5′-phosphate (Natuzzi et al. 1999). Finally, complete cysteine-scanning mutagenesis of OGC revealed all functionally important residues (Palmieri et al. 1996, Stipani et al. 2001, Cappello et al. 2006, Cappello et al. 2007, Miniero et al. 2011). By replacing one amino acid with a cysteine, one at a time, it was possible to measure its importance in

substrate transport and/or inhibition. So far, complete cysteine mutagenesis exists only for OGC, and it revealed several groups of functionally relevant residues.

The first group of residues are those important for specific substrate binding, namely R90, Y94, R98, R190, and R288 (Stipani et al. 2001, Cappello et al. 2006). They fit into the contact points of the proposed binding site of the MCF family and are found on the even-numbered helices at the mid-point of the IMM (Fig. 6). Even though their role in substrate transport was confirmed by leucine replacements as well (Palmieri et al. 1996), it is still not clear how they coordinate the binding of different parts of the substrate molecules. The second important group of OGC´s residues forms the salt-bridge networks among the protein´s helices, thereby supporting the changes in conformation necessary for active function.

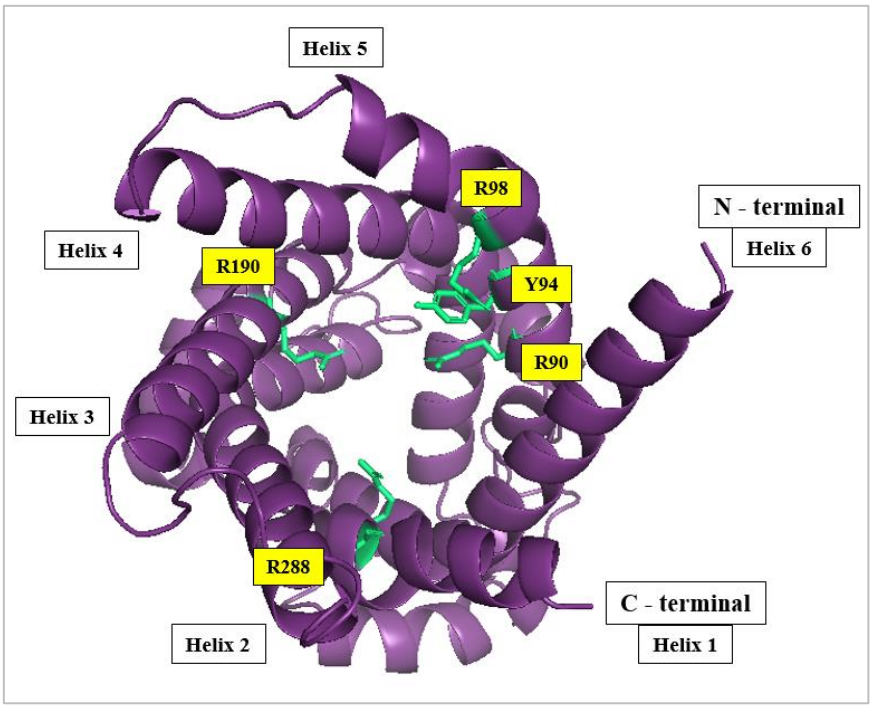

Figure 6. Topological view of OGC from the cytosolic side. Yellow-labeled residues represent the substrate binding site. Image created with an AlphaFold-predicted murine OGC structure (PDB: AF-Q9CR62) and PyMOL.

Salt bridges found on the matrix side of the protein belong to the signature MCF motifs PX[DE]XX[RK], and those are P41, D43, and K46; P139 and E141; and P239, D241, and K244, found on the odd-numbered helices (Cappello et al. 2007). Residues Y and [ED]G, found on the beginnings and ends of matrix helices h_{12}, h_{34}, and h_{56}, are forming additional salt bridges with the residues below the signature motifs to add extra support to the closing of the matrix gate (Miniero et al. 2007). The cytoplasmic part of OGC is formed somewhat differently from other MCF carriers, mainly because the signature motifs [DE]XX[RK], found on even-

numbered helices, are only party conserved (Miniero et al. 2011). Many other singular amino acids, such as prolines and glycines, are found throughout OGC´s sequence and were proven functionally relevant. They most likely support salt-bridge networks during substrate translocation or induce helix kinks, used for opening and closing the gates (Robinson et al. 2008, Palmieri & Pierri 2010).

Table 1. Sequence similarity of murine mitochondrial carrier sequences. The carriers are the 2-oxoglutarate/malate carrier (OGC), adenine nucleotide translocase 1 (ANT1), uncoupling proteins 1-4 (UCP1-4), aspartate glutamate carrier 1 (AGC1), phosphate carrier (PiC) and dicarboxylate carrier (DIC).

	OGC	ANT1	UCP1	UCP2	UCP3	UCP4	AGC1	PiC	DIC
OGC	**100%**	27,7%	33,3%	34%	35%	32,3%	24,5%	24,5%	39%
ANT1	27,7%	**100%**	22%	24%	25,5%	24,3%	28,9%	21,8%	23%
UCP1	33,3%	22%	**100%**	56,6%	55,5%	30,8%	26,2%	26,5%	33,3%
UCP2	34%	24%	56,6%	**100%**	73,8%	34,9%	26,4%	22,1%	36,2%
UCP3	35%	25,5%	55,5%	73,8%	**100%**	34,9%	28,1%	26,9%	35,8%
UCP4	32,3%	24,3%	30,8%	34,9%	34,9%	**100%**	25%	28%	30,8%
AGC1	24,5%	28,9%	26,2%	26,4%	28,1%	25%	**100%**	25,5%	26,3%
PiC	24,5%	21,8%	26,5%	22,1%	26,9%	28%	25,5%	**100%**	22,2%
DIC	39%	23%	33,3%	36,2%	35,8%	30,8%	26,3%	22,2%	**100%**

Given the similarities between OGC and other members of the SLC25 family (Palmieri 2013), it was proposed that it performs substrate transport in the same manner. According to the central gate pore mechanism (Klingenberg 2008), OGC would have one binding site for substrates, which would enter either from the cytoplasmic or the matrix side. In each case, one molecule of substrate would bind to the substrate binding site, which would trigger conformational changes needed for the opposite gate of the protein to open and release the substrate. This transport cycle is simultaneous, with gates opening and closing on opposite sides as needed. However, a 3D structure of OGC hasn´t yet been resolved, and such a transport mechanism is proposed solely based on the structure homology between carriers. Since OGC´s cytoplasmic MCF signature motifs are only partly conserved, the cytoplasmic gate´s opening might be triggered through a set of functions individual for OGC.

1.5.3. Physiological significance of OGC

The main and most impactful function of OGC is the indirect involvement in energy production through the malate/aspartate shuttle (Borst cycle) (For review see Borst 2020). OGC transports malate for 2-oxoglutarate, while the aspartate/glutamate carrier transports aspartate for glutamate across the IMM. The enzymes malate dehydrogenase and glutamate oxaloacetate transaminase, which exist in the cytosol and the mitochondrial matrix, convert these substrates to their oxidized/reduced counterparts (Fig. 7). The result is equivalent to the oxidation of one NAD^+ in the cytosol reduction of one NADH in the matrix, which enters the electron transport chain. The described function of OGC is crucial for proper energy production in the cell, and the knockout of OGC in mice is embryonically lethal (Lee et al. 2019).

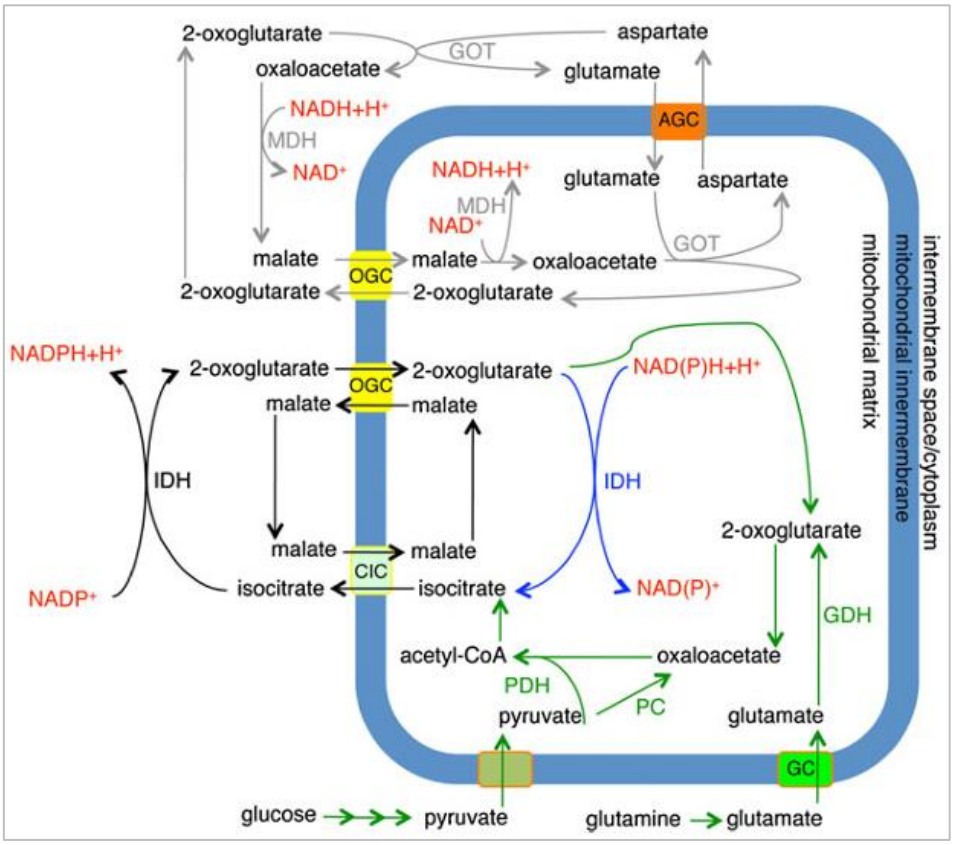

Figure 7. OGC participates in the malate/aspartate shuttle, the 2-oxoglutarate/(iso)citrate shuttle, and the pyruvate/isocitrate pathway. The enzymes are malate dehydrogenase (MDH), glutamate oxaloacetate transaminase (GOT), isocitrate dehydrogenase (IDH), pyruvate carboxylase (PC), pyruvate dehydrogenase (PDH), glutamate dehydrogenase (GDH), citrate carrier (CIC), aspartate/glutamate carrier (AGC), and the glutamate carrier (GC). Image published in Monné et al. 2013 and reposted with the permission of PubMed Central.

OGC participates in the 2-oxoglutarate/isocitrate shuttle similarly, together with the citrate carrier (CIC). Isocitrate, transported by the citrate carrier, is converted to 2-oxoglutarate by isocitrate dehydrogenase that exists in both the matrix and the cytosol. In the end, the reducing molecule NADPH is replenished in the cytosol, where it can be used in anabolic processes such as in the synthesis of cytosolic fatty acids or cholesterol (Williamson & Cooper 1980). OGC is also involved in the 2-oxoglutarate/citrate shuttle in the same way, with the addition of matrix aconitase and cytosolic citrate lyase, which convert isocitrate to citrate and citrate to acetyl-Co, respectively (Castegna et al. 2010).

By transporting 2-oxoglutarate, OGC also supports the pyruvate/isocitrate pathway, where isocitrate exists in the mitochondrial matrix through CIC after pyruvate has entered the Krebs cycle. Isocitrate is converted to 2-oxoglutarate by the isocitrate dehydrogenase, and the 2-oxoglutarate can return to the matrix via OGC. The cycle produces one molecule of cytosolic NADPH necessary for anabolic processes (Joseph et al. 2006). It was proposed that OGC takes part in gluconeogenesis as well when the starting compound is lactate. The initial step in glycolysis is the transport of oxaloacetate from the matrix to the cytosol. Since oxaloacetate cannot cross the IMM, it crosses as malate through OGC or CIC and is converted to oxaloacetate by the cytosolic malate dehydrogenase (Meijer & Van Dam 1981).

Glutathione transport is another proposed function of OGC, which remains highly controversial. Initial studies suggested both OGC and the dicarboxylate carrier are responsible for the mitochondrial uptake of glutathione (Putt 2000, Coll et al. 2003, Estrela et al. 2004, Xu et al. 2006), but this was later disputed by testing the function of recombinant proteins reconstituted in liposomes (Booty et al. 2015). However, OGC´s unresolved function of binding porphyrin derivatives, such as hemin, has been proven only recently after the protein was purified and reconstituted from rat brain mitochondria (Miniero er al. 2021). This suggests OGC might be indirectly involved in several metabolic pathways that are regulated by the breakdown of heme-containing proteins, such as apoptosis.

Furthermore, by reconstituting OGC in an isolated system of planar lipid bilayers, we proved that it participates in FA and DNP-mediated proton transport. This was direct proof of OGC´s role in uncoupling after years of debate (See section 1.5.4.). The multitude of OGC´s essential physiological roles explains the embryonic lethality of OGC-deficient mice and underlines the importance of conducting further research on the vast number of its undiscovered roles.

1.5.4. The hidden role of OGC in uncoupling

OGC has been used as a negative control for uncoupling since the study of Sanchis et al., where it was compared to UCP5 in yeast mitochondria (Sanchis et al. 1998). OGC overexpression did not affect the MMP compared to the wild type. However, an increase of another proton motive force or a changed number of mitochondria could have diminished an uncoupling effect if there was one. Zhang et al. later chose to overexpress OGC as a negative control as well, solely based on the previously mentioned study. They noted a slightly decreased MMP in yeast mitochondria (Zhang et al. 1999). Surprisingly, Yu et al. found that overexpression of OGC significantly decreases the MMP in HEK293 cells (Yu et al. 2001).

Initially, OGC was not considered for uncoupling due to its electroneutral substrate exchange (2-oxoglutarate^{2-} for L-malate^{2-}) and clear localization in the IMM (Sanchis et al. 1998). However, even though the substrate exchange process seems neutral from the overall net charge perspective, each step involves interaction with positively charged amino acids in the protein´s cavity, which can also explain the binding of the negatively charged FAs. Two substrates from opposite sides of the membrane are not transported simultaneously (Robinson et al. 2008), which means the transport of each molecule results in a change of electrical potential, even though the finished substrate exchange cycle does not. Furthermore, the argument that OGC does not participate in uncoupling due to its localization is not valid, given that all proteins that potentiate FA-mediated uncoupling are exclusively integrated into the IMM.

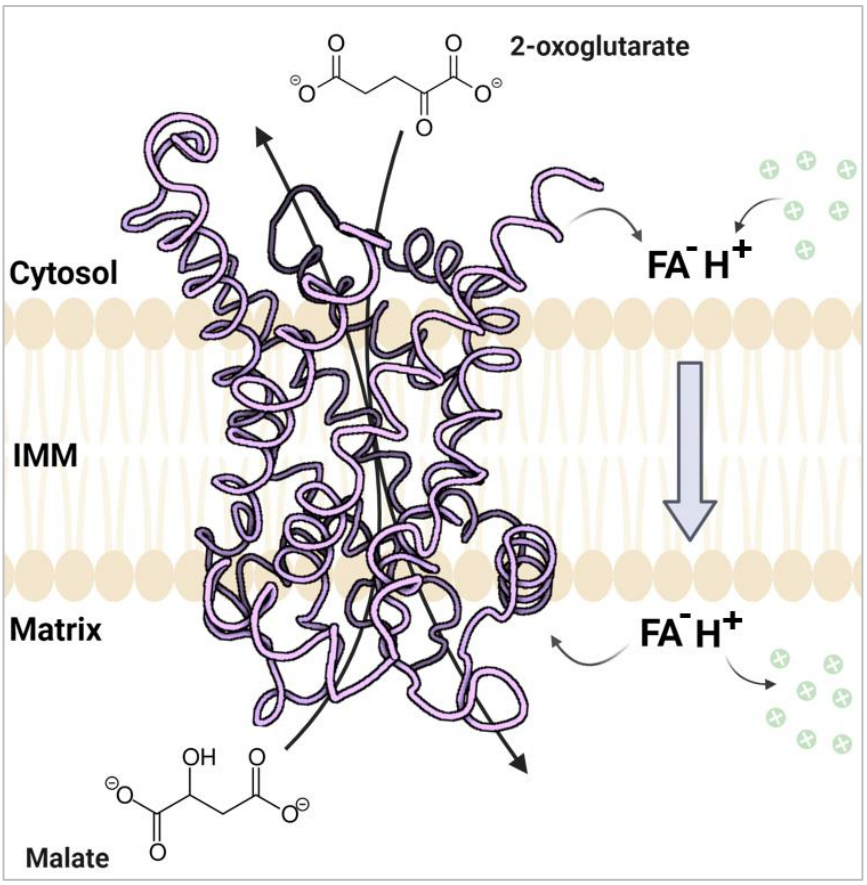

Figure 8. Two functions of OGC – 2-oxoglutarate/malate transport and fatty acid (FA)-mediated proton transport. Image created with BioRender using the AlphaFold predicted murine OGC structure (PDB: AF-Q9CR62).

One cannot easily conclude what is the effect of a single overexpressed protein in complex expression systems, such as yeast and cancer cells. A global effect can be attributed to changes in the expression of the desired protein, but many cellular processes can play a role in between. For example, higher expression of mitochondrial carriers might result in a changed number or morphology of mitochondria, which can unintentionally change the observed effects. Furthermore, if there is an intentional knock-out or knock-down of a certain protein, other proteins might become more expressed to compensate for the lost function. A false correlation can be recorded, even though it was impossible to distinguish it from other cell processes. Therefore, only by testing proton transport in an isolated system containing purified OGC and various protonophores, it is possible to conclude that it does indeed take part both in substrate transport and FA-mediated proton transport (Fig. 8) (Žuna et al. 2024).

1.6. Aims of the PhD work

Chemical protonophores such as DNP are of great pharmacological potential, but their action mechanisms have not been studied in detail. Given the implications regarding DNP´s effect on mitochondria, it is worth investigating whether and how it affects mitochondrial transporters of the SLC25 family involved in uncoupling, specifically ANT1 and UCP1-3. On the other hand, the involvement of other mitochondrial transporters from the SLC25 family, such as OGC, in physiological or chemically induced uncoupling has not been studied at all.

We hypothesize that (i) DNP-mediated uncoupling can be significantly enhanced by mitochondrial carriers that are capable of potentiating FAs-mediated uncoupling and (ii) OGC belongs to the group of proteins that catalyze the translocation of substrates and enhances both FAs and DNP-mediated uncoupling. We also hypothesize that the OGC-mediated uncoupling in the presence of FA may have a fatty acid cycling mechanism and may be regulated by lipid oxidation products.

Therefore, the aims of the PhD thesis are:

1. To investigate whether OGC facilitates uncoupling in the presence of FAs and DNP, and how these processes are inhibited.
2. To examine the effect of DNP on the mitochondrial carriers OGC, ANT1, and UCP1-3.
3. To establish important binding sites for DNP and FAs in OGC and ANT1.
4. To test how ROS products, such as RAs, affect lipid headgroups and influence mitochondrial carrier-mediated uncoupling.

We used an *E. coli* expression system to produce recombinant mitochondrial carriers. After purification, the proteins were reconstituted into planar lipid bilayer systems, which were used for conductance measurements and radioactive substrate transport measurements. Site-directed mutagenesis and molecular dynamics simulations were used to observe the effects of specific amino acid mutations and measurements of the membrane elastic parameters were used to observe changes in lipid bilayers upon addition of RAs.

2. Results

2.1. The 2-oxoglutarate/malate carrier extends the family of mitochondrial carriers capable of fatty acid and 2,4-dinitrophenol-activated proton transport.

Received: 19 October 2023 | Revised: 6 March 2024 | Accepted: 11 March 2024

DOI: 10.1111/apha.14143

ACTA PHYSIOLOGICA

RESEARCH PAPER

The 2-oxoglutarate/malate carrier extends the family of mitochondrial carriers capable of fatty acid and 2,4-dinitrophenol-activated proton transport

Kristina Žuna | **Tatyana Tyschuk** | **Taraneh Beikbaghban** | **Felix Sternberg** | **Jürgen Kreiter** | **Elena E. Pohl**

Physiology and Biophysics, Department of Biological Sciences and Pathobiology, University of Veterinary Medicine, Vienna, Austria

Correspondence
Elena E. Pohl, Physiology and Biophysics, Department of Biological Sciences and Pathobiology, University of Veterinary Medicine, 1210 Vienna, Austria.
Email: elena.pohl@vetmeduni.ac.at

Present address
Tatyana Tyschuk, Ludwig Boltzmann Institute for Traumatology, The Research Centre in Cooperation with AUVA, Vienna, Austria

Jürgen Kreiter, Institute of Molecular and Cellular Physiology, Stanford University School of Medicine, Stanford, California, USA

Funding information
Austrian Science Fund

Abstract

Aims: Metabolic reprogramming in cancer cells has been linked to mitochondrial dysfunction. The mitochondrial 2-oxoglutarate/malate carrier (OGC) has been suggested as a potential target for preventing cancer progression. Although OGC is involved in the malate/aspartate shuttle, its exact role in cancer metabolism remains unclear. We aimed to investigate whether OGC may contribute to the alteration of mitochondrial inner membrane potential by transporting protons.

Methods: The expression of OGC in mouse tissues and cancer cells was investigated by PCR and Western blot analysis. The proton transport function of recombinant murine OGC was evaluated by measuring the membrane conductance (G_m) of planar lipid bilayers. OGC-mediated substrate transport was measured in proteoliposomes using ^{14}C-malate.

Results: OGC increases proton G_m only in the presence of natural (long-chain fatty acids, FA) or chemical (2,4-dinitrophenol) protonophores. The increase in OGC activity directly correlates with the increase in the number of unsaturated bonds of the FA. OGC substrates and inhibitors compete with FA for the same protein binding site. Arginine 90 was identified as a critical amino acid for the binding of FA, ATP, 2-oxoglutarate, and malate, which is a first step towards understanding the OGC-mediated proton transport mechanism.

Conclusion: OGC extends the family of mitochondrial transporters with dual function: (i) metabolite transport and (ii) proton transport facilitated in the presence of protonophores. Elucidating the contribution of OGC to uncoupling may be essential for the design of targeted drugs for the treatment of cancer and other metabolic diseases.

KEYWORDS

long-chain fatty acids, mitochondrial transport, planar bilayer membranes, proton transport, SLC25A11, total membrane conductance

1 | INTRODUCTION

Cancer cells demonstrate distinctive metabolic reprogramming, relying more on aerobic glycolysis than oxidative phosphorylation (OXPHOS) for energy production, and exhibiting increased glutaminolysis and oxidative stress.[1,2] In particular, glutamine-derived α-ketoglutarate (α-KG), also known as 2-oxoglutarate, can participate in the OXPHOS pathway or the reductive carboxylation pathway, deviating from the usual TCA cycle. The 2-oxoglutarate/malate carrier (OGC) aids this by transporting 2-oxoglutarate and malate across the mitochondrial membrane.[2] Recent evidence shows that knockdown of OGC results in a 75% reduction in ATP production in non-small cell lung cancer.[3] In addition, a heterozygous OGC knockout reduced the growth of spontaneous lung cancer in mice by 50%, while inhibition of OGC by N-phenylmaleimide resulted in a 50% reduction in melanoma formation in human xenograft models.[4] The inhibitory effect on malignant growth has been attributed to the involvement of OGC in the replenishment of NADH required for ATP production via the malate–aspartate shuttle. Neutralization of excessive amounts of reactive oxygen species (ROS) by increasing proton transport across the membrane may be an alternative strategy and has been shown to induce apoptosis in mature tumors or prevent damage early in cancer development and after radiation therapy.[5] Application of chemical protonophores such as BAM15, niclosamide, or oxyclozanide to in vitro and in vivo systems resulted in a significant reduction in tumor proliferation.[6–8]

OGC, a member of the mitochondrial solute carrier 25 (SLC25) superfamily, is located in the inner mitochondrial membrane (IMM), where it transports 2-oxoglutarate for L-malate or other C4 metabolites.[9] Notably, the double knockout of OGC is embryonically lethal.[3] OGC was previously used as a negative control for uncoupling[10,11] until Yu et al. observed a significant decrease in mitochondrial membrane potential (MMP) after its overexpression in HEK293 cells.[12] Later, glutathione transport by OGC was proposed to play a role in reducing of oxidative stress in neuronal cells,[13] but this function remained controversial.[14] Since oxidative stress is reduced by mitochondrial uncoupling,[15,16] the real reason may be OGC-mediated H^+ transport, which has never been confirmed and further investigated in a well-defined system.

Since the homologs of OGC—adenine nucleotide transporter 1 (ANT1, 28% homology to OGC) and uncoupling proteins 1 (UCP1, 33% homology to OGC)—enhance H^+ transport in the presence of free fatty acids (FAs) and 2,4-dinitrophenol (DNP)[17,18] we hypothesized that also OGC dissipates the IMM proton gradient under similar conditions. Therefore, in this work, we used a well-defined system of planar lipid bilayer membranes reconstituted with OGC to (i) investigate its contribution to FA- and DNP-mediated proton transport, (ii) evaluate the efficiency of OGC inhibitors in reducing the proton transport rate, and (iii) identify amino acids critical for the interaction of OGC with FAs.

Unraveling the physiological function and mechanism of OGC-mediated mitochondrial uncoupling has the potential to provide insight into its involvement in cancer metabolism and aid in the development of targeted drugs for other metabolic diseases.

2 | RESULTS

2.1 | OGC is present in a wide range of murine tissues and cancer cell lines

To understand the physiological role of OGC, we first investigated its tissue expression in mice. Based on immunohistochemical staining experiments and testing the mRNA abundance, OGC has been reported to be ubiquitously expressed in the human body,[19] and in various rat tissues.[20] However, mRNA levels are not reliable predictors of protein presence[21] and there are no experimental data on OGC protein expression in mice. The main problem in testing the expression of SLC25 superfamily proteins is the lack of specific antibodies capable of distinguishing close homologs. To address this issue, we first validated the anti-OGC (anti-SLC25A11) antibody using inclusion bodies (IBs) of mouse OGC (mOGC) and other SLC25 family members, as well as heterozygous mouse knockout tissues. As shown in Figure S1, the antibody was specifically bound only to OGC IBs. We found that OGC was expressed on the protein level in all tested murine tissues (Figure 1A,B), with an expected decrease in heterozygous knockout samples. OGC was also present at the mRNA level in all tissues (Figure 1C), and in both cases, the highest expression was found in the heart, brain, and kidney. In addition, we have shown that OGC is expressed at different levels in murine and human cancer cell lines (Figure 1D).

2.2 | Production and reconstitution of mouse OGC in liposomes

OGC was the first eukaryotic protein to be expressed in Escherichia *coli* (*E. coli*) and functionally reconstituted in proteoliposomes.[9] The homology between OGC and other proteins of the SLC25 superfamily, such as ANT1, UCP1, and the dicarboxylate carrier is high, especially in conserved mitochondrial carrier motifs and substrate binding sites (Figure 2). Therefore, it is possible to express and purify them by using similar protocols.

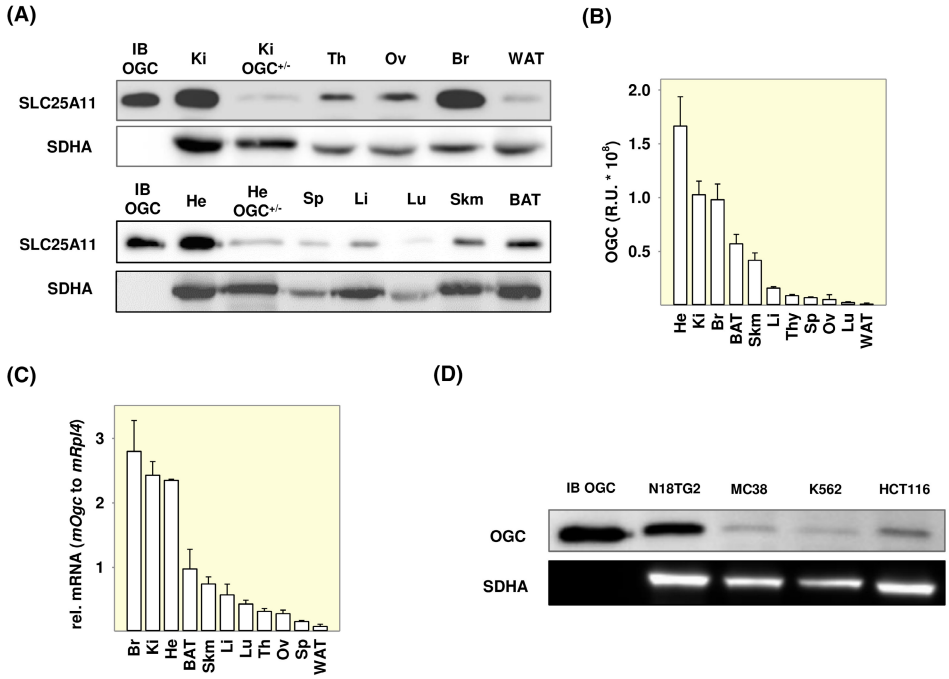

FIGURE 1 Detection of OGC (SLC25A11) in mice tissues and cancer cell lines. (A) Representative Western blot of OGC in mouse tissues. Tissues are labeled as follows: kidney (Ki), thymus (Th), ovary (Ov), brain (Br), white adipose tissue (WAT), heart (He), spleen (Sp), liver (Li), lung (Lu), skeletal muscle (Skm), and brown adipose tissue (BAT). (B) Quantification of OGC band intensity in all tissue samples in relative units. (C) mOGC mRNA levels (2-ΔCt) relative to mitochondrial ribosomal protein L4 (mRPL4) used as a reference gene. (D) Western blot analysis of OGC in mouse neuroblastoma (N18TG2), mouse colon adenocarcinoma (MC38), human myeloid leukemia (K562), and human colorectal carcinoma (HCT116) cell lines. 40 µg (A) or 20 µg (D) of total protein was loaded per lane. Recombinant mouse OGC (mOGC) inclusion bodies (IBs) (IB OGC, 2 µg) were used as positive controls, and mOGC heterozygous heart (He+/−) and kidney (Ki+/−) knockouts as negative controls in (A). OGC is detected at the corresponding size of 34 kDa. Succinate dehydrogenase (SDHA) was used as a mitochondrial control. Reversible Ponceau S staining loading control, full blots, and anti-OGC antibody validation are shown in Figure S1. See Section "4" for more details.

In this study, we adapted previously established protocols to produce murine OGC (mOGC) in *E. coli* IBs.[9,17,22] After purification and reconstitution into proteoliposomes (see Section 4), it was present as a dimer (Figure 3A). Early cross-linking studies suggested possible cysteine-linked dimerization of OGC in detergent,[23] although the issue remained controversial,[24] and the observed dimerization may be a result of aggregation under SDS-PAGE conditions.[25,26]

2.3 | mOGC transports ^{14}C-malate for 2-oxoglutarate

To confirm the functionality of mOGC and its correct refolding in proteoliposomes, we performed substrate transport exchange measurements using ^{14}C-malate and 2-oxoglutarate (Figure 3B). Figure 3C shows the decrease in ^{14}C-malate concentration in proteoliposomes reconstituted with mOGC upon the addition of 2-oxoglutarate. The transport rate, τ, was estimated from the decrease in ^{14}C-malate concentration over time, normalized to the protein concentration. The determined τ was approximately 47.24 µmol/min/mg, which is in good agreement with previous results for mitochondrial carriers (Table S1). Transport was completely inhibited by phenylsuccinate (PS), a substrate analog and a known inhibitor of the transport function of OGC.[27]

2.4 | Fatty acid and 2,4-dinitrophenol-mediated proton transport is facilitated by mOGC in planar lipid bilayers

Next, we tested whether mOGC contributes to the proton conductance in pure lipid membranes composed of DOPC, DOPE, and cardiolipin (45:45:10 mol%) in the model system.[28] We first measured the increase in the total membrane conductance (G_m) in the presence of a representative natural protonophore, arachidonic acid (AA), and DNP, a very potent chemical uncoupler that was previously used for obesity treatment.[29] G_m of protein-free planar lipid bilayers ($G_m = 8.75 \pm 3.2$ nS/cm^2) is comparable to the conductance of membranes

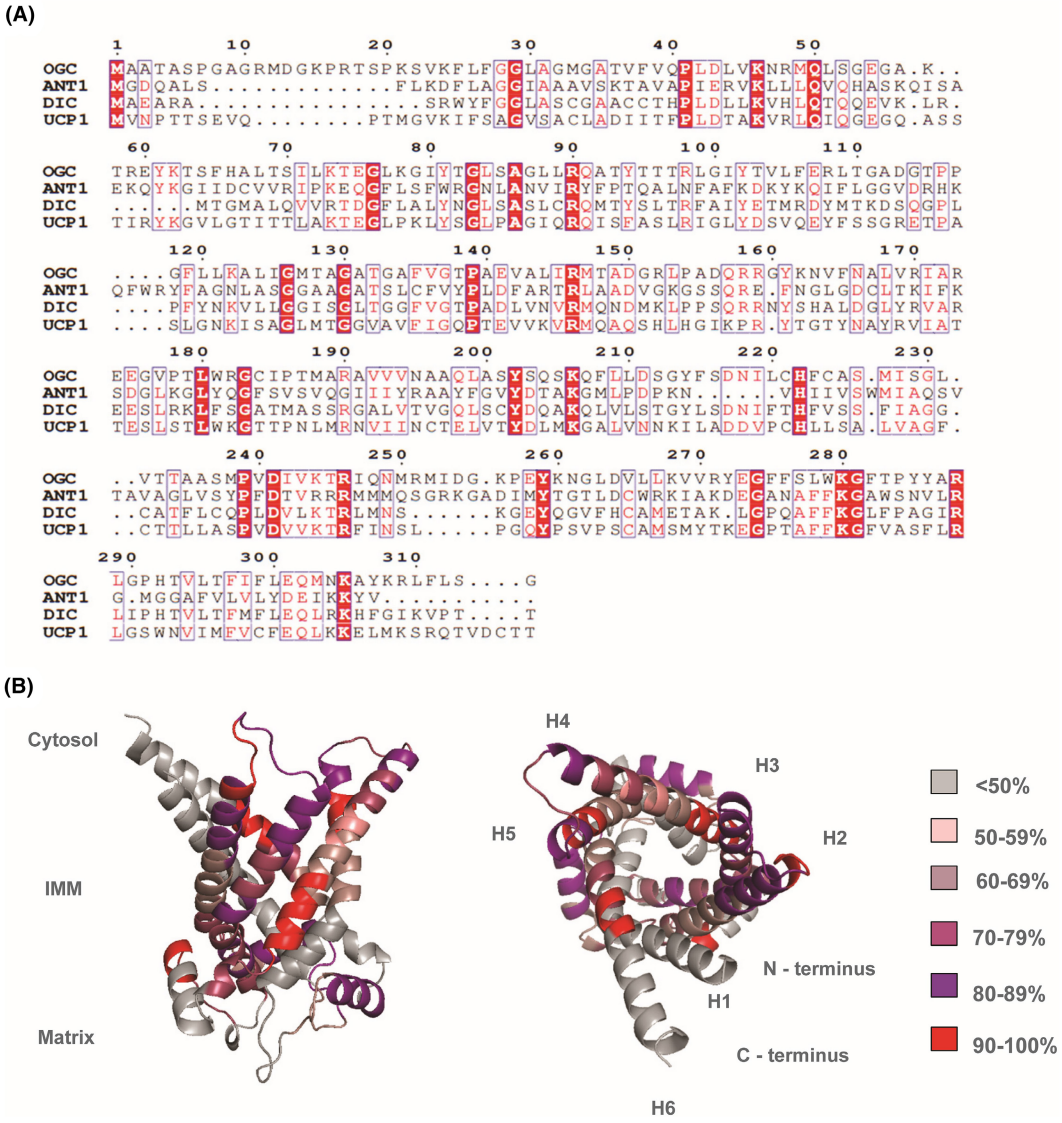

FIGURE 2 High sequence homology in substrate binding sites and signature motifs between OGC and other members of the SLC25 family. (A) Sequence alignment of murine OGC, adenine nucleotide translocase 1 (ANT1), dicarboxylate carrier (DIC), and uncoupling protein 1 (UCP1) generated with ClustalW and colored with ESPript. (B) Sequence homology scores between mOGC and mANT1. Homology scores are averaged for every 5 amino acids, based on their individual homology percentage scores calculated in the alignment. The image was generated in PyMOL using the AlphaFold structure of mOGC (AF-Q9CR62-F1) as a template. Alpha helices are numbered as H1–H6. First 20 amino acids of the N-terminus are not shown for simplicity.

reconstituted with mOGC alone ($G_m = 9.23 \pm 3\,nS/cm^2$). The G_m of bilayers containing AA ($G_m = 34.1 \pm 7.1$ nS/cm^2) or DNP ($G_m = 46.8 \pm 6.1\,nS/cm^2$) was significantly increased in the presence of mOGC ($G_m = 92.5 \pm 16.5\,nS/cm^2$ for AA, $G_m = 69.6 \pm 7.5\,nS/cm^2$ for DNP; Figure 4A and Figure S2).

To confirm that in the presence of AA, mOGC facilitates the transport of protons, and not other ions present in the buffer, we measured current–voltage characteristics in the presence and absence of a transmembrane pH gradient of 0.4 (ΔpH 0.4) (Figure 4B). Solutions on both the *cis* and *trans* sides of the planar lipid bilayer had the same concentrations of all ions except H^+ and OH^-, similar ionic strength, and similar osmolarity. The pH values on the *cis* and *trans* sides were 7.34 and 7.74, the latter being adjusted with 2.39 mM of Tris dissolved in water (pH 7.34) after bilayer membrane formation. In this case, the experimentally obtained shift of the reversal potential, ΔV_0, is equal to the theoretical H^+ Nernst potential (Ψ_N) at ΔpH 0.4. The shift of intersection points of I/V curves with the x-axis, for ΔpH 0 and ΔpH 0.4, resulted in $V_0 = 25.8 \pm 6.8$ mV (Figure 4B). We then calculated the transfer number of H^+ and OH^- ions across the membrane (Equation 1),

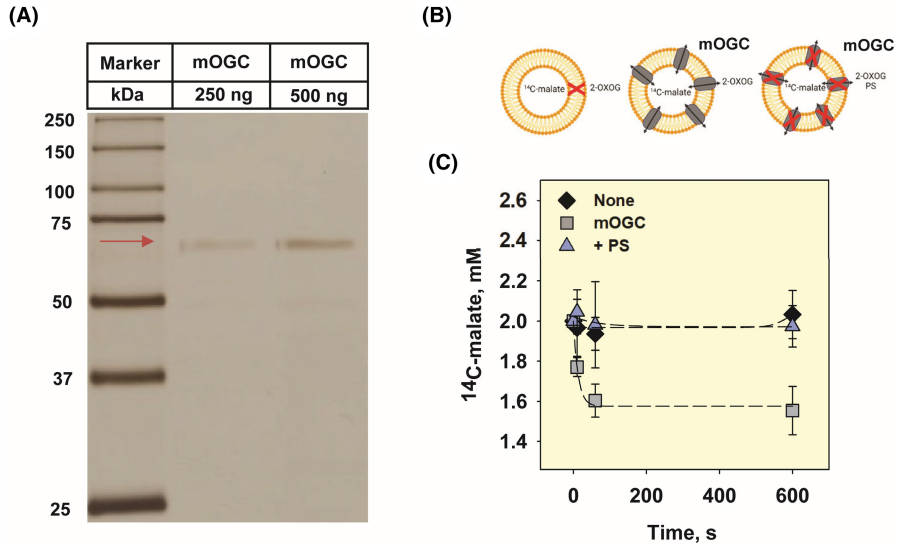

FIGURE 3 Reconstituted mOGC transports 14C-malate for 2-oxoglutarate. (A) Representative silver staining of mOGC reconstituted into proteoliposomes. 250 and 500 ng of proteoliposomes were loaded in separate lanes on a 15% acrylamide gel, separated by SDS-PAGE and visualized by silver staining. Reconstituted mOGC appears at the expected dimer size (~69 kDa, red arrow). Precision Plus Protein Dual Color Standard was loaded as a molecular weight marker. (B) The scheme shows the three experimental setups: empty liposomes (left), active transport with mOGC (middle), and inhibition of transport by phenylsuccinate (PS, right). (C) Decrease in 14C-malate concentration upon initiation of 2-oxoglutarate/malate exchange in proteoliposomes containing reconstituted mOGC (squares). Transport was not measured in empty liposomes (diamonds) and was completely inhibited by the addition of 20 mM of the substrate analog PS (triangles). For all measurements, membranes were prepared DOPC:DOPE:CL (45:45:10 mol%). Lipid and protein concentrations were 1.5 mg/mL and 4 μg/(mg lipid), respectively. The buffer solution consisted of 50 mM Na_2SO_4, 10 mM Tris, 10 mM MES, and 0.6 mM EGTA at pH 7.34 and $T = 32°C$. Hundred nanometer proteoliposomes were filled with 2 mM 14C-malate and transport was initiated by the addition of 2 mM 2-oxoglutarate from the outside. 14C-malate, oxoglutarate, and PS were dissolved in buffer (pH 7.34). Data are mean ± SD of at least three independent experiments.

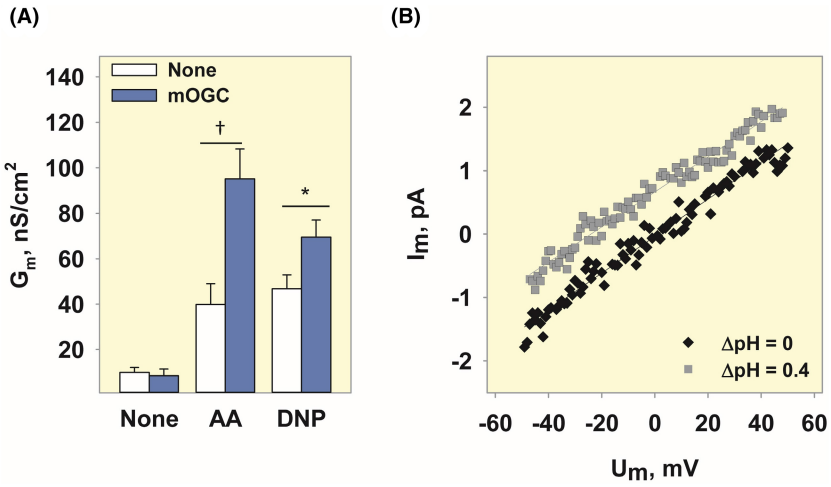

FIGURE 4 mOGC-mediated proton conductance in the presence of AA or DNP in planar lipid bilayers. (A) Increase in total membrane conductance (G_m) in the presence of 15 mol% arachidonic acid (AA) or 50 μM DNP without (white) and with (blue) mOGC. (B) Current–voltage (I/V) recordings of lipid bilayer membranes reconstituted with mOGC in the presence and absence of a transmembrane pH gradient of 0.4 pH units. For all measurements, membranes were made prepared from DOPC:DOPE:CL (45:45:10 mol%). Lipid and protein concentrations were 1.5 mg/mL and 4 μg/(mg lipid), respectively. The buffer solution consisted of 50 mM Na_2SO_4, 10 mM Tris, 10 mM MES, and 0.6 mM EGTA at pH 7.34 and $T = 32°C$. DNP and ATP were dissolved in DMSO and buffer (pH 7.34), respectively. Data are mean ± SD of at least three independent experiments.

$$T_{H^+/OH^-} = V_0 / \Psi_N \quad (1)$$

where Ψ_N is the theoretical value of H^+ Nernst potential at ΔpH 0.4 (23.9 mV). T_{H^+/OH^-} was 1.08 ± 0.3, which confirms that the observed increase in G_m is exclusively due to the transport of protons.

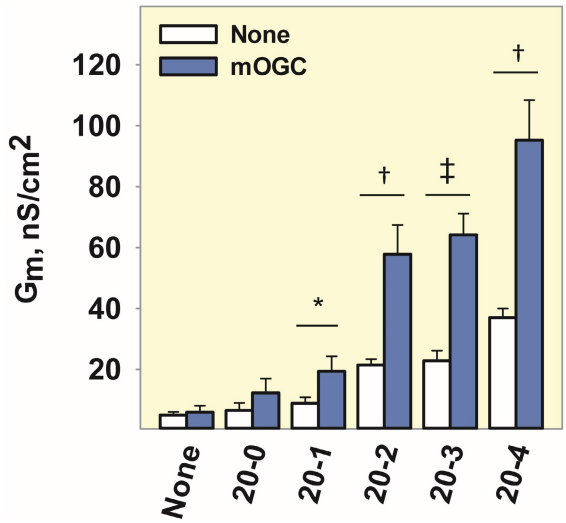

FIGURE 5 The increase in mOGC-mediated proton transport directly correlates with the increase in the number of unsaturated bonds of FAs. Increase in G_m in the presence of arachidic acid (20-0), cis-11-eicosaenoic acid (20-1), cis-11,14-eicosadienoic acid (20-2), cis-8,11,14-trienoic acid (20-3), and AA (20-4). The experimental conditions were similar to those described in Figure 4.

2.5 | mOGC mediates proton transport in the presence of free fatty acid with different structures

Under oxidative stress, the cell concentration of ROS increases and subsequently activates phospholipase A (PLA).[30] PLA_2 cleaves unsaturated FAs from the IMM, the most abundant of which is AA. Therefore, to understand how OGC-mediated proton transport correlates with the degree of FA saturation as a response to oxidative stress in cells, we measured the G_m of mOGC-reconstituted lipid bilayers in the presence of FAs with increasing number of double bonds—arachidic acid (20–0), cis-11-eicosaenoic acid (20–1), cis-11,14-eicosadienoic acid (20–2), cis-8,11,14-trienoic acid (20–3), and AA (20–4) (Figure 5). Our results show that the G_m is directly correlated with the increase in the number of unsaturated bonds of the FA, similar to what was observed for UCP1, UCP2, and ANT1.[31,32]

2.6 | The activation of mOGC by arachidonic acid can be inhibited by ATP, its substrates, and substrate analog

We further tested whether ATP could inhibit mOGC-enhanced proton transport in the presence of AA. Figure 6A and Figure S3A show that ATP can inhibit mOGC-mediated proton conductance by 75%, indicating a possible common binding site for ATP and AA.

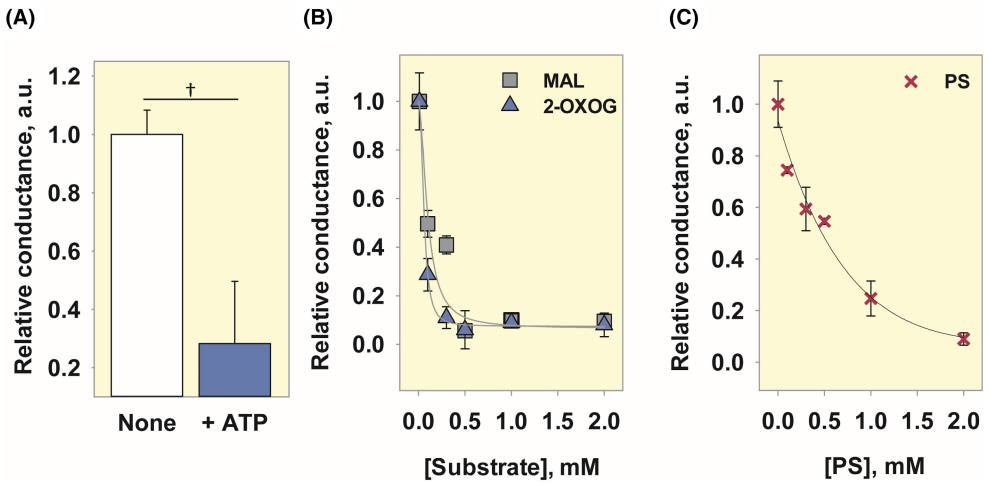

FIGURE 6 Inhibition of mOGC-mediated proton transport in the presence of AA by ATP, 2-oxoglutarate (2-OXOG), malate (MAL) and phenylsuccinate (PS). Relative conductance of mOGC activated by 15 mol% AA and inhibited by 4 mM ATP (A), 2-OXOG or MAL (B), or PS (C). The relative conductance is the ratio of the total membrane conductance in the presence and absence of the protein inhibitors to the membrane conductance measured in the presence of lipid and AA (see Section 4). The curves in (B) and (C) were fitted with a 4-parameter sigmoidal function (least squares method) and IC50 values of (0.06 ± 0.01) mM for 2-OXOG, (0.1 ± 0.06) mM for MAL and (1 ± 0.11) mM for PS were obtained. ATP, 2-OXOG, and MAL were dissolved in buffer (pH 7.34). PS was dissolved in DMSO. Other experimental conditions were similar to those described in Figure 4.

Next, we tested whether the main substrates transported by OGC, 2-oxoglutarate, and malate, show a similar effect. Figure 6B and Figure S3B show that the rate of AA-mediated proton transport inhibition in the presence of mOGC depends on the substrate concentration with IC50s of (0.06 ± 0.01) mM and (0.1 ± 0.06) mM for 2-oxoglutarate and malate, respectively. This is consistent with the substrate transport function of OGC, and its highest affinity for 2-oxoglutarate.[9] We then found that the IC50 of PS was (1 ± 0.11) mM (Figure 6C, Figure S3C), higher than both substrates tested.

None of the tested compounds altered the G_m values when only mOGC or AA were present in the system (Figure S3D), confirming that there is no unspecific proton leak. Taken together, these results may indicate a common binding site, or a shared part of the binding site in OGC for AA, ATP, 2-oxoglutarate, malate, and PS.

2.7 | R90 is involved in the binding of free fatty acids, ATP, and substrates

Residues R90, Y94, R98, R190, and R288 were identified as critical for substrate transport of OGC by substitution with cysteine and leucine.[33–35] Using site-directed mutagenesis, we produced mOGC-R90S (Figure 7A) and compared the specific membrane conductance of the bilayer membranes reconstituted with the wild-type and mutant proteins. Figure 7B shows that G_m is 50% lower in the presence of mOGC-R90S (63.28 ± 5.12 nS/cm^2 versus 92.47 ± 16.49 nS/cm^2 measured for mOGC, relative to the AA-induced G_m). Furthermore, mutation of R90 to serine completely abolished the ability of ATP to inhibit mOGC. We also tested how efficiently the AA-induced G_m of mOGC-R90S can be inhibited by malate and 2-oxoglutarate. Figure 7C and Figure S4 show that 1 mM of 2-oxoglutarate or malate inhibited the activated mOGC by 0% and 20%, respectively, whereas 2 mM of 2-oxoglutarate or malate inhibited the protein by 19% and 74%, respectively. These results suggest that R90 may be more important in the binding of 2-oxoglutarate than malate in the protein's cavity, or that malate competes more efficiently with AA for the rest of the binding site.

3 | DISCUSSION

Our results show that OGC can participate in uncoupling under similar conditions as ANT1 and UCP1-3 and that proton transport is enhanced only in the presence of the artificial uncoupler DNP or long-chain FAs.[17] Proton transport facilitated by OGC increased with the degree of unsaturation of the FA, as has been shown for other carriers.[31,32] Furthermore, ATP can competitively inhibit the activity of ANT1, UCP1-UCP3, and OGC in the presence of AA, suggesting a common binding site for nucleotides. We identified R90 as one of the residues involved in the binding of AA and ATP to OGC (Figure 7). This amino acid is a part of the conserved common substrate binding

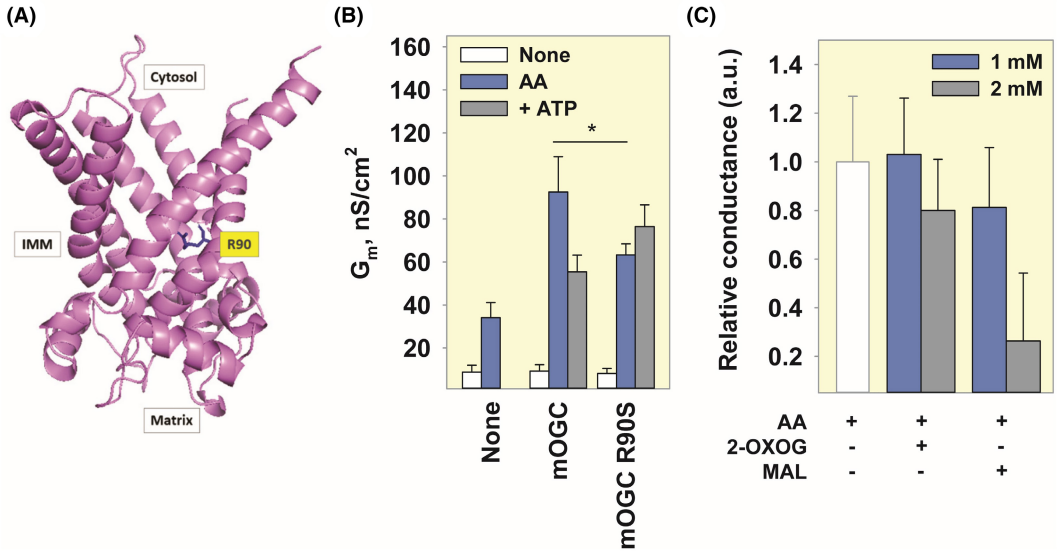

FIGURE 7 Substrate-binding residue R90 is involved in uncoupling. (A) Side view of mOGC with R90 shown in blue licorice and labeled in yellow. The image was generated in PyMOL using the AlphaFold structure of mOGC (AF-Q9CR62-F1) as a template. The N-terminal sequence has been truncated for simplicity. (B) Comparison of total membrane conductance (G_m) between mOGC and mOGC R90S in the presence of 15 mol% AA (blue) or 4 mM ATP (gray). C. Relative G_m measured in the presence of different concentrations of 2-OXOG or MAL. Other experimental conditions were similar to those described in Figure 4.

site of the SLC25 family and is a homolog of R79 in ANT1 and R84 in UCP1, which are critical for the binding of nucleotides, FAs, and DNP.[32,36–40] It also has a homolog in UCP2 (R88) and dicarboxylate carrier (R69). Since these proteins are involved in both substrate transport and FA-mediated proton transport, we propose that OGC is a protein with dual function whose substrate binding site is part of the interaction site with negatively charged uncouplers such as FAs or DNPs (Figure 8).

A possible explanation for thermogenesis-independent uncoupling would be mild uncoupling or lowering of MMP to prevent the generation of damaging ROS.[41,42] Under normal physiological conditions, OGC regulates the supply of the relevant metabolites—malate and 2-oxoglutarate—for OXPHOS (Figure 8A). During oxidative stress, the activity of phospholipid hydrolysis catalyzed by PLA increases significantly.[43] As a result, the blood concentration of FAs increases in pathological conditions such as obesity and type II diabetes.[44] In addition to the increase in free FAs, oxidative stress leads to the formation of lipid hydroperoxides and reactive aldehydes, which can modify and activate UCPs.[45,46] Under these conditions, OGC is likely to be involved in FA-mediated proton transport (Figure 8B).

We found that 2-oxoglutarate is a competitive inhibitor of OGC-mediated proton leak, with an EC50 value of 60 μM (Figure 6B). Considering that human plasma, liver, and brain contain 8–12 μM,[47] 150–300 μM,[48] and 600–800 μM[49] of 2-oxoglutarate, respectively, it seems that the cavity of OGC is permanently occupied and not available to bind FAs. Yet, it has been observed that 2-oxoglutarate levels are significantly reduced when mitochondrial function is impaired or damaged by oxidative stress, such as in diabetes[50] and breast cancer.[51] Under conditions that promote elevated levels of FAs and reactive aldehydes, it is plausible that OGC participates in proton transport to prevent further damage. It remains to be unraveled whether OGC alone contributes to significant proton leak in vivo. Unlike UCP1 in BAT under cold acclimation conditions, individual proteins such as OGC, ANT1, UCP2, or UCP3 may not induce a substantial amount of proton transport. However, their collective uncoupling function could lead to a beneficial and transient decrease in MMP, mitigating further

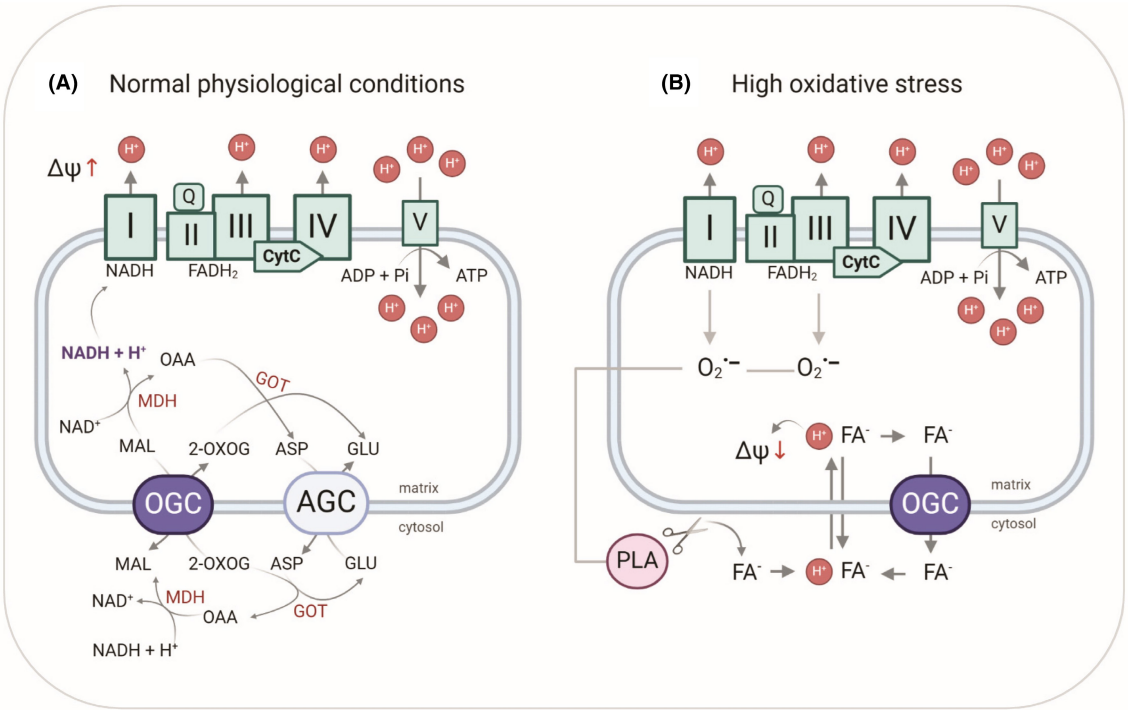

FIGURE 8 OGC catalyzes substrate transport and participates in FA-mediated uncoupling. (A) Under physiological conditions, OGC transports 2-oxoglutarate for malate to support the regeneration of NADH for oxidative phosphorylation (OXPHOS). The enzymes are the electron chain complex (I–IV), ATP synthase (V), aspartate/glutamate carrier (AGC), malate dehydrogenase (MDH), and glutamate oxaloacetate transaminase (GOT), and the substrates are malate (MAL), 2-oxoglutarate (2-OXOG), aspartate (ASP), glutamate (GLU), and oxaloacetate (OAA). (B) Under high oxidative stress, OGC is involved in FA-mediated uncoupling. Leakage of electrons from electron transport complexes I and III generates reactive oxygen species (ROS), which in turn activate phospholipase A (PLA), which cleaves FAs from the IMM. After neutralization and transfer to the matrix, FAs release protons and decrease MMP. FA anions are transported back into the cytosol by OGC and similar proteins. Image is created in BioRender.

oxidative damage without the need for upregulation of protein expression.

The use of mitochondrial carriers through targeted activation of their uncoupling function could be a promising approach for future cancer therapy. Cancer cells have an abnormally high MMP (~220 mV compared to 140 mV in normal cells),[2] which is associated with increased metastasis and more invasive tumor properties.[52,53] Therefore, they take up lipophilic chemical protonophores with a higher affinity than normal cells, which results in uncoupling of the IMM through activation of several proteins of the SLC25 family and a substantial decrease in MMP, which induces apoptosis. OGC is a good candidate for targeted uncoupling because it is ubiquitously expressed in healthy tissues and therefore most likely in all cancer types (Figure 1).

In conclusion, by reconstituting OGC as the only protein in the lipid bilayer membrane, we have demonstrated its role in facilitating proton transport in the presence of FAs and DNP. ATP, OGC substrates, and PS inhibited this effect, indicating competition for the same binding site. We identified residue R90 which is involved in both uncoupling and substrate transport in OGC and may play a critical role in the conserved mechanism of uncoupling in the entire SLC25 family.

4 | MATERIALS AND METHODS

4.1 | Chemicals

1,2-Dioleoyl-*sn*-glycero-3-phosphotidylcholine (DOPC, #SLCF9767), 1,2-dioleoyl-*sn*-glycero-3-phosphoethanola mine (DOPE, #SLCB7462), cardiolipin (CL, #SLCC2621), adenosine 5′-triphosphate (ATP, #SLBZ3783), α-ketoglutaric acid (2-oxoglutaric acid, #BCCC4294), phenylsuccinic acid (#MKBS0493V), L-malic acid (#SLCD6882), N-laurylsarcosine (#L5125), Triton X-114 (#MKCL3391), Triton X-100 (#STBJ5677), dithiothreitol (DTT, #BCCG5712), 2,4-dinitrophenol (D198501), dimethylsulfoxide (DMSO, #276855), bovine serum albumin (BSA, #SLCM9403), arachidic acid (Ara, #0000145297), cis-11-eicosaenoic acid (20-1, #MKCP4439), cis-11,14-eicosadienoic acid (20-2, #SLCL2548), cis-8,11,14-trienoic acid (#SLCG0821), protease inhibitor cocktail (#P8340), bromophenol blue (#BCBF8233V), hexane (#296090), hexadecane (#296317), and isopropanol (#I9516) were purchased from Sigma-Aldrich (Vienna, Austria). Sodium sulfate (Na_2SO_4, #8560.3), sodium chloride (NaCl, #9265.1), potassium chloride (KCl, #6781.3), 2-(N-morpholino) ethanesulfonic acid (MES, #4256.2), tris(hydroxymethyl)-aminomethane (Tris, #4855.2), ethylenediaminetetraacetic acid (EDTA, #8043.2), ethylene glycol-bis(β-aminoethyl ether)-N,N,N′,N′-tetraacetic acid (EGTA, #8043.1), isopropyl β-D-1-thiogalactopyranoside (IPTG, #2316.3), chloramphenicol (#3886.2), kanamycin (#T832.1), β-mercaptoethanol (#4227.3), glycerine (#3783.1), ethanol (#T913.1), desoxycholic acid sodium salt (#3484.2), sodium dodecyl sulfate (SDS, #0183.3), agarose (#3810.2), and Ponceau S staining solution (#5938.2) were purchased from Carl Roth GmbH & Co. K.G. (Karlsruhe, Germany). Chloroform (#AE 54.1) was obtained from either Carl Roth GmbH & Co. K.G. (Karlsruhe, Germany) or PanReac AppliChem (UN1888, Darmstadt, Germany). We purchased arachidonic acid (AA, #10-2004-7) from Larodan (Solna, Sweden), n-octylpolyoxyethylene (#1000013726) from BACHEM (Bubendorf, Switzerland), and hydroxyapatite (#130-0420), Bio-Beads SM-2 (#152-3920) and the enhanced chemiluminescence (ECL) western blotting reagent (#170-50001) from Bio-Rad Laboratories (Hercules, CA, USA). Dulbecco's phosphate-buffered saline (DPBS, #14190144) was obtained from Thermo Fisher Scientific, Waltham, MA, USA, PhosSTOP™ (#59124600) from Roche Diagnostics (Mannheim, Germany), and nuclease-free water (#7732-18-5) from VWR (Vienna, Austria). ^{14}C-malic acid was purchased either from Perkin Elmer (Waltham, MA, USA) (#2625350) or from Hartmann Analytic (Braunschweig, Germany) (ARC 0771). The Ultima-Gold™ scintillation liquid (#7722011) was purchased from Perkin Elmer (Waltham, MA, USA) and Sephadex™ G-50 (#10297028) from Cytiva Sweden AB (Uppsala, Sweden).

4.2 | Animals and protein sample preparation

Two-month-old female C57BL/6 wild-type mice used in this study were kept under standardized laboratory conditions (12:12 h light/dark cycle, room temperature (24°C), food and water ad libitum) and sacrificed by CO_2 asphyxiation. Mouse organ and tissue samples were pooled from at least five mice to obtain enough protein. They were homogenized with a mixer mill (MM200, Retsch, Germany) in RIPA buffer (50 mM Tris, 150 mM NaCl, 1% desoxycholic acid sodium salt, 1 mM EDTA, 1% Triton X-100, 0.1% SDS) supplemented with a protease inhibitor cocktail. After 30 min of incubation on ice, the lysates were centrifuged 2 × 10 min at 2500 ×*g*. The supernatants were collected, aliquoted, and stored frozen at −20°C.

Total protein isolation from cancer cells was performed as described in Ref.[54] In brief, the cells were washed twice in ice-cold DPBS and centrifuged at 300 ×*g* for 5 min. Pellets were snap frozen and sonicated in RIPA buffer supplemented with a protease inhibitor cocktail and

PhosSTOP™. Lysates were centrifuged 2×10 min at 2500 ×*g*, and the collected supernatants were aliquoted and stored at −20°C. Total protein concentrations of tissue and cancer cell samples were determined using the Pierce BCA Protein Assay Kit (#RG235622, Thermo Fisher Scientific, Waltham, MA, USA). Further steps were performed as described for protein isolation from mouse organ tissues.

4.3 | Western blot analysis

Western blotting was adapted to the previously published protocol.[55] In brief, total protein was separated on 15% SDS-PAGE gels and transferred to nitrocellulose membranes. Reversible Ponceau S staining was used as a loading control (Figure S1A). After blocking the membranes in 2% BSA blocking solution at RT, they were incubated with primary antibodies against OGC (anti-SLC25A11, sc-515 593, #G2016, Santa Cruz Biotechnology, Dallas, TX, USA) or succinate dehydrogenase (SDHA, ab14715, #G3365497-8, Abcam, Cambridge, UK) overnight at 4°C. Detection was performed with the UVP ChemStudio Imaging System (Analytik Jena, Jena, Germany) using horseradish peroxidase-linked anti-mouse (#38) and anti-rabbit (#29) secondary antibodies (Cell Signaling Technology, Danvers, MA, USA), and the ECL western blotting reagent. All primary and secondary antibodies were diluted with 2% BSA block solution. The semi-quantitative analysis of western blots was done using Vision Works software version 9.1 (Analytik Jena, Jena, Germany). SDHA was used as a mitochondrial marker. The values were averaged from at least three different membranes and two biological replicates. For each biological replicate, tissues from five mice were pooled together to isolate sufficient protein levels.

4.4 | mRNA expression analysis

RNA isolation and quantitative reverse transcription (qRT–PCR) were performed as previously described.[55] RNA was isolated using the innuSOLV RNA Reagent (Analytik Jena, Jena, Germany) according to the guanidine isothiocyanate/phenol method. Briefly, homogenized tissue samples were incubated with 1 mL of the innuSOLV RNA reagent per 100 mg. Phase separation was done by the addition of chloroform, and RNA was precipitated with isopropanol and washed with ethanol. Air-dried RNA was dissolved in nuclease-free water and quantified using the NanoDrop® UV–Vis Spectrophotometer (Thermo Fisher Scientific, Waltham, MA, USA).

Two μg of RNA were subjected to DNase digestion and reverse transcribed to cDNA using random hexamer primers and the High-Capacity cDNA Reverse Transcription Kit (both Thermo Fisher Scientific, Waltham, MA, USA). RT-qPCR was conducted on qTOWER[3] 84 (Analytik Jena, Jena, Germany) at a 62°C annealing temperature using the Luna® Universal qPCR Master Mix (New England BioLabs GmbH, Frankfurt am Main, Germany) and primers for *Mus musculus* solute carrier family 25 member 11 (SLC25A11) sourced from the NCBI primer-blast [NM_024211.3]. Primers targeting both murine splice variants were used: (5′–>3′ forward: GTTGTTTGAGCGCCTGACTG, reverse: CAGCTGGAAGCCGACCAT). Relative expression levels of *mOgc* were calculated by the Δ cycle threshold (Ct) to the housekeeping gene *mRpl4* ($2^{-[Ct(mOgc)-Ct(mRpl4)]}$).

4.5 | Recombinant protein production and purification

Cloning, purification, and reconstitution of murine OGC were adapted to the previously established protocols.[9,56] In brief, pET24a expression plasmids containing selected OGC cDNA sequences were transformed into the *E. coli* Rosetta (DE3) pLysS strain (Novagen®, Darmstadt, Germany) and selected on kanamycin (25 μg/mL) and chloramphenicol (34 μg/mL) containing plates. Successful transformants were inoculated into the growth medium containing chloramphenicol (34 μg/mL) and grown until the optical density at 600 nm reached 0.5. Protein production was then induced with 0.5 mM IPTG, and the cells were collected by centrifugation after 3 h. IBs containing the expressed protein were isolated via high-pressure homogenization and centrifugation. The expression of mOGC in IBs was confirmed using the Western blot analysis (Figure S1C).

4.6 | Reconstitution of OGC into liposomes

To purify and reconstitute the protein, 2 mg of IBs were solubilized in a TE/G buffer containing 2% N-lauroylsarcosine, 1.3% Triton X-114, 0.3% N-octylpolyoxyethylene, 1 mM DTT, and 2 mM phenylsuccinate (PS) at pH 7.5. The lipid mixture (DOPC:DOPE:CL; 45:45:10 mol%) was hydrated overnight and added in gradually. The mixture was concentrated and dialyzed against a buffer used in the experiments (50 mM Na_2SO_4, 10 mM MES, 10 mM Tris, and 0.6 mM EGTA at pH 7.34). The dialysate was centrifuged and applied to a hydroxyapatite column to remove unfolded and aggregated protein fractions. Subsequently, non-ionic detergents were removed by Bio-Beads SM-2. The final protein concentration was measured with the Micro BCA Protein Assay Kit (#OI191202, Thermo Fisher Scientific, Waltham, MA, USA). Protein purity was

verified by SDS-PAGE and silver staining (Figure 3A). Proteoliposomes were produced in independent batches. The following batch numbers were used for this study: OGC #5, #9, #11, #12, #15, #23, #24, and #25.

4.7 | Generation of the OGC R90S mutant

In vitro site-directed mutagenesis was carried out on expression plasmids containing the cDNA of mOGC as a template. The mutation was introduced with an oligonucleotide designed to alter codon Arg90 (CGC) to Ser (AGC) using a Q5™ site-directed mutagenesis kit (#EO552, #EO554S, New England BioLabs GmbH, Frankfurt am Main, Germany). The successful introduction of mutations was confirmed by sequencing. Mutant OGC expression plasmids were transformed in the *E. coli* expression strain Rosetta(DE3)pLysS. The rest of the protocol was as described above for the OGC wild-type, and the batch numbers used for this study were #2, #4, and #5.

4.8 | Substrate exchange rate measurements of OGC

OGC-containing proteoliposomes (as described above) were filled with 2 mM malate (L-malic acid dissolved in the experimental buffer at pH 7.34) and 2 mM ^{14}C labeled malate prior to extrusion. 1 mM of DTT was added to proteoliposomes after extrusion to prevent any free sulfhydryl group-mediated aggregation. OGC facilitated transport was initiated by adding 2 mM 2-oxoglutarate (2-oxoglutaric acid dissolved in the experimental buffer at pH 7.34) and stopped immediately by size exclusion chromatography using SephadexTM G-50 dextran gels at corresponding times (Figure 3B). The remaining radioactivity in proteoliposomes was measured by liquid scintillation counting (Tri-Carb 2100TR, Perkin Elmer, Waltham, MA, USA). In the case of inhibition, 20 mM phenylsuccinate (PS, phenylsuccinic acid dissolved in the experimental buffer at pH 7.34) was added to proteoliposomes prior to extrusion to account for the random orientation of OGC in the membrane. For control measurements, the same protocol was used on empty liposomes.

4.9 | Formation of planar bilayer membrane and measurements of the electrical parameters

Planar lipid bilayers were formed from liposomes on the tip of the dispensable plastic pipettes as previously described.[28] Membrane formation and bilayer quality were verified by capacitance measurements ($C = 0.715 \pm 0.03\,\mu F/cm^2$). Capacitance did not depend on the presence of the protein, AA, or other substrates, which were added to the lipid phase before membrane formation. Current–voltage (I–U) characteristics were measured by a patch-clamp amplifier (EPC 10, HEKA Elektronik Dr. Schulze GmbH, Germany). Total membrane conductance (G_m) was derived from the slope of a linear fit of the experimental data at applied voltages in the range of −50 mV to +50 mV. Lipid concentration was 1.5 mg/mL (1.875 mM) in all experiments. AA was dissolved in chloroform and added to the lipid phase before vacuuming. ATP, 2-oxoglutaric acid, L-malic acid, and phenylsuccinic acid were dissolved in the buffer solution (pH adjusted to 7.34) and DNP in DMSO. The amount of DMSO added to the measuring sample never exceeded 10 µL, which was previously shown not to alter the membrane conductance.[17] The concentrations of each substrate used in the experiments are indicated in the figure legends. The relative membrane conductance was calculated according to Equation 2:

$$G_{rel} = \frac{G - G_0}{G_1 - G_0} \quad (2)$$

where G_0 is the total membrane conductance of lipid membranes reconstituted with AA, G_1 is the total membrane conductance of lipid membranes reconstituted with OGC and AA, and G is the total specific membrane conductance of lipid membranes reconstituted with OGC, AA, and/or ATP/PS/2-oxoglutarate/L-malate (Figure 6).

4.10 | Statistical analysis

Statistical analyses were performed using Sigma Plot 12.5 (Systat Software GmbH, Erkrath, Germany). Data from the electrophysiological and substrate exchange measurements are represented as mean ± standard deviation of at least three technical replicates performed on three different days. In electrophysiological measurements, each technical replicate was the mean conductance of three to ten lipid bilayer membranes formed on the same day. In substrate exchange measurements, each technical replicate stands for a new preparation of the measuring sample. Electrophysiological data were tested using the unpaired two-tailed Student's t-test. Statistical significance was defined at $p < 0.05$ (*), $p < 0.01$ (†), $p < 0.001$.

AUTHOR CONTRIBUTIONS

Kristina Žuna: Investigation; writing – original draft; visualization; writing – review and editing; formal analysis. **Tatyana Tyschuk:** Investigation; writing – review

and editing; formal analysis. **Taraneh Beikbaghban:** Investigation; writing – review and editing; formal analysis. **Felix Sternberg:** Investigation; formal analysis; writing – review and editing. **Jürgen Kreiter:** Writing – review and editing; formal analysis; supervision. **Elena E. Pohl:** Conceptualization; funding acquisition; writing – original draft; writing – review and editing; data curation; project administration; supervision; resources.

ACKNOWLEDGMENTS

We thank Sarah Bardakji and Deniz Hofbauer for the excellent technical assistance, and Prof. Soo-Youl Kim (National Cancer Center, Seoul, Republic of Korea) for providing us with murine knockout samples.

FUNDING INFORMATION

This research was supported by the Austrian Science Fund (P31559-B20 and Sonderforschungsbereich F83 to E.E.P.).

CONFLICT OF INTEREST STATEMENT

The authors declare no conflict of interest.

DATA AVAILABILITY STATEMENT

The datasets generated and/or analyzed during this study are available from the corresponding authors upon reasonable request.

ORCID

Kristina Žuna https://orcid.org/0000-0003-3585-2679
Felix Sternberg https://orcid.org/0000-0003-3487-362X
Jürgen Kreiter https://orcid.org/0000-0001-5877-762X
Elena E. Pohl https://orcid.org/0000-0002-0604-5950

REFERENCES

1. Warburg O. On the origin of cancer cells. *Science*. 1956;123(3191):309-314.
2. Weinberg SE, Sena LA, Chandel NS. Mitochondria in the regulation of innate and adaptive immunity. *Immunity*. 2015;42(3):406-417.
3. Lee JS, Lee H, Lee S, et al. Loss of SLC25A11 causes suppression of NSCLC and melanoma tumor formation. *EBioMedicine*. 2019;40:184-197.
4. Lee JS, Choi J, Lee SH, et al. Oxoglutarate carrier inhibition reduced melanoma growth and invasion by reducing ATP production. *Pharmaceutics*. 2020;12(11):1128.
5. Rai Y, Anita KN, Singh S, Kalra N, Soni R, Bhatt AN. Mild mitochondrial uncoupling protects from ionizing radiation induced cell death by attenuating oxidative stress and mitochondrial damage. *Biochim Biophys Acta Bioenerg*. 2021;1862(1):148325.
6. Kumar R, Coronel L, Somalanka B, et al. Mitochondrial uncoupling reveals a novel therapeutic opportunity for p53-defective cancers. *Nat Commun*. 2018;9(1):3931.
7. Alasadi A, Chen M, Swapna GVT, et al. Effect of mitochondrial uncouplers niclosamide ethanolamine (NEN) and oxyclozanide on hepatic metastasis of colon cancer. *Cell Death Dis*. 2018;9(2):215.
8. Zunica ERM, Axelrod CL, Cho E, et al. Breast cancer growth and proliferation is suppressed by the mitochondrial targeted furazano[3,4-b]pyrazine BAM15. *Cancer Metab*. 2021;9(1):36.
9. Fiermonte G, Walker JE, Palmieri F. Abundant bacterial expression and reconstitution of an intrinsic membrane-transport protein from bovine mitochondria. *Biochem J*. 1993;294(Pt 1):293-299.
10. Sanchis D, Fleury C, Chomiki N, et al. BMCP1, a novel mitochondrial carrier with high expression in the central nervous system of humans and rodents, and respiration uncoupling activity in recombinant yeast. *J Biol Chem*. 1998;273(51):34611-34615.
11. Zhang CY, Hagen T, Mootha VK, Slieker LJ, Lowell BB. Assessment of uncoupling activity of uncoupling protein 3 using a yeast heterologous expression system. *FEBS Lett*. 1999;449(2–3):129-134.
12. Yu XX, Lewin DA, Zhong A, et al. Overexpression of the human 2-oxoglutarate carrier lowers mitochondrial membrane potential in HEK-293 cells: contrast with the unique cold-induced mitochondrial carrier CGI-69. *Biochem J*. 2001;353(Pt. 2):369-375.
13. Wilkins HM, Brock S, Gray JJ, Linseman DA. Stable overexpression of the 2-oxoglutarate carrier enhances neuronal cell resistance to oxidative stress via Bcl-2-dependent mitochondrial GSH transport. *J Neurochem*. 2014;130(1):75-86.
14. Booty LM, King MS, Thangaratnarajah C, et al. The mitochondrial dicarboxylate and 2-oxoglutarate carriers do not transport glutathione. *FEBS Lett*. 2015;589(5):621-628.
15. Korshunov SS, Skulachev VP, Starkov AA. High protonic potential actuates a mechanism of production of reactive oxygen species in mitochondria. *FEBS Lett*. 1997;416(1):15-18.
16. Brookes PS. Mitochondrial H(+) leak and ROS generation: an odd couple. *Free Radic Biol Med*. 2005;38(1):12-23.
17. Zuna K, Jovanovic O, Khailova LS, et al. Mitochondrial uncoupling proteins (UCP1-UCP3) and adenine nucleotide translocase (ANT1) enhance the protonophoric action of 2,4-dinitrophenol in mitochondria and planar bilayer membranes. *Biomol*. 2021;11(8):1178. doi:10.3390/biom11081178
18. Bertholet AM, Natale AM, Bisignano P, et al. Mitochondrial uncouplers induce proton leak by activating AAC and UCP1. *Nature*. 2022;606(7912):180-187.
19. Uhlen M, Fagerberg L, Hallstrom BM, et al. Proteomics. Tissue-based map of the human proteome. *Science*. 2015;347(6220):1260419.
20. Dolce V, Messina A, Cambria A, Palmieri F. Cloning and sequencing of the rat cDNA encoding the mitochondrial 2-oxoglutarate carrier protein. *DNA Seq*. 1994;5(2):103-109.
21. Wang D. Discrepancy between mRNA and protein abundance: insight from information retrieval process in computers. *Comput Biol Chem*. 2008;32(6):462-468.
22. Smith VR, Walker JE. Purification and folding of recombinant bovine oxoglutarate/malate carrier by immobilized metal-ion affinity chromatography. *Protein Expr Purif*. 2003;29(2):209-216.
23. Bisaccia F, Zara V, Capobianco L, Iacobazzi V, Mazzeo M, Palmieri F. The formation of a disulfide cross-link between the two subunits demonstrates the dimeric structure of the mitochondrial oxoglutarate carrier. *Biochim Biophys Acta*. 1996;1292(2):281-288.
24. Kunji ER, Crichton PG. Mitochondrial carriers function as monomers. *Biochim Biophys Acta*. 2010;1797(6–7):817-831.
25. Sagne C, Isambert MF, Henry JP, Gasnier B. SDS-resistant aggregation of membrane proteins: application to the purification of

the vesicular monoamine transporter. *Biochem J*. 1996;316(Pt. 3):825-831.
26. Bonaventura C, Bonaventura J, Stevens R, Millington D. Acrylamide in polyacrylamide gels can modify proteins during electrophoresis. *Anal Biochem*. 1994;222(1):44-48.
27. Palmieri F, Quagliariello E, Klingenberger M. Kinetics and specificity of the oxoglutarate carrier in rat-liver mitochondria. *Eur J Biochem*. 1972;29(3):408-416.
28. Beck V, Jaburek M, Breen EP, Porter RK, Jezek P, Pohl EE. A new automated technique for the reconstitution of hydrophobic proteins into planar bilayer membranes. Studies of human recombinant uncoupling protein 1. *Biochim Biophys Acta*. 2006;1757(5–6):474-479.
29. Cutting W, Mehrtens H, Tainter M. Actions and uses of dinitrophenol: promising metabolic applications. *JAMA*. 1933;101(3):193-195.
30. Jaburek M, Pruchova P, Holendova B, Galkin A, Jezek P. Antioxidant synergy of mitochondrial phospholipase PNPLA8/iPLA2gamma with fatty acid-conducting SLC25 gene family transporters. *Antioxidants (Basel)*. 2021;10(5):678.
31. Beck V, Jaburek M, Demina T, et al. Polyunsaturated fatty acids activate human uncoupling proteins 1 and 2 in planar lipid bilayers. *FASEB J*. 2007;21(4):1137-1144.
32. Kreiter J, Rupprecht A, Skulj S, et al. ANT1 activation and inhibition patterns support the fatty acid cycling mechanism for proton transport. *Int J Mol Sci*. 2021;22(5):2490.
33. Stipani V, Cappello AR, Daddabbo L, et al. The mitochondrial oxoglutarate carrier: cysteine-scanning mutagenesis of transmembrane domain IV and sensitivity of Cys mutants to sulfhydryl reagents. *Biochemistry*. 2001;40(51):15805-15810.
34. Cappello AR, Curcio R, Valeria Miniero D, et al. Functional and structural role of amino acid residues in the even-numbered transmembrane alpha-helices of the bovine mitochondrial oxoglutarate carrier. *J Mol Biol*. 2006;363(1):51-62.
35. Palmieri F, Bisaccia F, Capobianco L, et al. Mitochondrial metabolite transporters. *Biochim Biophys Acta*. 1996;1275(1–2):127-132.
36. Kunji ER, Robinson AJ. The conserved substrate binding site of mitochondrial carriers. *Biochim Biophys Acta*. 2006;1757(9–10):1237-1248.
37. Dehez F, Pebay-Peyroula E, Chipot C. Binding of ADP in the mitochondrial ADP/ATP carrier is driven by an electrostatic funnel. *J Am Chem Soc*. 2008;130(38):12725-12733.
38. Jones SA, Gogoi P, Ruprecht JJ, et al. Structural basis of purine nucleotide inhibition of human uncoupling protein 1. *Sci Adv*. 2023;9(22):eadh4251.
39. Kreiter J, Skulj S, Brkljaca Z, Bardakji S, Vazdar M, Pohl EE. FA sliding as the mechanism for the ANT1-mediated fatty acid anion transport in lipid bilayers. *Int J Mol Sci*. 2023;24(18):13701.
40. Kang Y, Chen L. Structural basis for the binding of DNP and purine nucleotides onto UCP1. *Nature*. 2023;620(7972):226-231.
41. Skulachev VP. Uncoupling: new approaches to an old problem of bioenergetics. *Biochim Biophys Acta*. 1998;1363(2):100-124.
42. Brand M. Uncoupling to survive? The role of mitochondrial inefficiency in ageing. *Exp Gerontol*. 2000;35(6):811-820.
43. Asai K, Hirabayashi T, Houjou T, Uozumi N, Taguchi R, Shimizu T. Human group IVC phospholipase A2 (cPLA2gamma). Roles in the membrane remodeling and activation induced by oxidative stress. *J Biol Chem*. 2003;278(10):8809-8814.
44. Boden G, Jadali F, White J, et al. Effects of fat on insulin-stimulated carbohydrate metabolism in normal men. *J Clin Invest*. 1991;88(3):960-966.
45. Jovanovic O, Pashkovskaya AA, Annibal A, et al. The molecular mechanism behind reactive aldehyde action on transmembrane translocations of proton and potassium ions. *Free Radic Biol Med*. 2015;89:1067-1076.
46. Pohl EE, Jovanovic O. The role of phosphatidylethanolamine adducts in modification of the activity of membrane proteins under oxidative stress. *Molecules*. 2019;24(24):4545.
47. Ingraham L, Li M, Renfro JL, et al. A plasma concentration of alpha-ketoglutarate influences the kinetic interaction of ligands with organic anion transporter 1. *Mol Pharmacol*. 2014;86(1):86-95.
48. Holloway GP, Holwerda AM, Miotto PM, Dirks ML, Verdijk LB, van Loon LJC. Age-associated impairments in mitochondrial ADP sensitivity contribute to redox stress in senescent human skeletal muscle. *Cell Rep*. 2018;22(11):2837-2848.
49. Tashlitsky VN, Artiukhov AV, Fedorova NV, et al. Analysis of content of 2-oxoacids in rat brain extracts using high-performance liquid chromatography. *Biochemistry (Mosc)*. 2022;87(4):356-365.
50. Wu H, Esteve E, Tremaroli V, et al. Metformin alters the gut microbiome of individuals with treatment-naive type 2 diabetes, contributing to the therapeutic effects of the drug. *Nat Med*. 2017;23(7):850-858.
51. Mullen AR, Wheaton WW, Jin ES, et al. Reductive carboxylation supports growth in tumour cells with defective mitochondria. *Nature*. 2011;481(7381):385-388.
52. Heerdt BG, Houston MA, Augenlicht LH. The intrinsic mitochondrial membrane potential of colonic carcinoma cells is linked to the probability of tumor progression. *Cancer Res*. 2005;65(21):9861-9867.
53. Houston MA, Augenlicht LH, Heerdt BG. Stable differences in intrinsic mitochondrial membrane potential of tumor cell subpopulations reflect phenotypic heterogeneity. *Int J Cell Biol*. 2011;2011:978583.
54. Rupprecht A, Moldzio R, Modl B, Pohl EE. Glutamine regulates mitochondrial uncoupling protein 2 to promote glutaminolysis in neuroblastoma cells. *Biochim Biophys Acta Bioenerg*. 2019;1860(5):391-401.
55. Sternberg F, Sternberg C, Dunkel A, et al. Ketogenic diets composed of long-chain and medium-chain fatty acids induce cardiac fibrosis in mice. *Mol Metab*. 2023;72:101711.
56. Rupprecht A, Sokolenko EA, Beck V, et al. Role of the transmembrane potential in the membrane proton leak. *Biophys J*. 2010;98(8):1503-1511.

SUPPORTING INFORMATION

Additional supporting information can be found online in the Supporting Information section at the end of this article.

How to cite this article: Žuna K, Tyschuk T, Beikbaghban T, Sternberg F, Kreiter J, Pohl EE. The 2-oxoglutarate/malate carrier extends the family of mitochondrial carriers capable of fatty acid and 2,4-dinitrophenol-activated proton transport. *Acta Physiol*. 2024;00:e14143. doi:10.1111/apha.14143

2.2. Mitochondrial Uncoupling Proteins (UCP1-UCP3) and Adenine Nucleotide Translocase (ANT1) Enhance the Protonophoric Action of 2,4-Dinitrophenol in Mitochondria and Planar Bilayer Membranes.

biomolecules

MDPI

Article

Mitochondrial Uncoupling Proteins (UCP1-UCP3) and Adenine Nucleotide Translocase (ANT1) Enhance the Protonophoric Action of 2,4-Dinitrophenol in Mitochondria and Planar Bilayer Membranes

Kristina Žuna [1], Olga Jovanović [1], Ljudmila S. Khailova [2], Sanja Škulj [3], Zlatko Brkljača [4], Jürgen Kreiter [1], Elena A. Kotova [2], Mario Vazdar [4,5], Yuri N. Antonenko [2,*] and Elena E. Pohl [1,*]

1 Institute of Physiology, Pathophysiology and Biophysics, University of Veterinary Medicine, A-1210 Vienna, Austria; kristina.zuna@vetmeduni.ac.at (K.Ž.); olga.jovanovic@vetmeduni.ac.at (O.J.); jürgen.kreiter@vetmeduni.ac.at (J.K.)
2 Belozersky Institute of Physico-Chemical Biology, Lomonosov Moscow State University, Leninskie Gory 1/40, 119991 Moscow, Russia; khailova@genebee.msu.ru (L.S.K.); kotova@belozersky.msu.ru (E.A.K.)
3 Department of Chemistry, Faculty of Science, University of Zagreb, Horvatovac 102a, 10000 Zagreb, Croatia; Sanja.Skulj@irb.hr
4 Division of Organic Chemistry and Biochemistry, Ruđer Bošković Institute, Bijenička 54, 10000 Zagreb, Croatia; Zlatko.Brkljaca@irb.hr (Z.B.); Mario.Vazdar@irb.hr (M.V.)
5 Institute of Organic Chemistry and Biochemistry, Czech Academy of Sciences, Flemingovo nám. 2, 16610 Prague, Czech Republic
* Correspondence: antonen@belozersky.msu.ru (Y.N.A.); elena.pohl@vetmeduni.ac.at (E.E.P.)

Abstract: 2,4-Dinitrophenol (DNP) is a classic uncoupler of oxidative phosphorylation in mitochondria which is still used in "diet pills", despite its high toxicity and lack of antidotes. DNP increases the proton current through pure lipid membranes, similar to other chemical uncouplers. However, the molecular mechanism of its action in the mitochondria is far from being understood. The sensitivity of DNP's uncoupling action in mitochondria to carboxyatractyloside, a specific inhibitor of adenine nucleotide translocase (ANT), suggests the involvement of ANT and probably other mitochondrial proton-transporting proteins in the DNP's protonophoric activity. To test this hypothesis, we investigated the contribution of recombinant ANT1 and the uncoupling proteins UCP1-UCP3 to DNP-mediated proton leakage using the well-defined model of planar bilayer lipid membranes. All four proteins significantly enhanced the protonophoric effect of DNP. Notably, only long-chain free fatty acids were previously shown to be co-factors of UCPs and ANT1. Using site-directed mutagenesis and molecular dynamics simulations, we showed that arginine 79 of ANT1 is crucial for the DNP-mediated increase of membrane conductance, implying that this amino acid participates in DNP binding to ANT1.

Keywords: mitochondrial uncoupler; protonophore; membrane potential; proton conductance; artificial membranes; molecular dynamics simulations

Citation: Žuna, K.; Jovanović, O.; Khailova, L.S.; Škulj, S.; Brkljača, Z.; Kreiter, J.; Kotova, E.A.; Vazdar, M.; Antonenko, Y.N.; Pohl, E.E. Mitochondrial Uncoupling Proteins (UCP1-UCP3) and Adenine Nucleotide Translocase (ANT1) Enhance the Protonophoric Action of 2,4-Dinitrophenol in Mitochondria and Planar Bilayer Membranes. *Biomolecules* **2021**, *11*, 1178. https://doi.org/10.3390/biom11081178

Academic Editor: Brigita Urbanc

Received: 21 June 2021
Accepted: 4 August 2021
Published: 9 August 2021

1. Introduction

Obesity is one of the most acute health problems in developed countries worldwide. Recent statistics from the World Health Organization show that obesity has nearly tripled worldwide since 1975 (https://www.who.int/news-room/fact-sheets/detail/obesity-and-overweight, accessed on 5 June 2021). Although the uncoupling of oxidative phosphorylation (OxPhos) in the mitochondria was long ago proposed as a target for treating obesity, no breakthrough therapy has yet been established. 2,4-Dinitrophenol (DNP) has been known since the mid-1930s as an effective component of "diet pills" that is capable of reducing obesity by increasing the basal metabolic rate [1]. Severe side effects forced its withdrawal from the pharmaceutical market [2,3]. However, DNP can still be illegally purchased under

different names over the internet as a drug conferring rapid and supposedly safe weight loss, and is also used as an illegal food supplement [4].

Sustained scientific interest in DNP is based not only on its much higher efficacy than other drugs but also on the need to develop antidotes against its toxicity to prevent the increasing number of deaths associated with its uncontrolled use. The detailed molecular mechanism of the uncouplers' action in the mitochondria remains unclear, which hinders the use of DNP and its derivatives as therapeutic drugs.

Since DNP increases the conductance of pure lipid membranes, similar to other uncouplers [5–14], its effect on the mitochondria was ascribed to an increase in proton permeability through the lipid part of the inner mitochondrial membrane (IMM). On the other hand, the azido-substituted analog of DNP, 2-azido-4-nitrophenol, was shown to bind effectively to mitochondrial proteins [15–17]. In addition, the uncoupling effect of DNP on the mitochondria was shown to be partially blocked by carboxyatractyloside (CATR) [18,19], a specific inhibitor of the adenine nucleotide translocase (ANT), indicating the participation of ANT in the uncoupling action of DNP in the mitochondria.

Partial suppression of the uncoupling effect was also found for other protonophores, including BAM15 [19–24]. These findings support the hypothesis of ANT's participation in the uncoupling action of certain protonophores in the mitochondria [25].

Our previous study demonstrated the ability of ANT1 to enhance the proton current across artificial membranes in the presence of weak uncouplers—long-chain fatty acids (FA) [26]. We now hypothesize that DNP's protonophoric function may be also potentiated by mitochondrial proton-transporting proteins, in addition to the DNP-mediated increase in the selective lipid membrane's permeability for protons. To test this hypothesis, we used a well-defined model of lipid bilayer membranes reconstituted with recombinant ANT1 or UCPs (1) to investigate the contribution of these proteins to DNP-mediated proton leakage, (2) to evaluate the efficiency of the inhibitors of proton transport mediated by ANT1/UCP, and (3) to reveal the amino acids crucial for ANT1 activation by DNP.

2. Materials and Methods

2.1. Chemicals

2,4-Dinitrophenol (DNP), chloroform, dimethyl sulfoxide (DMSO), 1,2-dioleoyl-sn-glycero-3-phosphotidylcholine (DOPC), 1,2-dioleoyl-sn-glycero-3-phosphoethanolamine (DOPE), cardiolipin (CL), sodium sulfate (Na_2SO_4), 2-(*N*-morpholino) ethanesulfonic acid (MES), tris(hydroxymethyl)-aminomethane (Tris), adenosine 5′-triphosphate (ATP), guanosine 5′-triphosphate (GTP), carboxyatractyloside (CATR), ethylenediaminetetraacetic acid (EDTA), ethylene glycol-bis(β-aminoethyl ether)-N,N,N′,N′-tetraacetic acid (EGTA), *N*-lauroylsarcosine, Triton X-114, dithiothreitol (DTT), bovine serum albumin (BSA), sucrose, 3-(*N*-morpholino) propanesulfonic acid (MOPS), rotenone, and safranin O were purchased from Sigma-Aldrich (Vienna, Austria). Arachidonic acid (AA) was purchased from Larodan (Solna, Sweden), n-octylpolyoxyethylene was purchased from BACHEM (Bubendorf, Switzerland), and hydroxyapatite was purchased from Bio-Rad Laboratories (Hercules, CA, USA).

2.2. Cloning, Purification, and Reconstitution of Murine ANT1 and UCPs

Cloning, purification, and reconstitution of murine ANT1, UCP1, UCP2, and UCP3 followed previously established protocols [27–29]. In brief, expression plasmids containing selected cDNA sequences were transformed into the *E. coli* Rosetta DE3 strain (Novagen (Merck), Darmstadt, Germany). After induction, high-pressure homogenization, and centrifugation, the proteins were isolated as inclusion bodies. For protein refolding, purification, and reconstitution, 1 mg of the inclusion bodies was solubilized in a TE/G buffer containing 2% *N*-lauroylsarcosine, 1.3% Triton X-114, 0.3% n-octylpolyoxyethylene, 1 mM DTT, and GTP at pH 7.5. Fifty milligrams of the lipid mixture (DOPC:DOPE:CL; 45:45:10 mol%) was mixed in gradually. The mixture was concentrated and dialyzed against a buffer used in the experiments (50 mM Na_2SO_4, 10 mM MES, 10 mM Tris, and

0.6 mM EGTA at pH 7.34). Unfolded and aggregated proteins were removed from the dialysate by centrifugation and through a column containing hydroxyapatite; non-ionic detergents were removed by applying Bio-Beads SM-2 (Bio-Rad Laboratories, Hercules, CA, USA). The protein concentration in proteoliposomes was measured with the Micro BCA Protein Assay Kit (Thermo Fisher Scientific, Waltham, MA, USA). Protein purity was verified by SDS-PAGE and silver staining (Figure S1). Proteoliposomes were produced in independent batches. The following batch numbers were used for this study: ANT1 #42 and #47, UCP1 #117, UCP2 #39, UCP3 #31, and ANT1 R79S #3.

2.3. Generation of the ANT1 R79S Mutant

In vitro site-directed mutagenesis was carried out on expression plasmids containing the cDNA of mANT1 as a template. The mutation was introduced with an oligonucleotide designed to alter codon Arg79 (CGG) to Ser (TCG) using a QuikChange II site-directed mutagenesis kit (Agilent Technologies, Vienna, Austria). The successful introduction of mutations was confirmed by sequencing. Mutant ANT1 expression plasmids were transformed in the *E. coli* expression strain Rosetta DE3. Expression induction, inclusion body isolation, and reconstitution into liposomes of the ANT1 mutant were performed as described above for the ANT1 wild-type.

2.4. Formation of Planar Lipid Bilayer Membranes and Membrane Conductance Measurements

Planar lipid bilayers were formed from proteoliposomes as described previously [30,31]. Correct membrane formation was verified by measuring the membrane capacitance ($C = 0.72 \pm 0.02$ μF/cm^2), which was independent of the presence of protein, AA and DNP. Current voltage measurements were performed with a patch-clamp amplifier (EPC 10, HEKA Elektronik, Dr. Schulze GmbH, Lambrecht, Germany). The specific total membrane conductance (G_m) at 0 mV was obtained as the slope of a linear fit of the experimental data at the applied voltages from −50 mV to +50 mV, normalized to the membrane area. AA solved in chloroform was added to the membrane-forming lipid solution. ATP dissolved in the assay buffer (pH = 7.34), CATR, and DNP (both dissolved in DMSO) were added to the buffer solution before forming bilayer membranes. Control experiments showed that DMSO did not change the total membrane conductance of the lipid bilayers in the range of concentrations used [32]. The concentrations of each substrate are indicated in the figure legends. The relative conductance was calculated according to Equation (1):

$$G_{rel} = \frac{G - G_0}{G_1 - G_0} \quad (1)$$

where G_0 is the total membrane conductance of lipid membranes reconstituted with DNP, G_1 is the total membrane conductance of lipid membranes reconstituted with ANT1 and DNP, and G is the total specific membrane conductance of lipid membranes reconstituted with ANT1, DNP, and/or CATR/ATP (Figure 3).

2.5. Isolation of Rat Liver Mitochondria

Rat liver or heart mitochondria (RLM, RHM) were isolated by differential centrifugation [33] in a medium containing 250 mM sucrose, 5 mM MOPS, 1 mM EGTA, and bovine serum albumin (0.5 mg/mL) at pH 7.4. The final washing was performed in a medium with the same composition. Protein concentration was determined using the Biuret method. Handling of animals and experimental procedures were conducted in accordance with international guidelines for animal care and use and were approved by the Ethics Committee of the Belozersky Institute of Physico-Chemical Biology at Moscow State University (protocol #3 from 12 February 2018).

2.6. Membrane Potential (Δψ) Measurements in Isolated Mitochondria

The transmembrane electric potential difference (Δψ) was measured using safranin O dye [34]. An incubation medium containing 250 mM sucrose, 5 mM MOPS, 1 mM

EGTA, 2 μM rotenone, 5 mM succinate (pH 7.4), and 15 μM safranin O was used. The mitochondrial protein content measured by the Biuret method was 0.6 mg protein/mL. The experiments were carried out at 26 °C.

The difference in absorbance between 555 and 523 nm (ΔA) was recorded with an Aminco DW-2000 spectrophotometer (Olis Inc., Bogart, GA, USA) in dual wavelength mode.

Mitochondrial membrane potential (MMP) was normalized according to Equation (2):

$$\text{Absorbance, \% of the maximum} = \frac{\Delta A_{max} - \Delta A}{\Delta A_{max} - \Delta A_{min}} \times 100 \quad (2)$$

where ΔA is the difference between A_{523} and A_{555}, ΔA_{max} is the highest membrane potential measured without the presence of DNP, and ΔA_{min} is the lowest MMP measured in the presence of DNP at the highest concentration. Statistical analysis was performed using a Student's test with a level of significance of 0.01.

2.7. Molecular Dynamic Simulations

We performed all-atom molecular dynamic (MD) simulations of wild-type and mutated (R79 to S79) ANT1 protein in a 1,2-dioleoyl-sn-glycero-3-phosphocholine (DOPC) bilayer. The initial structure for both the wild-type and mutated forms of ANT1 was taken from the end of the 2 μs simulation of the wild-type ANT1 protein in the DOPC bilayer [35], with the mutation of R79 into S79 and the subsequent introduction of the mutated form of ANT1 into the DOPC bilayer being performed using CHARMM-GUI (http://www.charmm-gui.org/, accessed on 10 February 2021) [36–38]. Overall, 4 system set-ups were prepared: the wild-type ANT1 with the anionic form of 2,4-dinitrophenol (DNP) (i) or ATP^{4-} bound in the cytosolic-open state (ii), as well as the mutated ANT1 with the DNP anion (iii) or ATP^{4-} bound in the same position (iv). Since DNP has a p*K*a value in water of 4.1, we assumed it was anionic at the neutral pH used in MD simulations. All simulation boxes contained ANT1 protein (wild-type or the R79-to-S79 mutant) (with a total charge of +19e or +18e, respectively), 73 DOPC molecules per leaflet (146 per system), 11,500 water molecules, a single DNP anion or ATP^{4-}, and the necessary number of Cl^- anions to neutralize the net charge, depending on whether wild-type ANT1 or its mutant was present in the system. ANT1 protein, ATP^{4-} ion, and DOPC lipids were described by the CHARMM36m force field [39]. The force field for the anionic form of the DNP (2,4-dinitrophenol) anion was built on the basis of the CHARMM general force field (CGenFF) [40] (https://cgenff.umaryland.edu/, accessed on 10 February 2021).

The system containing mutated ANT1 protein, DOPC molecules, and water/ions (no DNP anion or ATP^{4-} present at this stage) was first minimized and equilibrated in 6 steps using the CHARMM-GUI protocol [41] and then simulated for a further 500 ns without any restraints with a 2 fs time step in a periodic rectangular box of 7.9 nm × 7.9 nm × 9.4 nm using the isobaric–isothermal ensemble (NPT) and periodic boundary conditions in all directions at T = 310 K, maintained via a Nosé–Hoover thermostat [42] independently for the DOPC, water/ions, and protein subsystems, with a coupling constant of 1.0 ps^{-1}. The pressure was set to 1.013 bar and controlled with a semi-isotropic Parrinello–Rahman barostat [43], with a time constant for pressure coupling of 5 ps^{-1}. Long-range electrostatics were calculated using the particle-mesh Ewald (PME) method [44] with real-space Coulomb interactions cut off at 1.2 nm using a Fourier spacing of 0.12 nm and a Verlet cut-off scheme.

To prepare the investigated systems, one molecule of DNP anion (or ATP^{4-}) was placed in the cytosolic-open state of the equilibrated systems containing wild-type ANT1 (obtained after 2 μs of free MD simulation) or mutated ANT1 (see previous paragraph). More precisely, the DNP anion (or ATP^{4-}) was placed in the cavity of the ANT1 protein, in proximity to the R79 (wild-type) or S79 (mutated ANT1) amino acid residue, using the VMD molecular graphics program [45]. The prepared systems were then minimized, and short preliminary simulations (2 ns) with positional restraints on the DNP (or ATP) molecule (500 kJ mol^{-1} nm^{-2}) were conducted to relax the protein around the DNP

molecule. Subsequently, both investigated systems were propagated for a duration of 500 ns, with MD parameters equal to those used to propagate the mutated ANT1 system (see previous paragraph). All simulations were run with the GROMACS 2018 software package [46].

2.8. Statistics

Data analysis and fitting of electrophysiological measurements were performed using Sigma Plot 12.5 (Systat Software GmbH, Erkrath, Germany) and are displayed as the mean ± SD of at least 3 independent experiments. Each independent experiment involved at least 3 measurements using independently formed bilayer membranes.

3. Results

3.1. CATR Recouples Mitochondria Uncoupled by DNP

Measurements of oxygen consumption in isolated rat liver mitochondria (RLM) and skeletal muscle mitochondria showed that CATR can partially reverse the uncoupling effect of low DNP concentrations [18,47]. Because mitochondrial membrane potential (MMP) is a more sensitive indicator of mitochondrial coupling, we measured the MMP of isolated RLM in the presence of DNP and CATR using the potential-sensitive dye safranin O [34]. Figure 1A shows that, after the addition of 10–50 µM DNP to RLM, MMP decreased in a concentration-dependent manner. CATR at a concentration of 3 µM partially restored MMP at all concentrations, supporting the data obtained from oxygen consumption measurements earlier.

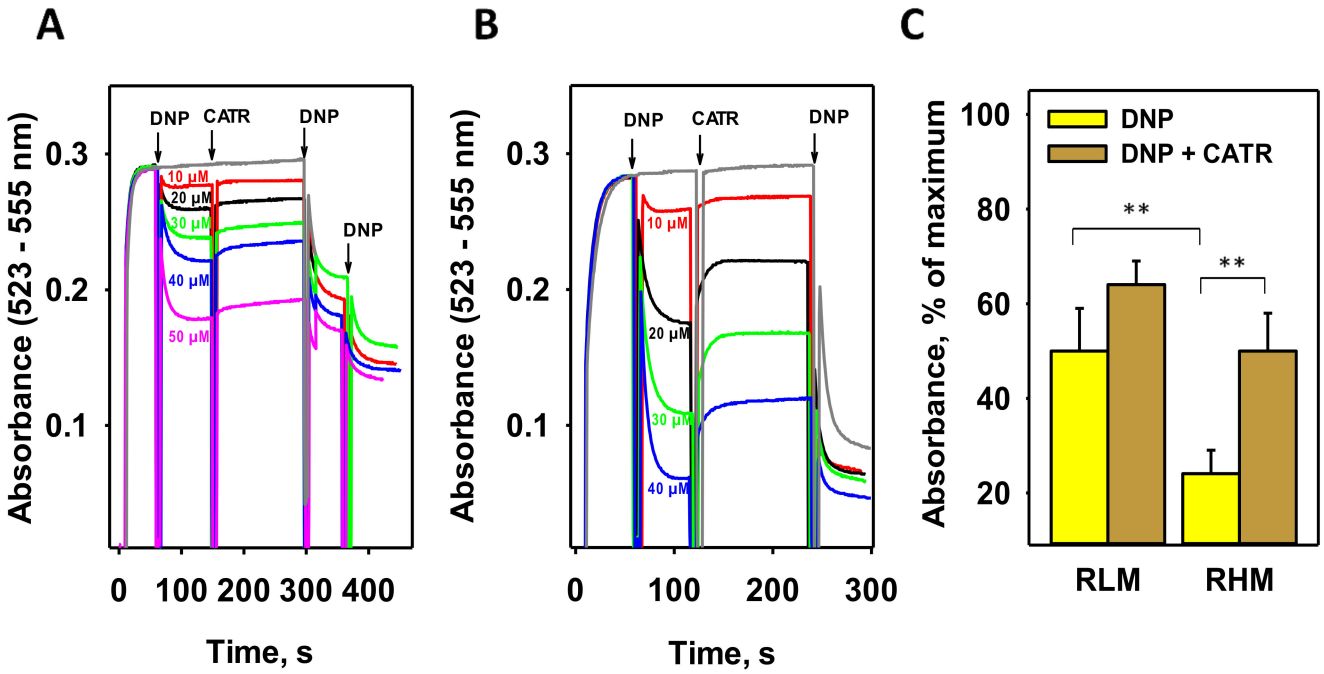

Figure 1. CATR recovers the DNP-mediated decrease in mitochondrial membrane potential (MMP) in isolated rat mitochondria. Representative recordings of MMP in rat liver mitochondria (**A**) and heart (**B**) mitochondria correspond to changes in the absorbance of the potential-sensitive dye safranin O (15 µM). CATR was added at a final concentration of 3 µM; the concentration of DNP (unless otherwise indicated) was 50 µM. The gray line represents the control measurement without the addition of CATR or DNP. (**C**) Quantification of MMP recovery by CATR (brown) in the presence of 30 µM DNP (yellow, brown). Data are the mean ± SD of at least three independent experiments; ** $p < 0.01$. For other conditions, see Section 2 (Materials and Methods).

Because the DNP effect was small in RLM, we performed similar experiments with mitochondria isolated from rat hearts (RHM), which are known to have a higher ANT1 abundance [48]. The heart is also known to express another proton-transporting protein,

UCP3 [49,50]. Figure 1B shows that the uncoupling effect of DNP in RHM was significantly higher than that in RLM. Importantly, the subsequent recoupling effect of CATR was also much more pronounced in RHM. A significant difference ($p < 0.01$) was found between RLM and RHM for both DNP-mediated uncoupling and recoupling in the presence of CATR (Figure 1C). Nonetheless, no complete recoupling was observed, suggesting a significant contribution of the DNP-assisted proton shuttling through the lipid part of membranes to the overall DNP-mediated proton transport and/or the involvement of other carrier proteins of IMM in this process.

3.2. DNP Increases the Proton Conductance of the Membranes Reconstituted with Mitochondrial Membrane Proteins

It was previously shown that ANT1 mediates proton transport in the presence of free long-chain fatty acids (FA), similar to UCPs [26,47,51]. To test whether DNP also activates ANT1, we used a well-defined model of planar bilayer membranes reconstituted with recombinant murine ANT1 (Figure S1) [27]. In contrast to the well-known Müller–Rudin technique, in which the membrane is "painted" by lipids dissolved in n-decane, we folded bilayers from the solvent-free monolayer formed from the proteoliposomes. The specific conductance (G_m) of the membranes reconstituted with ANT1 (G_m = 11.1 ± 0.8 nS/cm^2) was comparable with the conductance of pure lipid membranes made from DOPC, DOPE, and cardiolipin (CL) (45:45:10 mol%; G_m = 10.81 ± 2.72 nS/cm^2, Figure 2A).

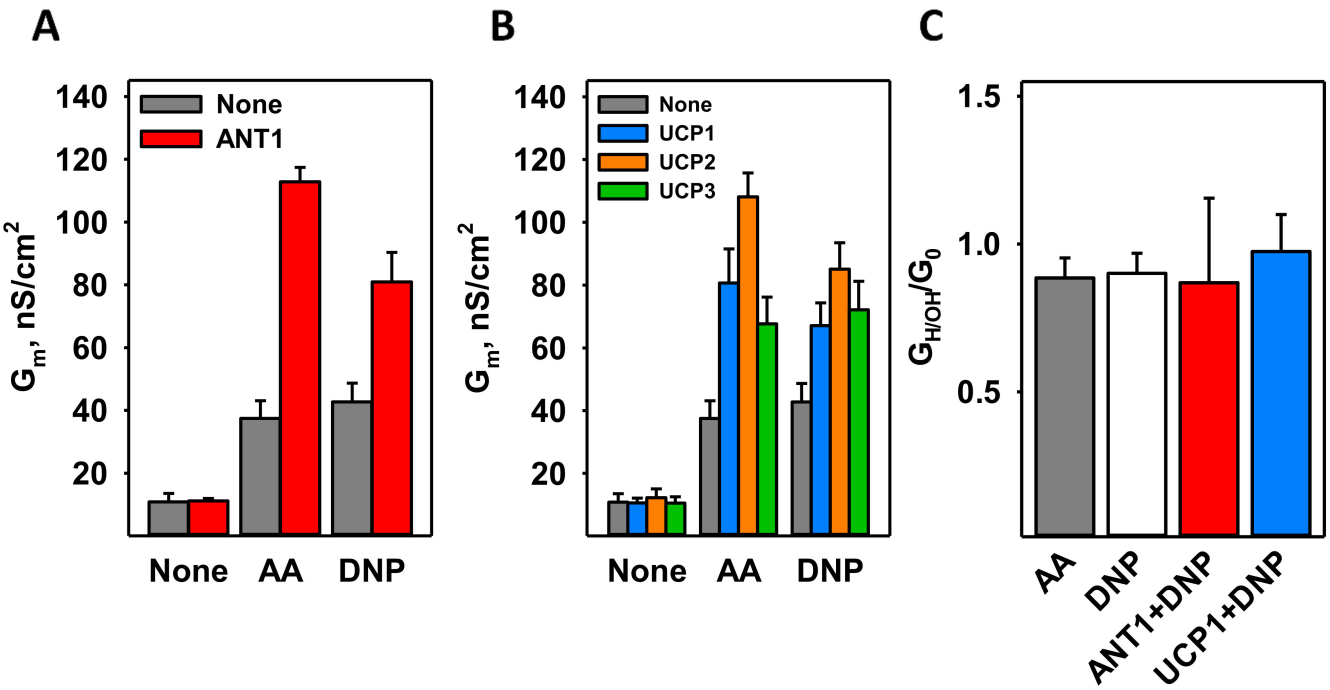

Figure 2. DNP-mediated proton transport in the presence of mitochondrial membrane proteins reconstituted in planar lipid bilayers. (**A**) Increase in the total specific membrane conductance (G_m) in the presence of arachidonic acid (AA) or DNP without (gray) and with ANT1 (red). (**B**) Increase in G_m in the presence of AA or DNP without protein (gray) or with UCP1 (blue), UCP2 (orange), or UCP3 (green). (**C**) The ratio of proton conductance to total membrane conductance ($G_{H/OH}/G_0$) was measured at a transmembrane pH gradient of 0.4. The concentrations of AA and DNP were 15 mol% and 50 μM. For all measurements, the membranes were made of DOPC:DOPE:CL (45:45:10 mol%). Lipid and protein concentrations were 1.5 mg/mL and 4 μg per mg of lipid. The buffer solution consisted of 50 mM Na_2SO_4, 10 mM Tris, 10 mM MES, and 0.6 mM EGTA at pH = 7.34 and T = 32 °C. Data are the mean ± SD of at least three independent experiments.

Figure 2A shows that the specific conductance of membranes containing DNP in the presence of ANT1 (ANT1 + DNP, red column; G_m = 80.9 ± 9.4 nS/cm^2) was approximately double that of membranes containing only DNP at a concentration of 50 μM (DNP, gray

column; G_m = 42.7 ± 5.9 nS/cm^2). Until now, only FAs have been shown to activate ANT1 directly (Figure 2A) [18,26,51,52].

To test whether uncoupling proteins can be activated by DNP in the absence of FA, we reconstituted recombinant murine UCP1, UCP2, and UCP3 (Figure S1) in bilayer membranes made of DOPC, DOPE, and CL. G_m in the presence of UCPs and DNP ($G_{m,\,UCP1}$ = 67.1 ± 7.2 nS/cm^2, $G_{m,\,UCP2}$ = 85.1 ± 8.4 nS/cm^2; $G_{m,\,UCP3}$ = 72.1 ± 9.1 nS/cm^2) was again approximately double that in the presence of DNP alone (G_m = 42.7 ± 5.9 nS/cm^2) (Figure 2B).

The contribution of proton conductance to the total membrane conductance ($G_{H/OH}/G_0$) was determined from the shift in reverse potential in the presence of a transmembrane pH gradient of 0.4 [30]. Figure 2C shows that in the presence of DNP and protein (ANT1 or UCP1), the $G_{H/OH}/G_0$ was approximately 1, confirming the specificity of the proton transport in all cases.

3.3. CATR and ATP Inhibit DNP-Mediated Activation of ANT1 Only If Added before DNP

Because CATR was able to partially restore MMP in mitochondria treated with DNP (Figure 1), we tested whether its addition would deplete the proton transport mediated by DNP in the presence of reconstituted ANT1. Interestingly, CATR decreased G_m more effectively if added prior to DNP (Figure 3A). The decrease was more pronounced at the higher CATR concentration of 100 µM (~98%), indicating the specificity of the interaction.

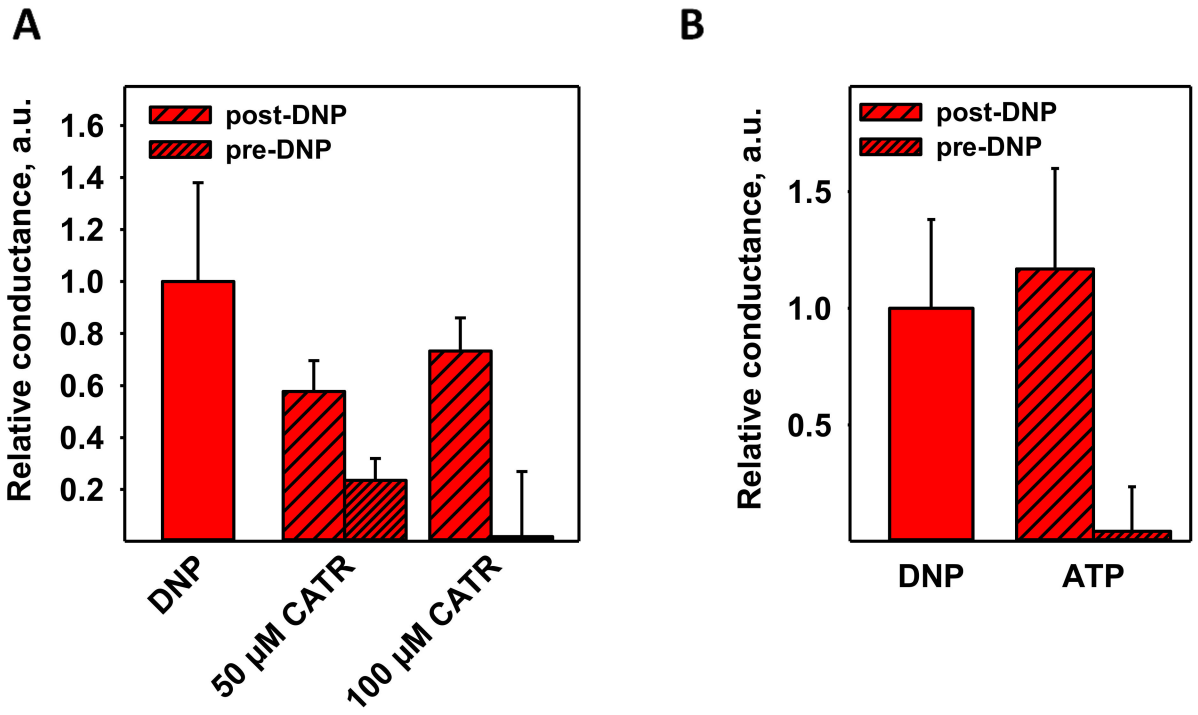

Figure 3. DNP-mediated proton transport in the presence of ANT1 can be inhibited by CATR or ATP. (**A**) Relative conductance of bilayer lipid membranes reconstituted with ANT1 in the presence of DNP and CATR added either after DNP (post-DNP) or before DNP (pre-DNP). (**B**) Relative conductance of bilayer membranes reconstituted with ANT1 in the presence of DNP and 4 mM ATP. Relative conductance describes the ratio between the total membrane conductance, G_m, in the presence or absence of inhibitors to the membrane conductance measured in the presence of lipids alone (see Equation (1)). Other experimental conditions were the same as in Figure 2.

ATP was shown to be an inhibitor of FA-activated ANT1 [26], so we examined its effect on DNP-mediated proton transport as well. Figure 3B shows that 4 mM ATP inhibited the effect of DNP by ~96%, further suggesting the same putative binding site for DNP, CATR, ATP, and FA. The total membrane conductance (G_m) values of Figure 3 are shown

in Figure S2. ATP inhibited the UCP1–UCP3-enhanced DNP-mediated uncoupling in the same manner as it did in case of ANT1 (Figure 4).

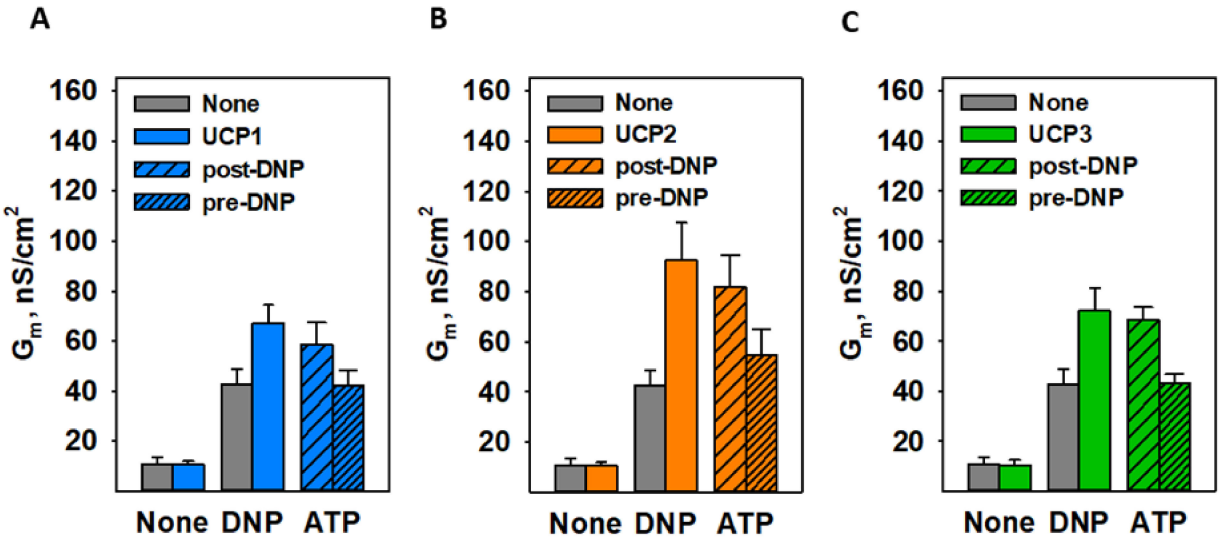

Figure 4. ATP decreased DNP-mediated proton transport enhanced by UCP1 (**A**), UCP2 (**B**), and UCP3 (**C**). Here, 4 mM of ATP was added either post-DNP (medium pattern) or pre-DNP (fine pattern). The experimental conditions were similar to those in Figure 2.

3.4. R79 Is Crucial for DNP–Protein Interaction

Because arginine 79 (R79) was previously shown to be important for the binding of CATR and ATP to ANT1 [53–55], we further evaluated the role of R79 in the interaction between DNP and ANT1. Indeed, the recombinant ANT1 in which R79 was substituted by serine using site-directed mutagenesis (ANT1 R79S) was unable to facilitate proton transport mediated by DNP (Figure 5, dark red columns). This result supported the idea that the R79 of ANT1 is crucial for the increase in proton transport in the presence of DNP.

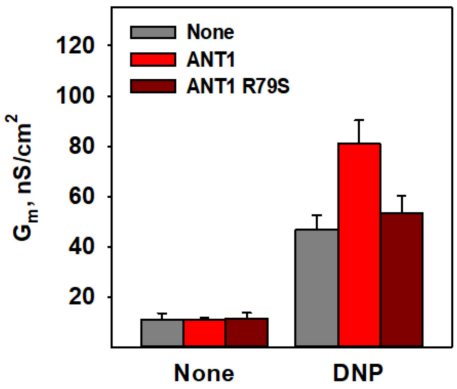

Figure 5. Effect of the ANT1 R79S mutation on DNP-mediated proton transport. Total specific membrane conductance (G_m) of the lipid bilayer membranes reconstituted with ANT1 (red) or ANT1 R79S (dark red) in the presence and absence of 50 μM DNP. The experimental conditions were the same as in Figure 2.

3.5. Molecular Dynamic Simulations Show the Binding of DNP to R79 but Not to S79

To test the putative role of R79 in the interaction of DNP with ANT1, we performed 500 ns molecular dynamic (MD) simulations for two systems: ANT1 and ANT1 R79S. Figure 6 shows that DNP bound easily to R79 in ANT1, whereas in the case of ANT1 R79S the binding was absent. Analysis of the distances between DNP and the C_Z atom of R79 (Figure 6A) shows that the binding of DNP to R79 was not very strong and persistent, as

evidenced by the relatively large corresponding average distance (Figure 6B). However, DNP frequently makes close contact with R79 by forming bidentate hydrogen bonds with its guanidinium side chain, which is apparently responsible for DNP binding in addition to attractive electrostatic interactions (Figure 6B, arrows; Figure 6C). In contrast, a mutation of R79 to S79 in ANT1 abolished the close contacts between DNP and the C_B atom of serine due to the loss of attractive electrostatic interactions and favorable hydrogen bonding (Figure 6D).

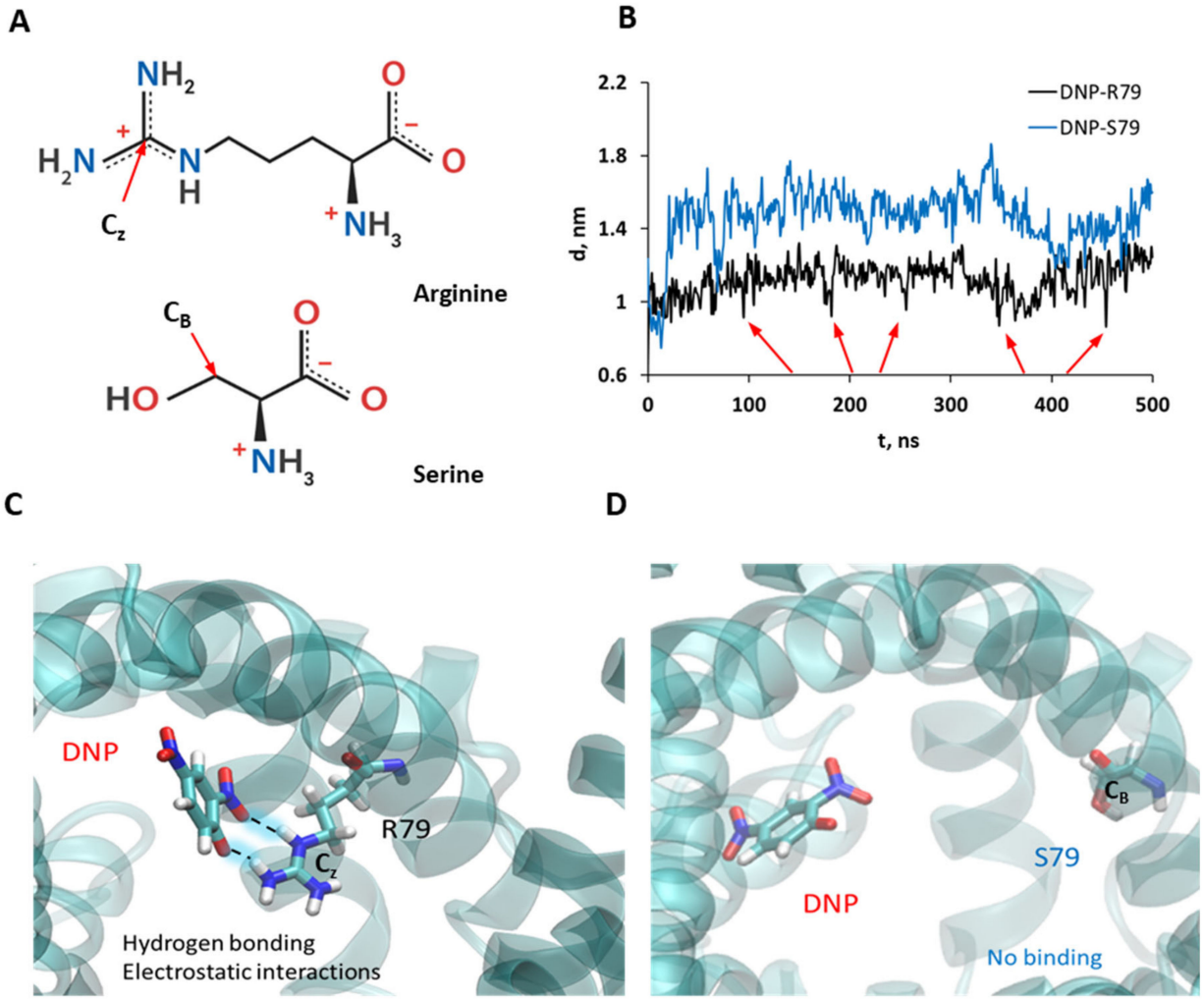

Figure 6. DNP binding in ANT1 and ANT1 R79S. (**A**) Structure of arginine and serine at pH = 7 in water. C_Z is the central carbon atom of the guanidinium side chain in R79, and C_B is the carbon atom in the side chain of S79. (**B**) Analysis of the distances between DNP's center of mass and the C_Z atom in R79 (black) and the C_B atom in the S79 residue (blue). Red arrows indicate close contacts between DNP and R79. Selected snapshots from MD simulations of DNP in ANT1 (**C**) and DNP in ANT1 R79S (**D**).

However, the binding of DNP to R79 was not as strong as in the case of ATP [56,57]. Figure S4 presents an analysis of the corresponding distances between phosphorous atoms in the phosphate groups of ATP (Pα, Pβ, and Pγ) and the C_Z atom in R79 in ANT1 (Figure S4A) and the C_B atom in S79 in the ANT1 R79S (Figure S4B), respectively. We can see that ATP bound very strongly to R79, as evidenced by the short and persistent contacts between Pα and Pβ atoms and R79 throughout the MD simulations. However, when R79 was mutated, the average distances from all three phosphate groups to S79 increased, showing weaker binding to S79 due to the loss of electrostatic interactions.

4. Discussion

Comparing the conductance of the pure lipid bilayer membranes and membranes reconstituted with recombinant ANT1, UCP1, UCP2, or UCP3, we revealed that proteins potentiate DNP-mediated proton transport through the membrane. Until now, only FAs were known to serve as a co-factor of the uncoupling function of these proteins. The mutation R79 in ANT1 abolished the increment in the conductance of the bilayer membrane reconstituted with protein, thus indicating DNP's putative binding site.

Our experiments on isolated mitochondria and membranes reconstituted with ANT1 or UCPs showed that DNP at a concentration of 50 μM can significantly decrease the MMP (Figure 1) and increase G_m (Figure 2). This is in agreement with a previous report about the large effects of 30 μM DNP on the mitochondria [58]. Interestingly, the fact that IMM has very high protein to lipid ratio of approximately 3:1 implies that the interaction of DNP with a protein contributes significantly to the DNP's action on the mitochondria.

Both CATR and ATP were able to prevent the increase in the protonophoric action of DNP in the presence of protein, which suggested the involvement of a similar binding site. MD simulation results supported the idea that ATP binds to R79 more strongly than DNP, showing much shorter distances between ATP phosphate groups and R79, and persistent contacts between them (Figure S4). DNP also bound to R79 but, based on the distance analysis (Figure 6B), the binding of DNP was not as strong, and close contacts between DNP and R79 are not as frequent as in ATP binding.

The results of the site-directed mutagenesis showed that R79 is crucial for the DNP effect, since its replacement completely abolished the G_m increase in the presence of protein. R79 is a component of the arginine ring made of three arginine residues, which was found to protrude into the center of the protein's cavity [55]. At the alkaline pH of the cytosol and mitochondrial matrix, which we imitated in our experiments, the aforementioned molecules possess at least one negative charge and interact with positively charged amino acids, with R79 either being one of them or being the critical one. As R79 plays an important role in the binding of all ANT1-specific substrates, it is possibly a highly conserved residue for the protein's functions—ATP/ADP and proton transport—regardless of which molecule acts as an uncoupler. This was also shown by the MD simulations, suggesting that the mutation of R79 to S79 weakens the interaction between DNP and the protein due to the loss of electrostatic attraction and hydrogen bonding possibilities (Figure 6C,D).

We suggest that the mechanism of the enhancement of DNP's protonophoric function by ANT1 is similar to that of fatty acids. So far, two hypotheses have been proposed to explain the induction of proton conductance by fatty acids involving ANT and uncoupling proteins (for a review, see [59]): (1) Protein accelerates the transport of the FA anion, which limits total proton transport by FA flip-flop through the lipid membrane [26,60]; (2) FA induces a conformational transition in protein, leading to proton leakage through the protein [51,61]. The present work argued in favor of the first mechanism of the induction of proton conductance by ANT1 [26] because FA and DNP share the R79 residue as a common binding site [62]. Further experiments investigating the exact interaction between ANT1 and DNP and outlining the mechanism are required.

Besides ANT1, UCP1–UCP3 enhance the proton transport mediated by DNP (Figure 2B). This is in agreement with the experiments on isolated rat heart mitochondria, in which we observed a more pronounced effect of DNP than in liver. Heart mitochondria not only have a higher level of ANT1 than RLM [48] but also express UCP3, which is not found in the liver [49,63,64]. Notably, the R79 of ANT1 is highly conserved among the SLC25 protein family, with the residues R84, R88, and R84 being homologs of it in UCP1, UCP2, and UCP3, respectively. These residues likely form a putative DNP binding site in uncoupling proteins, and their depletion would result in the complete loss of DNP-mediated proton leakage, as occurred in R79S ANT1. Furthermore, we suggest that other proton-transporting proteins, such as the aspartate/glutamate carrier, the dicarboxylate carrier, the phosphate carrier, and the 2-oxoglutarate carrier [65–68], will also potentiate the protonophoric function of DNP.

Supplementary Materials: The following are available online at https://www.mdpi.com/article/10.3390/biom11081178/s1, Figure S1: Representative silver staining of proteins used in the study, Figure S2: Representative current-voltage recordings of pure lipid bilayer membranes and membranes reconstituted with ANT1 or without ANT1 in the presence of DNP, Figure S3: Effect of ANT1 specific inhibitors on the total conductance (G_m) of membranes reconstituted with ANT1 and DNP, Figure S4: ATP binding to the arginine 79 of the ANT1 or ANT1-R79S, Figure S5: DNP and ATP binding in ANT1.

Author Contributions: Conceptualization, E.E.P. and Y.N.A.; funding acquisition, E.E.P., Y.N.A., and M.V.; investigation, K.Ž., O.J., J.K., S.Š., Z.B., L.S.K., and M.V.; project administration, E.E.P.; resources, E.E.P., Y.N.A., and M.V.; supervision, E.E.P., Y.N.A., and M.V.; writing—original draft, E.E.P., K.Ž., Y.N.A., E.A.K., and M.V.; writing—review and editing, E.E.P., K.Ž., Y.N.A., O.J., J.K., E.A.K., S.Š., Z.B., L.S.K. and M.V. All authors have read and agreed to the published version of the manuscript.

Funding: This paper was supported by the European Union's Horizon 2020 MSCA-ITN-860592-PROTON and the Austrian Research Fund (P31559) (to E.P.), the Russian Science Foundation (grant 21-14-00062 to Y.N.A.), and the Croatian Science Foundation (Project No. IP-2019-04-3804 to M.V.).

Institutional Review Board Statement: Not applicable.

Informed Consent Statement: Not applicable.

Data Availability Statement: The datasets generated and/or analyzed during the current study can be obtained upon reasonable request from the corresponding authors or at the following link: DOI:10.5281/zenodo.5113039.

Acknowledgments: We thank Sarah Bardakji for the excellent technical assistance. We are also grateful to Peter Pohl for helpful discussions. We thank the computer cluster Isabella based at SRCE—University of Zagreb, University Computing Centre, for computational resources. M.V. thanks the UOCHB Sabbatical visit program for support.

Conflicts of Interest: The authors declare no conflict of interest.

References

1. Cutting, W.; Mehrtens, H.; Tainter, M. Actions and uses of dinitrophenol: Promising metabolic applications. *J. Am. Med. Assoc.* **1933**, *101*, 193–195. [CrossRef]
2. Tainter, M.L.; Cutting, W.C.; Stockton, A. Use of Dinitrophenol in Nutritional Disorders* A Critical Survey of Clinical Results. *Am. J. Public Health Nations Health* **1934**, *24*, 1045–1053. [CrossRef]
3. Colman, E. Dinitrophenol and obesity: An early twentieth-century regulatory dilemma. *Regul. Toxicol. Pharmacol.* **2007**, *48*, 115–117. [CrossRef]
4. Koncz, D.; Tóth, B.; Roza, O.; Csupor, D. A Systematic Review of the European Rapid Alert System for Food and Feed: Tendencies in Illegal Food Supplements for Weight Loss. *Front. Pharmacol.* **2021**, *11*, 611361. [CrossRef]
5. Ebert, A.; Hannesschlaeger, C.; Goss, K.-U.; Pohl, P. Passive Permeability of Planar Lipid Bilayers to Organic Anions. *Biophys. J.* **2018**, *115*, 1931–1941. [CrossRef] [PubMed]
6. Hannesschlaeger, C.; Horner, A.; Pohl, P. Intrinsic Membrane Permeability to Small Molecules. *Chem. Rev.* **2019**, *119*, 5922–5953. [CrossRef] [PubMed]
7. Liberman, E.A.; Topaly, V.P.; Silberstein, A.Y. Charged and neutral ion carriers through bimolecular phospholipid membranes. *Biochim. Biophys. Acta* **1970**, *196*, 221–234. [CrossRef]
8. Bakker, E.; Heuvel, E.V.D.; Wiechmann, A.; Van Dam, K. A comparison between the effectiveness of uncouplers of oxidative phosphorylation in mitochondria and in different artificial membrane systems. *Biochim. Biophys. Acta Bioenerg.* **1973**, *292*, 78–87. [CrossRef]
9. Bielawski, J.; Thompson, T.E.; Lehninger, A.L. The effect of 2,4-dinitrophenol on the electrical resistance of phospholipid bilayer membranes. *Biochem. Biophys. Res. Commun.* **1966**, *24*, 948–954. [CrossRef]
10. Hopfer, U.; Lehninger, A.L.; Thompson, T.E. Protonic conductance across phospholipid bilayer membranes induced by uncoupling agents for oxidative phosphorylation. *Proc. Natl. Acad. Sci. USA* **1968**, *59*, 484–490. [CrossRef]
11. Skulachbv, V.; Sharaf, A.; Yagujzinsky, L.; Jasaitis, A.; Liberman, E.; Topali, V. The effect of uncouplers on mitochondria, respiratory enzyme complexes and artificial phospholipid membranes. *Biosystems* **1968**, *2*, 98–105. [CrossRef]
12. Liberman, E.A.; Topaly, V.P.; Tsofina, L.M.; Jasaitis, A.A.; Skulachev, V.P. Mechanism of coupling of oxidative phosphorylation and the membrane potential of mitochondria. *Nature* **1969**, *222*, 1076–1078. [CrossRef]
13. Liberman, E.; Topaly, V. Selective transport of ions through bimolecular phospholipid membranes. *Biochim. Biophys. Acta Biomembr.* **1968**, *163*, 125–136. [CrossRef]

14. Ting, H.; Wilson, D.F.; Chance, B. Effects of uncouplers of oxidative phosphorylation on the specific conductance of bimolecular lipid membranes. *Arch. Biochem. Biophys.* **1970**, *141*, 141–146. [CrossRef]
15. Hanstein, W.G.; Hatefi, Y. Trinitrophenol: A Membrane-Impermeable Uncoupler of Oxidative Phosphorylation. *Proc. Natl. Acad. Sci. USA* **1974**, *71*, 288–292. [CrossRef]
16. Cyboron, G.W.; Dryer, R. Uncoupling of hamster brown adipose and liver mitochondria by 2-azido-4-nitrophenol and binding properties of the reagent. *Arch. Biochem. Biophys.* **1977**, *179*, 141–146. [CrossRef]
17. Kurup, C.K.R.; Sanadi, D.R. Photoaffinity labeling of uncoupler binding sites on mitochondrial membrane. *J. Bioenerg. Biomembr.* **1977**, *9*, 1–15. [CrossRef] [PubMed]
18. Andreyev, A.; Bondareva, T.; Dedukhova, V.; Mokhova, E.; Skulachev, V.; Volkov, N. Carboxyatractylate inhibits the uncoupling effect of free fatty acids. *FEBS Lett.* **1988**, *226*, 265–269. [CrossRef]
19. Lou, P.-H.; Hansen, B.S.; Olsen, P.H.; Tullin, S.; Murphy, M.P.; Brand, M.D. Mitochondrial uncouplers with an extraordinary dynamic range. *Biochem. J.* **2007**, *407*, 129–140. [CrossRef]
20. Kopustinskiene, D.M.; Jovaisiene, J.; Liobikas, J.; Toleikis, A. Diazoxide and Pinacidil Uncouple Pyruvate–Malate-Induced Mitochondrial Respiration. *J. Bioenerg. Biomembr.* **2002**, *34*, 49–53. [CrossRef]
21. Ortega, R.; Garcia, N. The flavonoid quercetin induces changes in mitochondrial permeability by inhibiting adenine nu-cleotide translocase. *J. Bioenerg. Biomembr.* **2009**, *41*, 41–47. [CrossRef]
22. Lu, Y.; Liu, S.; Wang, Y.; Wang, D.; Gao, J.; Zhu, L. Asiatic acid uncouples respiration in isolated mouse liver mitochondria and induces HepG2 cells death. *Eur. J. Pharmacol.* **2016**, *786*, 212–223. [CrossRef]
23. Antonenko, Y.N.; Denisov, S.; Khailova, L.S.; Nazarov, P.A.; Rokitskaya, T.; Tashlitsky, V.N.; Firsov, A.M.; Korshunova, G.A.; Kotova, E.A. Alkyl-substituted phenylamino derivatives of 7-nitrobenz-2-oxa-1,3-diazole as uncouplers of oxidative phosphorylation and antibacterial agents: Involvement of membrane proteins in the uncoupling action. *Biochim. Biophys. Acta Biomembr.* **2017**, *1859*, 377–387. [CrossRef] [PubMed]
24. Firsov, A.M.; Popova, L.B.; Khailova, L.S.; Nazarov, P.A.; Kotova, E.A.; Antonenko, Y.N. Protonophoric action of BAM15 on planar bilayers, liposomes, mitochondria, bacteria and neurons. *Bioelectrochemistry* **2021**, *137*, 107673. [CrossRef]
25. Skulachev, V.P. Uncoupling: New approaches to an old problem of bioenergetics. *Biochim. Biophys. Acta Bioenerg.* **1998**, *1363*, 100–124. [CrossRef]
26. Kreiter, J.; Rupprecht, A.; Škulj, S.; Brkljača, Z.; Žuna, K.; Knyazev, D.; Bardakji, S.; Vazdar, M.; Pohl, E. ANT1 Activation and Inhibition Patterns Support the Fatty Acid Cycling Mechanism for Proton Transport. *Int. J. Mol. Sci.* **2021**, *22*, 2490. [CrossRef]
27. Kreiter, J.; Beitz, E.; Pohl, E.E. A Fluorescence-Based Method to Measure ADP/ATP Exchange of Recombinant Adenine Nucleotide Translocase in Liposomes. *Biomolecules* **2020**, *10*, 685. [CrossRef] [PubMed]
28. Rupprecht, A.; Sokolenko, E.A.; Beck, V.; Ninnemann, O.; Jaburek, M.; Trimbuch, T.; Klishin, S.S.; Jezek, P.; Skulachev, V.; Pohl, E.E. Role of the Transmembrane Potential in the Membrane Proton Leak. *Biophys. J.* **2010**, *98*, 1503–1511. [CrossRef]
29. Macher, G.; Koehler, M.; Rupprecht, A.; Kreiter, J.; Hinterdorfer, P.; Pohl, E.E. Inhibition of mitochondrial UCP1 and UCP3 by purine nucleotides and phosphate. *Biochim. Biophys. Acta Biomembr.* **2018**, *1860*, 664–672. [CrossRef] [PubMed]
30. Kreiter, J.; Pohl, E.E. A Micro-agar Salt Bridge Electrode for Analyzing the Proton Turnover Rate of Recombinant Membrane Proteins. *J. Vis. Exp.* **2019**, *143*, e58552. [CrossRef] [PubMed]
31. Beck, V.; Jabůrek, M.; Breen, E.P.; Porter, R.K.; Ježek, P.; Pohl, E.E. A new automated technique for the reconstitution of hydrophobic proteins into planar bilayer membranes. Studies of human recombinant uncoupling protein 1. *Biochim. Biophys. Acta Bioenerg.* **2006**, *1757*, 474–479. [CrossRef] [PubMed]
32. Kreiter, J.; Rupprecht, A.; Zimmermann, L.; Moschinger, M.; Rokitskaya, T.; Antonenko, Y.N.; Gille, L.; Fedorova, M.; Pohl, E.E. Molecular Mechanisms Responsible for Pharmacological Effects of Genipin on Mitochondrial Proteins. *Biophys. J.* **2019**, *117*, 1845–1857. [CrossRef]
33. Johnson, D.; Lardy, H. Isolation of liver or kidney mitochondria. *Anal. Biochem.* **1967**, 94–96. [CrossRef]
34. Åkerman, K.E.; Wikström, M.K. Safranine as a probe of the mitochondrial membrane potential. *FEBS Lett.* **1976**, *68*, 191–197. [CrossRef]
35. Škulj, S.; Brkljača, Z.; Vazdar, M. Molecular Dynamics Simulations of the Elusive Matrix-Open State of Mitochondrial ADP/ATP Carrier. *Isr. J. Chem.* **2020**, *60*, 735–743. [CrossRef]
36. Jo, S.; Lim, J.B.; Klauda, J.B.; Im, W. CHARMM-GUI Membrane Builder for mixed bilayers and its application to yeast membranes. *Biophys. J.* **2009**, *97*, 50–58. [CrossRef]
37. Wu, E.L.; Cheng, X.; Jo, S.; Rui, H.; Song, K.C.; Davila-Contreras, E.M.; Qi, Y.; Lee, J.; Monje-Galvan, V.; Venable, R.M.; et al. CHARMM-GUI Membrane Builder toward realistic biological membrane simulations. *J. Comput. Chem.* **2014**, *35*, 1997–2004. [CrossRef] [PubMed]
38. Lee, J.; Cheng, X.; Swails, J.M.; Yeom, M.S.; Eastman, P.K.; Lemkul, J.A.; Wei, S.; Buckner, J.; Jeong, J.C.; Qi, Y.; et al. CHARMM-GUI Input Generator for NAMD, GROMACS, AMBER, OpenMM, and CHARMM/OpenMM Simulations Using the CHARMM36 Additive Force Field. *J. Chem. Theory Comput.* **2016**, *12*, 405–413. [CrossRef]
39. Huang, J.; Rauscher, S.; Nawrocki, G.; Ran, T.; Feig, M.; de Groot, B.L.; Grubmuller, H.; MacKerell, A.D., Jr. CHARMM36m: An improved force field for folded and intrinsically disordered proteins. *Nat. Methods* **2017**, *14*, 71–73. [CrossRef]

40. Vanommeslaeghe, K.; Hatcher, E.; Acharya, C.; Kundu, S.; Zhong, S.; Shim, J.; Darian, E.; Guvench, O.; Lopes, P.E.M.; Vorobyov, I.; et al. CHARMM general force field: A force field for drug-like molecules compatible with the CHARMM all-atom additive biological force fields. *J. Comput. Chem.* **2009**, *31*, 671–690. [CrossRef] [PubMed]
41. Jo, S.; Kim, T.; Im, W. Automated Builder and Database of Protein/Membrane Complexes for Molecular Dynamics Simulations. *PLoS ONE* **2007**, *2*, e880. [CrossRef] [PubMed]
42. Nosé, S. A molecular dynamics method for simulations in the canonical ensemble. *Mol. Phys.* **1984**, *52*, 255–268. [CrossRef]
43. Parrinello, M.; Rahman, A. Polymorphic transitions in single crystals: A new molecular dynamics method. *J. Appl. Phys.* **1981**, *52*, 7182–7190. [CrossRef]
44. Essmann, U.; Perera, L.; Berkowitz, M.L.; Darden, T.; Lee, H.; Pedersen, L.G. A smooth particle mesh Ewald method. *J. Chem. Phys.* **1995**, *103*, 8577–8593. [CrossRef]
45. Humphrey, W.; Dalke, A.; Schulten, K. VMD: Visual molecular dynamics. *J. Mol. Graph.* **1996**, *14*, 33–38. [CrossRef]
46. Abraham, M.J.; Murtola, T.; Schulz, R.; Páll, S.; Smith, J.; Hess, B.; Lindahl, E. GROMACS: High performance molecular simulations through multi-level parallelism from laptops to supercomputers. *SoftwareX* **2015**, *1-2*, 19–25. [CrossRef]
47. Andreyev, A.Y.; Bondareva, T.O.; Dedukhova, V.I.; Mokhova, E.N.; Skulachev, V.P.; Tsofina, L.M.; Volkov, N.I.; Vygodina, T.V. The ATP/ADP-antiporter is involved in the uncoupling effect of fatty acids on mitochondria. *Eur. J. Biochem.* **1989**, *182*, 585–592. [CrossRef] [PubMed]
48. Schonfeld, P. Does the function of adenine nucleotide translocase in fatty acid uncoupling depend on the type of mitochondria? *FEBS Lett.* **1990**, *264*, 246–248. [CrossRef]
49. Hilse, K.E.; Rupprecht, A.; Egerbacher, M.; Bardakji, S.; Zimmermann, L.; Wulczyn, A.; Pohl, E.E. The Expression of Un-coupling Protein 3 Coincides with the Fatty Acid Oxidation Type of Metabolism in Adult Murine Heart. *Front. Physiol.* **2018**, *9*, 747. [CrossRef]
50. Skárka, L.; Bardová, K.; Brauner, P.; Flachs, P.; Jarkovská, D.; Kopecký, J.; Ostádal, B. Expression of mitochondrial uncoupling protein 3 and adenine nucleotide translocase 1 genes in developing rat heart: Putative involvement in control of mitochondrial membrane potential. *J. Mol. Cell. Cardiol.* **2003**, *35*.
51. Bertholet, A.M.; Chouchani, E.T.; Kazak, L.; Angelin, A.; Fedorenko, A.; Long, J.Z.; Vidoni, S.; Garrity, R.; Cho, J.; Terada, N.; et al. H+ transport is an integral function of the mitochondrial ADP/ATP carrier. *Nat. Cell Biol.* **2019**, *571*, 515–520. [CrossRef] [PubMed]
52. Brustovetsky, N.; Klingenberg, M. The reconstituted ADP/ATP carrier can mediate H+ transport by free fatty acids, which is further stimulated by mersalyl. *J. Biol. Chem.* **1994**, *269*, 27329–27336. [CrossRef]
53. Nelson, D.; Lawson, J.E.; Klingenberg, M.; Douglas, M.G. Site-directed Mutagenesis of the Yeast Mitochondrial ADP/ATP Translocator: Six Arginines and One Lysine are Essential. *J. Mol. Biol.* **1993**, *230*, 1159–1170. [CrossRef] [PubMed]
54. Heidkämper, D.; Müller, V.; Nelson, D.; Klingenberg, M. Probing the Role of Positive Residues in the ADP/ATP Carrier from Yeast. The Effect of Six Arginine Mutations on Transport and the Four ATP versus ADP Exchange Modes. *Biochemistry* **1996**, *35*, 16144–16152. [CrossRef] [PubMed]
55. Pebay-Peyroula, E.; Dahout-Gonzalez, C.; Kahn, R.; Trézéguet, V.; Lauquin, G.J.-M.; Brandolin, G. Structure of mitochondrial ADP/ATP carrier in complex with carboxyatractyloside. *Nat. Cell Biol.* **2003**, *426*, 39–44. [CrossRef]
56. Wang, Y.; Tajkhorshid, E. Electrostatic funneling of substrate in mitochondrial inner membrane carriers. *Proc. Natl. Acad. Sci. USA* **2008**, *105*, 9598–9603. [CrossRef] [PubMed]
57. Dehez, F.; Pebay-Peyroula, E.; Chipot, C. Binding of ADP in the Mitochondrial ADP/ATP Carrier Is Driven by an Electrostatic Funnel. *J. Am. Chem. Soc.* **2008**, *130*, 12725–12733. [CrossRef]
58. Parker, V.H. Uncouplers of rat-liver mitochondrial oxidative phosphorylation. *Biochem. J.* **1965**, *97*, 658–662. [CrossRef] [PubMed]
59. Pohl, E.E.; Rupprecht, A.; Macher, G.; Hilse, K.E. Important Trends in UCP3 Investigation. *Front. Physiol.* **2019**, *10*, 470. [CrossRef]
60. Skulachev, V.P. Fatty acid circuit as a physiological mechanism of uncoupling of oxidative phosphorylation. *FEBS Lett.* **1991**, *294*, 158–162. [CrossRef]
61. Klingenberg, M. Wanderings in bioenergetics and biomembranes. *Biochim. Biophys. Acta* **2010**, *1797*, 579–594. [CrossRef]
62. Kreiter, J.; Skulj, S.; Brkljaca, Z.; Zuna, K.; Vazdar, M.; Pohl, E.E. The transport of fatty acid anions across the inner mitochondrial membrane by the adenine nucleotide translocase. *Eur. Biophys. J.* **2021**, *50* (Suppl. 1), S57.
63. Langdown, M.L.; Smith, N.D.; Sugden, M.C.; Holness, M.J. Excessive glucocorticoid exposure during late intrauterine development modulates the expression of cardiac uncoupling proteins in adult hypertensive male offspring. *Pflügers Archiv.* **2001**, *442*, 248–255. [CrossRef]
64. Hilse, K.E.; Kalinovich, A.V.; Rupprecht, A.; Smorodchenko, A.; Zeitz, U.; Staniek, K.; Erben, R.G.; Pohl, E.E. The expression of UCP3 directly correlates to UCP1 abundance in brown adipose tissue. *Biochim. Biophys. Acta Bioenerg.* **2016**, *1857*, 72–78. [CrossRef]
65. Samartsev, V.N.; Smirnov, A.V.; Zeldi, I.P.; Markova, O.V.; Mokhova, E.N.; Skulachev, V.P. Involvement of aspartate/glutamate antiporter in fatty acid-induced uncoupling of liver mitochondria. *Biochim. Biophys. Acta* **1997**, *1319*, 251–257. [CrossRef]
66. Wieckowski, M.; Wojtczak, L. Involvement of the Dicarboxylate Carrier in the Protonophoric Action of Long-Chain Fatty Acids in Mitochondria. *Biochem. Biophys. Res. Commun.* **1997**, *232*, 414–417. [CrossRef] [PubMed]

64. Hilse, K.E.; Kalinovich, A.V.; Rupprecht, A.; Smorodchenko, A.; Zeitz, U.; Staniek, K.; Erben, R.G.; Pohl, E.E. The expression of UCP3 directly correlates to UCP1 abundance in brown adipose tissue. *Biochim. Biophys. Acta (BBA) Bioenerg.* **2016**, *1857*, 72–78, doi:10.1016/j.bbabio.2015.10.011.
65. Samartsev, V.N.; Smirnov, A.V.; Zeldi, I.P.; Markova, O.V.; Mokhova, E.N.; Skulachev, V.P. Involvement of aspartate/glutamate antiporter in fatty acid-induced uncoupling of liver mitochondria. *Biochim. Biophys. Acta* **1997**, *1319*, 251–257.
66. Wieckowski, M.; Wojtczak, L. Involvement of the Dicarboxylate Carrier in the Protonophoric Action of Long-Chain Fatty Acids in Mitochondria. *Biochem. Biophys. Res. Commun.* **1997**, *232*, 414–417, doi:10.1006/bbrc.1997.6298.
67.
68. Engstová, H.; Žáčková, M.; Růžička, M.; Meinhardt, A.; Hanuš, J.; Krämer, R.; Jezek, P. Natural and Azido Fatty Acids Inhibit
69. Phosphate Transport and Activate Fatty Acid Anion Uniport Mediated by the Mitochondrial Phosphate Carrier. *J. Biol. Chem.*
70. **2001**, *276*, 4683–4691. [CrossRef] [PubMed]
68. Yu, X.X.; Lewin, D.A.; Zhong, A.; Brush, J.; Shemin, R.; Shenvood, S.W.; Adams, S.H. Overexpression of the human
71. Yu, X.X.; Lewin, D.A.; Zhong, A.; Brush, J.; Shemin, R.; Sherwood, S.W.; Adams, S.H. Overexpression of the human mitochondrial carrier homologue in HEK-293 cells: contrast with the unique cold-induced mitochondrial carrier CGI-69. *Biochem. J.* **2001**, *353*, 369–375. [CrossRef]

2.3. Membrane Lipid Reshaping Underlies Oxidative Stress Sensing by the Mitochondrial Proteins UCP1 and ANT1.

antioxidants

MDPI

Article

Membrane Lipid Reshaping Underlies Oxidative Stress Sensing by the Mitochondrial Proteins UCP1 and ANT1

Olga Jovanović [1], Ksenia Chekashkina [2,3], Sanja Škulj [4], Kristina Žuna [1], Mario Vazdar [5], Pavel V. Bashkirov [2,6] and Elena E. Pohl [1,*]

1 Institute of Physiology, Pathophysiology and Biophysics, Department of Biomedical Sciences, University of Veterinary Medicine Vienna, 1210 Vienna, Austria
2 Federal Research and Clinical Center of Physical-Chemical Medicine, 119435 Moscow, Russia
3 A.N. Frumkin Institute of Physical Chemistry and Electrochemistry, 119071 Moscow, Russia
4 Department of Chemistry, Faculty of Science, University of Zagreb, 10000 Zagreb, Croatia
5 Department of Mathematics, University of Chemistry and Technology, 16628 Prague, Czech Republic
6 Scientific Research Institute of System Biology and Medicine, 117246 Moscow, Russia
* Correspondence: elena.pohl@vetmeduni.ac.at

Abstract: Oxidative stress and ROS are important players in the pathogenesis of numerous diseases. In addition to directly altering proteins, ROS also affects lipids with negative intrinsic curvature such as phosphatidylethanolamine (PE), producing PE adducts and lysolipids. The formation of PE adducts potentiates the protonophoric activity of mitochondrial uncoupling proteins, but the molecular mechanism remains unclear. Here, we linked the ROS-mediated change in lipid shape to the mechanical properties of the membrane and the function of uncoupling protein 1 (UCP1) and adenine nucleotide translocase 1 (ANT1). We show that the increase in the protonophoric activity of both proteins occurs due to the decrease in bending modulus in lipid bilayers in the presence of lysophosphatidylcholines (OPC and MPC) and PE adducts. Moreover, MD simulations showed that modified PEs and lysolipids change the lateral pressure profile of the membrane in the same direction and by the similar amplitude, indicating that modified PEs act as lipids with positive intrinsic curvature. Both results indicate that oxidative stress decreases stored curvature elastic stress (SCES) in the lipid bilayer membrane. We demonstrated that UCP1 and ANT1 sense SCES and proposed a novel regulatory mechanism for the function of these proteins. The new findings should draw the attention of the scientific community to this important and unexplored area of redox biochemistry.

Keywords: lipid shape; bending moduli; lateral pressure profile; reactive aldehydes; mitochondrial membrane protein; lipid–protein interaction; stored curvature elastic stress; protonophoric function

Citation: Jovanović, O.; Chekashkina, K.; Škulj, S.; Žuna, K.; Vazdar, M.; Bashkirov, P.V.; Pohl, E.E. Membrane Lipid Reshaping Underlies Oxidative Stress Sensing by the Mitochondrial Proteins UCP1 and ANT1. *Antioxidants* **2022**, *11*, 2314. https://doi.org/10.3390/antiox11122314

Academic Editor: Stanley Omaye

Received: 13 October 2022
Accepted: 18 November 2022
Published: 23 November 2022

1. Introduction

Lipid heterogeneity, observed between the membranes of cells and cell organelles, as well as between membrane leaflets and subdomains, is essential for proper cell functioning [1–5]. The most abundant lipids in cell membranes are phospholipids. Variations in their structure lead to different shapes, which is related to their basic property, intrinsic lipid curvature (C_0) [6–8]. Phosphatidylglycerol and phosphatidylcholine (PC), which spontaneously assemble into lamellar bilayer structures at physiological concentration of ions in water, have a cylindrical shape and negligible C_0 (≈0). Non-bilayer lipids or conical lipids such as phosphatidylethanolamine (PE; $C_0 < 0$) and lysolipids (lysoPC; $C_0 > 0$) form highly curved lipid structures such as HII phase (PE) or micelles. PE accounts for approximately 25% of all membrane lipids that significantly affect the mechanical properties of membranes [9,10].

The embedding of conical lipids into a flat monolayer composed of cylindrical lipids modifies the lateral pressure profile (LPP) so that the bending moment produced by LPP in the monolayer is no longer zero [11]. The bending rigidity, quantified by the bending

modulus, k, is an intrinsic mechanical material constant that defines the amount of energy required to deform a membrane out of the spontaneous state [12]. Membrane bending rigidity is critical for membrane remodeling during vesicular transport, exocytosis, and endocytosis. Maintaining the flatness of the lipid monolayer containing conical lipids leads to the induction of the stored elastic curvature stress (SCES) in the bilayer membrane [13]. SCES induced by PE supports the docking and insertion of membrane-associated/peripheral proteins [10,14,15], membrane budding [16], and membrane remodeling [17,18]. SCES is also suggested to influence the functioning of transmembrane proteins. However, only a few studies have shown this relationship [13,19–24].

The role of conical lipids is especially apparent in the inner mitochondrial membrane (IMM), which contains the highest percentage of phospholipids with a negative C_0 (38−45% PE and 15−25% cardiolipin [CL]) [25,26]. Their shape supports the characteristic architecture of the IMM, which is necessary for the proper functioning of the mitochondrion [27–30]. Because PE senses membrane curvature, the curvature-driven redistribution leads to its accumulation in strongly concave regions [31–34]. As an example, CL and PE support adenosine 5-triphosphate (ATP) synthase dimer formation, generating strong membrane curvature on the top of the cristae and thereby potentiating protein activity [35,36].

Under oxidative stress conditions, membrane lipids undergo shape transformation. The products of reactive oxygen species (ROS), which include the biologically important reactive aldehydes (RAs) 4-hydroxy-2-nonenal (HNE) and 4-oxo-2-nonenal, covalently modify the PE headgroup to form RA-PE adducts [37–40]. RA-PE adducts increase the protonophoric activity of mitochondrial uncoupling protein 1 (UCP1), an essential player in non-shivering thermogenesis [37]. Based on results obtained by mass spectrometry and molecular dynamic (MD) simulations, we previously suggested that the formation of RA-PE adducts reshapes PE, thereby changing the intrinsic curvature of this lipid [41]. Another contribution to the transformation of the lipid shape during oxidative stress in mitochondria comes from the amplified action of membrane-bound phospholipase A2 (mPLA2) [42,43], which converts membrane lipids to lysolipids ($C_0 > 0$) and free fatty acids (FAs). The released FAs represent the raw material for the production of more RAs, which then target the headgroup of the PE and form more RA-PE adducts. As a result of these events, the ratio of lipids with opposite shapes in IMM can rapidly alter, leading to a modification of the LPP and the bending rigidity of the IMM [44].

We hypothesized that the SCES change caused by the lipid shape transformation is a crucial event by which IMM proteins (particularly uncoupling proteins) respond rapidly to oxidative stress. To investigate the impact of ROS-modified lipids on mitochondrial protein function, we combined experimental measurements of membrane elastic properties and total conductance of membranes reconstituted with recombinant UCP1 and ANT1 with calculations of membrane LPPs using MD simulations.

2. Materials and Methods

2.1. Chemicals

1,2-dioleoyl-sn-glycero-3-phosphocholine (DOPC), 1,2-dioleoyl-sn-glycero-3-phosphoethanolamine (DOPE), 1-oleoyl-2-hydroxy-sn-glycero-3-phosphocholine (OPC), bovine heart cardiolipin (CL), arachidonic acid (AA), hexane, hexadecane, KCl, HEPES, EDTA, Na_2SO_4, MES, Tris, adenosine 5-triphosphate (ATP), and guanosine 5-triphosphate (GTP) were purchased from Sigma-Aldrich (Munich, Germany). MPC (1-myristoyl-2-hydroxy-sn-glycero-3-phosphocholine) was obtained from Avanti Polar Lipids (Alabaster, AL, USA). Plain silica beads (22-µm diameter) were from Microspheres-Nanospheres (Corpuscular Co., Cold Spring, NY, USA). Chloroform was purchased from Carl Roth (Karlsruhe, Germany). 4-oxo-trans-2-nonenal (4-ONE) and 4-hydroxy-trans-2-nonenal (4-HNE) were purchased from Cayman Chemical (Ann Arbor, MI, USA) or synthesized as previously described [45].

2.2. Reconstitution of UCP1 and ANT1 in Liposomes

Recombinant uncoupling protein (murine UCP1) and adenine nucleotide translocase 1 (murine ANT1) were purified from *E. coli* inclusion bodies and reconstituted into liposomes made of DOPC, DOPE and CL as previously described [46,47]. AA (20:4, ω6), at a concentration of 15 mol%, and lyso-PCs (OPC and MPC), at the concentrations indicated in the figure descriptions, were added to the lipid phase before membrane formation.

2.3. Formation of the Planar Lipid Bilayer Membranes and Measurements of the Membrane Electrical Parameters

Solvent-depleted planar lipid bilayers for the experiments with the recombinant proteins UCP1 and ANT1 were formed from proteoliposomes at the tip of a disposable plastic pipette [48]. The disposable container was filled with 0.75 mL buffer containing 50 mM Na_2SO_4, 10 mM MES, 10 mM Tris, and 0.6 mM EGTA at pH 7.32 and T = 305 K. Membrane formation and bilayer quality were monitored by capacitance measurements. Current–voltage (*I*–*V*) characteristics were measured by a patch-clamp amplifier (EPC 10; HEKA Elektronik Dr Schulze GmbH, Lambrecht, Germany). Total membrane conductance G_m was calculated from a linear fit of experimental data (*I*) at applied voltages (*V*) in the range of −50 mV to 50 mV [49]. The relative conductance, G_{rel}, was calculated according to Equation (1):

$$G_{rel} = \frac{G_m - G_0}{G_0 - G_{AA}} \quad (1)$$

where G_m and G_0 are the total membrane conductance of the lipid membranes reconstituted with transmembrane protein and arachidonic acid (*AA*), with or without lysolipids, respectively, while G_{AA} is the total membrane conductance of the lipid membranes reconstituted with AA alone.

2.4. Measurements of the Membrane Elastic Parameters

Bilayer lipid membranes (BLMs) for the experiments shown in Figure 1 were formed by applying the "painting" technique to mesh openings [50]. In brief, the openings were pretreated with a small drop of lipid mixture (10 mg/mL total lipid) dissolved in decane:octane (1:1 *v*/*v*). The solvents were evaporated under a stream of argon. Then, a small amount of the lipid mixture dissolved in squalene (20–30 mg/mL, total lipid) was painted on the openings of the grid fixed at a small distance from the bottom of a Petri dish filled with a buffer solution. BLMs formed spontaneously after the excess lipid solution was forced to the periphery, forming a "toroidal meniscus"—a reservoir that maintains the lateral tension of the lipid bilayer (Figure 1A). BLMs were made of DOPC, DOPE, CL, and OPC in the ratios indicated in the figures. The experimental chamber was filled with buffer containing 100 mM KCl, 10 mM HEPES, and 1 mM EDTA at pH 7 and room temperature (295 K). We added RAs to the buffer solution, which surrounded the formed BLM in the container and incubated for 15 min, then the nanotubes were pooled.

Nanotubes (*NT*s) were pulled from BLMs vertically using a fire-polished borosilicate patch pipette with a tip diameter of ~1 µm filled with the same buffer as the experimental chamber. The tip of the pipette was placed in close contact with the BLM. The hydrostatic pressure pulse ruptured the small membrane patch isolated inside the pipette while the pipette rim remained in contact with the parent BLM. The cylindrical *NT* formed spontaneously when the pipette was slowly moved away from the membrane [51]. A precise nanopositioning system (piezo linear actuator and Actuator Controller ESA-CSA, Newport, Irvine, CA, USA) controlled the vertical position of the pipette (Δ*L*). The formation of the *NT* was detected by conductance measurements using Ag/AgCl electrodes placed in the pipette and bath solution. The *NT* radius was recalculated from the ion current *I*, measured by an Axopatch 200 B amplifier (Molecular Devices, Sunnyvale, CA, USA), and acquired by a low-noise data acquisition system (Axon Digidata 1550, Molecular Devices, Sunnyvale, CA, USA). The amplifier was set in the voltage-clamp mode to measure the ion conductance $G = I/U$. We used the hyperbolic approximation of *G* (Δ*L*) (Figure 1B) to

fit the measured conductance dependence [50]. Briefly, the conductance of the *NT* lumen, G_{NT}, was obtained as the difference between the *G* and the patch leakage conductance, G_p ($G_p = G$ at the infinite *NT* length): $G_{NT} = G - G_p$. The vertical asymptotes of the fit provided the length measurement offset, which should be subtracted from ΔL to measure the length of *NT* (L_{NT}). *NT* radius (r_{NT}) was determined as given in Equation (2),

$$r_{NT} = \langle \sqrt{\frac{G_{NT} L_{NT} \rho NT}{\pi}} \rangle \quad (2)$$

where the ρ_{NT} denotes the specific electrical resistance of the electrolyte inside *NT* lumen. For electrically neutral *NT*, we considered ρ_{NT} to be equal to the bulk value, ρ_0. ρ_0 was 1 Ohm*m for the buffer we used (100 mM KCl). For CL-containing membranes the impact of electrical double layer on total ion concentration inside *NT* was taken into consideration [50].

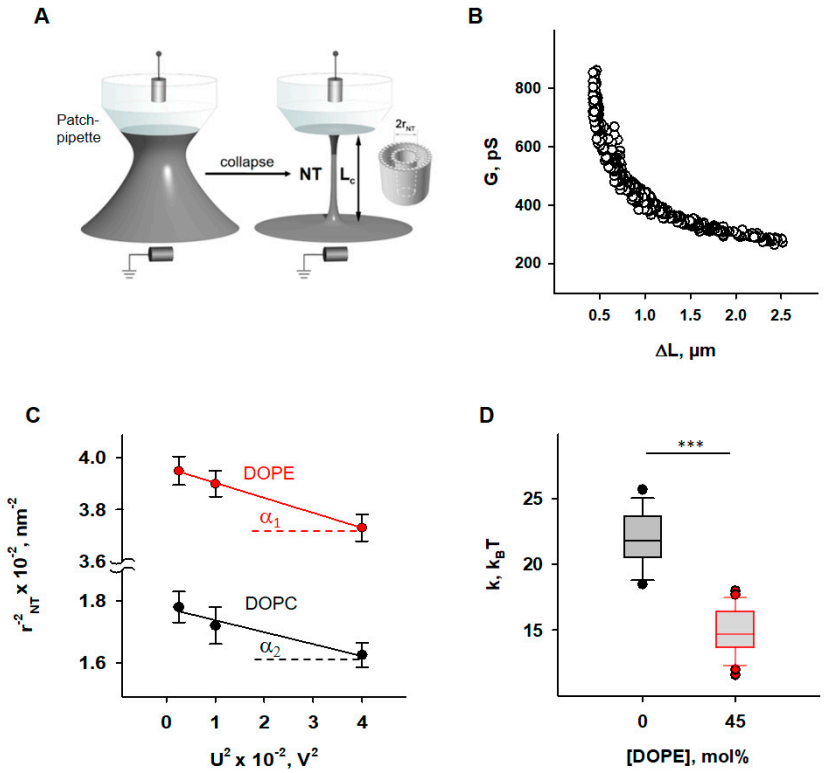

Figure 1. Determination of the elastic parameters of the lipid bilayer membrane based on nanotube (*NT*) pulling. (**A**) Scheme of *NT*s pulled from a bilayer lipid membrane (grey) and held by a patch-pipette (white). A voltage applied to the ends of the *NT*s (U) induces an ion current (I_{NT}) flowing through the *NT* interior. (**B**) A representative measurement shows the dependence of measured membrane conductance (G) (black circles) on the *NT* length change (ΔL), required for calculation of the *NT* radius (r_{NT}) (see Methods). (**C**) Dependence r_{NT} on U, obtained for the membrane lipid compositions DOPC:CL 90:10 (black) and DOPC:DOPE:CL 45:45:10 (red). (**D**) Box plot and distribution of the bending modulus, *k*, depending on the molar concentration of the phosphatidylethanolamine (DOPE). The buffer solution contained 100 mM KCl, 10 mM HEPES, and 1 mM EDTA at pH 7.0 and 295 K. Data points represent the mean and standard deviation from more than 10 independent experiments. *** $p < 0.001$, *t*-test.

Bending modulus, *k*, and lateral tension, *σ*, were measured as previously described [50]. Briefly, the expansion of *NT* under the action of electrical field [52] was used. The same potential difference, *U*, that is applied to the ends of the *NT* to induce an ionic current through its lumen leads to a transmembrane potential in the nanotube wall, which reduces the lateral tension of the nanotube membrane according to Lippmann's law of electrocapillarity. Since *NT* transmembrane potential grows linearly from 0 at the "BLM" end to *U* at the pipette rim remained in contact with the patent BLM. The cylindrical *NT* formed spontaneously when the pipette was slowly moved away from the membrane [51]. A precise nanopositioning system (piezo linear actuator and Actuator Controller ESA-CSA, Newport) controlled the vertical position of the pipette (ΔL). The formation of the *NT* was detected by conductance measurements using Ag/AgCl electrodes placed in the pipette and bath solution. The *NT* radius was recalculated from the ion current *I*, measured by an Axopatch 200 B amplifier (Molecular Devices, Sunnyvale, CA), and acquired by a low-

at the "pipette's tip" end of the *NT* (Figure 1A), the expansion of *NT* is non-uniform [52]. However, the hyperbolic dependence of *G* (Δ*L*) of such a non-cylindrical *NT* is preserved, and the effective radius determined from the hyperbolic approximation of *G* (Δ*L*) is related to the elastic characteristics of the membrane and the applied voltage by the Equation (3):

$$\frac{1}{(r_{NT}+h)^2} = \frac{2\sigma}{k} - \frac{c_{sp}U^2}{3k} \quad (3)$$

where h = 2 nm is the monolayer thickness and c_{sp}—the specific capacitance of BLM.

$c_{sp} \approx 1$ μF·cm^{-2} for the membranes prepared from lipid solution in squalene [53]. Thus, r_{NT} was measured at different U and the dependence $(r_{NT}+h)^{-2}$ on U^2 was plotted. The linear regression of this plot gave k as the tangent to the slope of the line and σ was determined from the intersection of the line with the ordinate axis (Figure 1C).

2.5. Molecular Dynamics Simulations

We performed molecular dynamics (MD) simulations for lipid bilayers of different compositions—DOPC, DOPC:DOPE (50:50), DOPC:ONE-PE (50:50), and DOPC:OPC (50:50). DOPC, DOPE, ONE-PE Schiff base adduct [37,41], and OPC were described with Slipids force field [54–56]. All missing bonding and non-bonding parameters of lipid molecules in the existing Slipids force field were updated with compatible CHARMM36 parameters [57] when needed. Atomic charges were recalculated by the standard Slipids procedure using the Merz–Singh–Kollman scheme [58], which is composed of B3LYP/6-31G (d) geometry optimization of the molecule of interest, a subsequent single point ESP charge calculation using the B3LYP/cc-pVTZ method, and a final charge refinement with the RESP method [59].

Bilayers containing 128 lipid molecules were constructed from two monolayers containing 64 individual lipid molecules, with symmetrical lipid distribution across the leaflets in mixed systems. All systems were placed in a unit cell and solvated by about 12,000 water molecules using the TIP3P water model [60]. The unit cell size was approximately 6.5 × 6.5 × 12.0 nm. Three-dimensional periodic boundary conditions were used with long-range electrostatic interactions beyond the non-bonded cut-off of 1 nm using the particle-mesh Ewald procedure [61] with a Fourier spacing of 1.2 nm. Real-space Coulomb interactions were cut off at 1 nm, while van der Waals interactions were cut-off at 1.4 nm. We performed 100 ns MD simulations with semi-isotropic pressure coupling, independently in the directions parallel and perpendicular to the bilayer's normal using the Parrinello–Rahman algorithm [62]. The pressure was set to 1 bar, and a coupling constant of 10 ps^{-1} was used. All simulations were performed at 310 K and controlled with the Nose–Hoover thermostat [63] independently for the lipid–water sub-systems, with a coupling constant of 0.5 ps^{-1}. Bond lengths within the simulated molecules were constrained using the LINCS [64]. Water bond lengths were kept constant by using the SETTLE method [65]. Equations of motion were integrated using the leap-frog algorithm with a time step of 2 fs. For the LPP, a custom version of GROMACS-LS package [66,67] was used to re-run trajectories and output local stress tensors. Because long-range electrostatics via PME is not available in GROMACS-LS, an increased cut-off distance of 2 nm was used for Coulomb interaction calculations as suggested by the package developers [66].

2.6. Statistics

Data from the electrophysiological measurements are displayed as mean ± standard deviation of at least three technical replicates (on three different days). Each replicate was the mean membrane conductance of three to ten bilayer membranes formed on the same day. Error bars for pressure profiles of lipids were calculated as the difference between symmetrized and unsymmetrized pressure profiles in different leaflets. Smoothed data were obtained from the average of two points.

3. Results

3.1. Impact of DOPE on Membrane Elastic Parameters and SCES

First, we examined how the presence of PE influences the elastic properties of lipid bilayer membranes. To do so, we measured the radii (r_{NT}) of nanotubes (*NT*s) pulled from BLM at different voltage biases (U) applied to the *NT* interior (Figure 1A).

To evaluate the impact of PE on membrane elastic parameters, we compared *NT* pulled from BLM made of either (i) DOPC:DOPE:CL (45:45:10 mol%), mimicking the IMM, or (ii) DOPC:CL (90:10 mol%), as a model of a PE-free membrane. The r_{NT} was measured for both lipid compositions at U values varying from 50 to 200 mV. The membrane bending rigidity modulus (k) and lateral tension (σ) of BLMs were calculated from the linear regression of $(r_{NT}+h)^{-2}\left(U^2\right)$ according to Equation (3) (see Section 2).

We found that membranes containing 45 mol% DOPE were considerably less resistant to bending than DOPE-free membranes (Figure 1D). The measured bending modulus decreased from k = (22.1 ± 2.0) k_BT for PE-free membranes to k = (4.8 ± 1.8) k_BT for PE-containing membranes.

This observation qualitatively confirmed the previously reported effect of membrane softening by PE, demonstrating that the addition of 30 mol% DOPE significantly reduced the k [68]. At the molecular level, the effect was attributed to the curvature-induced redistribution of DOPE between *NT* monolayers and the reservoir membrane during *NT* formation. Conical lipids with a pronounced $C_0 < 0$ tend to accumulate in the inner leaflet and to be deposited from the outer monolayer of the highly curved *NT* membrane, which remained connected to a flat reservoir membrane during the measurement [32,33]. Reduction in the apparent bending rigidity modulus, k, due to curvature-driven DOPE redistribution in the membrane can be estimated according to the Equation (4) [69]:

$$k = \frac{\widetilde{k}}{1 + \frac{a\widetilde{k}C_{0,DOPE}^2\,\varphi(1-\varphi)}{2k_BT}} \tag{4}$$

where $\widetilde{k}$ is the bending modulus of membranes with a restricted PE curvature-composition coupling, a—the area per lipid (about 0.7 nm^2), $C_{0,DOPE}$—the intrinsic curvature of DOPE, and φ—the molar fraction of DOPE in the lipid reservoir.

For PE-containing membranes, we considered $\widetilde{k}$ equal to the bending modulus measured for PE-free membranes and characteristic of DOPC membranes [50]. Using Equation (4), we calculated $C_{0,DOPE} \approx -0.45$ nm^{-1}, which is in agreement with previously published data obtained for DOPE in the inverted HII phase [70], confirming the reduction in apparent bending rigidity of PE-containing membrane due to PE curvature-composition coupling [44]. At the same time, lateral tension in PE-containing membranes was almost twice as high (σ = (1.4 ± 0.4)·mN·m^{-1} versus σ = (0.8 ± 0.3) mN·m^{-1} in PE-free membrane). BLM is an open system, in which a lipid bilayer is connected to a large lipid reservoir that defines the chemical potentials of the lipids. The lateral tension, σ, is related to the surface free energy, required for keeping lipids in a flat bilayer or the same SCES = $\frac{1}{2}kC_m^2$, where C_m is the average spontaneous curvature of the lipid mixture. Thus, the lateral tension of BLM should increase with DOPE content by the SCES magnitude caused by the insertion of conical PE lipids into a flat membrane. Indeed, we found that σ gradually increases in DOPC membranes with increasing DOPE content, so that it almost doubles at 50 mol% DOPE, confirming the direct contribution of SCES to the lateral tension of membranes connected to the lipid reservoir.

We considered the contribution of the CL curvature-composition coupling to the apparent bending rigidity to be the same in both types of the membrane (PE-containing and PE-free) because of its lower concentration (10 mol% of total lipid composition) and smaller C_0 ($C_{0,CL} \approx -0.15$ nm^{-1} [70]) compared to PE.

membranes connected to the lipid reservoir.

We considered the contribution of the CL curvature-composition coupling to the a parent bending rigidity to be the same in both types of the membrane (PE-containing a PE-free) because of its lower concentration (10 mol% of total lipid composition) a smaller C_0 ($C_{0,CL} \approx -0.15$ nm^{-1} [70]) compared to PE.

3.2. Reactive Aldehydes Modify the Elastic Properties of the PE-Containing Lipid Bilayer Membranes

3.2. Reactive Aldehydes Modify the Elastic Properties of the PE-Containing Lipid Bilayer Membranes

Next, we studied the effects of the modification of the lipids by RAs [37] on the elastic properties of membranes. We incubated the reservoir membranes of different lipid compositions with a RA (4-hydroxy-2-hexenal [HHE], HNE, or ONE) at the concentrations of 0.5–0.7 mM, which are in accordance with the concentrations found under physiological conditions (~0.3 mM) and under oxidative stress (up to 5 mM in cellular membranes) [71,72]. We found that HNE and ONE induced a pronounced reduction in the apparent bending modulus k in DOPE-containing membranes, resulting in k_{HNE} = 11.7 k_BT and k_{ONE} = 7.1 k_BT (Figure 2A and Supplementary Figure S1A). HHE had no detectable impact on k (Figures 2A and S1A). We explained the lack of the HHE effect by its weaker adsorption to the lipid membrane [37]. It is noteworthy that in the PE-free membranes, none of the RAs caused a measurable change in the bending modulus k (Figure 2B and Supplementary Figure S1B).

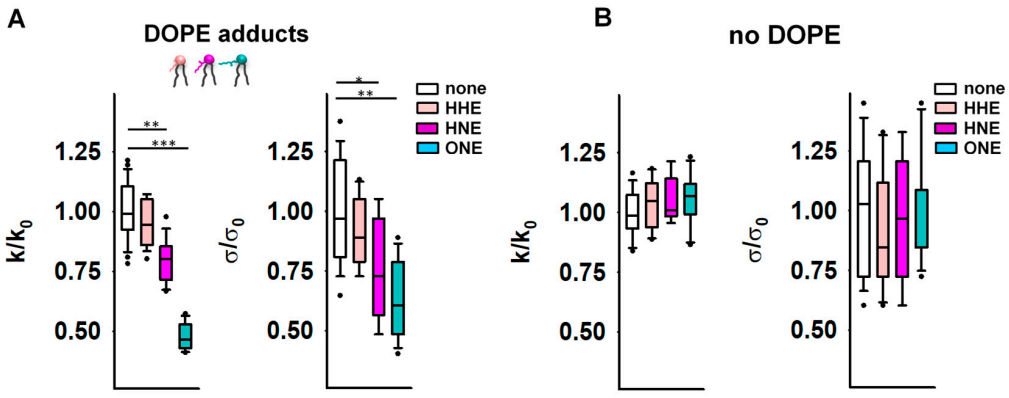

Figure 2. Elastic properties of the lipid bilayer membrane in the presence of reactive aldehydes (RAs). (**A**,**B**) Relative bending rigidity k/k_0 and relative lateral tension σ/σ_0 for lipid membranes composed of DOPC:DOPE:CL 45:45:10 in (**A**) and DOPC:CL 90:10 in (**B**), incubated with the RAs 4-hydroxy-2-hexenal (HHE), 4-hydroxy-2-nonenal (HNE), and 4-oxo-2-nonenal (ONE). k_0 and σ_0 are bending modulus and lateral tension in the absence of RAs, respectively. RAs were added in a concentration range of 0.5–0.7 mM. Buffer composition: 100 mM KCl, 10 mM HEPES, 1 mM EDTA pH = 7.0, T = 295 K. Data points represent mean and standard deviation from more than 10 independent experiments. * $p < 0.05$; ** $p < 0.01$; *** $p < 0.001$, *t*-test.

Figure 2. Elastic properties of the lipid bilayer membrane in the presence of reactive aldehyd (RAs). (**A**,**B**) Relative bending rigidity k/k_0 and relative lateral tension σ/σ_0 for lipid membranes co posed of DOPC:DOPE:CL 45:45:10 in (**A**) and DOPC:CL 90:10 in (**B**), incubated with the RAs hydroxy-2-hexenal (HHE), 4-hydroxy-2-nonenal (HNE), and 4-oxo-2-nonenal (ONE). k_0 and σ_0 bending modulus and lateral tension in the absence of RAs, respectively. RAs were added in a c centration range of 0.5–0.7 mM. Buffer composition: 100 mM KCl, 10 mM HEPES, 1 mM EDTA =7.0, T = 295 K. Data points represent mean and standard deviation from more than 10 independ experiments. * $p < 0.05$; ** $p < 0.01$; *** $p < 0.001$, *t*-test.

Alongside enhanced compliance to bending, we observed a decrease in σ for PE-containing membranes after their incubation with RAs (Figure 2A). Again, this effect was absent in PE-free membranes (Figure 2B). MD simulations predicted a significant alteration of the PE molecular shape caused by its modification by RAs [41]. Such lipid reshaping is highly likely to be the reason for the simultaneous reduction in both the k and σ caused by RAs in PE-containing membranes.

Alongside enhanced compliance to bending, we observed a decrease in σ for PE-co taining membranes after their incubation with RAs (Figure 2A). Again, this effect w absent in PE-free membranes (Figure 2B). MD simulations predicted a significant alte tion of the PE molecular shape caused by its modification by RAs [41]. Such lipid resha ing is highly likely to be the reason for the simultaneous reduction in both the k and caused by RAs in PE-containing membranes.

3.3. OPC Alters the Elastic Properties of the Lipid Bilayer Membrane

Next, we measured the impact of inverted conical lipid 1-hydroxy-2-oleoyl-sn-glycero-3-phosphocholine (OPC; $C_{0,OPC} > 0$) on the elasticity of PE-containing membranes. The presence of OPC mimics the accumulation of lysolipids in the IMM due to increased phospholipase activity in response to oxidative stress [42,43]. Therefore, we measured the changes in the σ and k of DOPC membranes ($C_{0,DOPC} \approx 0$) induced by the addition of DOPE alone or simultaneously with OPC in the molar ratios indicated in the figure descriptions (Figure 3 and Supplementary Figure S1C,D). In these particular studies, we did not add CL to the BLM compositions because we aimed to use lipids whose molecular shapes were as complementary as possible: the absolute C_0 values of DOPE and OPC are practically the same ($C_{0,OPC} = 0.41$ nm^{-1} [70]).

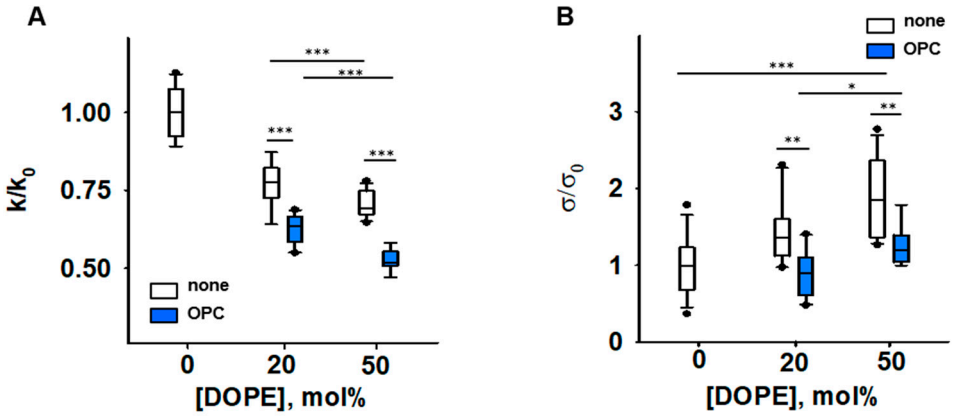

Figure 3. Impact of PE and OPC on the elastic parameters k/k_0 (**A**) and σ/σ_0 (**B**). k_0 and σ_0 are bending modulus and lateral tension in the absence of PE, respectively. Buffer solution contained 100 mM KCl, 10 mM HEPES, 1mM EDTA, pH = 7.0, T = 295 K. Data points represent mean and standard deviation from more than 10 independent experiments. * $p < 0.05$; ** $p < 0.01$; *** $p < 0.001$, *t*-test.

Our results showed that the presence of both conical lipids, OPC and DOPE, made membranes significantly more compliant to bending than DOPC alone, and the effect is potentiated with an increase in DOPE by constant OPC. The bending modulus of a DOPC membrane containing DOPC:DOPE:OPC (60:20:20) mol% was $k = [13.6 \pm 0.63]$ *kT* and lower than that of a DOPC:DOPE (50:50) lipid mixture ($k = [16.7 \pm 1.05]$ *kT*). The bending modulus of the membrane containing DOPC:DOPE:OPC (30:50:20) mol% was the lowest ($k = [11.4 \pm 0.79]$ *kT*). Thus, the OPC-induced changes in elastic parameters of PE-containing membranes (Figure 3) were similar to those caused by the accumulation of PE-RAs adducts in the membrane (Figure 2A). Both OPC and PE-RA adducts diminished the SCES initially produced by PE.

The replacement of DOPC with DOPE led to a concentration-dependent increase in the lateral tension σ in the lipid bilayer membrane (Figure 3B) [44]. Replacement of 20 mol% DOPC with the lysolipid OPC abolished the DOPE-induced increase in σ. This indicates that the effect of OPC on SCES was due to the complementarity of DOPE and OPC shapes (Figure 3B and Supplementary Figure S1D).

3.4. The IMM Proteins UCP1 and ANT1 Sense Stored Curvature Elastic Stress

To test our hypothesis about the impact of SCES on mitochondrial membrane protein function, we performed measurements of total conductance (G_m) of membranes reconstituted with recombinant UCP1 and ANT1. Both proteins are known to assist FA in the transport of protons from the cytosol to the mitochondrial matrix [73–76]. To test the role of lipid shape and thus conditioned SCES in the lipid membrane, we reconstituted UCP1 or ANT1 in lipid bilayer membranes containing lysolipids with pronounced positive individual curvature, 1-myristoyl-2-hydroxy-sn-glycero-3-phosphocholine (MPC; 14:0) and OPC (18:1). Because the acyl chain length defines the intrinsic lipid curvature (the shorter the acyl chain, the higher the individual lipid curvature), we achieved different SCESs in the lipid bilayer membrane at the same concentration of lysolipids.

We compared G_m of membranes formed from (i) DOPE:DOPC:CL (45:45:10 mol%), (ii) MPC:DOPC:DOPE:CL (5:45:40:10 mol%), or (iii) OPC:DOPC:DOPE:CL X:(45 − X/2):(45 − X/2):10, (X = 5, 10, and 12.5 mol%), thereby keeping a constant protein to lipid ratio. In all experiments, the UCP1 and ANT1 activities were measured in the presence of the arachidonic acid (AA; 20:4, ω6), because this fatty acid is released from phospholipids by the activity of phospholipase A2 (PLA2) [77]. With 5 mol% MPC, the G_m (MPC) increased to (124.6 ± 13.7) nS/cm^2, in contrast to the G_m = (79.9 ± 5.3) nS/cm^2 in the absence of MPC (Figure 4A). In the experiments with OPC, we demonstrated a concentration-dependent increase in G_m, from G_m = (89.9 ± 6.7) nS/cm^2 in the absence of OPC to the G_m (OPC) = (158.5 ± 15.8) nS/cm^2 at 12.5 mol% OPC (Figure 4B). We failed to measure the

all experiments, the UCP1 and ANT1 activities were measured in the presence of the arachidonic acid (AA; 20:4, ω6), because this fatty acid is released from phospholipids by the activity of phospholipase A2 (PLA2) [77]. With 5 mol% MPC, the G_m (MPC) increased to (124.6 ± 13.7) nS/cm², in contrast to the G_m = (79.9 ± 5.3) nS/cm² in the absence of MPC (Figure 4A). In the experiments with OPC, we demonstrated a concentration-dependent increase in G_m, from G_m = (89.9 ± 6.7) nS/cm² in the absence of OPC to the G_m (OPC) = (158.5 ± 15.8) nS/cm² at 12.5 mol% OPC (Figure 4B). We failed to measure the conductance of the protein-containing membranes at lysolipid concentrations higher than 5 mol% MPC or 12.5 mol% OPC because of the high membrane instability in the presence of higher amounts of lysolipids. We showed that, in the absence of AA, use of 15 mol% OPC does not affect UCP1-mediated G_m, which means we could compare the G_m (OPC) = (11.2 ± 1.5) nS/cm² of neat lipid bilayer membranes (Supplementary Figure S2A) to the G_m (OPC) = (11.2 ± 1.65) nS/cm² mediated by ANT1 reconstituted in lipid bilayer membranes containing 10 mol% OPC (Figure 4C), was comparable to the $G_{m,UCP1}$ = 1.5, measured for the membranes reconstituted with UCP1 in the presence of OPC (Figure 4B and Supplementary Figure S2).

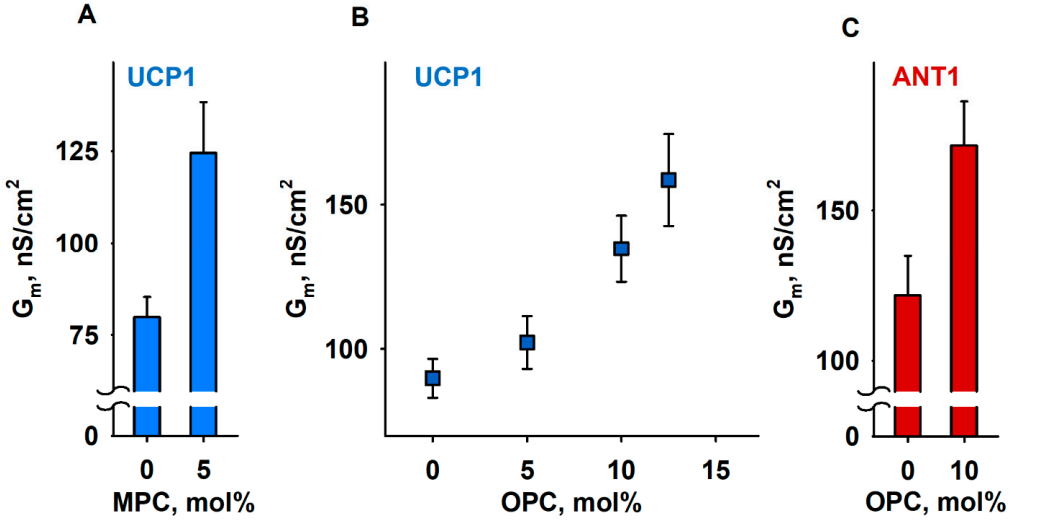

Figure 4. Lipid shape effects UCP1- and ANT1-mediated total membrane conductance (G_m). (**A**,**B**) Dependence of G_m measured in membranes reconstituted with recombinant UCP1 on the concentration of lysolipids MPC (**A**) and OPC (**B**). (**C**) Dependence of G_m measured in membranes reconstituted with recombinant ANT1 on the concentration of OPC. The lipid composition in control experiments was DOPC:DOPE:CL (45:45:10). The specified lysolipid amount (mol%) was used instead of DOPC and DOPE. The concentrations of UCP1 and ANT1 were 4–5 µg/(mg lipid). The concentrations of lipid and AA were 1.5 mg/mL and 15 mol%, respectively. The buffer solution contained 50 mM Na_2SO_4, 10 mM MES, 10 mM Tris, and 0.6 mM EGTA, at pH = 7.32 and T = 305 K. Data points represent means and standard deviation from 3–5 independent experiments.

We tested how SCES affects the inhibition of ANT1 by adding 4 mM ATP to the ANT1 reconstituted with 10% OPC (Supplementary Figure S2C). A slight decrease in the relative ANT1 inhibition (~66% in the presence of OPC vs. ~76% in its absence; Supplementary Figure S2C) suggests that the binding of ATP to R79 of ANT1 [74] was unaffected by SCES.

3.5. Impact of Lipid Shape on the Lateral Pressure Profiles across the Lipid Bilayer Membrane

The results shown above suggest that lipids with different intrinsic curvatures promote activation of the membrane proteins to different extents. Therefore, we used MD simulations to investigate the impact of lipid shape on the LPP in lipid membranes comprising (i) DOPC, (ii) DOPC:ONE-DOPE, (iii) DOPC:OPC, and (iv) DOPC:DOPE (Figures 5A–C and S3). We omitted CL from our MD simulations because (1) CL has low intrinsic curvature ($C_{0,CL} \approx -0.15\ nm^{-1}$) [78], and (2) we focused only on lipids that change shape as a consequence of oxidative stress, such as PE or lysolipids. The ONE-DOPE adduct is chosen as a prototypical Schiff base adduct formed via the reaction of ONE with PE [37], while OPC mimics lysolipids formed due to increased PLA2 activity. The LPP arises in the lipid bilayer membrane due to the repulsive interaction in the lipid headgroup and acyl chain regions and strong attraction at the lipid–water interface.

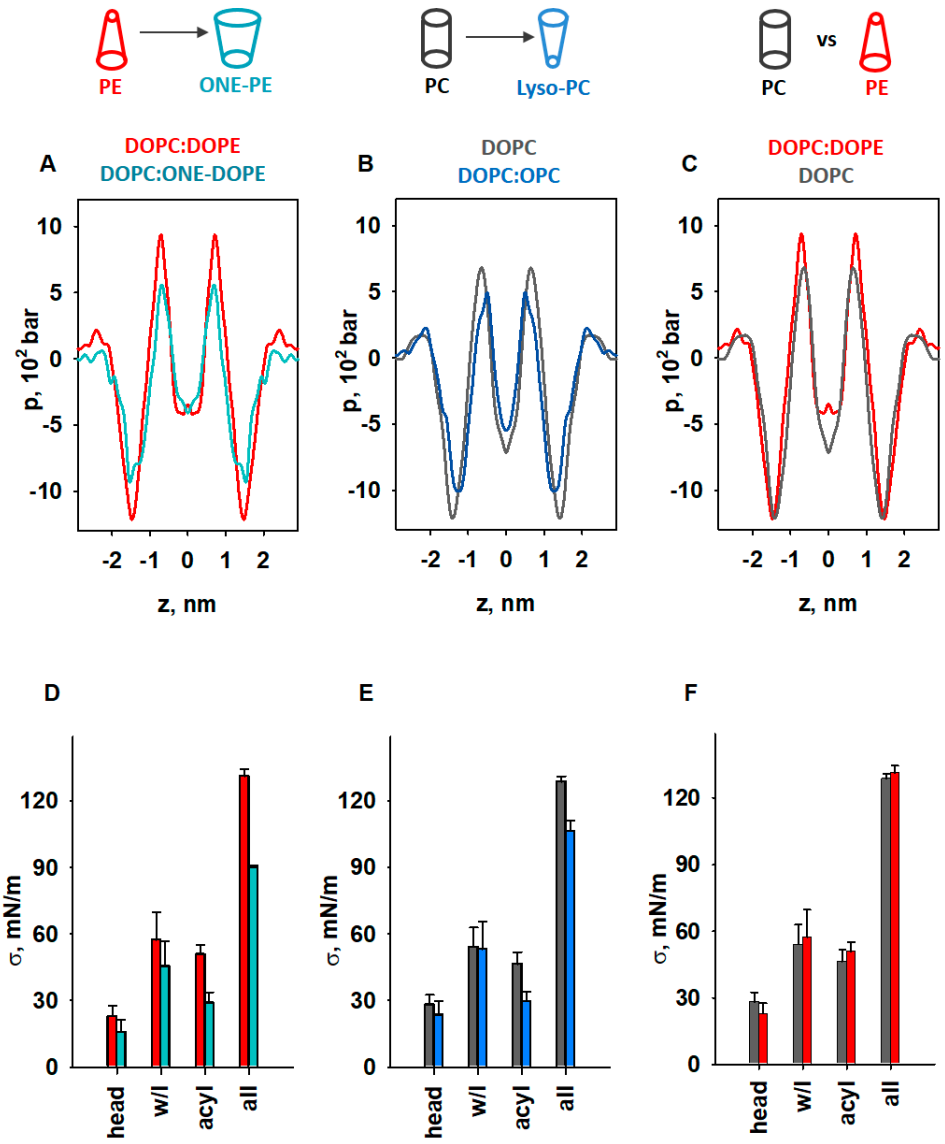

Figure 5. MD simulations of LPP dependency on lipid shape. (**A**–**C**) Impact of lipids with pronounced SC on the LPP, *p*. (**D**–**F**) Comparison of areas below the pressure profiles in the headgroup (head), water–lipid interface (w/l), and acyl chains (acyl) and for the whole bilayer profile (all) for *p* shown in (**A**–**C**). The lipid ratio in bi-component membranes was 50:50 mol%. Color labels: DOPC:DOPE (red), DOPC (grey), DOPC:ONE-DOPE (cyan), and DOPC:OPC (blue).

Our results showed that transformation of the PE headgroup (PE→ONE-PE) reduced the σ value by 29.6%, whereas deletion of the acyl chain (DOPC→OPC)—by 17% (Figure 5D,E). More precisely, the decreases in the σ values for the PE→ONE-PE and DOPC→OPC modifications were 10% and 8.3% in the water–lipid interface region and 43.1% and 37.6% in the acyl chains region (Figure 5D,E). In contrast, PE insertion into the lipid bilayer increased the σ value by only 4.3% in total, and by 11.9% in the acyl chain region (Figure 5F). These observations are in agreement with the data of Zoni et al. [79] that were obtained for LPP's and areas under the curve in the hydrophobic core region for mixed bilayers containing DOPC, DAG, DOPE, and DLPC, where DLPC can be considered a lipid with a positive individual curvature [21].

To highlight the fact that the changes originated from the modified PE headgroup due to the formation of the RA-PE adducts, we compared the LPPs in DOPC:DOPE and DOPC:ONE-DOPE membranes (Figure 5A). A substantial drop in the pressure occurred across the whole membrane profile, in the headgroup region, hydrophobic core, and water–lipid interface. In the membrane–water interface region, $\Delta p_{ONE\text{-}PE} = (p_{PE} - p_{ONE\text{-}PE})$ was equal to 302 bar (25%), while in the acyl chain region, the $\Delta p_{ONE\text{-}PE}$ was 72.5 bar (40%). To evaluate the contribution of lysolipids to the LPP, we compared the DOPC and DOPC:OPC membrane bilayers (Figure 5B). The decrease in lateral pressure due to the replacement of DOPC with OPC occurred at the water–lipid interface and in the acyl tail regions and was slightly pushed to the center of the bilayer. Compared to the LPP of pure DOPC membranes, the lateral pressure in the OPC-containing membranes (Figure 5B) decreased in the membrane–water interface region, from $\Delta p_{OPC} = (p_{DOPC} - p_{OPC}) = 188.6$ bar (15.76%), to $\Delta p_{OPC} = 182$ bar (27%) in the acyl chain region, and to $\Delta p_{OPC} = 38.6$ bar in the center of the bilayer. We also analyzed the effect of DOPE ($C_0 < 0$) on the LPP in the lipid bilayer by

Interestingly, the variability of the lipid acyl chains in the mitochondrion [80] could also influence the modification of the PE headgroup. However, Bacot et al. [39] showed that a reduction in the unsaturation of the mixed acyl chains (18:0/20:4 PE versus 18:0/22:6

comparing the membrane with DOPC membrane with near-neutral curvature ($C_0 \approx 0$). In contrast to OPC and ONE-PE, insertion of DOPE into the lipid bilayer slightly increased the lateral pressure in the acyl chain region ($\Delta p_{DOPE} = (p_{DOPE} - p_{DOPC}) = 256.2$ bar [27.5%]), and slightly shifted the profile outwards from the bilayer center (Figure 5C). Importantly, the changes in LPP caused by the introduction of DOPE or ONE-PE or OPC into the DOPC bilayer are in qualitative agreement with the lateral stress measurements (Figures 2 and 3).

We quantified the distribution of LPP for each lipid bilayer by calculating the lateral tension σ, which is equal to the area under the pressure profile curve (Supplementary Figure S3). This allowed us to determine σ for the headgroup, water–lipid interface, and hydrophobic regions in the lipid bilayer membrane and compare the results for unmodified and modified lipids (PE vs. ONE-PE, DOPC vs. OPC, and PE vs. PC) (Figure 5D–F).

Our results showed that transformation of the PE headgroup (PE→ONE-PE) reduced the σ value by 29.6%, whereas deletion of the acyl chain (DOPC→OPC)—by 17% (Figure 5D,E). More precisely, the decreases in the σ values for the PE→ONE-PE and DOPC→OPC modifications were 10% and 6.5% in the water–lipid interface region and 43.1% and 37.6% in the acyl chains region (Figure 5D,E). In contrast, PE insertion into the lipid bilayer increased the σ value by only 4.3% in total, and by 11.9% in the acyl chain (Figure 5F). These observations are in agreement with the data of Zoni et al. [79] that were obtained for LPPs and areas under the curve in the hydrophobic core region for mixed bilayers containing DOPC, DAG, DOPE, and DLPC, where DLPC can be considered a lipid with a positive individual curvature [21].

Interestingly, the variability of the lipid acyl chains in the mitochondrion [80] could also influence the modification of the PE headgroup. However, Bacot et al. [39] showed that a reduction in the unsaturation of the mixed acyl chains (18:0/20:4 PE versus 18:0/22:6 PE) only slightly reduced the modification of the PE headgroup by hydroxyalkenals (HHE, HNE, and HDDE).

The results shown in Figure 5D (PE→ONE-PE) are consistent with the experimental results obtained for the PE→ONE-PE modification (Figure 2A). Figure 5E indicates the weakening of the membrane lateral tension due to DOPC→OPC modification but it cannot be directly compared with the result shown in Figure 3B, because the MD simulation did not include DOPE (Figure 5E). As mentioned before, we applied MD simulations exclusively to demonstrate the contribution of lipid shape change to lateral pressure. The very small changes in surface tension, σ, of the lipid bilayer due to the presence of DOPE (Figure 5F) are consistent with published data [79,81]. In contrast, an increase of nearly 100% is shown for the same composition of the membrane (Figure 3B). Due to the fundamental difference between the applied experimental and in silico methods, obtained values in Figures 3B and 5F are not directly comparable. A bilayer lipid membrane (Figure 3) is an open system in which a lipid bilayer is connected to a large lipid reservoir. Therefore, lateral tension, σ, which arises in the lipid bilayer, is related to the surface free energy density of the lipids from a lipid reservoir. The lateral tension of the membrane increases by the SCES magnitude due to the insertion of the conical PE into the flat membrane.

In contrast, in the MD simulations (Figure 5), we consider a closed system consisting of a certain number of lipid molecules. In this system, SCES does not directly contribute to the lateral tension, which we calculate as the area under the curve obtained for the lateral pressure distribution. MD simulations in this case show the qualitative change in direction (increase/decrease), but not the quantitative magnitude of the change.

Based on the analysis presented above, the individual curvature of the ONE-PE should be more like that of OPC and, in any case, substantially different from the shape of the endogenous PE. Taken together, our results suggest that membrane protein activity increases if the lateral pressure at the water–lipid interface and in acyl chain regions decreases due to lipid modification; otherwise, it stays unchanged.

4. Discussion

The importance of the membrane lipid shape/reshaping for the mitochondria functioning under oxidative stress conditions (Figure 6A) can be summarized in two related categories: (i) softening of the lipid bilayer membrane, and (ii) a regulatory effect on the action of membrane proteins. In our previous study, we demonstrated the increase in G_m by AA-activated UCP1 due to the formation of RA-PE adducts and linked it for the first

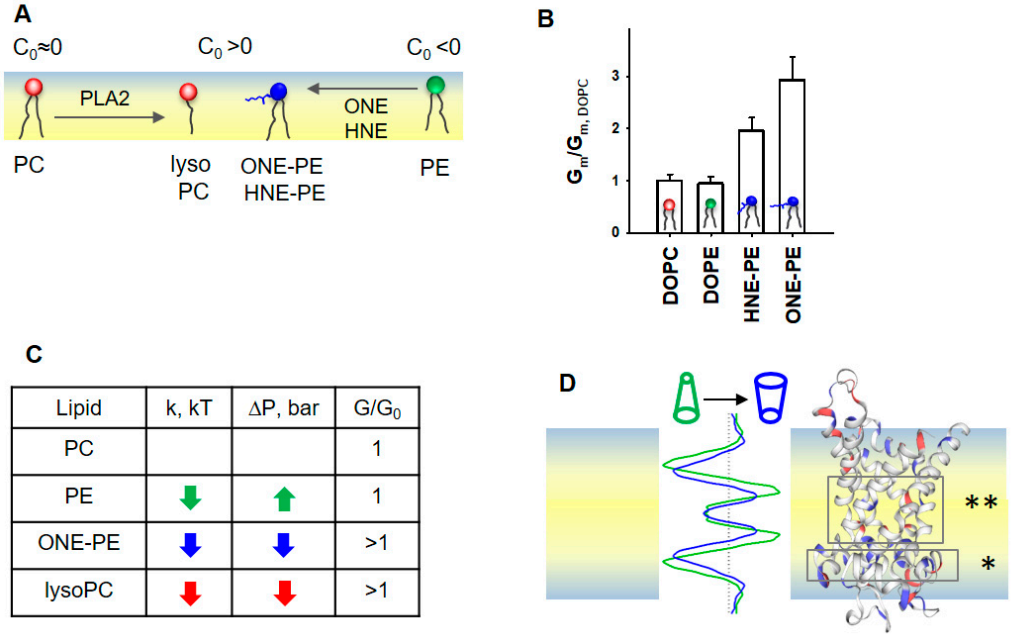

Figure 6. Proposed mechanism for the SCES sensing by mitochondrial proteins ANT1 and UCP1. (**A**) Schematic representation of the lipid membrane leaflet and change in lipid shapes under oxidative stress in mitochondria. (**B**) Effect of PE adducts, ONE-PE and HNE-PE, on the UCP1-mediated G_m in the presence of AA. The relative membrane conductance $G_m/G_{m,DOPC}$ was calculated based on data from [37]. $G_{m,DOPC}$ and G_m are specific membrane conductance in the absence or presence of PE or RA-PEs, respectively. (**C**) Schematic representation of the LPP redistribution in the lipid bilayer membrane caused by a change in the lipid shape. A comparison of the LPP (left) and protein structure (right) suggests that the decreased lateral pressure (dark blue), which appeared in the area of the FA binding site (*) and in the protein cavity region (**), promotes FA translocation. Most likely, the transformed lipid environment (i) increases the probability that anionic FA reaches a protein binding site and (ii) facilitates a protein conformational change, which in turn supports a faster translocation of FA to the opposite leaflet. (**D**) The increase in the UCP1- and ANT1- mediated G_m correlates with a decrease in both the lateral pressure, p, and bending rigidity, k, in the lipid bilayer membrane. If the change in p and k goes in the opposite direction, the protein-mediated G_m is not affected, as demonstrated here for the DOPE-containing membrane.

More importantly, the impact of PE-adducts on the elastic parameters k and σ in the order HHE < HNE < ONE perfectly matches their ability to enhance the UCP1-mediated proton translocation in the presence of FAs in membranes of the same lipid composition (Figure 4A) [37]. This supports the hypothesis that RA-induced changes in a lipid environment, and not a modification of protein amino acid residues, increase the G_m. Azwitterionic lysoPC lipids increased UCP1- and ANT1-mediated proton translocation similarly to PE-adducts. Thus, we propose that lipid shape and associated membrane mechanical properties [37], such as bending rigidity and lateral pressure, play a regulatory role in the catalytic activity of UCPs and ANTs. In contrast, the membrane surface potential, which increases due to the formation of RA-PEs [37], is most likely irrelevant for the SCES sensing of UCP1 and ANT1 because zwitterionic lysolipids do not affect the surface potential.

Here, we show that the integral proteins, UCP1 and ANT1, embedded in IMM-like membranes, sense changes in SCES caused by oxidative stress. The experimental results and MD simulations revealed that the modified phospholipids—PE adducts and lysolipids—induce similar changes in the bending rigidity, lateral tension, and LPP of lipid bilayer membranes (Figure 6C,D). The observed variations in k and σ among RAs can be explained by differences in the types of RA-PE adducts and their localization in the lipid bilayer membrane [37]. Because OPC's ($C_{0,OPC} > 0$) induced similar changes as k, σ, and p as a ONE-PE adduct in PE-containing membranes, we speculate that this PE adduct has a positive intrinsic curvature. Thus, RA-driven shape transformation in a fraction of PE molecules with a negative C_0 reduce dipolar packing stress due to mutual compensation with lipids with the opposite C_0, thereby decreasing the membrane SCES.

Notably, MD simulations suggested decreased lateral pressure over the whole membrane profile for bilayer membranes containing ONE-PE adduct or OPC (Figure 6D). We suggest that the altered lipid environment at the molecular level results in increased G_m in the presence of UCP1 or ANT1. The changes in the lipid environment are caused by the nature of the lipid transformation, in which the ratio (lipid head)/(acyl chains) is increased

More importantly, the impact of PE-adducts on the elastic parameters k and σ in the order HHE < HNE < ONE perfectly matches their ability to enhance the UCP1-mediated proton translocation in the presence of FAs in membranes of the same lipid composition (Figure 4A) [37]. This supports the hypothesis that RA-induced changes in a lipid environment, and not a modification of protein amino acid residues, increase the G_m. A zwitterionic lysoPC lipids increased UCP1- and ANT1-mediated proton translocation similarly to PE adducts. Thus, we propose that lipid shape and associated membrane mechanical properties, such as bending rigidity and lateral pressure, play a regulatory role in the protonophoric activity of UCPs and ANTs. In contrast, the membrane surface potential, which increases due to the formation of RA-PEs [37], is most likely irrelevant for the activation of UCP1 and ANT1, because zwitterionic lysolipids do not affect the surface potential.

Notably, MD simulations suggested decreased lateral pressure over the whole membrane profile for bilayer membranes containing ONE-PE adduct or OPC (Figure 6D). We suggest that the altered lipid environment at the molecular level results in increased G_m in the presence of UCP1 or ANT1. The changes in the lipid environment are caused by the nature of the lipid transformation, in which the ratio (lipid head)/(acyl chains) is increased compared to the "initial form" of the lipid (e.g., DOPC→OPC, PE→RA-PE). These modifications decreased both the bending modulus k and the lateral pressure p in the lipid bilayer membrane (Figures 2A and 5A,B).

The insertion of PE into the PC lipid bilayer resulted in an increase in lateral tension (Figure 3B), while the UCP1-mediated conductance remained unchanged (Figure 4A). In the case of RA-PE and lysolipids, decreased lateral pressure in the acyl tail region (Figure 6D) could increase the probability that anionic free fatty acids (i) reach the protein binding site, which is located in the hydrophobic region on the matrix side of the IMM [74], (ii) are protonated in the position near the center of the bilayer (asterisks in Figure 6D and reference [82]), and dissociate from the protein. Eventually, the same lipid environment supports the protein conformation change, ensuring faster FA^- translocation. Notably, protein modifications, such as crosslinking of RA amino acid adducts or protein mutations, can lead to loss of the protein transport function, whereas lipid modification potentiates the protein-mediated FA^- translocation. Remarkably, in the absence of oxidative stress lipids with distinctly positive curvature, such as lysolipids and phosphoinositides, are found only in trace amounts (<1%) and are primarily involved in direct lipid–protein interaction and signaling [9].

5. Conclusions

Identification of the mechanisms by which the transformation of lipid shape affects the functioning of mitochondria helps to explain the onset of diseases associated with oxidative stress in a way that has not been considered so far. Our results show that lysolipids and PEs modified by RAs similarly affect membrane mechanical properties by decreasing the bending modulus k and SCES. Furthermore, we showed that UCP1 and ANT1 sense SCES and proposed a new mechanism for regulating the protonophoric function of IMM proteins under oxidative stress.

Supplementary Materials: The following supporting information can be downloaded at: https://www.mdpi.com/article/10.3390/antiox11122314/s1, Figure S1: The lipid shape changes the elastic properties of the membrane; Figure S2: Lipid shape affects UCP1 and ANT1-mediated total membrane conductance; Figure S3: Impact of lipids with pronounced intrinsic curvature on the lateral pressure profile.

Author Contributions: Conceptualization, O.J. and E.E.P.; investigation, O.J., K.C., P.V.B., K.Ž., S.Š. and M.V.; resources, E.E.P., P.V.B. and M.V.; writing—original draft preparation, O.J. and E.E.P.; writing—review and editing, O.J., E.E.P., P.V.B. and M.V.; visualization, O.J., P.V.B.; supervision, E.E.P., P.V.B. and M.V.; project administration, E.E.P., P.V.B. and M.V.; funding acquisition, E.E.P., P.V.B. and M.V. All authors have read and agreed to the published version of the manuscript.

Funding: This research was funded by the Austrian Research Fund (P31559) (to E.E.P.), the Croatian Science Foundation (IP-2019-04-3804 to M.V.), and the Russian Science Foundation (grant # № 22-15-00265) to P.V.B. The authors are grateful to COST Action 19105 (Pan-European Network in Lipidomics and EpiLipidomics) for the scientific exchange and cooperation.

Institutional Review Board Statement: Not applicable.

Informed Consent Statement: Not applicable.

Data Availability Statement: The data supporting the findings are available in the Supplementary Information and from the corresponding author upon reasonable request.

Acknowledgments: We are grateful to Sarah Bardakji for the excellent technical assistance and for helping with the production and evaluation of recombinant proteins. We thank the computer cluster Isabella based in SRCE at the University of Zagreb, University Computing Centre for computational resources.

Conflicts of Interest: The authors declare no conflict of interest. The funders had no role in the design of the study; in the collection, analyses, or interpretation of data; in the writing of the manuscript; or in the decision to publish the results.

References

1. Harayama, T.; Riezman, H. Understanding the diversity of membrane lipid composition. *Nat. Rev. Mol. Cell Biol.* **2018**, *19*, 281–296. [CrossRef] [PubMed]
2. Lamari, F.; Mochel, F.; Sedel, F.; Saudubray, J.M. Disorders of phospholipids, sphingolipids and fatty acids biosynthesis: Toward a new category of inherited metabolic diseases. *J. Inherit. Metab. Dis.* **2013**, *36*, 411–425. [CrossRef] [PubMed]
3. Jo, D.S.; Park, N.Y.; Cho, D.H. Peroxisome quality control and dysregulated lipid metabolism in neurodegenerative diseases. *Exp. Mol. Med.* **2020**, *52*, 1486–1495. [CrossRef] [PubMed]
4. Sam, P.N.; Calzada, E.; Acoba, M.G.; Zhao, T.; Watanabe, Y.; Nejatfard, A.; Trinidad, J.C.; Shutt, T.E.; Neal, S.E.; Claypool, S.M. Impaired phosphatidylethanolamine metabolism activates a reversible stress response that detects and resolves mutant mitochondrial precursors. *iScience* **2021**, *24*, 102196. [CrossRef]
5. Eckmann, J.; Eckert, S.H.; Leuner, K.; Muller, W.E.; Eckert, G.P. Mitochondria: Mitochondrial membranes in brain ageing and neurodegeneration. *Int. J. Biochem. Cell Biol.* **2013**, *45*, 76–80. [CrossRef]
6. Kozlov, M.M. Spontaneous and Intrinsic Curvature of Lipid Membranes: Back to the Origins. In *Physics of Biological Membranes*; Bassereau, P., Sens, P., Eds.; Springer International Publishing: Berlin/Heidelberg, Germany, 2018; pp. 287–309.
7. Helfrich, W. Elastic properties of lipid bilayers: Theory and possible experiments. *Z. Nat. C* **1973**, *28*, 693–703. [CrossRef]
8. Dymond, M.K. Lipid monolayer spontaneous curvatures: A collection of published values. *Chem. Phys. Lipids* **2021**, *239*, 105117. [CrossRef]
9. van Meer, G.; Voelker, D.R.; Feigenson, G.W. Membrane lipids: Where they are and how they behave. *Nat. Rev. Mol. Cell Biol.* **2008**, *9*, 112–124. [CrossRef]
10. Vance, J.E.; Tasseva, G. Formation and function of phosphatidylserine and phosphatidylethanolamine in mammalian cells. *Biochim. Biophys. Acta* **2013**, *1831*, 543–554. [CrossRef]
11. Marsh, D. Lateral pressure profile, spontaneous curvature frustration, and the incorporation and conformation of proteins in membranes. *Biophys. J.* **2007**, *93*, 3884–3899. [CrossRef]
12. Bochicchio, D.; Monticelli, L. The Membrane Bending Modulus in Experiments and Simulations. In *Advances in Biomembranes and Lipid Self-Assembly*; Iglič, A., Kulkarni, C.V., Rappolt, M., Eds.; Academic Press: Cambridge, MA, USA, 2016; Volume 23, pp. 117–143.
13. van den Brink-van der Laan, E.; Killian, J.A.; de Kruijff, B. Nonbilayer lipids affect peripheral and integral membrane proteins via changes in the lateral pressure profile. *Biochim. Biophys. Acta* **2004**, *1666*, 275–288. [CrossRef] [PubMed]
14. Kirsten, M.L.; Baron, R.A.; Seabra, M.C.; Ces, O. Rab1a and Rab5a preferentially bind to binary lipid compositions with higher stored curvature elastic energy. *Mol. Membr. Biol.* **2013**, *30*, 303–314. [CrossRef] [PubMed]
15. Cullis, P.R.; de Kruijff, B. Lipid polymorphism and the functional roles of lipids in biological membranes. *Biochim. Biophys. Acta* **1979**, *559*, 399–420. [CrossRef] [PubMed]
16. Tuck, S. Extracellular vesicles: Budding regulated by a phosphatidylethanolamine translocase. *Curr. Biol.* **2011**, *21*, R988-990. [CrossRef]
17. Verkleij, A.J.; Leunissen-Bijvelt, J.; de Kruijff, B.; Hope, M.; Cullis, P.R. Non-bilayer structures in membrane fusion. *Ciba Found. Symp.* **1984**, *103*, 45–59. [CrossRef]
18. Siegel, D.P.; Epand, R.M. The mechanism of lamellar-to-inverted hexagonal phase transitions in phosphatidylethanolamine: Implications for membrane fusion mechanisms. *Biophys. J.* **1997**, *73*, 3089–3111. [CrossRef]
19. McDonald, C.; Jovanovic, G.; Ces, O.; Buck, M. Membrane Stored Curvature Elastic Stress Modulates Recruitment of Maintenance Proteins PspA and Vipp1. *mBio* **2015**, *6*, e01188-15. [CrossRef]
20. Agrawal, H.; Liu, L.; Sharma, P. Revisiting the curvature-mediated interactions between proteins in biological membranes. *Soft Matter* **2016**, *12*, 8907–8918. [CrossRef]

21. Strandberg, E.; Tiltak, D.; Ehni, S.; Wadhwani, P.; Ulrich, A.S. Lipid shape is a key factor for membrane interactions of amphipathic helical peptides. *Biochim. Biophys. Acta* **2012**, *1818*, 1764–1776. [CrossRef]
22. Nath, S.; Dancourt, J.; Shteyn, V.; Puente, G.; Fong, W.M.; Nag, S.; Bewersdorf, J.; Yamamoto, A.; Antonny, B.; Melia, T.J. Lipidation of the LC3/GABARAP family of autophagy proteins relies on a membrane-curvature-sensing domain in Atg3. *Nat. Cell Biol.* **2014**, *16*, 415–424. [CrossRef]
23. Putta, P.; Rankenberg, J.; Korver, R.A.; van Wijk, R.; Munnik, T.; Testerink, C.; Kooijman, E.E. Phosphatidic acid binding proteins display differential binding as a function of membrane curvature stress and chemical properties. *Biochim. Biophys. Acta* **2016**, *1858*, 2709–2716. [CrossRef] [PubMed]
24. Strahl, H.; Ronneau, S.; Gonzalez, B.S.; Klutsch, D.; Schaffner-Barbero, C.; Hamoen, L.W. Transmembrane protein sorting driven by membrane curvature. *Nat. Commun.* **2015**, *6*, 8728. [CrossRef] [PubMed]
25. Daum, G.; Vance, J.E. Import of lipids into mitochondria. *Prog. Lipid Res.* **1997**, *36*, 103–130. [CrossRef] [PubMed]
26. Mejia, E.M.; Hatch, G.M. Mitochondrial phospholipids: Role in mitochondrial function. *J. Bioenerg. Biomembr.* **2016**, *48*, 99–112. [CrossRef]
27. Basu Ball, W.; Neff, J.K.; Gohil, V.M. The role of nonbilayer phospholipids in mitochondrial structure and function. *FEBS Lett.* **2018**, *592*, 1273–1290. [CrossRef]
28. Bottinger, L.; Horvath, S.E.; Kleinschroth, T.; Hunte, C.; Daum, G.; Pfanner, N.; Becker, T. Phosphatidylethanolamine and cardiolipin differentially affect the stability of mitochondrial respiratory chain supercomplexes. *J. Mol. Biol.* **2012**, *423*, 677–686. [CrossRef]
29. Baker, C.D.; Basu Ball, W.; Pryce, E.N.; Gohil, V.M. Specific requirements of nonbilayer phospholipids in mitochondrial respiratory chain function and formation. *Mol. Biol. Cell* **2016**, *27*, 2161–2171. [CrossRef]
30. Calzada, E.; Avery, E.; Sam, P.N.; Modak, A.; Wang, C.; McCaffery, J.M.; Han, X.; Alder, N.N.; Claypool, S.M. Phosphatidylethanolamine made in the inner mitochondrial membrane is essential for yeast cytochrome bc1 complex function. *Nat. Commun.* **2019**, *10*, 1432. [CrossRef]
31. Cooke, I.R.; Deserno, M. Coupling between lipid shape and membrane curvature. *Biophys. J.* **2006**, *91*, 487–495. [CrossRef]
32. Bashkirov, P.V.; Chekashkina, K.V.; Akimov, S.A.; Kuzmin, P.I.; Frolov, V.A. Variation of Lipid Membrane Composition Caused by Strong Bending. *Biochem. Mosc. Suppl. Ser. A Membr. Cell Biol.* **2011**, *28*, 145–152. [CrossRef]
33. Beltran-Heredia, E.; Tsai, F.C.; Salinas-Almaguer, S.; Cao, F.J.; Bassereau, P.; Monroy, F. Membrane curvature induces cardiolipin sorting. *Commun. Biol.* **2019**, *2*, 225. [CrossRef] [PubMed]
34. Elias-Wolff, F.; Linden, M.; Lyubartsev, A.P.; Brandt, E.G. Curvature sensing by cardiolipin in simulated buckled membranes. *Soft Matter* **2019**, *15*, 792–802. [CrossRef] [PubMed]
35. Davies, K.M.; Strauss, M.; Daum, B.; Kief, J.H.; Osiewacz, H.D.; Rycovska, A.; Zickermann, V.; Kuhlbrandt, W. Macromolecular organization of ATP synthase and complex I in whole mitochondria. *Proc. Natl. Acad. Sci. USA* **2011**, *108*, 14121–14126. [CrossRef] [PubMed]
36. Acehan, D.; Malhotra, A.; Xu, Y.; Ren, M.; Stokes, D.L.; Schlame, M. Cardiolipin affects the supramolecular organization of ATP synthase in mitochondria. *Biophys. J.* **2011**, *100*, 2184–2192. [CrossRef] [PubMed]
37. Jovanovic, O.; Pashkovskaya, A.A.; Annibal, A.; Vazdar, M.; Burchardt, N.; Sansone, A.; Gille, L.; Fedorova, M.; Ferreri, C.; Pohl, E.E. The molecular mechanism behind reactive aldehyde action on transmembrane translocations of proton and potassium ions. *Free Radic. Biol. Med.* **2015**, *89*, 1067–1076. [CrossRef] [PubMed]
38. Guichardant, M.; Taibi-Tronche, P.; Fay, L.B.; Lagarde, M. Covalent modifications of aminophospholipids by 4-hydroxynonenal. *Free Radic. Biol. Med.* **1998**, *25*, 1049–1056. [CrossRef]
39. Bacot, S.; Bernoud-Hubac, N.; Baddas, N.; Chantegrel, B.; Deshayes, C.; Doutheau, A.; Lagarde, M.; Guichardant, M. Covalent binding of hydroxy-alkenals 4-HDDE, 4-HHE, and 4-HNE to ethanolamine phospholipid subclasses. *J. Lipid Res.* **2003**, *44*, 917–926. [CrossRef]
40. Vazdar, K.; Vojta, D.; Margetic, D.; Vazdar, M. Reaction Mechanism of Covalent Modification of Phosphatidylethanolamine Lipids by Reactive Aldehydes 4-Hydroxy-2-nonenal and 4-Oxo-2-nonenal. *Chem. Res. Toxicol.* **2017**, *30*, 840–850. [CrossRef]
41. Jovanovic, O.; Skulj, S.; Pohl, E.E.; Vazdar, M. Covalent modification of phosphatidylethanolamine by 4-hydroxy-2-nonenal increases sodium permeability across phospholipid bilayer membranes. *Free Radic. Biol. Med.* **2019**, *143*, 433–440. [CrossRef]
42. Jezek, J.; Jaburek, M.; Zelenka, J.; Jezek, P. Mitochondrial phospholipase A2 activated by reactive oxygen species in heart mitochondria induces mild uncoupling. *Physiol. Res.* **2010**, *59*, 737–747. [CrossRef]
43. Jaburek, M.; Pruchova, P.; Holendova, B.; Galkin, A.; Jezek, P. Antioxidant Synergy of Mitochondrial Phospholipase PNPLA8/iPLA2gamma with Fatty Acid-Conducting SLC25 Gene Family Transporters. *Antioxidants* **2021**, *10*, 678. [CrossRef] [PubMed]
44. Bashkirov, P.V.; Kuzmin, P.I.; Vera Lillo, J.; Frolov, V.A. Molecular Shape Solution for Mesoscopic Remodeling of Cellular Membranes. *Annu. Rev. Biophys.* **2022**, *51*, 473–497. [CrossRef] [PubMed]
45. Zimmermann, L.; Moldzio, R.; Vazdar, K.; Krewenka, C.; Pohl, E.E. Nutrient deprivation in neuroblastoma cells alters 4-hydroxynonenal-induced stress response. *Oncotarget* **2017**, *8*, 8173–8188. [CrossRef] [PubMed]
46. Macher, G.; Koehler, M.; Rupprecht, A.; Kreiter, J.; Hinterdorfer, P.; Pohl, E.E. Inhibition of mitochondrial UCP1 and UCP3 by purine nucleotides and phosphate. *Biochim. Biophys. Acta Biomembr.* **2018**, *1860*, 664–672. [CrossRef] [PubMed]
47. Kreiter, J.; Beitz, E.; Pohl, E.E. A Fluorescence-Based Method to Measure ADP/ATP Exchange of Recombinant Adenine Nucleotide Translocase in Liposomes. *Biomolecules* **2020**, *10*, 685. [CrossRef]

48. Beck, V.; Jaburek, M.; Breen, E.P.; Porter, R.K.; Jezek, P.; Pohl, E.E. A new automated technique for the reconstitution of hydrophobic proteins into planar bilayer membranes. Studies of human recombinant uncoupling protein 1. *Biochim. Biophys. Acta* **2006**, *1757*, 474–479. [CrossRef]
49. Rupprecht, A.; Sokolenko, E.A.; Beck, V.; Ninnemann, O.; Jaburek, M.; Trimbuch, T.; Klishin, S.S.; Jezek, P.; Skulachev, V.P.; Pohl, E.E. Role of the transmembrane potential in the membrane proton leak. *Biophys. J.* **2010**, *98*, 1503–1511. [CrossRef]
50. Bashkirov, P.V.; Kuzmin, P.I.; Chekashkina, K.; Arrasate, P.; Vera Lillo, J.; Shnyrova, A.V.; Frolov, V.A. Reconstitution and real-time quantification of membrane remodeling by single proteins and protein complexes. *Nat. Protoc.* **2020**, *15*, 2443–2469. [CrossRef]
51. Frolov, V.A.; Lizunov, V.A.; Dunina-Barkovskaya, A.Y.; Samsonov, A.V.; Zimmerberg, J. Shape bistability of a membrane neck: A toggle switch to control vesicle content release. *Proc. Natl. Acad. Sci. USA* **2003**, *100*, 8698–8703. [CrossRef]
52. Ivchenkov, D.V.; Kuzmin, P.I.; Galimzyanov, T.R.; Shnyrova, A.V.; Bashkirov, P.V.; Frolov, V.A. Nonlinear material and ionic transport through membrane nanotubes. *Biochim. Biophys. Acta Biomembr.* **2021**, *1863*, 183677. [CrossRef]
53. Galimzyanov, T.R.; Bashkirov, P.V.; Blank, P.S.; Zimmerberg, J.; Batishchev, O.V.; Akimov, S.A. Monolayerwise application of linear elasticity theory well describes strongly deformed lipid membranes and the effect of solvent. *Soft Matter* **2020**, *16*, 1179–1189. [CrossRef] [PubMed]
54. Jaembeck, J.P.; Lyubartsev, A.P. An extension and further validation of an all-atomistic force field for biological membranes. *J. Chem. Theory Comput.* **2012**, *8*, 2938–2948. [CrossRef] [PubMed]
55. Jaembeck, J.P.; Lyubartsev, A.P. Derivation and systematic validation of a refined all-atom force field for phosphatidylcholine lipids. *J. Phys. Chem. B* **2012**, *116*, 3164–3179. [CrossRef] [PubMed]
56. Jaembeck, J.P.M.; Lyubartsev, A.P. Another piece of the membrane puzzle: Extending slipids further. *J. Chem. Theory Comput.* **2012**, *9*, 774–784. [CrossRef]
57. Klauda, J.B.; Venable, R.M.; Freites, J.A.; O'Connor, J.W.; Tobias, D.J.; Mondragon-Ramirez, C.; Vorobyov, I.; MacKerell, A.D., Jr.; Pastor, R.W. Update of the CHARMM all-atom additive force field for lipids: Validation on six lipid types. *J. Phys. Chem. B* **2010**, *114*, 7830–7843. [CrossRef]
58. Singh, U.C.; Kollman, P.A. An Approach to Computing Electrostatic Charges for Molecules. *J. Comput. Chem.* **1984**, *5*, 129–145. [CrossRef]
59. Bayly, C.I.; Cieplak, P.; Cornell, W.D.; Kollman, P.A. A Well-Behaved Electrostatic Potential Based Method Using Charge Restraints for Deriving Atomic Charges-the Resp Model. *J. Phys. Chem.* **1993**, *97*, 10269–10280. [CrossRef]
60. Jorgensen, W.L.; Chandrasekhar, J.; Madura, J.D.; Impey, R.W.; Klein, M.L. Comparison of Simple Potential Functions for Simulating Liquid Water. *J. Chem. Phys.* **1983**, *79*, 926–935. [CrossRef]
61. Essmann, U.; Perera, L.; Berkowitz, M.L.; Darden, T.; Lee, H.; Pedersen, L.G. A Smooth Particle Mesh Ewald Method. *J. Chem. Phys.* **1995**, *103*, 8577–8593. [CrossRef]
62. Parrinello, M.; Rahman, A. Polymorphic Transitions in Single-Crystals-a New Molecular-Dynamics Method. *J. Appl. Phys.* **1981**, *52*, 7182–7190. [CrossRef]
63. Nosé, S. A molecular dynamics method for simulations in the canonical ensemble. *Mol. Phys.* **1984**, *52*, 255–268. [CrossRef]
64. Hess, B.; Bekker, H.; Berendsen, H.J.C.; Fraaije, J.G.E.M. LINCS: A linear constraint solver for molecular simulations. *J. Comput. Chem.* **1997**, *18*, 1463–1472. [CrossRef]
65. Miyamoto, S.; Kollman, P.A. Settle-an Analytical Version of the Shake and Rattle Algorithm for Rigid Water Models. *J. Comput. Chem.* **1992**, *13*, 952–962. [CrossRef]
66. Vanegas, J.M.; Torres-Sanchez, A.; Arroyo, M. Importance of Force Decomposition for Local Stress Calculations in Biomembrane Molecular Simulations. *J. Chem. Theory Comput.* **2014**, *10*, 691–702. [CrossRef]
67. Torres-Sanchez, A.; Vanegas, J.M.; Arroyo, M. Examining the Mechanical Equilibrium of Microscopic Stresses in Molecular Simulations. *Phys. Rev. Lett.* **2015**, *114*, 258102. [CrossRef]
68. Shi, Z.; Baumgart, T. Membrane tension and peripheral protein density mediate membrane shape transitions. *Nat. Commun.* **2015**, *6*, 5974. [CrossRef]
69. Sorre, B.; Callan-Jones, A.; Manzi, J.; Goud, B.; Prost, J.; Bassereau, P.; Roux, A. Nature of curvature coupling of amphiphysin with membranes depends on its bound density. *Proc. Natl. Acad. Sci. USA* **2012**, *109*, 173–178. [CrossRef]
70. Fuller, N.; Rand, R.P. The influence of lysolipids on the spontaneous curvature and bending elasticity of phospholipid membranes. *Biophys. J.* **2001**, *81*, 243–254. [CrossRef]
71. Esterbauer, H.; Schaur, R.J.; Zollner, H. Chemistry and biochemistry of 4-hydroxynonenal, malonaldehyde and related aldehydes. *Free Radic. Biol. Med.* **1991**, *11*, 81–128. [CrossRef]
72. Uchida, K. 4-Hydroxy-2-nonenal: A product and mediator of oxidative stress. *Prog. Lipid Res.* **2003**, *42*, 318–343. [CrossRef]
73. Andreyev, A.; Bondareva, T.O.; Dedukhova, V.I.; Mokhova, E.N.; Skulachev, V.P.; Tsofina, L.M.; Volkov, N.I.; Vygodina, T.V. The ATP/ADP-antiporter is involved in the uncoupling effect of fatty acids on mitochondria. *Eur. J. Biochem.* **1989**, *182*, 585–592. [CrossRef] [PubMed]
74. Kreiter, J.; Rupprecht, A.; Skulj, S.; Brkljaca, Z.; Zuna, K.; Knyazev, D.G.; Bardakji, S.; Vazdar, M.; Pohl, E.E. ANT1 Activation and Inhibition Patterns Support the Fatty Acid Cycling Mechanism for Proton Transport. *Int. J. Mol. Sci.* **2021**, *22*, 2490. [CrossRef] [PubMed]
75. Malingriaux, E.A.; Rupprecht, A.; Gille, L.; Jovanovic, O.; Jezek, P.; Jaburek, M.; Pohl, E.E. Fatty acids are key in 4-hydroxy-2-nonenal-mediated activation of uncoupling proteins 1 and 2. *PLoS ONE* **2013**, *8*, e77786. [CrossRef]

76. Garlid, K.D.; Orosz, D.E.; Modriansky, M.; Vassanelli, S.; Jezek, P. On the mechanism of fatty acid-induced proton transport by mitochondrial uncoupling protein. *J. Biol. Chem.* **1996**, *271*, 2615–2620. [CrossRef] [PubMed]
77. Dennis, E.A. Diversity of group types, regulation, and function of phospholipase A2. *J. Biol. Chem.* **1994**, *269*, 13057–13060. [CrossRef]
78. Chen, Y.F.; Tsang, K.Y.; Chang, W.F.; Fan, Z.A. Differential dependencies on [Ca2+] and temperature of the monolayer spontaneous curvatures of DOPE, DOPA and cardiolipin: Effects of modulating the strength of the inter-headgroup repulsion. *Soft Matter* **2015**, *11*, 4041–4053. [CrossRef]
79. Zoni, V.; Khaddaj, R.; Campomanes, P.; Thiam, A.R.; Schneiter, R.; Vanni, S. Pre-existing bilayer stresses modulate triglyceride accumulation in the ER versus lipid droplets. *Elife* **2021**, *10*, e62886. [CrossRef]
80. Renne, M.F.; Bao, X.; Hokken, M.W.; Bierhuizen, A.S.; Hermansson, M.; Sprenger, R.R.; Ewing, T.A.; Ma, X.; Cox, R.C.; Brouwers, J.F.; et al. Molecular species selectivity of lipid transport creates a mitochondrial sink for di-unsaturated phospholipids. *EMBO J.* **2022**, *41*, e106837. [CrossRef]
81. Orsi, M.; Essex, J.W. Physical properties of mixed bilayers containing lamellar and nonlamellar lipids: Insights from coarse-grain molecular dynamics simulations. *Faraday Discuss.* **2013**, *161*, 249–272; discussion 273–303, discussion 273–303. [CrossRef]
82. Kreiter, J.; Brkljača, Z.; Škulj, S.; Bardakji, S.; Vazdar, M.; Pohl, E.E. Mechanism of the ANT-mediated transport of fatty acid anions across the inner mitochondrial membrane. *bioRxiv* **2022**. [CrossRef]

2.4. ANT1 Activation and Inhibition Patterns Support the Fatty Acid Cycling Mechanism for Proton Transport.

International Journal of
Molecular Sciences

MDPI

Article

ANT1 Activation and Inhibition Patterns Support the Fatty Acid Cycling Mechanism for Proton Transport

Jürgen Kreiter [1], Anne Rupprecht [1,2], Sanja Škulj [3], Zlatko Brkljača [3], Kristina Žuna [1], Denis G. Knyazev [4], Sarah Bardakji [1], Mario Vazdar [3,5] and Elena E. Pohl [1,*]

1 Institute of Physiology, Pathophysiology and Biophysics, Department of Biomedical Sciences, University of Veterinary Medicine, 1210 Vienna, Austria; juergen.kreiter@vetmeduni.ac.at (J.K.); anne.rupprecht@med.uni-rostock.de (A.R.); kristina.zuna@vetmeduni.ac.at (K.Ž.); sarah.bardakji@vetmeduni.ac.at (S.B.)
2 Institute of Pharmacology and Toxicology, Rostock University Medical Center, 18057 Rostock, Germany
3 Division of Organic Chemistry and Biochemistry, Rudjer Bošković Institute,10000 Zagreb, Croatia; Sanja.Skulj@irb.hr (S.Š.); Zlatko.Brkljaca@irb.hr (Z.B.); Mario.Vazdar@irb.hr (M.V.)
4 Institute of Biophysics, Johannes Kepler University, 4020 Linz, Austria; denis.knyazev@jku.at
5 Institute of Organic Chemistry and Biochemistry, Czech Academy of Sciences, 16610 Prague 6, Czech Republic
* Correspondence: elena.pohl@vetmeduni.ac.at

Abstract: Adenine nucleotide translocase (ANT) is a well-known mitochondrial exchanger of ATP against ADP. In contrast, few studies have shown that ANT also mediates proton transport across the inner mitochondrial membrane. The results of these studies are controversial and lead to different hypotheses about molecular transport mechanisms. We hypothesized that the H^+-transport mediated by ANT and uncoupling proteins (UCP) has a similar regulation pattern and can be explained by the fatty acid cycling concept. The reconstitution of purified recombinant ANT1 in the planar lipid bilayers allowed us to measure the membrane current after the direct application of transmembrane potential $\Delta\Psi$, which would correspond to the mitochondrial states III and IV. Experimental results reveal that ANT1 does not contribute to a basal proton leak. Instead, it mediates H^+ transport only in the presence of long-chain fatty acids (FA), as already known for UCPs. It depends on FA chain length and saturation, implying that FA's transport is confined to the lipid-protein interface. Purine nucleotides with the preference for ATP and ADP inhibited H^+ transport. Specific inhibitors of ATP/ADP transport, carboxyatractyloside or bongkrekic acid, also decreased proton transport. The H^+ turnover number was calculated based on ANT1 concentration determined by fluorescence correlation spectroscopy and is equal to $14.6 \pm 2.5\ s^{-1}$. Molecular dynamic simulations revealed a large positively charged area at the protein/lipid interface that might facilitate FA anion's transport across the membrane. ANT's dual function—ADP/ATP and H^+ transport in the presence of FA—may be important for the regulation of mitochondrial membrane potential and thus for potential-dependent processes in mitochondria. Moreover, the expansion of proton-transport modulating drug targets to ANT1 may improve the therapy of obesity, cancer, steatosis, cardiovascular and neurodegenerative diseases.

Keywords: fatty acid anion transport; proton transport; ADP/ATP carrier protein; mitochondrial transporter; arachidonic acid; long-chain fatty acids

Citation: Kreiter, J.; Rupprecht, A.; Škulj, S.; Brkljača, Z.; Žuna, K.; Knyazev, D.G.; Bardakji, S.; Vazdar, M.; Pohl, E.E. ANT1 Activation and Inhibition Patterns Support the Fatty Acid Cycling Mechanism for Proton Transport. *Int. J. Mol. Sci.* **2021**, *22*, 2490. https://doi.org/10.3390/ijms22052490

Academic Editor: Masoud Jelokhani-Niaraki

Received: 8 January 2021
Accepted: 24 February 2021
Published: 2 March 2021

1. Introduction

In mitochondria, oxidative phosphorylation accounts for ATP production by phosphorylating ADP using proton (H^+) gradient generated by the respiratory chain proteins (coupling). H^+ can return to the matrix by alternative pathways (uncoupling): (i) inhibitor-non sensitive basal H^+ leak (J_B) and (ii) protein-mediated inhibitor-sensitive proton transport (J_H) [1–3]. J_B is sensitive to the membrane potential, mitochondrial inner membrane surface area, the composition of phospholipids and free fatty acids (FA) and was observed in

mitochondria of all tissues [1]. Uncoupling proteins (UCP) are implicated in the mediation of J_H [4–9]. As several tissues such as liver, kidney, skin, and others lack any UCPs under physiological conditions (for review, see [10]), mitochondrial adenine nucleotide translocase (ANT, also cited in the literature as AAC or ADP/ATP carrier) was proposed to provide an alternative pathway for proton transport alongside its well-known function to exchange ADP for ATP [11–15].

The H^+ transporting function of ANT in the presence of palmitate has been first observed in experiments with isolated mitochondria [16,17]. The addition of free FA to the proteoliposomes reconstituted with purified ANT caused the transmembrane potential ($\Delta\Phi$) decrease, which was restored by carboxyatractyloside (CATR) and bongkrekic acid (BA) [18]. In brown-fat mitochondria from mice knockout for UCP1, fatty-acid-induced uncoupling could also be inhibited by CATR [19]. The H^+ conductance of muscle mitochondria from mice knockout for ANT1 was reported to be half that of wild-type controls [20]. Recently, ANT-mediated H^+ transport was observed in patched mitoplasts [21]. Although the H^+ transporting function of ANT1 seems to be accepted, discrepancies in results obtained in various experimental systems led to different views on the proton transport mechanism. In the 1980–1990s, several groups recognized that the proton transport could occur by the flip-flop of the protonated form of long-chain fatty acid (FA) without membrane proteins' participation [22,23]. However, a fatty acid anion (FA^-) transport is a rate-limiting step in FA circulation and has to be accelerated by proteins. In 1991, Skulachev proposed the "fatty acid circuit hypothesis", claiming that proteins such as ANT1 and UCP1 mediate the return of the FA^- to the cytosolic side of the membrane, resulting in net proton transport catalyzed by the protein [24]. Our previous results obtained for UCP1-UCP3 can be well described based on the FA cycling model and are consistent with the translocation of FA^- at the protein/lipid interface.

In contrast, Bertholet et al. proposed FA to be co-factors in H^+ transport by ANT based on patch-clamp experiments [21]. In this model, FA is not translocated but stays in one place as a part of the protein translocating pathway, where it is (de-)protonated. This mechanism differed from the mechanism suggested by the same group for UCP1, in which UCP1 was regarded as a FA^-/H^+ symporter [25]. Moreover, this model does not necessarily assume direct binding of H^+ to the FA anion and allows the proton transport in both directions.

Here, we hypothesized that the H^+-transport mediated by ANT has a regulation pattern similar to UCPs and can be explained by the FA cycling concept. The goals of this study were (i) to investigate the dependence of ANT-mediated H^+ transport on FA structure, (ii) to estimate ANT-specific H^+ turnover number, and (iii) to examine whether the specific ANT substrates inhibit H^+ transport.

2. Results

2.1. ANT1-Mediated Substrate Transport

To evaluate whether recombinant murine ANT1 was correctly refolded in proteoliposomes, we performed ADP/ATP transport measurements using proteoliposomes initially filled with radioactively labeled ^{3}H-ATP [26]. After adding ADP to the bulk solution, we measured the release of ^{3}H-ATP with time (Supplementary Figure S2). The determined ADP/ATP exchange rate depends on ANT1 content (k_{ANT} = 5.53 ± 0.74 mmol/min/g) and corresponds well to the reported results for ANT reconstituted into liposomes (Supplementary Table S1) [26–29].

2.2. Basal Proton Leak

We further investigated the controversially discussed ANT1 involvement in the basal leak [20,21]. For this, we formed planar bilayer lipid membranes from proteoliposomes reconstituted with recombinant ANT1 [26]. Figure 1 demonstrates that the total specific conductances, G_m and G_0, of bilayer membranes made from DOPC, DOPE, and cardiolipin were similar in the presence and absence of ANT1 (G_m =10.0 ± 2.0 nS/cm^2 and G_0 =8.4

conductances, G_m and G_0, of bilayer membranes made from DOPC, DOPE, and ca
were similar in the presence and absence of ANT1 (G_m =10.0 ± 2.0 nS/cm² and G_0 =
nS/cm²) if no purine nucleotides (PN) were added. The addition of ATP and ADP
sides of the membrane led to a substantial G_m increase, which was directly prop
to the applied membrane potentials, reaching G_m = 39.5 ± 4.9 nS/cm² at 190 mV (
Supplementary Figure S3 and Supplementary Table S2). This increase vanished a
ing the specific inhibitor of ADP/ATP transport—CATR (Figure 1) and can be e
by the electrogenic shift due to ATP/ADP exchange by ANT1. This experiment
that ANT1 has no measurable impact on the proton leak without FAs.

± 2.3 nS/cm²) if no purine nucleotides (PN) were added. The addition of ATP and ADP on both sides of the membrane led to a substantial G_m increase, which was directly proportional to the applied membrane potentials, reaching G_m = 39.5 ± 4.9 nS/cm² at 190 mV (Figure 1; Supplementary Figure S3 and Supplementary Table S2). This increase vanished after adding the specific inhibitor of ADP/ATP transport—CATR (Figure 1) and can be explained by the electrogenic shift due to ATP/ADP exchange by ANT1. This experiment showed that ANT1 has no measurable impact on the proton leak without FAs.

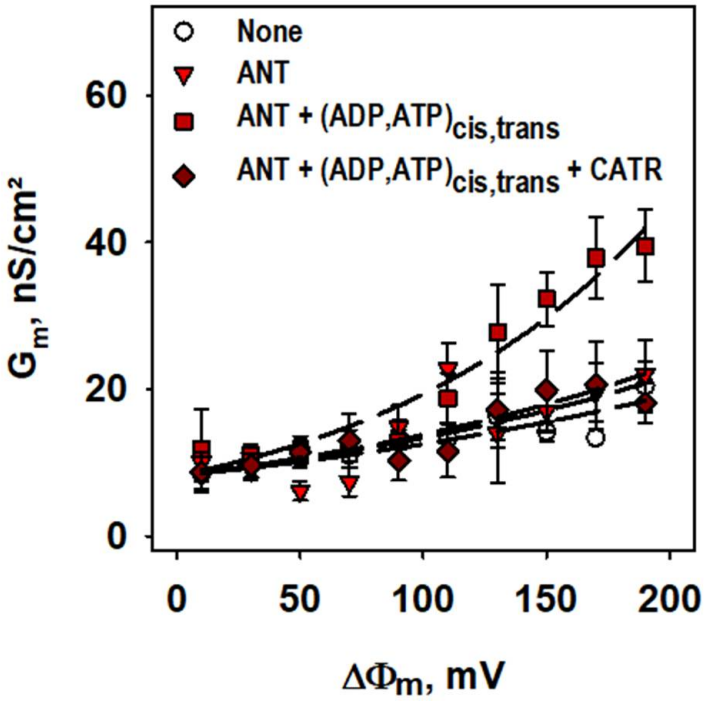

Figure 1. ANT1 does not contribute to the basal proton leak. Total membrane conductance (G_m) was measured at different membrane potentials (ΔΦ) and membrane compositions (s. legend). Planar bilayer membranes were made of 45:45:10 mol % PC:PE:CL. Lipid concentration was 1.5 mg/(mL of buffer solution). Protein concentration measured by BCA assay was 4 µg/(mg of lipid). Buffer contained 50 mM Na_2SO_4, 10 mM Tris, 10 mM MES and 0.6 mM EGTA at pH = 7.34 and T = 306 K. ADP, ATP and CATR were added at concentrations 2 mM, 2 mM and 100 µM. Lines represent the least square regression fit of an exponential function to the data. Data are the mean ± SD of at least three independent experiments.

Figure 1. ANT1 does not contribute to the basal proton leak. Total membrane conductance (G_m) was measured at different membrane potentials (ΔΦ) and membrane compositions (s. legend). Planar bilayer membranes were made of 45:45:10 mol % PC:PE:CL. Lipid concentration was 1.5 mg/(mL of buffer solution). Protein concentration measured by BCA assay was 4 µg/(mg of lipid). Buffer contained 50 mM Na_2SO_4, 10 mM Tris, 10 mM MES and 0.6 mM EGTA at pH = 7.34 and T = 306 K. ADP, ATP and CATR were added at concentrations 2 mM, 2 mM and 100 µM. Lines represent the least square regression fit of an exponential function to the data. Data are the mean ± SD of at least three independent experiments.

2.3. ANT1-Mediated Proton Transport in the Presence of FA

The addition of polyunsaturated arachidonic acid (AA) to the membrane in the absence of ANT1 led to a potential-dependent increase in G_m. It confirms FA's importance as weak uncouplers, especially at high potentials (G_m was one order of magnitude higher at 190 mV) relevant for mitochondrial membranes [30]. The reconstitution of ANT1 in the membrane increased G_m in the presence of AA 4-fold ($G_m^{ANT,AA}/G_m^{AA}$) (Figure 2a). At 190 mV $G_m^{ANT,AA}$, G_m^{AA} and G_0 were equal to 1750 ± 220 nS/cm², 440 ± 135 nS/cm² and 20.4 ± 3.4 nS/cm², respectively (Supplementary Figure S4 and Supplementary Table S2). Notably, ANT1-mediated G_m depended on the structure of FAs. It increased with the elongation of FA chain length in order palmitic (PA, 16:0) → arachidic (ArA, 20:0) acid and was the highest by unsaturated AA (20:4) (Figure 2b).

2.3. ANT1-Mediated Proton Transport in the Presence of FA

The addition of polyunsaturated arachidonic acid (AA) to the membrane in the absence of ANT1 led to a potential-dependent increase in G_m. It confirms FA's importance as weak uncouplers, especially at high potentials (G_m was one order of magnitude higher at 190 mV) relevant for mitochondrial membranes [30]. The reconstitution of ANT1 in the membrane increased G_m in the presence of AA 4-fold ($G_m^{ANT,AA}/G_m^{AA}$) (Figure 2a). At 190 mV $G_m^{ANT,AA}$, G_m^{AA} and G_0 were equal to 1750 ± 220 nS/cm², 440 ± 135 nS/cm² and 20.4 ± 3.4 nS/cm², respectively (Supplementary Figure S4 and Supplementary Table S2). Notably, ANT1-mediated G_m depended on the structure of FAs. It increased with the elongation of FA chain length in order palmitic (PA, 16:0) → arachidic (ArA, 20:0) acid and was the highest by unsaturated AA (20:4) (Figure 2b).

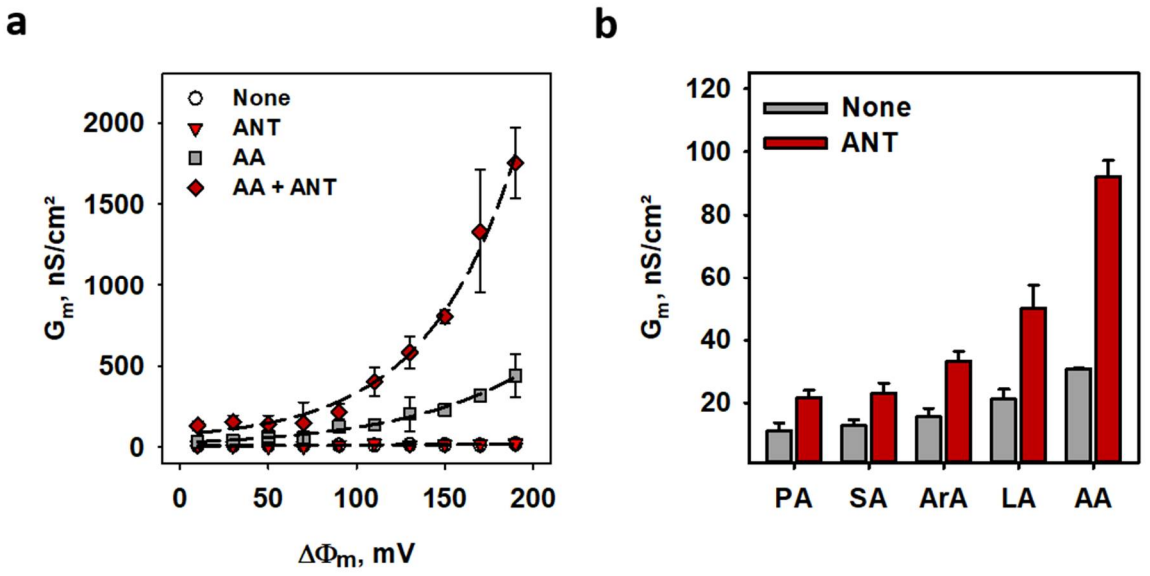

Figure 2. Fatty acids are required to activate ANT1-mediated proton transport. (**a**) Total membrane conductance (G_m) of lipid bilayers in the presence of AA (gray squares), ANT1 (red triangles), ANT1 and AA (dark red diamonds) and in the absence of AA and ANT1 (white circles) at different membrane potentials ($\Delta\Phi_m$). Lines represent the least square regression fit of an exponential function to the data. (**b**) Dependence of total membrane conductance (G_m) on fatty acid chain length and unsaturation in the presence (red) and absence (gray) of ANT1. PA, SA, ArA, LA, and AA indicate palmitic, stearic, arachidic, linoleic, and arachidonic acids. In all measurements, planar bilayer membranes were made of 45:45:10 mol % PC:PE:CL reconstituted with 15 mol % FA, except indicated otherwise. Lipid concentration was 1.5 mg/(mL of buffer solution). Protein concentration measured by BCA assay was 4 µg/(mg of lipid). The buffer solution contained 50 mM Na_2SO_4, 10 mM Tris, 10 mM MES and 0.6 mM EGTA at pH = 7.34 and T = 306 K. Data are the mean ± SD of at least three independent experiments.

2.4. Proton Turnover Number of ANT1

To determine the H^+ turnover number of ANT, we recorded current-voltage characteristics in the presence and absence of a transmembrane pH gradient (Figure 3, insert) [31].

To estimate a protein to lipid ratio, we measured the number of fluorescently-labeled ANT per liposome using fluorescence correlation spectroscopy (FCS) [32] (s. Methods and Supplementary Figure S5). By comparing the number of the fluorescent particles in proteoliposomes before ($N_{ANT,\ none}$ = 1.60 ± 0.01) and after ($N_{ANT,\ SDS}$ = 13.83 ± 0.04) the addition of 2 % (*v*/*v*) SDS, and assuming one ANT protein per detergent micelle after micellization, we calculated 8.67 ± 0.74 ANT molecules per liposome. The protein to lipid ratio estimated according to Equation (4) was 1:12000.

From the potential shift and proton/lipid ratio, we then estimated that ANT has a turnover rate of 1446 ± 2.5 H^+/s (Figure 3), being similar to those of uncoupling proteins (Supplementary Table S3) [6,7,33–35].

2.5. Inhibition of ANT1-Mediated Proton Transport

Specific inhibitors of nucleotide transport lock ANT either in its cytosolic-opened c-side (CATR) or in its matrix-opened m-side (BA) [15] and inhibit both ADP/ATP exchange and FA-mediated proton leak. The comparison of CATR and BA effect on G_m (Figure 4a) showed that inhibition by CATR was more effective than by BA. It is displayed by the EC50 values of 18.9 ± 1.8 µM for CATR and 32.3 ± 11.4 µM for BA, respectively (Figure 4b and Supplementary Table S4). Maximum inhibition values (I_{max} = 64.2 ± 2.8% and I_{max} = 44.3 ± 5.7% in the presence of CATR or BA) indicate that ANT conformation in the bilayer is approximately 60% in the c-state and 40% in the m-state in our system (Figure 4c and Supplementary Table S4).

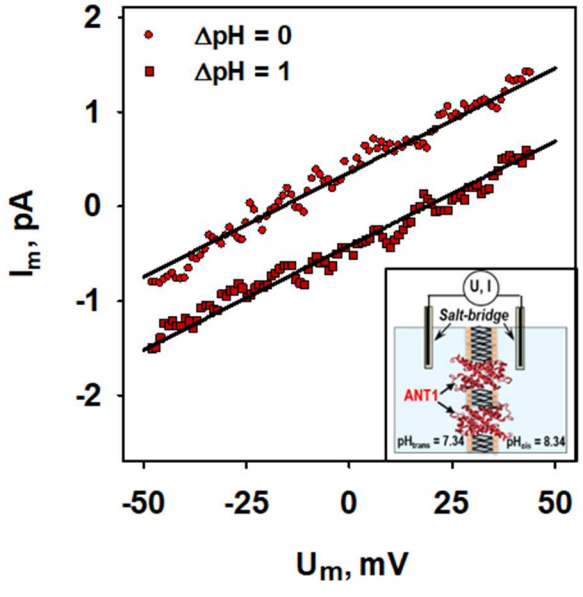

Figure 3. The proton turnover number of ANT is similar to UCPs. Representative current-voltage recordings of lipid bilayer membranes reconstituted with ANT1 in the presence (squares) and absence (circles) of ΔpH = 1.0 across the membrane. Lines represent a linear fit to the data. Planar bilayer membranes were made of 45:45:10 mol % PC:PE:CL reconstituted with 15 mol % AA. Buffer contained 50 mM Na_2SO_4, 10 mM Tris, 10 mM MES and 0.6 mM EGTA at pH = 7.34 and T = 306 K. Lipid concentration was 1.5 mg/(mL of buffer solution). Protein concentration measured by BCA assay was 4 µg/(mg of lipid). Insert: Experimental setup of the measurements to establish a transmembrane pH gradient.

Figure 3. The proton turnover number of ANT is similar to UCPs. Representative current-voltage recordings of lipid bilayer membranes reconstituted with ANT1 in the presence (squares) and absence (circles) of ΔpH = 1.0 across the membrane. Lines represent a linear fit to the data. Planar bilayer membranes were made of 45:45:10 mol % PC:PE:CL reconstituted with 15 mol % AA. Buffer contained 50 mM Na_2SO_4, 10 mM Tris, 10 mM MES and 0.6 mM EGTA at pH = 7.34 and T = 306 K. Lipid concentration was 1.5 mg/(mL of buffer solution). Protein concentration measured by BCA assay was 4 µg/(mg of lipid). Insert: Experimental setup of the measurements to establish a transmembrane pH gradient.

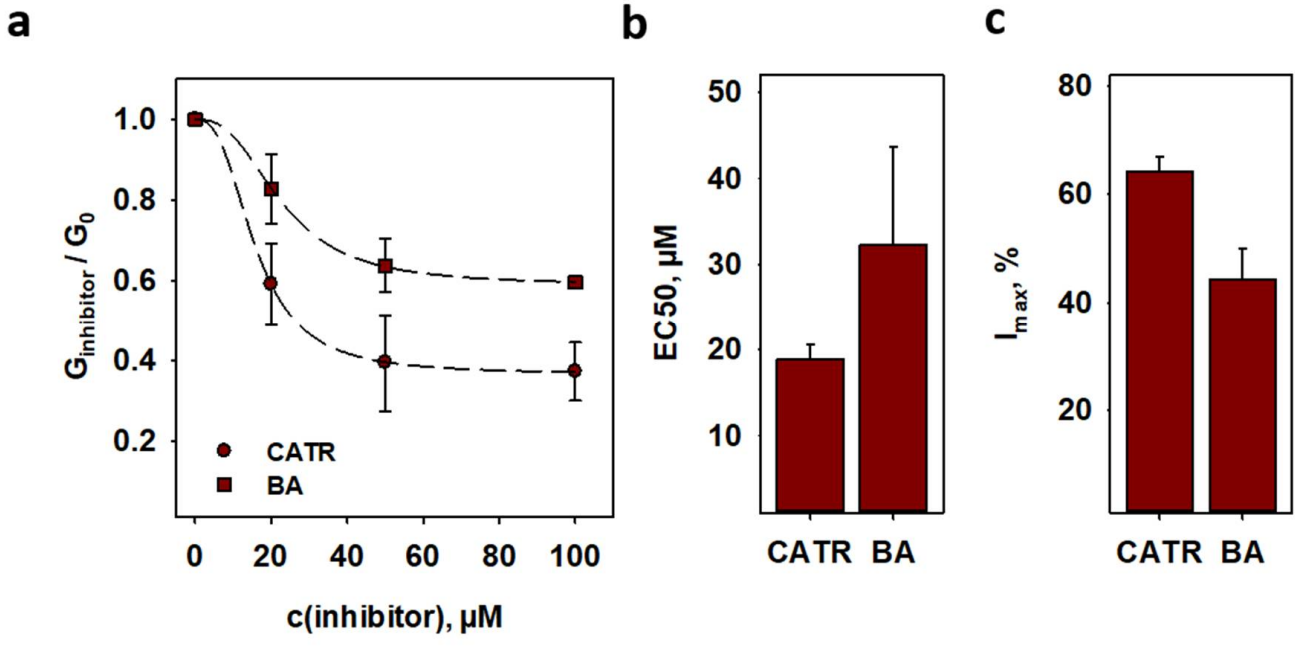

Figure 4. The ADP/ATP exchange inhibitors inhibit ANT-mediated proton leak. (**a**) Dose-dependent inhibition of ANT-mediated proton leak by the inhibitors CATR (circles) and bongkrekic acid (BA, triangles) on proton leak (dark red). Lines are a least square regression fit of a sigmoidal function to the data. (**b**) EC50 and (**c**) maximum inhibition I_{max} as fit parameters of (**a**). Planar bilayer membranes were made of 45:45:10 mol % PC:PE:CL reconstituted with 15 mol % AA. Buffer contained 50 mM Na_2SO_4, 10 mM Tris, 10 mM MES and 0.6 mM EGTA at pH = 7.34 and T = 306 K. Lipid concentration was 1.5 mg/(mL of buffer solution). Protein concentration measured by BCA assay was 4 µg/(mg of lipid). Data are the mean ± SD of at least three independent experiments.

Figure 4. The ADP/ATP exchange inhibitors inhibit ANT-mediated proton leak. (**a**) Dose-dependent inhibition of ANT-mediated proton leak by the inhibitors CATR (circles) and bongkrekic acid (BA, triangles) on proton leak (dark red). Lines are a least square regression fit of a sigmoidal function to the data. (**b**) EC50 and (**c**) maximum inhibition I_{max} as fit parameters of (**a**). Planar bilayer membranes were made of 45:45:10 mol % PC:PE:CL reconstituted with 15 mol % AA. Buffer contained 50 mM Na_2SO_4, 10 mM Tris, 10 mM MES and 0.6 mM EGTA at pH = 7.34 and T = 306 K. Lipid concentration was 1.5 mg/(mL of buffer solution). Protein concentration measured by BCA assay was 4 µg/(mg of lipid). Data are the mean ± SD of at least three independent experiments.

To investigate the interdependence of proton transport, activated by FA, a ADP/ATP transport, we measured G_m of ANT1-containing lipid bilayers reconstitu

eters of (**a**). Planar bilayer membranes were made of 45:45:10 mol % PC:PE:CL reconstituted with 15 mol % AA. Buffer contained 50 mM Na_2SO_4, 10 mM Tris, 10 mM MES and 0.6 mM EGTA at pH = 7.34 and T = 306 K. Lipid concentration was 1.5 mg/(mL of buffer solution). Protein concentration measured by BCA assay was 4 µg/(mg of lipid). Data are the mean ± SD of at least three independent experiments.

To investigate the interdependence of proton transport, activated by FA, and ADP/ATP transport, we measured G_m of ANT1-containing lipid bilayers reconstituted with AA in the presence and absence of purine nucleotides (PN). Adenine nucleotides inhibited H^+ transport much more effectively than guanosine nucleotides (Figure 5a). The EC50 values correlated well with the known narrow substrate specificity of ANT (Figure 5b and Supplementary Table S4) [36]. ATP and ADP fully inhibited G_m, whereas all other PN decreased G_m by 50% (Figure 5c and Supplementary Table S4).

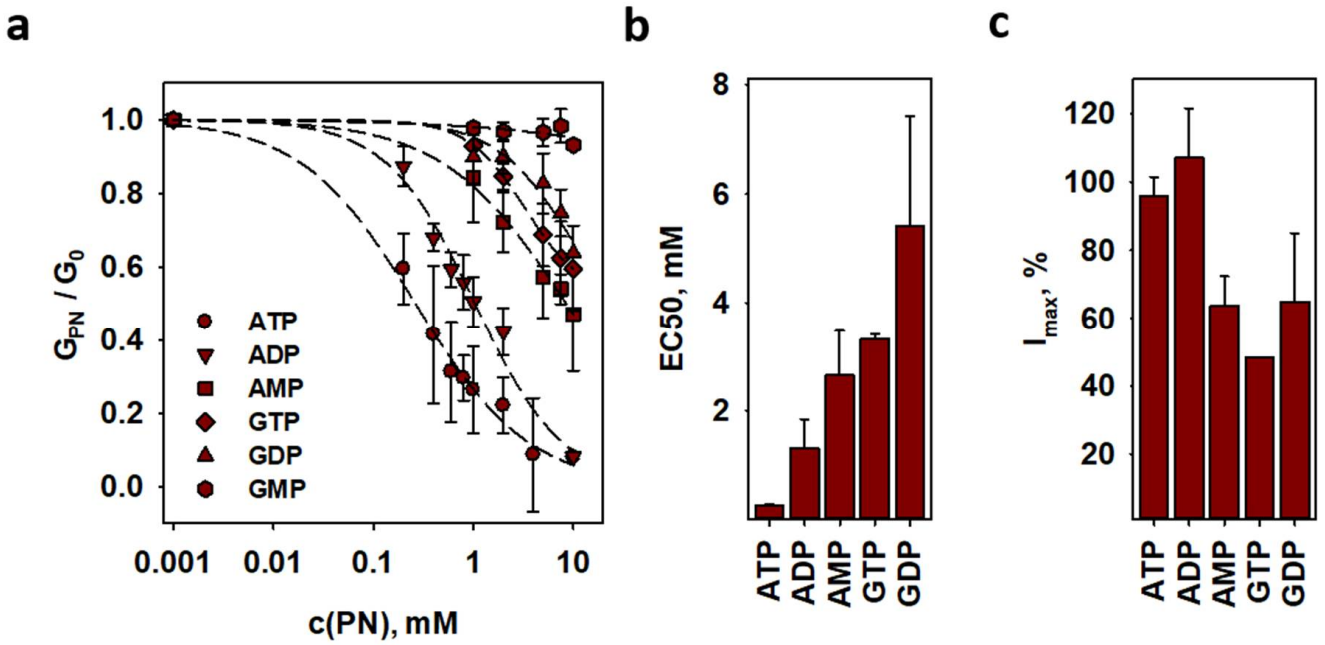

Figure 5. FA activated proton leak is preferably inhibited by ADP and ATP and maintains the substrate specificity of ANT. (**a**) Membrane conductance of lipid bilayers reconstituted with AA and ANT1 in the presence of different purine nucleotides. Lines are a least square regression fit of a sigmoidal function to the data. (**b**) EC50 and (**c**) maximum inhibition values as fit function parameters in (**a**). Values for GMP were dropped due to the low effect. For experimental conditions, see Figure 4. Data are the mean ± SD of at least three independent experiments.

2.6. Analysis of the ANT´s Surface Electrostatic Potential using Molecular Dynamic Simulations

The high similarity of the ANT activation pattern to those of UCP1, UCP2 and UCP3 [6,7,35] leads to the hypothesis that the H^+ transport can be explained by the FA cycling mechanism. We analyzed the ANT's surface electrostatic potential in the DOPC bilayers to test whether a possible FA translocation pathway may be localized at the lipid-protein interface. The calculation revealed a large positively charged patch (Figure 6a) that might facilitate FA anion's sliding alongside the protein. The ATP binding significantly decreased the positive electrostatic potential (Figure 6b) due to its strong screening at the bottom of the cavity [37]. The existence of such a patch would explain the inhibition of H^+ transport by ATP observed in electrophysiological experiments. GTP has less effect on the positive electrostatic potential (Figure 6c) because of its different orientation in the cavity (Figure 6d) and its "weaker interaction with the hydrophobic pocket that binds the adenine moiety" [36].

creased the positive electrostatic potential (Figure 6b) due to its strong screening at the bottom of the cavity [37]. The existence of such a patch would explain the inhibition of H^+ transport by ATP observed in electrophysiological experiments. GTP has less effect on the positive electrostatic potential (Figure 6c) because of its different orientation in the cavity (Figure 6d) and its "weaker interaction with the hydrophobic pocket that binds the adenine moiety" [36].

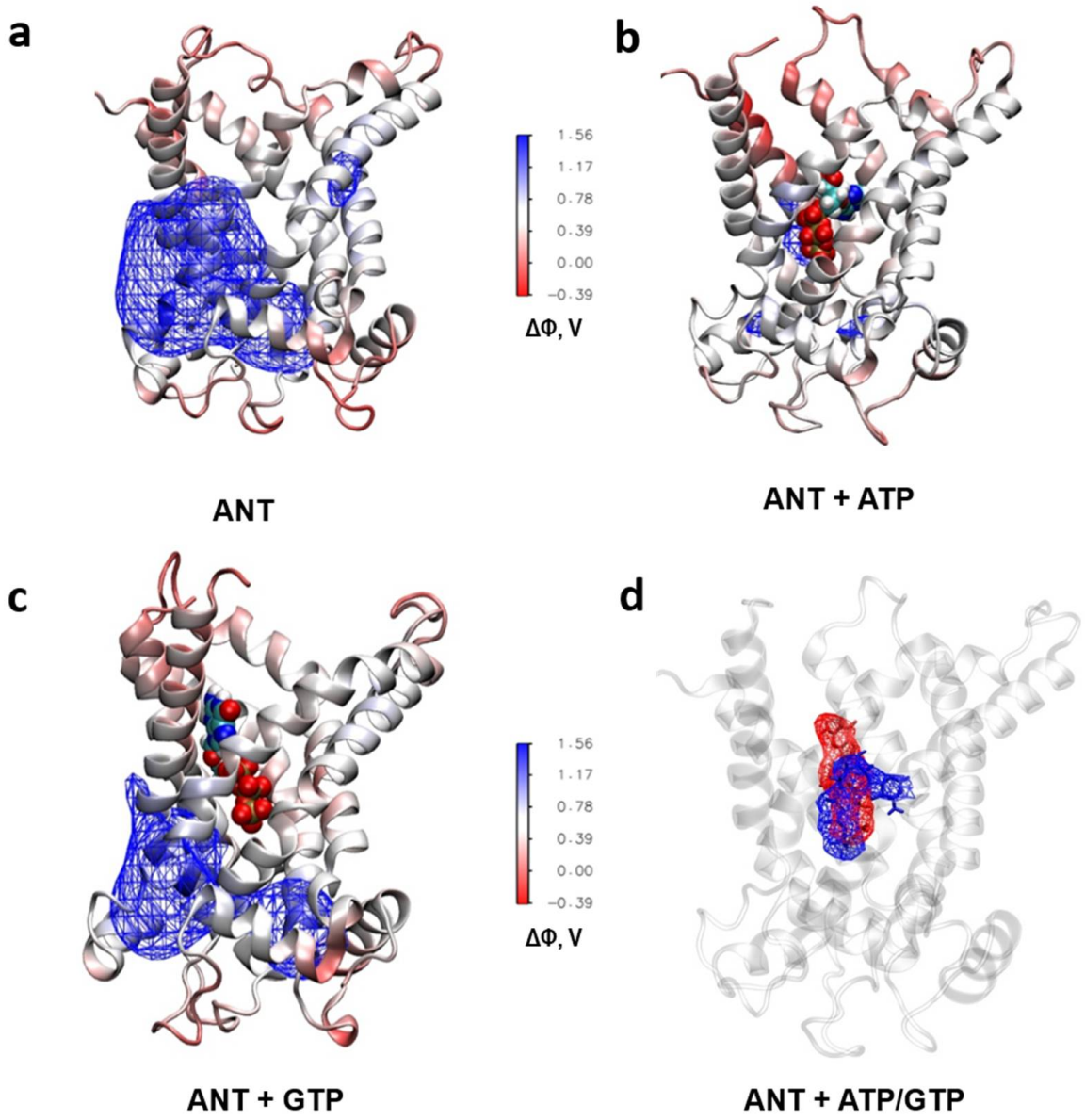

Figure 6. The purine nucleotides ATP and GTP differently modulate the electrostatic surface potential of ANT upon binding. (**a**–**c**) Electrostatic potential (Δ of ANT1 in the absence (**a**) and presence of bound ATP (**b**) and GTP (**c**) calculated by molecular dynamics simulations. The isosurface of the potential of 0.9 V is shown with the wireframe. (**d**) Different average binding location of ATP (blue wireframe) and GTP (red wireframe) in ANT1.

3. Discussion

We investigated the regulation of H^+ transport using planar bilayer membranes reconstituted with the recombinant mouse ANT1. This model allowed us (i) to measure membrane conductance at precisely defined lipid and buffer composition, (ii) to apply mitochondria-relevant potentials directly, and (iii) to separate the ANT1-originated effects from the simultaneous effects of other proteins. The latter is a main disadvantage by the interpretation of experiments on (isolated) mitochondria or mitoplasts representing swollen mitochondria lacking an intact outer membrane.

We confirmed that ANT1 has a dual function performing H^+ transport additionally to the substrate transport. Proton transport occurs only in the presence of the long-chain FAs and reveals high sensitivity to the FA chain length and saturation (Figure 7). The data on ANT1 activation showed remarkable similarity to the activation pattern of uncoupling

len mitochondria lacking an intact outer membrane.

We confirmed that ANT1 has a dual function performing H^+ transport additionally to the substrate transport. Proton transport occurs only in the presence of the long-chain FAs and reveals high sensitivity to the FA chain length and saturation (Figure 7). The data on ANT1 activation showed remarkable similarity to the activation pattern of uncoupling proteins (UCP1-UCP3) [6,7,35]. The dependence of proton transport rate on the FA structure can be explained by the FA cycling model, assuming that the transport of FA anions, which is the rate-limiting step, occurs at the lipid-protein interface as proposed for UCP2 [6].

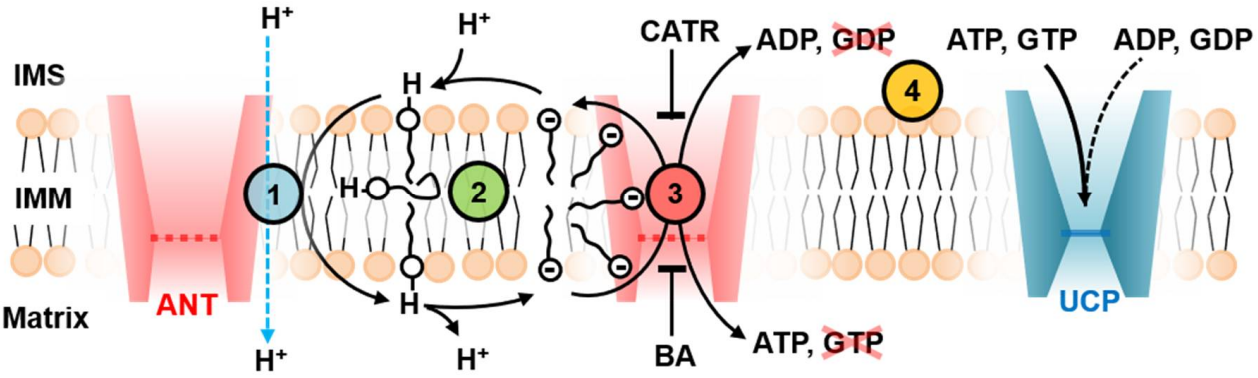

Figure 7. ANT1 transport features point to the fatty acid cycling mechanism. The proton transport rate of ANT1 (Table S3) in the presence of fatty acids (FA) is similar to that proposed for UCPs and depends on the FA structure (Circle 1, blue). ANT1 facilitates the FA anion's transport at the protein-lipid interface, which is supported by the membrane conductance dependence on the FA structure (Circle 2, green). The FA anions slide alongside the electrostatic surface potential of ANT1; its modulation by binding ADP/ATP specific substrates inhibits the FA anion transport (Circle 3, red). The inhibition of ANT1-mediated proton leak is the strongest for the ANT1 substrates—ADP and ATP. It is in contrast to UCPs, in which the triphosphate nucleotides ATP and GTP are the most potent inhibitors (Circle 4, yellow).

Figure 7. ANT1 transport features point to the fatty acid cycling mechanism. The proton transport rate of ANT1 (Tabl. S3) in the presence of fatty acids (FA) is similar to that proposed for UCPs and depends on the FA structure (Circle 1, blue). ANT1 facilitates the FA anion's transport at the protein-lipid interface, which is supported by the membrane conductance dependence on the FA structure (Circle 2, green). The FA anions slide alongside the electrostatic surface potential of ANT1; its modulation by binding ADP/ATP specific substrates inhibits the FA anion transport (Circle 3, red). The inhibition of ANT1-mediated proton leak is the strongest for the ANT1 substrates—ADP and ATP. It is in contrast to UCPs, in which the triphosphate nucleotides ATP and GTP are the most potent inhibitors (Circle 4, yellow).

Although the FA hydrophobicity increases with both chain length and unsaturation, the FA anions occupy similar positions at the lipid-water interface [38]. FA anions should also not further penetrate the ANT1 structure unless a hydrophobic pocket would pull the FA into the ANT1 interior. However, such a membrane-spanning pocket is not found in the ANT structure [39].

Whereas the FA activation pattern of the proton transport seems to be similar in ANT and UCPs, the inhibition pattern is not (Figure 7). We explain it by the fact that these proteins transport different substrates. However, all ANT-specific substrates bind at the substrate-binding site in the ANT cavity [39]. As shown by molecular dynamics simulation, after the ATP binding, the electrostatic potential is diminished, and FAs are potentially less attracted to the ANT surface (Figure 6a,b). Since all substrates (ATP^{4-}, ADP^{3-}, $CATR^{4-}$ and BA^{3-}) are similarly charged and bind to the same region, the electrostatic potential of ANT will be significantly altered upon their binding [36,39,40]. GTP has a different orientation when bound to ANT, which has less impact on ANT's electrostatic potential (Figures 6c,d and 7). The surface electric charge directly correlated with the inhibition potency of PNs. This observation strongly supports the data on the binding site competition between PNs and FAs.

Our model is in strong contrast to the model, which proposed that FAs bind within the ANT cavity and act as a co-factor of H^+ transport [21]. The authors based their model on the experiments showing that non-protonable sulfonated FA failed to induce any transmembrane current in isolated mitoplasts. The use of sulfonated FA is very controversial, as chemical and geometrical properties of the crucial head group are altered compared to the carboxylic head group of native FA. However, the absence of any transient current by non-protonable FA acids is well described by the FA cycling model, in which the net charge transport of H^+ is impaired by the inability of the sulfonated FA to transport a proton across the membrane [41,42]. Upon FA addition to the mitoplast matrix, Bertholet et al. [21] observed no current in contrast to the FA addition to the cytosolic side, showing that the H^+ transport is independent of ANT conformation. The authors claimed that FA reaches its putative binding site inside ANT only from the cytosolic side. However, it is questionable how FAs should activate H^+ transport inside ANT, as protons have to cross at least one salt-bridge network [29], independent of ANT conformation. The FA binding to

ANT and subsequently H^+ binding to the FA in the protein cavity will most probably not provide the energy of roughly 10 kcal/mol to break the strong salt-bridge network [42–46].

The inhibition of H^+ transport in the FA co-factor model can be clearly described as a competition between FA and purine nucleotides for the binding site that we also observed for UCP1 and UCP3 [7]. However, the FA binding site is not further characterized, and it is not clear if there is a common binding target for the FA anion and the adenine nucleotides and/or specific transport inhibitors. Nevertheless, the dependency on FA chain length and unsaturation would imply a loose binding of FAs inside the protein to account for the different structures, which contrasts the high energy required to break the salt-bridge network. Thus, the model proposed by Bertholet et al. [21] seems to fail in describing our experimental results.

We determined the ANT-specific H^+ turnover number of 14.6 $\pm$ 2.5 H^+/s, which is similar to turnover numbers determined earlier for UCPs. Besides ANT and UCPs, FA-activated H^+ leak was also shown for other mitochondrial carriers, including the aspartate/glutamate carrier, dicarboxylate carrier, 2-oxoglutarate carrier, and the phosphate carrier [47–50]. Thus, it is reasonable to conclude a dual transport function for the before mentioned proteins: (i) the substrate transport to maintain mitochondrial respiration and (ii) the proton transport, which may affect the inner mitochondrial membrane potential. We speculate that these carriers have a similar mechanism of FA-mediated activation of H^+ transport due to their high homology. Simultaneous activation of several proton transporters could ensure an essential drop in potential. The latter is crucial for regulating potential-dependent processes in mitochondria, such as reactive oxygen species production, cell death, autophagy, protein secretion, metabolic adaptations, and cell signaling [51]. The controlling of the mitochondrial uncoupling can be used to treat several human diseases, such as obesity, cardiovascular diseases, or neurological disorders.

4. Methods

4.1. Chemicals

Agarose (#3810), KCl (#6781), Na_2SO_4 (#8560), 2-(N-morpholino)ethanesulfonic acid (MES, #4256), sodium dodecyl sulfate (SDS, #0183), tris(hydroxymethyl)-aminomethane (Tris, #AE15), chloroform (#AE54) and ethylene glycol-bis(β-aminoethyl ether)-N,N,N′,N′-tetraacetic acid (EGTA, #3054) were purchased from Carl Roth GmbH & Co. KG (Karlsruhe, Germany). Hexane (#296090), hexadecane (#296317), palmitic acid (#P0500), stearic acid (#S4751), arachidic acid (#A3631), linoleic acid (#L1376) and arachidonic acid (#A3611), dimethyl sulfoxide (DMSO, #472301), the purine nucleotides adenine and guanine tri-, di-, and mono-phosphate (ATP, #A2383; ADP, #A2754; AMP, #01930; GTP #G8877; GDP, #G7127; and GMP, #G8377), carboxyatractyloside (CATR, #C4992) and bongkrekic acid (BA, #B6179) were purchased from Sigma-Aldrich (Vienna, Austria). 1,2-dioleoyl-sn-glycero-3-phosphocholine (DOPC, #850375P), 1,2-dioleoyl-sn-glycero-3-phosphoethanolamine (DOPE, #850725P) and cardiolipin (CL, #710335P) came from Avanti Polar Lipids Inc. (Alabaster, AL, USA).

4.2. Cloning, Purification and Reconstitution of Murine ANT1

Cloning, purification and reconstitution of murine ANT1 followed a previously established protocol [26]. The protein concentration in proteoliposomes was measured with the Micro BCA™ Protein Assay Kit (Thermo Fisher Scientific, Prod. #23235, Waltham, MA, USA). Protein purity was verified by SDS-PAGE and silver staining (Supplementary Figure S1).

4.3. Exchange Rate Measurements of mANT1

ANT-mediated exchange of ADP/ATP was measured radioactively using ^{3}H-ATP (Prod. #NET420250UC, Perkin Elmer, Waltham, MA, USA) following the protocol as described elsewhere [26] (Supplementary Figure S2).

4.4. Electrophysiological Measurements of mANT1

Planar lipid bilayers were formed from proteoliposomes as described previously [31,52]. FAs were added to the lipid phase before membrane formation. Proper membrane formation was verified by measuring membrane capacitance (C = 0.72 ± 0.05 μF/cm^2), which is independent of the presence of protein, FA and inhibitor. Current-voltage (I-U) measurements were performed with a patch-clamp amplifier (EPC 10USB, Werner Instruments, Holliston, MA, USA). The specific total membrane conductance (G_m) at 0 mV was obtained as the slope of a linear fit of the experimental data at applied voltages from −50 mV to + 50 mV and normalized to the membrane area in cm^2. Purine nucleotides (solved in distilled water, pH = 7.34) and ANT-specific inhibitors BA and CATR (solved in DMSO) were added to the buffer solution before forming bilayer membranes. The concentrations of each substrate are indicated in the figure legends. Membrane conductance expressed in relative units was calculated according to [7].

Measurement and calculation of H^+ turnover rate of ANT followed the established protocol [31]. The addition of Tris increased the pH value of the buffer solution on the cis side of the membrane to a value of pH = 8.34.

4.5. Fluorescence Correlation Spectroscopy (FCS)

The average number of ANT1 per liposome was measured using FCS [32,53]. In brief, proteoliposomes obtained after reconstitution of the ANT1 were extruded using a Mini-Extruder system (Avanti Polar Lipids Inc., Alabaster, AL, USA) with a membrane nanopore filter with a pore diameter of 100 nm (Avestin Europe GmbH, Mannheim, Germany, LFM-100). ANT1 was labeled with ATTO 488-maleimide [54] (Sigma-Aldrich, Vienna, Austria; 28562-1MG-F). We used size exclusion chromatography (Sephadex® G-50 Superfine, Merck, Vienna, Austria; GE17-0041-01) to remove the unbound dye. The average residence time, $\tau_{D,}$ and ANT1- containing proteoliposomes number in the focal volume were derived from the autocorrelation function (G(τ)) of the temporal fluorescence signal (Supplementary Figure S5). To measure the signal, a commercial laser scanning microscope (LSM 510 META/ConfoCor 3, Carl Zeiss, Jena, Germany) equipped with avalanche diodes and a 40× water immersion objective was used. The standard model for two-component free 3D diffusion was applied [55]:

$$G(\tau) = 1 + 1/(n\,(1+ \tau/\tau_D)) \quad (1)$$

where the number of fluorescent particles, n, in the detection volume, V_{eff}, was determined as $n = V_{eff}\,C$, where C is the particle concentration. The diffusion coefficient (D) was determined as $D = \omega^2/4\tau_D$, where ω = 0.16 μm is the diameter of the confocal volume cross-section as determined from the calibration experiments.

Dissolving the liposomes with 2% (*v*/*v*) SDS was expected to increase the particle number if liposomes contained more than one ANT1. The average number of ANT1 per liposome, $<N_{ANT1}>$, was obtained from the ratio of the particle number per confocal volume after and before the addition of SDS.

The protein per lipid ratio (ρ) was estimated by:

$$\rho = \frac{N_{ANT1}}{N_{Lipids}} = \left.\frac{< N_{ANT1} >}{< N_{Lipids} >}\right|_{Liposomes} \quad (2)$$

The average number of lipids per liposomes ($<N_{Lipids}>$) is calculated by the ratio of the surface area of the liposome with radius r and the average area per lipid ($A_L \approx 0.6$ nm^2) of a membrane containing DOPC, DOPE and CL [56,57]:

$$< N_{Lipids} >= 2\frac{4\pi r^2}{A_L} \quad (3)$$

Thus, Equation (2) gives:

$$\rho = < N_{ANT1} > \frac{1}{2}\frac{A_L}{4\pi r^2} \quad (4)$$

4.6. Molecular Dynamics Simulations

We performed all-atom molecular dynamics (MD) simulations of ANT1 protein in a 1,2-dioleoyl-sn-glycero-3-phosphocholine (DOPC) bilayer. Residues (residue 1 and residues 294–297) missing from the crystal structure of ANT1 (PDB code: 1okc) [40] without CATR were added using Modeller 9 [58] and implemented into the DOPC bilayer using CHARMM-GUI (http://www.charmm-gui.org/ (accessed on 7 January 2021)) [59–61]. Three system setups were prepared—the wild-type ANT1, the wild-type ANT1 with ATP^{4-} bound in the cytosolic-open state (c-state) [43], as well as GTP^{4-} bound in the same position. All simulation boxes contained ANT1 protein (with a total charge of +19), 73 DOPC molecules per leaflet (146 per system), ~11,500 water molecules, and the necessary number of Cl^- anions to neutralize the net charge, depending on whether ATP^{4-} or GTP^{4-} are added to the system. All systems were first minimized and equilibrated in six steps using the CHARMM-GUI protocol [62] and then simulated for a further 100 ns without any restraints with a 2 fs time step in a periodic rectangular box of 7.9 nm × 7.9 nm × 9.4 nm using the isobaric-isothermal ensemble (NPT) and periodic boundary conditions in all directions at T = 310 K, maintained via Nosé–Hoover thermostat [63] independently for the DOPC, water/ions and protein subsystems with a coupling constant of 1.0 ps^{-1}. The pressure was set to 1.013 bar and controlled with a semi-isotropic Parrinello-Rahman barostat [64] with a time constant for pressure coupling of 5 ps^{-1}. Long-range electrostatics were calculated using the particle-mesh Ewald (PME) method [65] with real space Coulomb interactions cut off at 1.2 nm using a Fourier spacing of 0.12 nm and a Verlet cut-off scheme. All simulated systems were described by the CHARMM36m force field [66]. The electrostatic potential maps of all systems were calculated using VMD's PMEPOT plugin [67]. All simulations were run with the GROMACS 5.1.4 software package [68] and visualized with the VMD molecular graphics program [69].

4.7. Statistics

Data analysis and fitting of electrophysiological measurements were performed using Sigma Plot 12.5 (Systat Software GmbH, Erkrath, Germany) and displayed as mean ± SD of at least three independent measurements.

Supplementary Materials: The following are available online at https://www.mdpi.com/1422-0067/22/5/2490/s1.

Author Contributions: Conceptualization, E.E.P., A.R., J.K. and M.V.; funding acquisition, E.E.P. and M.V.; investigation, J.K., D.G.K., K.Ž., S.Š., Z.B., S.B. and M.V.; project administration, E.E.P.; resources, E.E.P. and M.V.; supervision, E.E.P. and M.V.; writing—original draft, J.K., M.V. and E.E.P.; writing—review and editing, J.K., A.R., S.Š., Z.B., D.G.K., K.Ž., S.B., E.E.P. and M.V. All authors have read and agreed to the published version of the manuscript.

Funding: We acknowledge support from the Austrian Research Fund (FWF, P31559 to E.E.P.) and Croatian Science Foundation (Project No. IP-2019-04-3804 to M.V.). We thank the computer cluster Isabella based in SRCE—University of Zagreb, University Computing Centre for computational resources. M. V. thanks UOCHB Sabbatical visit program for support.

Institutional Review Board Statement: Not applicable.

Informed Consent Statement: Not applicable.

Data Availability Statement: The datasets generated and/or analyzed during this study are available from the corresponding authors on reasonable request.

Acknowledgments: We thank Y.N. Antonenko (Belozersky Institute of Physico-Chemical Biology, Lomonosov Moscow State University, Moscow, Russia) for the valuable comments on the manuscript.

Conflicts of Interest: The authors declare no conflict of interest.

References

1. Brand, M.D. The proton leak across the mitochondrial inner membrane. *Biochim. Biophys. Acta* **1990**, *1018*, 128–133. [CrossRef]
2. Rolfe, D.F.; Brand, M.D. Contribution of mitochondrial proton leak to skeletal muscle respiration and to standard metabolic rate. *Am. J. Physiol.* **1996**, *271 Pt 1*, C1380–C1389. [CrossRef]
3. Rolfe, D.F.; Brand, M.D. The physiological significance of mitochondrial proton leak in animal cells and tissues. *Biosci. Rep.* **1997**, *17*, 9–16. [CrossRef] [PubMed]
4. Krauss, S.; Zhang, C.Y.; Lowell, B.B. The mitochondrial uncoupling-protein homologues. *Nat. Rev. Mol. Cell Biol.* **2005**, *6*, 248–261. [CrossRef] [PubMed]
5. Skulachev, V.P. Uncoupling: New approaches to an old problem of bioenergetics. *Biochim. Biophys. Acta* **1998**, *1363*, 100–124. [CrossRef]
6. Beck, V.; Jaburek, M.; Demina, T.; Rupprecht, A.; Porter, R.K.; Jezek, P.; Pohl, E.E. Polyunsaturated fatty acids activate human uncoupling proteins 1 and 2 in planar lipid bilayers. *FASEB J.* **2007**, *21*, 1137–1144. [CrossRef]
7. Macher, G.; Koehler, M.; Rupprecht, A.; Kreiter, J.; Hinterdorfer, P.; Pohl, E.E. Inhibition of mitochondrial UCP1 and UCP3 by purine nucleotides and phosphate. *Biochim. Biophys. Acta Biomembr.* **2018**, *1860*, 664–672. [CrossRef] [PubMed]
8. Zackova, M.; Jezek, P. Reconstitution of novel mitochondrial uncoupling proteins UCP2 and UCP3. *Biosci. Rep.* **2002**, *22*, 33–46. [CrossRef]
9. Hoang, T.; Smith, M.D.; Jelokhani-Niaraki, M. Toward understanding the mechanism of ion transport activity of neuronal uncoupling proteins UCP2, UCP4, and UCP5. *Biochemistry* **2012**, *51*, 4004–4014. [CrossRef]
10. Pohl, E.E.; Rupprecht, A.; Macher, G.; Hilse, K.E. Important Trends in UCP3 Investigation. *Front. Physiol.* **2019**, *10*, 470. [CrossRef] [PubMed]
11. Heldt, H.W.; Jacobs, H.; Klingenberg, M. Endogenous Adp of Mitochondria, an Early Phosphate Acceptor of Oxidative Phosphorylation as Disclosed by Kinetic Studies with C14 Labelled Adp and Atp and with Atractyloside. *Biochem. Biophys. Res. Commun.* **1965**, *18*, 174–179. [CrossRef]
12. Pfaff, E.; Klingenberg, M.; Heldt, H.W. Unspecific permeation and specific exchange of adenine nucleotides in liver mitochondria. *Biochim. Biophys. Acta* **1965**, *104*, 312–315. [CrossRef]
13. Vignais, P.V. The mitochondrial adenine nucleotide translocator. *J. Bioenerg.* **1976**, *8*, 9–17. [CrossRef] [PubMed]
14. Kunji, E.R.; Aleksandrova, A.; King, M.S.; Majd, H.; Ashton, V.L.; Cerson, E.; Springett, R.; Kibalchenko, M.; Tavoulari, S.; Crichton, P.G.; et al. The transport mechanism of the mitochondrial ADP/ATP carrier. *Biochim. Biophys. Acta* **2016**, *1863*, 2379–2393. [CrossRef]
15. Klingenberg, M. The ADP and ATP transport in mitochondria and its carrier. *Biochim. Biophys. Acta* **2008**, *1778*, 1978–2021. [CrossRef] [PubMed]
16. Andreyev, A.Y.; Bondareva, T.O.; Dedukhova, V.I.; Mokhova, E.N.; Skulachev, V.P.; Volkov, N.I. Carboxyatractylate inhibits the uncoupling effect of free fatty acids. *FEBS Lett.* **1988**, *226*, 265–269. [CrossRef]
17. Andreyev, A.Y.; Bondareva, T.O.; Dedukhova, V.I.; Mokhova, E.N.; Skulachev, V.P.; Tsofina, L.M.; Volkov, N.I.; Vygodina, T.V. The ATP/ADP-antiporter is involved in the uncoupling effect of fatty acids on mitochondria. *Eur. J. Biochem.* **1989**, *182*, 585–592. [CrossRef]
18. Brustovetsky, N.; Klingenberg, M. The reconstituted ADP/ATP carrier can mediate H+ transport by free fatty acids, which is further stimulated by mersalyl. *J. Biol. Chem.* **1994**, *269*, 27329–27336. [CrossRef]
19. Shabalina, I.G.; Kramarova, T.V.; Nedergaard, J.; Cannon, B. Carboxyatractyloside effects on brown-fat mitochondria imply that the adenine nucleotide translocator isoforms Ant1 and Ant2 may be responsible for basal and fatty acid-induced uncoupling, respectively. *Biochem. J.* **2006**, *399*, 405–414. [CrossRef]
20. Brand, M.D.; Pakay, J.L.; Ocloo, A.; Kokoszka, J.; Wallace, D.C.; Brookes, P.S.; Cornwall, E.J. The basal proton conductance of mitochondria depends on adenine nucleotide translocase content. *Biochem. J.* **2005**, *392 Pt 2*, 353–362. [CrossRef]
21. Bertholet, A.M.; Chouchani, E.T.; Kazak, L.; Angelin, A.; Fedorenko, A.; Long, J.Z.; Vidoni, S.; Garrity, R.; Cho, J.; Terada, N.; et al. H(+) transport is an integral function of the mitochondrial ADP/ATP carrier. *Nature* **2019**, *571*, 515–520. [CrossRef] [PubMed]
22. Kamp, F.; Hamilton, J.A. pH gradients across phospholipid membranes caused by fast flip-flop of un-ionized fatty acids. *Proc. Natl. Acad. Sci. USA* **1992**, *89*, 11367–11370. [CrossRef] [PubMed]
23. Pohl, E.E.; Peterson, U.; Sun, J.; Pohl, P. Changes of intrinsic membrane potentials induced by flip-flop of long-chain fatty acids. *Biochemistry* **2000**, *39*, 1834–1839. [CrossRef] [PubMed]
24. Skulachev, V.P. Fatty acid circuit as a physiological mechanism of uncoupling of oxidative phosphorylation. *FEBS Lett.* **1991**, *294*, 158–162. [CrossRef]
25. Fedorenko, A.; Lishko, P.V.; Kirichok, Y. Mechanism of fatty-acid-dependent UCP1 uncoupling in brown fat mitochondria. *Cell* **2012**, *151*, 400–413. [CrossRef] [PubMed]
26. Kreiter, J.; Beitz, E.; Pohl, E.E. A Fluorescence-Based Method to Measure ADP/ATP Exchange of Recombinant Adenine Nucleotide Translocase in Liposomes. *Biomolecules* **2020**, *10*, 685. [CrossRef] [PubMed]
27. Kramer, R.; Klingenberg, M. Electrophoretic control of reconstituted adenine nucleotide translocation. *Biochemistry* **1982**, *21*, 1082–1089. [CrossRef] [PubMed]

28. Heidkamper, D.; Muller, V.; Nelson, D.R.; Klingenberg, M. Probing the role of positive residues in the ADP/ATP carrier from yeast. The effect of six arginine mutations on transport and the four ATP versus ADP exchange modes. *Biochemistry* **1996**, *35*, 16144–16152. [CrossRef] [PubMed]
29. King, M.S.; Kerr, M.; Crichton, P.G.; Springett, R.; Kunji, E.R.S. Formation of a cytoplasmic salt bridge network in the matrix state is a fundamental step in the transport mechanism of the mitochondrial ADP/ATP carrier. *Biochim. Biophys. Acta* **2016**, *1857*, 14–22. [CrossRef] [PubMed]
30. Rupprecht, A.; Sokolenko, E.A.; Beck, V.; Ninnemann, O.; Jaburek, M.; Trimbuch, T.; Klishin, S.S.; Jezek, P.; Skulachev, V.P.; Pohl, E.E. Role of the transmembrane potential in the membrane proton leak. *Biophys. J* **2010**, *98*, 1503–1511. [CrossRef] [PubMed]
31. Kreiter, J.; Pohl, E.E. A Micro-agar Salt Bridge Electrode for Analyzing the Proton Turnover Rate of Recombinant Membrane Proteins. *J. Vis. Exp.* **2019**, *143*, e58552. [CrossRef]
32. Erokhova, L.; Horner, A.; Kugler, P.; Pohl, P. Monitoring single-channel water permeability in polarized cells. *J. Biol. Chem.* **2011**, *286*, 39926–39932. [CrossRef]
33. Nicholls, D.G. The effective proton conductance of the inner membrane of mitochondria from brown adipose tissue. Dependency on proton electrochemical potential gradient. *Eur. J. Biochem.* **1977**, *77*, 349–356. [CrossRef] [PubMed]
34. Klingenberg, M.; Winkler, E. The reconstituted isolated uncoupling protein is a membrane potential driven H+ translocator. *EMBO J.* **1985**, *4*, 3087–3092. [CrossRef]
35. Urbankova, E.; Voltchenko, A.; Pohl, P.; Jezek, P.; Pohl, E.E. Transport kinetics of uncoupling proteins. Analysis of UCP1 reconstituted in planar lipid bilayers. *J. Biol. Chem.* **2003**, *278*, 32497–32500. [CrossRef] [PubMed]
36. Mifsud, J.; Ravaud, S.; Krammer, E.M.; Chipot, C.; Kunji, E.R.; Pebay-Peyroula, E.; Dehez, F. The substrate specificity of the human ADP/ATP carrier AAC1. *Mol. Membr. Biol.* **2013**, *30*, 160–168. [CrossRef] [PubMed]
37. Krammer, E.M.; Ravaud, S.; Dehez, F.; Frelet-Barrand, A.; Pebay-Peyroula, E.; Chipot, C. High-chloride concentrations abolish the binding of adenine nucleotides in the mitochondrial ADP/ATP carrier family. *Biophys. J.* **2009**, *97*, L25–L27. [CrossRef]
38. Pashkovskaya, A.A.; Vazdar, M.; Zimmermann, L.; Jovanovic, O.; Pohl, P.; Pohl, E.E. Mechanism of Long-Chain Free Fatty Acid Protonation at the Membrane-Water Interface. *Biophys. J.* **2018**, *114*, 2142–2151. [CrossRef] [PubMed]
39. Ruprecht, J.J.; Kunji, E.R. Structural changes in the transport cycle of the mitochondrial ADP/ATP carrier. *Curr. Opin. Struct. Biol.* **2019**, *57*, 135–144. [CrossRef] [PubMed]
40. Pebay-Peyroula, E.; Dahout-Gonzalez, C.; Kahn, R.; Trezeguet, V.; Lauquin, G.J.; Brandolin, G. Structure of mitochondrial ADP/ATP carrier in complex with carboxyatractyloside. *Nature* **2003**, *426*, 39–44. [CrossRef] [PubMed]
41. Jaburek, M.; Varecha, M.; Jezek, P.; Garlid, K.D. Alkylsulfonates as probes of uncoupling protein transport mechanism. Ion pair transport demonstrates that direct H(+) translocation by UCP1 is not necessary for uncoupling. *J. Biol. Chem.* **2001**, *276*, 31897–31905.
42. Jezek, P.; Holendova, B.; Garlid, K.D.; Jaburek, M. Mitochondrial Uncoupling Proteins: Subtle Regulators of Cellular Redox Signaling. *Antioxid. Redox Signal.* **2018**, *29*, 667–714. [PubMed]
43. Wang, Y.; Tajkhorshid, E. Electrostatic funneling of substrate in mitochondrial inner membrane carriers. *Proc. Natl. Acad. Sci. USA* **2008**, *105*, 9598–9603. [CrossRef] [PubMed]
44. Dehez, F.; Pebay-Peyroula, E.; Chipot, C. Binding of ADP in the mitochondrial ADP/ATP carrier is driven by an electrostatic funnel. *J. Am. Chem. Soc.* **2008**, *130*, 12725–12733. [CrossRef]
45. Pietropaolo, A.; Pierri, C.L.; Palmieri, F.; Klingenberg, M. The switching mechanism of the mitochondrial ADP/ATP carrier explored by free-energy landscapes. *Biochim. Biophys. Acta* **2016**, *1857*, 772–781. [CrossRef]
46. Škulj, S.; Brkljača, Z.; Vazdar, M. Molecular Dynamics Simulations of the Elusive Matrix-Open State of Mitochondrial ADP/ATP Carrier. *Isr. J. Chem.* **2020**, *60*, 735–743. [CrossRef]
47. Samartsev, V.N.; Smirnov, A.V.; Zeldi, I.P.; Markova, O.V.; Mokhova, E.N.; Skulachev, V.P. Involvement of aspartate/glutamate antiporter in fatty acid-induced uncoupling of liver mitochondria. *Biochim. Biophys. Acta* **1997**, *1319*, 251–257. [CrossRef]
48. Wieckowski, M.R.; Wojtczak, L. Involvement of the dicarboxylate carrier in the protonophoric action of long-chain fatty acids in mitochondria. *Biochem. Biophys. Res. Commun.* **1997**, *232*, 414–417. [PubMed]
49. Engstova, H.; Zackova, M.; Ruzicka, M.; Meinhardt, A.; Hanus, J.; Kramer, R.; Jezek, P. Natural and azido fatty acids inhibit phosphate transport and activate fatty acid anion uniport mediated by the mitochondrial phosphate carrier. *J. Biol. Chem.* **2001**, *276*, 4683–4691. [CrossRef]
50. Yu, X.X.; Lewin, D.A.; Zhong, A.; Brush, J.; Schow, P.W.; Sherwood, S.W.; Pan, G.; Adams, S.H. Overexpression of the human 2-oxoglutarate carrier lowers mitochondrial membrane potential in HEK-293 cells: Contrast with the unique cold-induced mitochondrial carrier CGI-69. *Biochem. J.* **2001**, *353 Pt 2*, 369–375. [CrossRef]
51. Demine, S.; Renard, P.; Arnould, T. Mitochondrial Uncoupling: A Key Controller of Biological Processes in Physiology and Diseases. *Cells* **2019**, *8*, 795. [CrossRef]
52. Beck, V.; Jaburek, M.; Breen, E.P.; Porter, R.K.; Jezek, P.; Pohl, E.E. A new automated technique for the reconstitution of hydrophobic proteins into planar bilayer membranes. Studies of human recombinant uncoupling protein 1. *Biochim. Biophys. Acta* **2006**, *1757*, 474–479. [CrossRef] [PubMed]
53. Knyazev, D.G.; Lents, A.; Krause, E.; Ollinger, N.; Siligan, C.; Papinski, D.; Winter, L.; Horner, A.; Pohl, P. The bacterial translocon SecYEG opens upon ribosome binding. *J. Biol. Chem.* **2013**, *288*, 17941–17946. [CrossRef] [PubMed]

54. Majima, H.J.; Oberley, T.D.; Furukawa, K.; Mattson, M.P.; Yen, H.C.; Szweda, L.I.; St Clair, D.K. Prevention of mitochondrial injury by manganese superoxide dismutase reveals a primary mechanism for alkaline-induced cell death. *J. Biol. Chem.* **1998**, *273*, 8217–8224. [CrossRef] [PubMed]
55. Magde, D.; Elson, E.L.; Webb, W.W. Fluorescence correlation spectroscopy. II. An experimental realization. *Biopolymers* **1974**, *13*, 29–61. [CrossRef]
56. Boscia, A.L.; Treece, B.W.; Mohammadyani, D.; Klein-Seetharaman, J.; Braun, A.R.; Wassenaar, T.A.; Klosgen, B.; Tristram-Nagle, S. X-ray structure, thermodynamics, elastic properties and MD simulations of cardiolipin/dimyristoylphosphatidylcholine mixed membranes. *Chem. Phys. Lipids* **2014**, *178*, 1–10. [CrossRef] [PubMed]
57. De Vries, A.H.; Mark, A.E.; Marrink, S.J. The Binary Mixing Behavior of Phospholipids in a Bilayer: A Molecular Dynamics Study. *J. Phys. Chem. B* **2004**, *108*, 2454–2463. [CrossRef]
58. Webb, B.; Sali, A. Comparative Protein Structure Modeling Using MODELLER. *Curr. Protoc. Bioinform.* **2014**, *47*, 5.6.1–5.6.37. [CrossRef]
59. Jo, S.; Lim, J.B.; Klauda, J.B.; Im, W. CHARMM-GUI Membrane Builder for mixed bilayers and its application to yeast membranes. *Biophys. J.* **2009**, *97*, 50–58. [CrossRef]
60. Wu, E.L.; Cheng, X.; Jo, S.; Rui, H.; Song, K.C.; Davila-Contreras, E.M.; Qi, Y.; Lee, J.; Monje-Galvan, V.; Venable, R.M.; et al. CHARMM-GUI Membrane Builder toward realistic biological membrane simulations. *J. Comput. Chem.* **2014**, *35*, 1997–2004. [CrossRef] [PubMed]
61. Lee, J.; Cheng, X.; Swails, J.M.; Yeom, M.S.; Eastman, P.K.; Lemkul, J.A.; Wei, S.; Buckner, J.; Jeong, J.C.; Qi, Y.; et al. CHARMM-GUI Input Generator for NAMD, GROMACS, AMBER, OpenMM, and CHARMM/OpenMM Simulations Using the CHARMM36 Additive Force Field. *J. Chem. Theory Comput.* **2016**, *12*, 405–413. [CrossRef] [PubMed]
62. Jo, S.; Kim, T.; Im, W. Automated Builder and Database of Protein/Membrane Complexes for Molecular Dynamics Simulations. *PLoS ONE* **2007**, *2*, e880. [CrossRef]
63. Nosé, S. A molecular dynamics method for simulations in the canonical ensemble. *Mol. Phys.* **1984**, *52*, 255–268. [CrossRef]
64. Parrinello, M.; Rahman, A. Polymorphic transitions in single crystals: A new molecular dynamics method. *J. Appl. Phys.* **1981**, *52*, 7182–7190. [CrossRef]
65. Essmann, U.; Perera, L.; Berkowitz, M.L.; Darden, T.; Lee, H.; Pedersen, L.G. A smooth particle mesh Ewald method. *J. Chem. Phys.* **1995**, *103*, 8577–8593. [CrossRef]
66. Huang, J.; Rauscher, S.; Nawrocki, G.; Ran, T.; Feig, M.; de Groot, B.L.; Grubmuller, H.; MacKerell, A.D., Jr. CHARMM36m: An improved force field for folded and intrinsically disordered proteins. *Nat. Methods* **2017**, *14*, 71–73. [CrossRef]
67. Aksimentiev, A.; Schulten, K. Imaging alpha-hemolysin with molecular dynamics: Ionic conductance, osmotic permeability, and the electrostatic potential map. *Biophys. J.* **2005**, *88*, 3745–3761. [CrossRef]
68. Abraham, M.J.; Murtola, T.; Schulz, R.; Páll, S.; Smith, J.C.; Hess, B.; Lindahl, E. GROMACS: High performance molecular simulations through multi-level parallelism from laptops to supercomputers. *SoftwareX* **2015**, *1–2*, 19–25. [CrossRef]
69. Humphrey, W.; Dalke, A.; Schulten, K. VMD: Visual molecular dynamics. *J. Mol. Graph.* **1996**, *14*, 33–38. [CrossRef]

3. Conclusions

In this study, we made a discovery finding that OGC increases proton conductance when in the presence of natural and chemical protonophores. The increase in OGC activity directly correlates with the increase in the number of unsaturated bonds of the FA. We identified arginine 90 as a crucial residue for the binding of FAs, substrates 2-oxoglutarate and malate, and inhibitors ATP and phenyl succinate.

Moreover, our results show that the protonophoric effect of DNP is not only significantly increased by OGC, but also by other mitochondrial carriers, such as ANT1 and UCP1-UCP3 as well. Thus, we highlight the importance of studying DNP as a very potent chemical protonophore that interacts with both biological membranes and multiple mitochondrial carriers. Furthermore, by using site-directed mutagenesis and molecular dynamics simulations, we showed that arginine 79 of ANT1, a homolog of arginine 90 of OGC, is crucial for DNP´s binding to the protein. We showed that this amino acid residue is also crucial for the binding of FAs, ANT1´s substrates, and inhibitors, in a manner similar to OGC.

Finally, we proved that the protein-mediated proton conductance is indirectly enhanced by a covalent modification of membrane lipids by oxidative stress products, such as RAs. This modification decreases the bending modulus in lipid bilayers and potentiates FA turnover, which consequently increases protein-mediated protonophoric activity.

Taken together, our results point to a preserved mechanism of proton-transport mediation among the SLC25 family, which resembles the fatty-acid cycling hypothesis and is strongly affected by increased oxidative stress.

4. Discussion

4.1. Advantages and shortages of model membrane systems

Biological membranes have complex compositions made out of lipids, proteins, and carbohydrates, where their ratios and presence depend on the membrane type. Doing experimental work with these membranes is often challenging, due to the difficult processes of isolating and maintaining them in their native conditions (van Meer et al. 2008).

On the other hand, model membrane systems have a defined lipid composition, and are used to mimic natural membranes. Unlike biological membranes, model membranes are easier to form and maintain, and given the predefined conditions, they are easier to obtain data from using them. They can be divided into lipid monolayers, lipid vesicles, and supported or tethered lipid bilayer systems (Labbé & Buriez 2021). In our case, the model membrane system is a unique patented system (US20060228402A1), where a lipid bilayer is created on the surface of a conventional plastic tip (Fig. 9) (Beck et al. 2006). The additional advantages of this system are: (i) no organic solution is used; (ii) the diameter of the membrane of approx. 300 µm enables the insertion of multiple protein copies (~107) into a single bilayer, which is important for the investigation of transporters; (iii) transmembrane voltages up to 200 mV can be applied; (iv) all components of the system are known and pre-defined (Beck et al. 2006).

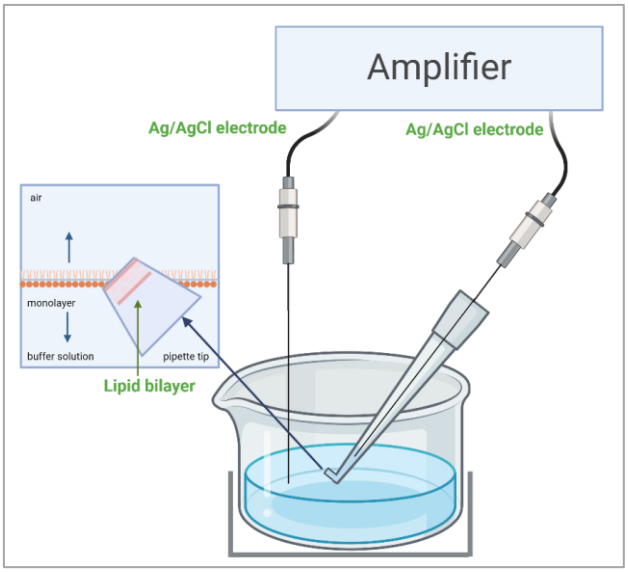

Figure 9. The lipid bilayer is created on the surface of a conventional plastic tip by a continuous insertion of the tip into the lipid-containing solution. The net current over the lipid bilayer is measured by silver chloride electrodes and amplified. Image created with BioRender.

One of the disadvantages of model membranes is the simplification of usually very complex and organized systems. It is possible to include up to four different lipid species in a model membrane, but natural membranes have more than hundreds (Muro et al. 2014). Natural membranes also contain cytoskeletal components as well as a variety of proteins, which are conditions rather difficult to replicate in model membranes. The preparation of model membranes can also be troublesome and often requires the use of organic solvents (Gustafson & Tagesson 1985). Therefore, one might doubt that the effects noticed on model membranes happen in a living organism. However, over the years, model membranes became more sophisticated which opened up the possibility of incorporating intricate and complex mixtures of lipids, asymmetric lipid bilayers, and membrane proteins into the system (Gutsmann et al. 2015, Pabst & Keller 2024).

Working with biological membranes offers a higher degree of similarity to the living system, but it does not guarantee any specificity. For example, one could study the contribution of only one protein to FA-mediated uncoupling by adding a certain amount of FA to the isolated mitoplasts containing the protein of interest overexpressed and measuring the net current, while comparing it to wild-type mitochondria and concluding that only that protein increases the current. However, given the complexity of the IMM, there might be many off-targeted or compensatory effects that come into place when a certain protein is overexpressed or activated. In the case of the SLC25 family and the high homology between its members, there are probably more undiscovered proteins that can uncouple the MMP in the presence of FAs, as was the case with OGC (Žuna et al. 2024). Therefore, purifying and reconstituting only one membrane protein in a model lipid bilayer system is the only way to know for sure if that protein is capable and directly responsible for performing a specific function.

4.2. Conserved mechanism of proton-transport mediation among the SLC25 family

Our findings suggest that SLC25 proteins that facilitate FA or DNP-mediated proton transport share a common mechanism for protonophore transport. This notion is supported by the high sequence homology between the carriers (Fig. 10) and structures that closely resemble each other. ANT1 and UCP1 are the only carriers in the family with resolved 3D structures (Pebay-Peyroula et al. 2003, Harding et al. 2020, Jones et al. 2023, Kang & Chen 2023), which differ only in a wider part of the cavity which determines the substrate specificity. Sequence prediction and artificial intelligence-based structural models anticipate that the other SLC25 carriers share the same structure as ANT1 and UCP1. Moreover, Kunji & Robinson proposed a common binding site for substrates, which consists of three distinct amino acid residues that are conserved across the entire protein family (Kunji & Robinson 2006).

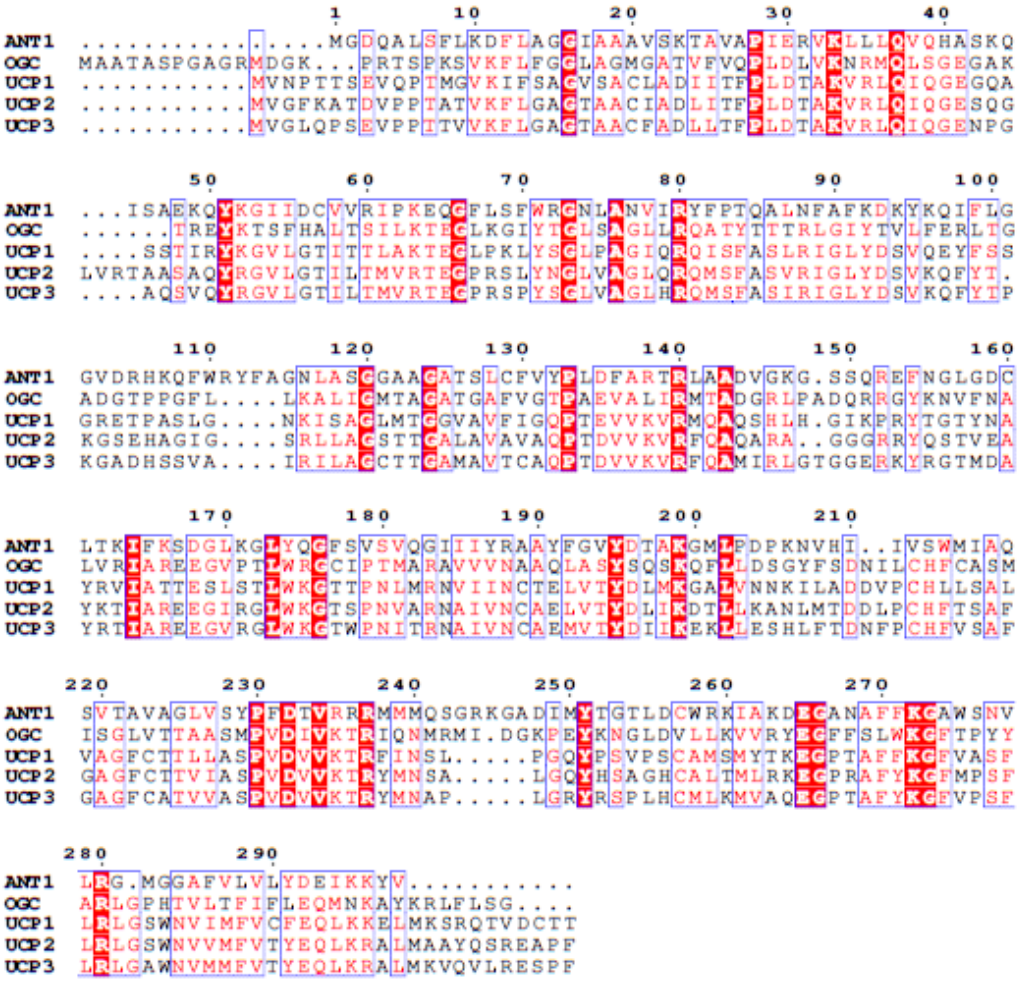

Figure 10. Sequence alignment of murine ANT1, OGC, and UCP1-3. Generated with ClustalW and colored with ESPript 3.0. The most conserved amino acid residues in mitochondrial signature motifs and the substrate binding sites are colored in dark red.

4.2.1. Competitive inhibition points to a common binding site for substrates and protonophores

We found that OGC, ANT1, and UCP1-UCP3 similarly interact with FA and DNP and that the binding site for protonophores overlaps partly with the substrate binding site. The increase in the protein-mediated protonophoric activity happened only in the presence of FAs/DNP, and in line with the increase in FA chain length and the number of unsaturated bonds (Kreiter et al. 2021, Žuna et al. 2021, Žuna et al. 2024).

In the case of both FA and DNP-mediated proton transport, the increase in proton conductance was inhibitable when we applied ATP to the protein-containing system. This implies the existence of competitive inhibition between the two molecules and the protein´s substrate binding site (Kreiter et al. 2021, Žuna et al. 2021, Žuna et al. 2024). Furthermore, the increase in protein-mediated proton transport in the presence of FA was diminished when we applied protein-specific substrates (2-oxoglutarate and malate for OGC, ADP/ATP for ANT1) and inhibitors (phenyl succinate for OGC, CATR, and BKA for ANT1), further implying a common binding site for all. By using site-directed mutagenesis and molecular dynamics simulations, we identified R90 of OGC as crucial for binding FAs (Žuna et al. 2024), and its homolog in ANT1, R79, for binding DNP (Žuna et al. 2021). This is in agreement with other results where R79 was identified as crucial for binding DNP in UCP1 (Kang & Chen 2023), ATP in UCP1 and UCP3 (Macher et al. 2017, Kang & Chen 2023), and ADP, ATP, CATR and BKA in ANT1 (Pebay-Peyroula et al. 2003, Robinson et al. 2008, Wang & Tajkhorshid 2008, Ruprecht & Kunji 2019). It was also later proposed as a crucial part of the newly proposed ANT1´s FA sliding pathway, which supports the fatty acid cycling mechanism (Kreiter et al. 2023).

The proposed “FA sliding” pathway for ANT1 (Kreiter et al. 2023) supports the fatty acid cycling pathway and involves protein parts that are conserved throughout the whole protein family. For example, positively charged residues on the matrix side that attract negatively charged FAs, the positively charged protein-lipid interface, and homologs to the R79 contact point and the D134 FA-protonation site, are conserved in OGC, UCP1-3, DIC, PiC, and AGC. Experimentally based evidence and high sequence homology across the family shows that SLC25 proteins are not transporters of protons, but rather transporters of FA anions.

4.2.2. Transient proton transport can rapidly shield cells from oxidative stress

Our results are of physiological significance because they show that proton uncoupling can be potentiated with multiple SLC25 carriers, probably even simultaneously. It would be more feasible for the cell to utilize all proton transport facilitating proteins at the same time compared to the time and energy-consuming overexpression of only one carrier.

Many members of the SLC25 family have already been identified as proton transport mediators, and given the high homology across the family, there are more to come. Proteins such as UCP2 and UCP3, which were originally considered only as proton transport facilitators, were proven to be substrate transporters as well (Vozza et al. 2014, Kreiter et al. 2023, De Leonardis et al. 2024). On the other hand, we proved that OGC, originally known and most studied for its substrate-transporting function, additionally functions as a facilitator of proton transport in the presence of FAs or DNP (Žuna et al. 2024). The same was shown for AGC (Samartsev et al. 1997, Samartsev & Mokhova 1997), PiC (Zácková et al. 2000, Engstová et al. 2001), and DIC (Wieckowski & Wojtczak 1997). Therefore, this "dual-functionality" is most likely a common feature of all proteins of the SLC25 family.

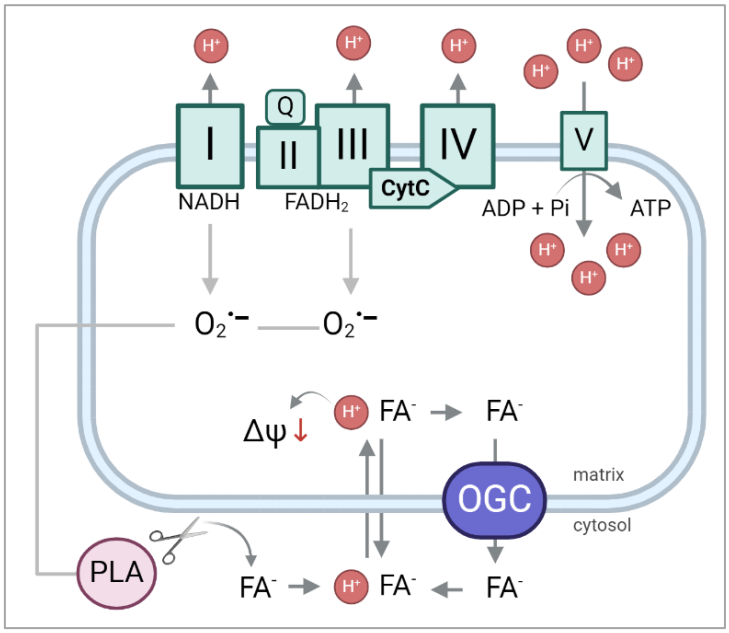

Figure 11. Under high oxidative stress, OGC potentiates FA-mediated uncoupling. Reactive oxygen species are created throughout the electron transport chain, and they activate phospholipase A (PLA), which cleaves FAs from the IMM. After neutralization and transfer to the matrix, FAs release protons and decrease MMP. FA anions are transported back to the cytosol by OGC and other SLC25 proteins. Image created with BioRender.

One might question the physiological state in which these proteins' cavities are free from substrates bound in either m- or c-state. However, it has been shown that the concentration of FAs in cells increases due to an increase in oxidative stress (ROS levels) and the activity of phospholipase A (Asai et al. 2003). Furthermore, we have shown that free radicals damage membrane lipids and create RAs, which in turn potentiate FA-mediated uncoupling, and consequently increase protein-mediated proton transport (Jovanovic et al. 2022). Under stressful conditions, the cell decreases the need for oxidative phosphorylation and decreases the amount of Kreb's cycle intermediates. For example, the levels of free 2-oxoglutarate and malate in plasma were shown to be significantly reduced in diabetes (Wu et al. 2017) or breast cancer (Mullen et al. 2011), when mitochondrial function has been impaired. In these conditions, OGC and other carriers most likely participate in FA-mediated uncoupling to prevent further mitochondrial damage through a transient decrease of MMP (Fig. 11).

4.3. Protein-mediated uncoupling holds promise for metabolic disorders, oxidative stress, and cancer treatment

4.3.1. Treatment and prevention of metabolic disorders

Uncoupling causes a decrease of MMP, needed for proper ATP production, which increases the nutrient demand to replenish the lost energy. Cells start utilizing FA oxidation more, which depletes stored FAs and prevents further accumulation. For this reason, uncoupling is considered a prospective tool in the fight against metabolic disorders like obesity, fatty liver disease, and type II diabetes (Harper et al. 2001, Bartelt et al. 2012).

Uncoupling was previously used as an obesity treatment in the form of DNP, which was extremely effective for weight loss (Colman 2007). Unfortunately, taking DNP as a weight-loss agent resulted in severe toxicities and deaths. There was no antidote because the mechanism of DNP-mediated uncoupling was unknown at the time, and it remained so ever since. For the first time, almost one hundred years after the discovery of DNP (Cutting et al. 1933), we showed that it interacts not only with lipid membranes but also with carriers of the SLC25 family, namely ANT1 and UCP1-3 (Žuna et al. 2021). This was later confirmed by the Kirichok group for ANT1 and UCP1 in isolated mitochondria (Bertholet et al. 2022), and we additionally proved it for OGC in a well-defined lipid-bilayer system (Žuna et al. 2024). DNP presumably acts similarly on other proton transport mediating SLC25 carriers. As proteins make up more

than 70% of the IMM (Cooper 2000), their participation in DNP´s action is equally significant to lipid membranes.

Notably, physiologically-induced proton transport can also be used to stimulate weight loss and prevent the development of metabolic disorders. Previous research has shown that the overexpression of UCP1 prevents the development of obesity in mice (Krauss et al 2005), while the depletion of UCP1 in mice augments the development of obesity (Feldmann et al. 2009). Ectopic expression of UCP1 in skeletal muscle in mice delayed the diet-induced development of obesity (Li et al. 2000, Keipert et al. 2013, Ost et al. 2014). UCP3, which is present in muscle in minute amounts, could also be used to lose weight. Even though UCP3´s presence in skeletal muscle is only 1% of UCP1´s presence in BAT, it should be noted that skeletal muscle is of much greater mass than BAT, and UCP3´s expression can be stimulated through muscle contraction (Clapham et al. 2000).

Finally, it was shown that UCP2 regulates the secretion of insulin through mild uncoupling in pancreatic β cells (Chan & Harper 2006). By lowering MMP, uncoupling prevents insulin secretion and regulates the switch between glucose and FA oxidation metabolism (Chan & Harper 2006), which can be used to prevent or treat diabetic conditions.

4.3.2. Reactive oxygen species and oxidative stress

It was previously shown that oxidative damage products, such as RAs, indirectly potentiate the proton-transporting function of proteins of the SLC25 family in the presence of FAs (Echtay et al. 2002, Echtay et al. 2003). Furthermore, Mailloux & Harper showed that the activation of uncoupling in UCP2 and UCP3 is directly controlled by ROS via a covalent modification of glutathione and that they may play a protective role in decreasing mitochondrial ROS production (Mailloux & Harper 2011). On the other hand, some groups found no experimental support for ROS regulation of proton-transport in UCPs (Couplan et al. 2002, Shabalina et al. 2006, Lombardi et al. 2008). The exact molecular mechanism of the interaction of ROS and ROS products, lipids, and mitochondrial proteins remained unclear.

Our results shed further light on the changes that oxidative stress has on the proton-transporting function of ANT1 and UCP1. Namely, we showed that ROS influence changes in the lipid environment by changing lipid shapes and creating lipid adducts, and not by covalently modifying the proteins (Jovanovic et al. 2022). This is in agreement with previous data showing that RAs do not activate proteins (in this case UCP1 and UCP2) directly, but that they rather

potentiate the uncoupling effect of FAs, which in turn increases the protein-mediated proton conductance (Esteves et al. 2006, Malingriaux et al. 2013, Jovanovic et al. 2015).

Given the high homology between members of the SLC25 family and localization in the IMM, other proteins that mediate proton transport such as OGC, AGC, PiC, and DIC, are most likely also affected by ROS-induced lipid reshaping in a similar manner. Since the increased proton transport rate neutralizes excess ROS in a negative feedback loop, any further oxidative damage to the cell may be prevented. In this way, the induction of proton-transport by the proteins of the SLC25 family in the presence of protonophores could be artificially potentiated to prevent cognitive disorders, inflammation, male infertility, aging, and other conditions caused or supported by high oxidative stress (Zhao et al. 2019, Shields et al. 2021).

4.3.3. Cancer and chemotherapy

We discovered that OGC belongs to a group of SLC25 proteins that exhibit protonophoric activity in the presence of natural and chemical uncouplers. Our results also showed that OGC, much like ANTs, is expressed throughout the whole organism (Žuna et al. 2024). Furthermore, we showed that the mechanism of protein-mediated proton transport is most likely conserved throughout the SLC25 family, both in the presence of FAs and DNP (Kreiter et al. 2021, Žuna et al. 2021, Žuna et al. 2024). These concepts have important implications for the potential use of potentiated proton transport in cancer treatment.

First, it is thought that the accumulation of ROS contributes to the early conversion of healthy cells to cancer cells by introducing DNA mutations and mediating the overall genetic instability. In fact, cancer cells constantly maintain high levels of ROS (Trachootham et al. 2009), and their IMMs are significantly more polarized than those of healthy cells ($\Psi_{\text{cancer IMM}} \sim$ -220 mV in comparison to $\Psi_{\text{healthy IMM}} \sim$-140 mV) (Chen 1988). This makes them susceptible to attracting negatively charged and potent chemical protonophores, such as DNP, FCCP, CCP, niclosamide, nitazoxanide, oxyclozanide, BAM15, and others. These chemical agents already show great potential for the treatment of cancers *in vitro* and *in vivo* (Shreshta et al. 2021), mainly because they induce a total collapse of their MMP and subsequent apoptosis. Furthermore, we have shown that five different proteins (OGC, ANT1, UCP1-UCP3) significantly augment DNP-mediated proton transport (Žuna et al. 2021, Žuna et al. 2024). The same was shown by Bertholet et al. for the interaction between chemical uncouplers DNP, BAM15, and FCCP, and the proteins ANT1 and UCP1 (Bertholet et al. 2022).

Second, by neutralizing ROS in the early stages of cancer development, it might be possible to prevent healthy cells from accumulating more oxidative damage and becoming malignant. As cancer can develop from any healthy cell in the body, this approach can work more efficiently by targeting proteins that are ubiquitously expressed, such as OGC and ANTs. Because their mechanism of mediating proton transport is conserved, they can be targeted at the same time with the same protonophore.

This approach can also work in the later stages of malignancy. In the late stages of malignancy, cancer cells may exploit uncoupling to protect themselves against chemotherapy, because many chemotherapeutic agents work on introducing high amounts of ROS to induce apoptosis. This has been proven in the case of UCP2, where overexpressing UCP2 in cancer cells protected them against chemotherapy (Derdak et al. 2008), while a knock-out restored sensitivity to chemotherapy (Pfefferle et al. 2013) and significantly increased the amount of ROS (Dando et al. 2013). Along those lines, targeted proton transport by several SLC25 proteins can be exploited at the same time to help with the side effects of radiation therapy. Namely, radiation often introduces oxidative damage to healthy cells (Wei et al. 2019), and proton transport could help decrease or prevent it.

However, the main obstacle to the use of chemical uncouplers in cancer therapy is the narrow concentration range between a therapeutic effect and toxicity. In addition, the exact mechanism of how these agents interact with natural membranes and membrane proteins (e.g., SLC25 carriers) is not clear yet and needs to be further investigated.

5. List of abbreviations

ADP - Adenosine diphosphate
AGC – Aspartate/glutamate carrier
ANT - Adenine nucleotide translocase
ATP - Adenosine triphosphate
BA - Bongkrekic acid
BAM15 - ((2-fluorophenyl)6-[(2-fluorophenyl) amino] (1,2,5-oxadiazolo[3,4-e]pyrazin-5-yl)amine)
BAT - Brown adipose tissue
C12TPP - Dodecyltriphenylphosphonium
CATR – Carboxyatractyloside
CCCP - Carbonylcyanide-3-chlorophenylhydrazone
cDNA – complementary DNA
CIC – Citrate carrier
CoA – Coenzyme A
DIC – Dicarboxylate carrier
DNA - Deoxyribonucleic acid
DNP – 2,4-dinitrophenol
ETC – Electron transport chain
FA – Fatty acid
$FADH_2$ - Flavin adenine dinucleotide
FCCP - Carbonyl cyanide p-trifluoro-methoxyphenyl hydrazone
HNE - 4-hydroxy-2-nonenal
IMM - Inner mitochondrial membrane
IMS - Intermembrane space
OGC – 2-oxoglutarate/malate carrier
MC – Mitochondrial carrier
MMP – Mitochondrial membrane potential
NAAA – N-acyl aminoacids
NADH - Nicotinamide adenine dinucleotide
NADPH - Nicotinamide adenine dinucleotide phosphate
NMR - Nuclear magnetic resonance
RA – Reactive alkenals
RNA - Ribonucleic acid
PIC – Phosphate carrier
pKa - Acid dissociation constant
ROS - Reactive oxygen species
SLC25 - Solute carrier family 25
OMM - Outer mitochondrial membrane
UCP - Uncoupling protein

6. References

Andreyev AYu, Bondareva TO, Dedukhova VI, Mokhova EN, Skulachev VP, Tsofina LM, Volkov NI, Vygodina TV. The ATP/ADP-antiporter is involved in the uncoupling effect of fatty acids on mitochondria. Eur J Biochem. 1989 Jul 1;182(3):585-92. doi: 10.1111/j.1432-1033.1989.tb14867.x

Andreyev AYu, Bondareva TO, Dedukhova VI, Mokhova EN, Skulachev VP, Volkov NI. Carboxyatractylate inhibits the uncoupling effect of free fatty acids. FEBS Lett. 1988 Jan 4;226(2):265-9. doi: 10.1016/0014-5793(88)81436-4

Antonenko YN, Denisov SS, Silachev DN, Khailova LS, Jankauskas SS, Rokitskaya TI, Danilina TI, Kotova EA, Korshunova GA, Plotnikov EY, Zorov DB. A long-linker conjugate of fluorescein and triphenylphosphonium as mitochondria-targeted uncoupler and fluorescent neuro- and nephroprotector. Biochim Biophys Acta. 2016 Nov;1860(11 Pt A):2463-2473. doi: 10.1016/j.bbagen.2016.07.014.

Asai K, Hirabayashi T, Houjou T, Uozumi N, Taguchi R, Shimizu T. Human group IVC phospholipase A2 (cPLA2gamma). Roles in the membrane remodeling and activation induced by oxidative stress. J Biol Chem. 2003 Mar 7;278(10):8809-14. doi: 10.1074/jbc.M212117200.

Bartelt A, Merkel M, Heeren J. A new, powerful player in lipoprotein metabolism: brown adipose tissue. J Mol Med (Berl). 2012 Aug;90(8):887-93. doi: 10.1007/s00109-012-0858-3

Beck V, Jabůrek M, Breen EP, Porter RK, Jezek P, Pohl EE. A new automated technique for the reconstitution of hydrophobic proteins into planar bilayer membranes. Studies of human recombinant uncoupling protein 1. Biochim Biophys Acta. 2006 May-Jun;1757(5-6):474-9. doi: 10.1016/j.bbabio.2006.03.006

Beck V, Jabůrek M, Demina T, Rupprecht A, Porter RK, Jezek P, Pohl EE. Polyunsaturated fatty acids activate human uncoupling proteins 1 and 2 in planar lipid bilayers. FASEB J. 2007 Apr;21(4):1137-44. doi: 10.1096/fj.06-7489com

Berardi MJ, Shih WM, Harrison SC, Chou JJ. Mitochondrial uncoupling protein 2 structure determined by NMR molecular fragment searching. Nature. 2011 Jul 24;476(7358):109-13. doi: 10.1038/nature10257

Bertholet AM, Chouchani ET, Kazak L, Angelin A, Fedorenko A, Long JZ, Vidoni S, Garrity R, Cho J, Terada N, Wallace DC, Spiegelman BM, Kirichok Y. H+ transport is an integral function of the mitochondrial ADP/ATP carrier. Nature. 2019 Jul;571(7766):515-520. doi: 10.1038/s41586-019-1400-3

Bertholet AM, Natale AM, Bisignano P, Suzuki J, Fedorenko A, Hamilton J, Brustovetsky T, Kazak L, Garrity R, Chouchani ET, Brustovetsky N, Grabe M, Kirichok Y. Mitochondrial uncouplers induce proton leak by activating AAC and UCP1. Nature. 2022 Jun;606(7912):180-187. doi: 10.1038/s41586-022-04747-5

Beyer K, Klingenberg M. ADP/ATP carrier protein from beef heart mitochondria has high amounts of tightly bound cardiolipin, as revealed by 31P nuclear magnetic resonance. Biochemistry. 1985 Jul 16;24(15):3821-6. doi: 10.1021/bi00336a001

Bielawski J, Thompson TE, Lehninger AL. The effect of 2,4-dinitrophenol on the electrical resistance of phospholipid bilayer membranes. Biochem Biophys Res Commun. 1966 Sep 22;24(6):948-54. doi: 10.1016/0006-291x(66)90342-1

Bisaccia F, Indiveri C, Palmieri F. Purification of reconstitutively active alpha-oxoglutarate carrier from pig heart mitochondria. Biochim Biophys Acta. 1985 Dec 16;810(3):362-9. doi: 10.1016/0005-2728(85)90222-1

Bisaccia F, Zara V, Capobianco L, Iacobazzi V, Mazzeo M, Palmieri F. The formation of a disulfide cross-link between the two subunits demonstrates the dimeric structure of the mitochondrial oxoglutarate carrier. Biochim Biophys Acta. 1996 Feb 8;1292(2):281-88. doi: 10.1016/0167-4838(95)00215-4

Booty LM, King MS, Thangaratnarajah C, Majd H, James AM, Kunji ER, Murphy MP. The mitochondrial dicarboxylate and 2-oxoglutarate carriers do not transport glutathione. FEBS Lett. 2015 Feb 27;589(5):621-8. doi: 10.1016/j.febslet.2015.01.027

Borst P. The malate-aspartate shuttle (Borst cycle): How it started and developed into a major metabolic pathway. IUBMB Life. 2020 Nov;72(11):2241-2259. doi: 10.1002/iub.2367

Boss O, Samec S, Paoloni-Giacobino A, Rossier C, Dulloo A, Seydoux J, Muzzin P, Giacobino JP. Uncoupling protein-3: a new member of the mitochondrial carrier family with tissue-specific expression. FEBS Lett. 1997 May 12;408(1):39-42. doi: 10.1016/s0014-5793(97)00384-0

Brand MD, Pakay JL, Ocloo A, Kokoszka J, Wallace DC, Brookes PS, Cornwall EJ. The basal proton conductance of mitochondria depends on adenine nucleotide translocase content. Biochem J. 2005 Dec 1;392(Pt 2):353-62. doi: 10.1042/BJ20050890

Brand MD, Turner N, Ocloo A, Else PL, Hulbert AJ. Proton conductance and fatty acyl composition of liver mitochondria correlates with body mass in birds. Biochem J. 2003 Dec 15;376(Pt 3):741-8. doi: 10.1042/BJ20030984

Brustovetsky N, Klingenberg M. The reconstituted ADP/ATP carrier can mediate H+ transport by free fatty acids, which is further stimulated by mersalyl. J Biol Chem. 1994 Nov 4;269(44):27329-36.

Brustovetsky NN, Dedukhova VI, Egorova MV, Mokhova EN, Skulachev VP. Inhibitors of the ATP/ADP antiporter suppress stimulation of mitochondrial respiration and H+ permeability by palmitate and anionic detergents. FEBS Lett. 1990 Oct 15;272(1-2):187-9. doi: 10.1016/0014-5793(90)80480-7

Cannon B, Nedergaard J. Brown adipose tissue: function and physiological significance. Physiol Rev. 2004 Jan;84(1):277-359. doi: 10.1152/physrev.00015.2003

Cappello AR, Curcio R, Valeria Miniero D, Stipani I, Robinson AJ, Kunji ER, Palmieri F. Functional and structural role of amino acid residues in the even-numbered transmembrane alpha-helices of the bovine mitochondrial oxoglutarate carrier. J Mol Biol. 2006 Oct 13;363(1):51-62. doi: 10.1016/j.jmb.2006.08.041

Cappello AR, Miniero DV, Curcio R, Ludovico A, Daddabbo L, Stipani I, Robinson AJ, Kunji ER, Palmieri F. Functional and structural role of amino acid residues in the odd-numbered transmembrane alpha-helices of the bovine mitochondrial oxoglutarate carrier. J Mol Biol. 2007 Jun 1;369(2):400-12. doi: 10.1016/j.jmb.2007.03.048

Carafoli E, Rossi CS. The effect of dinitrophenol on the permeability of the mitochondrial membrane. Biochem Biophys Res Commun. 1967 Oct 26;29(2):153-7. doi: 10.1016/0006-291x(67)90579-7

Castegna A, Scarcia P, Agrimi G, Palmieri L, Rottensteiner H, Spera I, Germinario L, Palmieri F. Identification and functional characterization of a novel mitochondrial carrier for citrate and oxoglutarate in Saccharomyces cerevisiae. J Biol Chem. 2010 Jun 4;285(23):17359-70. doi: 10.1074/jbc.M109.097188

Chan CB, Harper ME. Uncoupling proteins: role in insulin resistance and insulin insufficiency. Curr Diabetes Rev. 2006 Aug;2(3):271-83. doi: 10.2174/157339906777950660

Chappell JB, Greville GD. Effects of 2:4-dinitrophenol and other agents on the swelling of isolated mitochondria. Nature. 1959 Jun 20;183(4677):1737-8. doi: 10.1038/1831737a0

Chappell JB. Systems used for the transport of substrates into mitochondria. Br Med Bull. 1968 May;24(2):150-7. doi: 10.1093/oxfordjournals.bmb.a070618

Chen LB. Mitochondrial membrane potential in living cells. Annu Rev Cell Biol. 1988;4:155-81. doi: 10.1146/annurev.cb.04.110188.001103.

Chen Z, Putt DA, Lash LH. Enrichment and functional reconstitution of glutathione transport activity from rabbit kidney mitochondria: further evidence for the role of the dicarboxylate and 2-oxoglutarate carriers in mitochondrial glutathione transport. Arch Biochem Biophys. 2000 Jan 1;373(1):193-202. doi: 10.1006/abbi.1999.1527

Clapham JC, Arch JR, Chapman H, Haynes A, Lister C, Moore GB, Piercy V, Carter SA, Lehner I, Smith SA, Beeley LJ, Godden RJ, Herrity N, Skehel M, Changani KK, Hockings PD, Reid DG, Squires SM, Hatcher J, Trail B, Latcham J, Rastan S, Harper AJ, Cadenas S, Buckingham JA, Brand MD, Abuin A. Mice overexpressing human uncoupling protein-3 in skeletal muscle are hyperphagic and lean. Nature. 2000 Jul 27;406(6794):415-8. doi: 10.1038/35019082

Coll O, Colell A, García-Ruiz C, Kaplowitz N, Fernández-Checa JC. Sensitivity of the 2-oxoglutarate carrier to alcohol intake contributes to mitochondrial glutathione depletion. Hepatology. 2003 Sep;38(3):692-702. doi: 10.1053/jhep.2003.50351

Colman E. Dinitrophenol and obesity: an early twentieth-century regulatory dilemma. Regul Toxicol Pharmacol. 2007 Jul;48(2):115-7. doi: 10.1016/j.yrtph.2007.03.006

Cooper GM. The Cell: A Molecular Approach. 2nd edition. Sunderland (MA): Sinauer Associates; 2000. Mitochondria. Available from: https://www.ncbi.nlm.nih.gov/books/NBK9896/

Couplan E, del Mar Gonzalez-Barroso M, Alves-Guerra MC, Ricquier D, Goubern M, Bouillaud F. No evidence for a basal, retinoic, or superoxide-induced uncoupling activity of the uncoupling protein 2 present in spleen or lung mitochondria. J Biol Chem. 2002 Jul 19;277(29):26268-75. doi: 10.1074/jbc.M202535200

Cutting W, Mehrtens H, Tainter M. Actions and uses of dinitrophenol: Promising metabolic applications. J. Am. Med. Assoc. 1933;101:193–195. doi: 10.1001/jama.1933.02740280013006

Daems WT, Wisse E. Shape and attachment of the cristae mitochondriales in mouse hepatic cell mitochondria. J Ultrastruct Res. 1966 Sep;16(1):123-40. doi: 10.1016/s0022-5320(66)80027-8

Dando I, Fiorini C, Pozza ED, Padroni C, Costanzo C, Palmieri M, Donadelli M. UCP2 inhibition triggers ROS-dependent nuclear translocation of GAPDH and autophagic cell death in pancreatic adenocarcinoma cells. Biochim Biophys Acta. 2013 Mar;1833(3):672-9. doi: 10.1016/j.bbamcr.2012.10.028

Davies, K. M., Daum, B., Gold, V. A. M., Mühleip, A. W., Brandt, T., Blum, T. B., Mills, D. J., Kühlbrandt, W. Visualization of ATP Synthase Dimers in Mitochondria by Electron Cryo-tomography. J. Vis. Exp. 2014 (91), e51228, doi:10.3791/51228

De Leonardis F, Ahmed A, Vozza A, Capobianco L, Riley CL, Barile SN, Di Molfetta D, Tiziani S, DiGiovanni J, Palmieri L, Dolce V, Fiermonte G. Human mitochondrial uncoupling protein 3 functions as a metabolite transporter. FEBS Lett. 2024 Feb;598(3):338-346. doi: 10.1002/1873-3468.14784

Denisov SS, Kotova EA, Plotnikov EY, Tikhonov AA, Zorov DB, Korshunova GA, Antonenko YN. A mitochondria-targeted protonophoric uncoupler derived from fluorescein. Chem Commun (Camb). 2014 Dec 18;50(97):15366-9. doi: 10.1039/c4cc04996a

Derdak Z, Mark NM, Beldi G, Robson SC, Wands JR, Baffy G. The mitochondrial uncoupling protein-2 promotes chemoresistance in cancer cells. Cancer Res. 2008 Apr 15;68(8):2813-9. doi: 10.1158/0008-5472.CAN-08-0053

Dolce V, Scarcia P, Iacopetta D, Palmieri F. A fourth ADP/ATP carrier isoform in man: identification, bacterial expression, functional characterization and tissue distribution. FEBS Lett. 2005 Jan 31;579(3):633-7. doi: 10.1016/j.febslet.2004.12.034

Drew D, Boudker O. Shared Molecular Mechanisms of Membrane Transporters. Annu Rev Biochem. 2016 Jun 2;85:543-72. doi: 10.1146/annurev-biochem-060815-014520

Echtay KS, Roussel D, St-Pierre J, Jekabsons MB, Cadenas S, Stuart JA, Harper JA, Roebuck SJ, Morrison A, Pickering S, Clapham JC, Brand MD. Superoxide activates mitochondrial uncoupling proteins. Nature. 2002 Jan 3;415(6867):96-9. doi: 10.1038/415096a

Echtay KS, Esteves TC, Pakay JL, Jekabsons MB, Lambert AJ, Portero-Otín M, Pamplona R, Vidal-Puig AJ, Wang S, Roebuck SJ, Brand MD. A signalling role for 4-hydroxy-2-nonenal in regulation of mitochondrial uncoupling. EMBO J. 2003 Aug 15;22(16):4103-10. doi: 10.1093/emboj/cdg412

Engstová H, Zácková M, Růzicka M, Meinhardt A, Hanus J, Krämer R, Jezek P. Natural and azido fatty acids inhibit phosphate transport and activate fatty acid anion uniport mediated by the mitochondrial phosphate carrier. J Biol Chem. 2001 Feb 16;276(7):4683-91. doi: 10.1074/jbc.M009409200

Esteves TC, Parker N, Brand MD. Synergy of fatty acid and reactive alkenal activation of proton conductance through uncoupling protein 1 in mitochondria. Biochem J. 2006 May 1;395(3):619-28. doi: 10.1042/BJ20052004

Estrela JM, Ortega AL, Carretero J. A role for the 2-oxoglutarate carrier in glutathione transport into hepatocyte mitochondria? Hepatology. 2004 Feb;39(2):570-1; author reply 571. doi: 10.1002/hep.20041

Fedorenko A, Lishko PV, Kirichok Y. Mechanism of fatty-acid-dependent UCP1 uncoupling in brown fat mitochondria. Cell. 2012 Oct 12;151(2):400-13. doi: 10.1016/j.cell.2012.09.010

Feldmann HM, Golozoubova V, Cannon B, Nedergaard J. UCP1 ablation induces obesity and abolishes diet-induced thermogenesis in mice exempt from thermal stress by living at thermoneutrality. Cell Metab. 2009 Feb;9(2):203-9. doi: 10.1016/j.cmet.2008.12.014

Fiermonte G, Walker JE, Palmieri F. Abundant bacterial expression and reconstitution of an intrinsic membrane-transport protein from bovine mitochondria. Biochem J. 1993 Aug 15;294 (Pt 1)(Pt 1):293-9. doi: 10.1042/bj2940293

Fleury C, Neverova M, Collins S, Raimbault S, Champigny O, Levi-Meyrueis C, Bouillaud F, Seldin MF, Surwit RS, Ricquier D, Warden CH. Uncoupling protein-2: a novel gene linked to obesity and hyperinsulinemia. Nat Genet. 1997 Mar;15(3):269-72. doi: 10.1038/ng0397-269

Fontaine EM, Moussa M, Devin A, Garcia J, Ghisolfi J, Rigoulet M, Leverve XM. Effect of polyunsaturated fatty acids deficiency on oxidative phosphorylation in rat liver mitochondria. Biochim Biophys Acta. 1996 Sep 30;1276(3):181-7. doi: 10.1016/0005-2728(96)00075-8

Fonyó A, Palmieri F, Quagliariello E. Carrier-mediated transport of metabolites in mitochondria. Horiz Biochem Biophys. 1976;2:60-105.

Gao Y, Shabalina IG, Braz GRF, Cannon B, Yang G, Nedergaard J. Establishing the potency of N-acyl amino acids versus conventional fatty acids as thermogenic uncouplers in cells and mitochondria from different tissues. Biochim Biophys Acta Bioenerg. 2022 Apr 1;1863(4):148542. doi: 10.1016/j.bbabio.2022.148542

Genchi G, De Santis A, Ponzone C, Palmieri F. Partial Purification and Reconstitution of the alpha-Ketoglutarate Carrier from Corn (Zea mays L.) Mitochondria. Plant Physiol. 1991 Aug;96(4):1003-7. doi: 10.1104/pp.96.4.1003

Gimeno RE, Dembski M, Weng X, Deng N, Shyjan AW, Gimeno CJ, Iris F, Ellis SJ, Woolf EA, Tartaglia LA. Cloning and characterization of an uncoupling protein homolog: a potential molecular mediator of human thermogenesis. Diabetes. 1997 May;46(5):900-6. doi: 10.2337/diab.46.5.900

Goldgof M, Xiao C, Chanturiya T, Jou W, Gavrilova O, Reitman ML. The chemical uncoupler 2,4-dinitrophenol (DNP) protects against diet-induced obesity and improves energy homeostasis in mice at thermoneutrality. J Biol Chem. 2014 Jul 11;289(28):19341-50. doi: 10.1074/jbc.M114.568204

Gorgoglione R, Porcelli V, Santoro A, Daddabbo L, Vozza A, Monné M, Di Noia MA, Palmieri L, Fiermonte G, Palmieri F. The human uncoupling proteins 5 and 6 (UCP5/SLC25A14 and UCP6/SLC25A30) transport sulfur oxyanions, phosphate and dicarboxylates. Biochim Biophys Acta Bioenerg. 2019 Sep 1;1860(9):724-733. doi: 10.1016/j.bbabio.2019.07.010

Grav HI, Blix AS. A source of nonshivering thermogenesis in fur seal skeletal muscle. Science. 1979 Apr 6;204(4388):87-9. doi: 10.1126/science.219477

Gray MW, Burger G, Lang BF. The origin and early evolution of mitochondria. Genome Biol. 2001;2(6):REVIEWS1018. doi: 10.1186/gb-2001-2-6-reviews1018

Gutsmann T, Heimburg T, Keyser U, Mahendran KR, Winterhalter M. Protein reconstitution into freestanding planar lipid membranes for electrophysiological characterization. Nat Protoc. 2015 Jan;10(1):188-98. doi: 10.1038/nprot.2015.003.

Haguenauer A, Raimbault S, Masscheleyn S, Gonzalez-Barroso Mdel M, Criscuolo F, Plamondon J, Miroux B, Ricquier D, Richard D, Bouillaud F, Pecqueur C. A new renal mitochondrial carrier, KMCP1, is up-regulated during tubular cell regeneration and induction of antioxidant enzymes. J Biol Chem. 2005 Jun 10;280(23):22036-43. doi: 10.1074/jbc.M412136200

Hamilton JA. Transport of fatty acids across membranes by the diffusion mechanism. Prostaglandins Leukot Essent Fatty Acids. 1999 May-Jun;60(5-6):291-7. doi: 10.1016/s0952-3278(99)80002-7

Harper JA, Dickinson K, Brand MD. Mitochondrial uncoupling as a target for drug development for the treatment of obesity. Obes Rev. 2001 Nov;2(4):255-65. doi: 10.1046/j.1467-789x.2001.00043.x

Herrnhold M, Hamp I, Plettenburg O, Jastroch M, Keuper M. Adverse bioenergetic effects of N-acyl amino acids in human adipocytes overshadow beneficial mitochondrial uncoupling. Redox Biol. 2023 Oct;66:102874. doi: 10.1016/j.redox.2023.102874

Ho PW, Ho JW, Tse HM, So DH, Yiu DC, Liu HF, Chan KH, Kung MH, Ramsden DB, Ho SL. Uncoupling protein-4 (UCP4) increases ATP supply by interacting with mitochondrial Complex II in neuroblastoma cells. PLoS One. 2012;7(2):e32810. doi: 10.1371/journal.pone.0032810

Hoang T, Kuljanin M, Smith MD, Jelokhani-Niaraki M. A biophysical study on molecular physiology of the uncoupling proteins of the central nervous system. Biosci Rep. 2015 Jun 12;35(4):e00226. doi: 10.1042/BSR20150130

Hoang T, Matovic T, Parker J, Smith MD, Jelokhani-Niaraki M. Role of positively charged residues of the second transmembrane domain in the ion transport activity and conformation of human uncoupling protein-2. Biochemistry. 2015 Apr 14;54(14):2303-13. doi: 10.1021/acs.biochem.5b00177

Hoang T, Smith MD, Jelokhani-Niaraki M. Toward understanding the mechanism of ion transport activity of neuronal uncoupling proteins UCP2, UCP4, and UCP5. Biochemistry. 2012 May 15;51(19):4004-14. doi: 10.1021/bi3003378

Hollenbeck PJ, Bray D, Adams RJ. Effects of the uncoupling agents FCCP and CCCP on the saltatory movements of cytoplasmic organelles. Cell Biol Int Rep. 1985 Feb;9(2):193-9. doi: 10.1016/0309-1651(85)90094-3

Hopfer U, Lehninger AL, Lennarz WJ. The effect of the polar moiety of lipids on bilayer conductance induced by uncouplers of oxidative phosphorylation. J Membr Biol. 1970 Dec;3(1):142-55. doi: 10.1007/BF01868012

Huang SG, Klingenberg M. Chloride channel properties of the uncoupling protein from brown adipose tissue mitochondria: a patch-clamp study. Biochemistry. 1996 Dec 24;35(51):16806-14. doi: 10.1021/bi960989v

Indiveri C, Palmieri F, Bisaccia F, Krämer R. Kinetics of the reconstituted 2-oxoglutarate carrier from bovine heart mitochondria. Biochim Biophys Acta. 1987 Mar 4;890(3):310-8. doi: 10.1016/0005-2728(87)90158-7

Jardetzky O. Simple allosteric model for membrane pumps. Nature. 1966 Aug 27;211(5052):969-70. doi: 10.1038/211969a0

Ježek P, Holendová B, Garlid KD, Jabůrek M. Mitochondrial Uncoupling Proteins: Subtle Regulators of Cellular Redox Signaling. Antioxid Redox Signal. 2018 Sep 1;29(7):667-714. doi: 10.1089/ars.2017.7225

Jones SA, Gogoi P, Ruprecht JJ, King MS, Lee Y, Zögg T, Pardon E, Chand D, Steimle S, Copeman DM, Cotrim CA, Steyaert J, Crichton PG, Moiseenkova-Bell V, Kunji ERS. Structural basis of purine nucleotide inhibition of human uncoupling protein 1. Sci Adv. 2023 Jun 2;9(22):eadh4251. doi: 10.1126/sciadv.adh4251

Joseph JW, Jensen MV, Ilkayeva O, Palmieri F, Alárcon C, Rhodes CJ, Newgard CB. The mitochondrial citrate/isocitrate carrier plays a regulatory role in glucose-stimulated insulin secretion. J Biol Chem. 2006 Nov 24;281(47):35624-32. doi: 10.1074/jbc.M602606200

Jovanović O, Chekashkina K, Škulj S, Žuna K, Vazdar M, Bashkirov PV, Pohl EE. Membrane Lipid Reshaping Underlies Oxidative Stress Sensing by the Mitochondrial Proteins UCP1 and ANT1. (2022) Antioxidants (Basel) 11:2314. doi.org/10.3390/antiox11122314

Jovanovic O, Pashkovskaya AA, Annibal A, Vazdar M, Burchardt N, Sansone A, Gille L,Fedorova M, Ferreri C, Pohl EE. The molecular mechanism behind reactive aldehyde action on transmembrane translocations of proton and potassium ions. Free Radic Biol Med. 2015 Dec;89:1067-76. doi: 10.1016/j.freeradbiomed.2015.10.422

Kagawa Y, Ohta S. Regulation of mitochondrial ATP synthesis in mammalian cells by transcriptional control. Int J Biochem. 1990;22(3):219-29. doi: 10.1016/0020-711x(90)90333-x

Kane MS, Paris A, Codron P, Cassereau J, Procaccio V, Lenaers G, Reynier P, Chevrollier A. Current mechanistic insights into the CCCP-induced cell survival response. Biochem Pharmacol. 2018 Feb;148:100-110. doi: 10.1016/j.bcp.2017.12.018

Kang Y, Chen L. Structural basis for the binding of DNP and purine nucleotides onto UCP1. Nature. 2023 Aug;620(7972):226-231. doi: 10.1038/s41586-023-06332-w

Keipert S, Ost M, Chadt A, Voigt A, Ayala V, Portero-Otin M, Pamplona R, Al-Hasani H, Klaus S. Skeletal muscle uncoupling-induced longevity in mice is linked to increased substrate metabolism and induction of the endogenous antioxidant defense system. Am J Physiol Endocrinol Metab. 2013 Mar 1;304(5):E495-506. doi: 10.1152/ajpendo.00518.2012

Kenwood BM, Weaver JL, Bajwa A, Poon IK, Byrne FL, Murrow BA, Calderone JA, Huang L, Divakaruni AS, Tomsig JL, Okabe K, Lo RH, Cameron Coleman G, Columbus L, Yan Z, Saucerman JJ, Smith JS, Holmes JW, Lynch KR, Ravichandran KS, Uchiyama S, Santos WL, Rogers GW, Okusa MD, Bayliss DA, Hoehn KL. Identification of a novel mitochondrial uncoupler that does not depolarize the plasma membrane. Mol Metab. 2013 Nov 28;3(2):114-23. doi: 10.1016/j.molmet.2013.11.005

Khailova LS, Silachev DN, Rokitskaya TI, Avetisyan AV, Lyamsaev KG, Severina II, Il'yasova TM, Gulyaev MV, Dedukhova VI, Trendeleva TA, Plotnikov EY, Zvyagilskaya RA, Chernyak BV, Zorov DB, Antonenko YN, Skulachev VP. A short-chain alkyl derivative of Rhodamine 19 acts as a mild uncoupler of mitochondria and a neuroprotector. Biochim Biophys Acta. 2014 Oct;1837(10):1739-47. doi: 10.1016/j.bbabio.2014.07.006

Klingenberg M, Huang SG. Structure and function of the uncoupling protein from brown adipose tissue. Biochim Biophys Acta. 1999 Jan 8;1415(2):271-96. doi: 10.1016/s0005-2736(98)00232-6

Klingenberg M. The ADP and ATP transport in mitochondria and its carrier. Biochim Biophys Acta. 2008 Oct;1778(10):1978-2021. doi: 10.1016/j.bbamem.2008.04.011

Klingenberg M. UCP1 - A sophisticated energy valve. Biochimie. 2017 Mar;134:19-27. doi: 10.1016/j.biochi.2016.10.012

Krauss S, Zhang CY, Lowell BB. The mitochondrial uncoupling-protein homologues. Nat Rev Mol Cell Biol. 2005 Mar;6(3):248-61. doi: 10.1038/nrm1592

Kreiter J, Rupprecht A, Škulj S, Brkljača Z, Žuna K, Knyazev DG, Bardakji S, Vazdar M, Pohl EE. (2021) ANT1 Activation and Inhibition Patterns Support the Fatty Acid Cycling Mechanism for Proton Transport. International Journal of Molecular Sciences 22, 2490. doi.org/10.3390/ijms22052490

Kreiter J, Rupprecht A, Zimmermann L, Moschinger M, Rokitskaya TI, Antonenko YN, Gille L, Fedorova M, Pohl EE. Molecular Mechanisms Responsible for Pharmacological Effects of Genipin on Mitochondrial Proteins. Biophys J. 2019 Nov 19;117(10):1845-1857. doi: 10.1016/j.bpj.2019.10.021

Kreiter J, Škulj S, Brkljača Z, Bardakji S, Vazdar M, Pohl EE. FA Sliding as the Mechanism for the ANT1-Mediated Fatty Acid Anion Transport in Lipid Bilayers. Int J Mol Sci. 2023 Sep 5;24(18):13701. doi: 10.3390/ijms241813701

Kreiter J, Tyschuk T, Pohl EE. Uncoupling Protein 3 Catalyzes the Exchange of C4 Metabolites Similar to UCP2. Biomolecules. 2023 Dec 22;14(1):21. doi: 10.3390/biom14010021

Kunji ER, Robinson AJ. The conserved substrate binding site of mitochondrial carriers. Biochim Biophys Acta. 2006 Sep-Oct;1757(9-10):1237-48. doi: 10.1016/j.bbabio.2006.03.021

Kunji ERS, King MS, Ruprecht JJ, Thangaratnarajah C. The SLC25 Carrier Family: Important Transport Proteins in Mitochondrial Physiology and Pathology. Physiology (Bethesda). 2020 Sep 1;35(5):302-327. doi: 10.1152/physiol.00009.2020

Labbé E, Buriez O. Electrochem Sci. Adv. 2022, 2, e2100170. https://doi.org/10.1002/elsa.202100170

Lardy HA, Pressman BC. Effect of surface active agents on the latent ATPase of mitochondria. Biochim Biophys Acta. 1956 Sep;21(3):458-66. doi: 10.1016/0006-3002(56)90182-2

Lea EJ, Croghan PC. The effect of 2,4-dinitrophenol on the properties of thin phospholipid films. J Membr Biol. 1969 Dec;1(1):225-37. doi: 10.1007/BF01869783

Leblanc OH Jr. The effect of uncouplers of oxidative phosphorylation on lipid bilayer membranes: Carbonylcyanidem-chlorophenylhydrazone. J Membr Biol. 1971 Dec;4(1):227-51. doi: 10.1007/BF02431973

Lee JS, Lee H, Lee S, Kang JH, Lee SH, Kim SG, Cho ES, Kim NH, Yook JI, Kim SY. Loss of SLC25A11 causes suppression of NSCLC and melanoma tumor formation. EBioMedicine. 2019 Feb;40:184-197. doi: 10.1016/j.ebiom.2019.01.036

Liesa M, Shirihai OS. Mitochondrial dynamics in the regulation of nutrient utilization and energy expenditure. Cell Metab. 2013 Apr 2;17(4):491-506. doi: 10.1016/j.cmet.2013.03.002

Long JZ, Svensson KJ, Bateman LA, Lin H, Kamenecka T, Lokurkar IA, Lou J, Rao RR, Chang MR, Jedrychowski MP, Paulo JA, Gygi SP, Griffin PR, Nomura DK, Spiegelman BM. The

Secreted Enzyme PM20D1 Regulates Lipidated Amino Acid Uncouplers of Mitochondria. Cell. 2016 Jul 14;166(2):424-435. doi: 10.1016/j.cell.2016.05.071

Long Q, Yang K, Yang Q. Regulation of mitochondrial ATP synthase in cardiac pathophysiology. Am J Cardiovasc Dis. 2015 Mar 20;5(1):19-32.

Lou PH, Hansen BS, Olsen PH, Tullin S, Murphy MP, Brand MD. Mitochondrial uncouplers with an extraordinary dynamic range. Biochem J. 2007 Oct 1;407(1):129-40. doi: 10.1042/BJ20070606

Macher G, Koehler M, Rupprecht A, Kreiter J, Hinterdorfer P, Pohl EE. Inhibition of mitochondrial UCP1 and UCP3 by purine nucleotides and phosphate. Biochim Biophys Acta Biomembr. 2018 Mar;1860(3):664-672. doi: 10.1016/j.bbamem.2017.12.001

Mailloux RJ, Harper ME. Uncoupling proteins and the control of mitochondrial reactive oxygen species production. Free Radic Biol Med. 2011 Sep 15;51(6):1106-15. doi: 10.1016/j.freeradbiomed.2011.06.022

Malingriaux EA, Rupprecht A, Gille L, Jovanovic O, Jezek P, Jaburek M, Pohl EE. Fatty acids are key in 4-hydroxy-2-nonenal-mediated activation of uncoupling proteins 1 and 2. PLoS One. 2013 Oct 28;8(10):e77786. doi: 10.1371/journal.pone.0077786

Mannella CA, Pfeiffer DR, Bradshaw PC, Moraru II, Slepchenko B, Loew LM, Hsieh CE, Buttle K, Marko M. Topology of the mitochondrial inner membrane: dynamics and bioenergetic implications. IUBMB Life. 2001 Sep-Nov;52(3-5):93-100. doi: 10.1080/15216540152845885

Mao W, Yu XX, Zhong A, Li W, Brush J, Sherwood SW, Adams SH, Pan G. UCP4, a novel brain-specific mitochondrial protein that reduces membrane potential in mammalian cells. FEBS Lett. 1999 Jan 29;443(3):326-30. doi: 10.1016/s0014-5793(98)01713-x

McLaughlin S. The mechanism of action of DNP on phospholipid bilayer membranes. J Membr Biol. 1972 Dec;9(1):361-72. doi: 10.1007/BF01868062

Miniero DV, Cappello AR, Curcio R, Ludovico A, Daddabbo L, Stipani I, Robinson AJ, Kunji ER, Palmieri F. Functional and structural role of amino acid residues in the matrix alpha-helices, termini and cytosolic loops of the bovine mitochondrial oxoglutarate carrier. Biochim Biophys Acta. 2011 Mar;1807(3):302-10. doi: 10.1016/j.bbabio.2010.12.005

Miniero DV, Spagnoletta A, Gambacorta N, Scalera V, Pierri CL, Nicolotti O, De Palma A. The Interaction of Hemin, a Porphyrin Derivative, with the Purified Rat Brain 2-Oxoglutarate Carrier. Biomolecules. 2021 Aug 9;11(8):1175. doi: 10.3390/biom11081175

Modrianský M, Murdza-Inglis DL, Patel HV, Freeman KB, Garlid KD. Identification by site-directed mutagenesis of three arginines in uncoupling protein that are essential for nucleotide binding and inhibition. J Biol Chem. 1997 Oct 3;272(40):24759-62. doi: 10.1074/jbc.272.40.24759

Monné M, Miniero DV, Iacobazzi V, Bisaccia F, Fiermonte G. The mitochondrial oxoglutarate carrier: from identification to mechanism. J Bioenerg Biomembr. 2013 Feb;45(1-2):1-13. doi: 10.1007/s10863-012-9475-7

Mullen AR, Wheaton WW, Jin ES, Chen PH, Sullivan LB, Cheng T, Yang Y, Linehan WM, Chandel NS, DeBerardinis RJ. Reductive carboxylation supports growth in tumour cells with defective mitochondria. Nature. 2011 Nov 20;481(7381):385-8. doi: 10.1038/nature10642.

Muro E, Atilla-Gokcumen GE, Eggert US. Lipids in cell biology: how can we understand them better? Mol Biol Cell. 2014 Jun 15;25(12):1819-23. doi: 10.1091/mbc.E13-09-0516

Nass S. The significance of the structural and functional similarities of bacteria and mitochondria. Int Rev Cytol. 1969;25:55-129. doi: 10.1016/s0074-7696(08)60201-6

Natuzzi D, Daddabbo L, Stipani V, Cappello AR, Miniero DV, Capobianco L, Stipani I. Inactivation of the reconstituted oxoglutarate carrier from bovine heart mitochondria by pyridoxal 5'-phosphate. J Bioenerg Biomembr. 1999 Dec;31(6):535-41. doi: 10.1023/a:1026414826457

Nicholls DG. The influence of respiration and ATP hydrolysis on the proton-electrochemical gradient across the inner membrane of rat-liver mitochondria as determined by ion distribution. Eur J Biochem. 1974 Dec 16;50(1):305-15. doi: 10.1111/j.1432-1033.1974.tb03899.x

Nicholls DG. Mitochondrial proton leaks and uncoupling proteins. Biochim Biophys Acta Bioenerg. 2021 Jul 1;1862(7):148428. doi: 10.1016/j.bbabio.2021.148428

Ost M, Werner F, Dokas J, Klaus S, Voigt A. Activation of AMPKα2 is not crucial for mitochondrial uncoupling-induced metabolic effects but required to maintain skeletal muscle integrity. PLoS One. 2014 Apr 14;9(4):e94689. doi: 10.1371/journal.pone.0094689

Pabst G, Keller S. Exploring membrane asymmetry and its effects on membrane proteins. Trends Biochem Sci. 2024 Apr;49(4):333-345. doi: 10.1016/j.tibs.2024.01.007.

Palmieri F, Bisaccia F, Capobianco L, Dolce V, Fiermonte G, Iacobazzi V, Indiveri C, Palmieri L. Mitochondrial metabolite transporters. Biochim Biophys Acta. 1996 Jul 18;1275(1-2):127-32. doi: 10.1016/0005-2728(96)00062-x

Palmieri F, Pierri CL. Structure and function of mitochondrial carriers - role of the transmembrane helix P and G residues in the gating and transport mechanism. FEBS Lett. 2010 May 3;584(9):1931-9. doi: 10.1016/j.febslet.2009.10.063

Palmieri F, Quagliariello E, Klingenberger M. Kinetics and specificity of the oxoglutarate carrier in rat-liver mitochondria. Eur J Biochem. 1972 Sep 25;29(3):408-16. doi: 10.1111/j.1432-1033.1972.tb02003.x

Palmieri F. Mitochondrial transporters of the SLC25 family and associated diseases: a review. J Inherit Metab Dis. 2014 Jul;37(4):565-75. doi: 10.1007/s10545-014-9708-5

Palmieri F. The mitochondrial transporter family SLC25: identification, properties and physiopathology. Mol Aspects Med. 2013 Apr-Jun;34(2-3):465-84. doi: 10.1016/j.mam.2012.05.005

Park KS, Jo I, Pak K, Bae SW, Rhim H, Suh SH, Park J, Zhu H, So I, Kim KW. FCCP depolarizes plasma membrane potential by activating proton and Na+ currents in bovine aortic endothelial cells. Pflugers Arch. 2002 Jan;443(3):344-52. doi: 10.1007/s004240100703

Pashkovskaya AA, Vazdar M, Zimmermann L, Jovanovic O, Pohl P, Pohl EE. Mechanism of Long-Chain Free Fatty Acid Protonation at the Membrane-Water Interface. Biophys J. 2018 May 8;114(9):2142-2151. doi: 10.1016/j.bpj.2018.04.011

P. J. Pearce and R. J. J. Simkins. 1968. Acid strengths of some substituted picric acids. Canadian Journal of Chemistry. 46(2): 241-248. https://doi.org/10.1139/v68-038

Pebay-Peyroula E, Dahout-Gonzalez C, Kahn R, Trézéguet V, Lauquin GJ, Brandolin G. Structure of mitochondrial ADP/ATP carrier in complex with carboxyatractyloside. Nature. 2003 Nov 6;426(6962):39-44. doi: 10.1038/nature02056

Petróczi A, Ocampo JA, Shah I, Jenkinson C, New R, James RA, Taylor G, Naughton DP. Russian roulette with unlicensed fat-burner drug 2,4-dinitrophenol (DNP): evidence from a

multidisciplinary study of the internet, bodybuilding supplements and DNP users. Subst Abuse Treat Prev Policy. 2015 Oct 14;10:39. doi: 10.1186/s13011-015-0034-1

Pfefferle A, Mailloux RJ, Adjeitey CN, Harper ME. Glutathionylation of UCP2 sensitizes drug resistant leukemia cells to chemotherapeutics. Biochim Biophys Acta. 2013 Jan;1833(1):80-9. doi: 10.1016/j.bbamcr.2012.10.006

Pohl EE, Jovanovic O. The Role of Phosphatidylethanolamine Adducts in Modification of the Activity of Membrane Proteins under Oxidative Stress. Molecules. 2019 Dec 12;24(24):4545. doi: 10.3390/molecules24244545

Pohl EE, Peterson U, Sun J, Pohl P. Changes of intrinsic membrane potentials induced by flip-flop of long-chain fatty acids. Biochemistry. 2000 Feb 22;39(7):1834-9. doi: 10.1021/bi9919549

Pohl EE, Rupprecht A, Macher G, Hilse KE. Important Trends in UCP3 Investigation. Front Physiol. 2019 Apr 30;10:470. doi: 10.3389/fphys.2019.00470

Porter RK, Hulbert AJ, Brand MD. Allometry of mitochondrial proton leak: influence of membrane surface area and fatty acid composition. Am J Physiol. 1996 Dec;271(6 Pt 2):R1550-60. doi: 10.1152/ajpregu.1996.271.6.R1550

Ramsden DB, Ho PW, Ho JW, Liu HF, So DH, Tse HM, Chan KH, Ho SL. Human neuronal uncoupling proteins 4 and 5 (UCP4 and UCP5): structural properties, regulation, and physiological role in protection against oxidative stress and mitochondrial dysfunction. Brain Behav. 2012 Jul;2(4):468-78. doi: 10.1002/brb3.55

Rasmussen H. Mitochondrial ion transport: mechanism and physiological significance. Fed Proc. 1966 May-Jun;25(3):903-11.

Rial E, Aguirregoitia E, Jiménez-Jiménez J, Ledesma A. Alkylsulfonates activate the uncoupling protein UCP1: implications for the transport mechanism. Biochim Biophys Acta. 2004 Feb 15;1608(2-3):122-30. doi: 10.1016/j.bbabio.2003.11.001

Ricquier D. UCP1, the mitochondrial uncoupling protein of brown adipocyte: A personal contribution and a historical perspective. Biochimie. 2017 Mar;134:3-8. doi: 10.1016/j.biochi.2016.10.018

Robinson AJ, Kunji ER. Mitochondrial carriers in the cytoplasmic state have a common substrate binding site. Proc Natl Acad Sci U S A. 2006 Feb 21;103(8):2617-22. doi: 10.1073/pnas.0509994103

Robinson AJ, Overy C, Kunji ER. The mechanism of transport by mitochondrial carriers based on analysis of symmetry. Proc Natl Acad Sci U S A. 2008 Nov 18;105(46):17766-71. doi: 10.1073/pnas.0809580105

Rognstad R, Katz J. The effect of 2,4-dinitrophenol on adipose-tissue metabolism. Biochem J. 1969 Feb;111(4):431-44. doi: 10.1042/bj1110431

Rokitskaya TI, Khailova LS, Korshunova GA, Antonenko YN. Efficiency of mitochondrial uncoupling by modified butyltriphenylphosphonium cations and fatty acids correlates with lipophilicity of cations: Protonophoric vs leakage mechanisms. Biochim Biophys Acta Biomembr. 2023 Oct;1865(7):184183. doi: 10.1016/j.bbamem.2023.184183.

Rokitskaya TI, Khailova LS, Makarenkov AV, Ol'shevskaya VA, Kalinin VN, Antonenko YN. Weak C-H acids as protonophores can carry hydrogen ions through lipid membranes and mitochondria: a case of o-carborane. Phys Chem Chem Phys. 2016 Jun 28;18(24):16476-82. doi: 10.1039/c6cp02581a

Rolfe DF, Brand MD. The physiological significance of mitochondrial proton leak in animal cells and tissues. Biosci Rep. 1997 Feb;17(1):9-16. doi: 10.1023/a:1027327015957

Runswick MJ, Walker JE, Bisaccia F, Iacobazzi V, Palmieri F. Sequence of the bovine 2-oxoglutarate/malate carrier protein: structural relationship to other mitochondrial transport proteins. Biochemistry. 1990 Dec 18;29(50):11033-40. doi: 10.1021/bi00502a004

Ruprecht JJ, Hellawell AM, Harding M, Crichton PG, McCoy AJ, Kunji ER. Structures of yeast mitochondrial ADP/ATP carriers support a domain-based alternating-access transport mechanism. Proc Natl Acad Sci U S A. 2014 Jan 28;111(4):E426-34. doi: 10.1073/pnas.1320692111

Ruprecht JJ, King MS, Zögg T, Aleksandrova AA, Pardon E, Crichton PG, Steyaert J, Kunji ERS. The Molecular Mechanism of Transport by the Mitochondrial ADP/ATP Carrier. Cell. 2019 Jan 24;176(3):435-447.e15. doi: 10.1016/j.cell.2018.11.025

Ruprecht JJ, Kunji ERS. Structural changes in the transport cycle of the mitochondrial ADP/ATP carrier. Curr Opin Struct Biol. 2019 Aug;57:135-144. doi: 10.1016/j.sbi.2019.03.029

Ruprecht JJ, Kunji ERS. The SLC25 Mitochondrial Carrier Family: Structure and Mechanism. Trends Biochem Sci. 2020 Mar;45(3):244-258. doi: 10.1016/j.tibs.2019.11.001

Rupprecht A, Sokolenko EA, Beck V, Ninnemann O, Jaburek M, Trimbuch T, Klishin SS, Jezek P, Skulachev VP, Pohl EE. Role of the transmembrane potential in the membrane proton leak. Biophys J. 2010 Apr 21;98(8):1503-11. doi: 10.1016/j.bpj.2009.12.4301

Rupprecht A, Bräuer AU, Smorodchenko A, Goyn J, Hilse KE, Shabalina IG, Infante-Duarte C, Pohl EE. Quantification of uncoupling protein 2 reveals its main expression in immune cells and selective up-regulation during T-cell proliferation. PLoS One. 2012;7(8):e41406. doi: 10.1371/journal.pone.0041406

Sagan L. On the origin of mitosing cells. J Theor Biol. 1967 Mar;14(3):255-74. doi: 10.1016/0022-5193(67)90079-3

Samartsev VN, Mokhova EN. ATP/ADP antiporter- and aspartate/glutamate antiporter-mediated fatty acid-induced uncoupling of liver mitochondria in incubation media differing in ion composition. Biochem Mol Biol Int. 1997 Jun;42(1):29-34. doi: 10.1080/15216549700202401

Samartsev VN, Smirnov AV, Zeldi IP, Markova OV, Mokhova EN, Skulachev VP. Involvement of aspartate/glutamate antiporter in fatty acid-induced uncoupling of liver mitochondria. Biochim Biophys Acta. 1997 Apr 11;1319(2-3):251-7. doi: 10.1016/s0005-2728(96)00166-1

Sanchis D, Fleury C, Chomiki N, Goubern M, Huang Q, Neverova M, Grégoire F, Easlick J, Raimbault S, Lévi-Meyrueis C, Miroux B, Collins S, Seldin M, Richard D, Warden C, Bouillaud F, Ricquier D. BMCP1, a novel mitochondrial carrier with high expression in the central nervous system of humans and rodents, and respiration uncoupling activity in recombinant yeast. J Biol Chem. 1998 Dec 18;273(51):34611-5. doi: 10.1074/jbc.273.51.34611

Schauenstein E, Esterbauer H. Formation and properties of reactive aldehydes. Ciba Found Symp. 1978;(67):225-44. doi: 10.1002/9780470720493.ch15

Schwartz RM, Dayhoff MO. Origins of prokaryotes, eukaryotes, mitochondria, and chloroplasts. Science. 1978 Jan 27;199(4327):395-403. doi: 10.1126/science.202030

Severin FF, Severina II, Antonenko YN, Rokitskaya TI, Cherepanov DA, Mokhova EN, Vyssokikh MY, Pustovidko AV, Markova OV, Yaguzhinsky LS, Korshunova GA, Sumbatyan NV, Skulachev MV, Skulachev VP. Penetrating cation/fatty acid anion pair as a mitochondria-

targeted protonophore. Proc Natl Acad Sci U S A. 2010 Jan 12;107(2):663-8. doi: 10.1073/pnas.0910216107

Shabalina IG, Petrovic N, Kramarova TV, Hoeks J, Cannon B, Nedergaard J. UCP1 and defense against oxidative stress. 4-Hydroxy-2-nonenal effects on brown fat mitochondria are uncoupling protein 1-independent. J Biol Chem. 2006 May 19;281(20):13882-93. doi: 10.1074/jbc.M601387200

Shields HJ, Traa A, Van Raamsdonk JM. Beneficial and Detrimental Effects of Reactive Oxygen Species on Lifespan: A Comprehensive Review of Comparative and Experimental Studies. Front Cell Dev Biol. 2021 Feb 11;9:628157. doi: 10.3389/fcell.2021.628157

Shrestha R, Johnson E, Byrne FL. Exploring the therapeutic potential of mitochondrial uncouplers in cancer. Mol Metab. 2021 Sep;51:101222. doi: 10.1016/j.molmet.2021.101222

Skulachev VP. Fatty acid circuit as a physiological mechanism of uncoupling of oxidative phosphorylation. FEBS Lett. 1991 Dec 9;294(3):158-62. doi: 10.1016/0014-5793(91)80658-p

Škulj S, Brkljača Z, Kreiter J, Pohl EE, Vazdar M. Molecular Dynamics Simulations of Mitochondrial Uncoupling Protein 2. Int J Mol Sci. 2021 Jan 26;22(3):1214. doi: 10.3390/ijms22031214

Sluse FE, Goffart G, Liébecq C. Mechanism of the exchanges catalysed by the oxoglutarate translocator of rat-heart mitochondria. Kinetics of the external-product inhibition. Eur J Biochem. 1973 Jan 15;32(2):283-91. doi: 10.1111/j.1432-1033.1973.tb02609.x

Sluse FE, Liébecq C. Kinetics and mechanism of the exchange reactions catalysed by the oxoglutarate translocator of rat-heart mitochondria. Biochimie. 1973;55(6):747-54. doi: 10.1016/s0300-9084(73)80027-6

Smorodchenko A, Schneider S, Rupprecht A, Hilse K, Sasgary S, Zeitz U, Erben RG, Pohl EE. UCP2 up-regulation within the course of autoimmune encephalomyelitis correlates with T-lymphocyte activation. Biochim Biophys Acta Mol Basis Dis. 2017 Apr;1863(4):1002-1012. doi: 10.1016/j.bbadis.2017.01.019

Stipani V, Cappello AR, Daddabbo L, Natuzzi D, Miniero DV, Stipani I, Palmieri F. The mitochondrial oxoglutarate carrier: cysteine-scanning mutagenesis of transmembrane domain IV and sensitivity of Cys mutants to sulfhydryl reagents. Biochemistry. 2001 Dec 25;40(51):15805-10. doi: 10.1021/bi011616j

Stuart JA, Brindle KM, Harper JA, Brand MD. Mitochondrial proton leak and the uncoupling proteins. J Bioenerg Biomembr. 1999 Oct;31(5):517-25. doi: 10.1023/a:1005456725549

Terada H. The interaction of highly active uncouplers with mitochondria. Biochim Biophys Acta. 1981 Dec 30;639(3-4):225-42. doi: 10.1016/0304-4173(81)90011-2

Trachootham D, Alexandre J, Huang P. Targeting cancer cells by ROS-mediated mechanisms: a radical therapeutic approach? Nat Rev Drug Discov. 2009 Jul;8(7):579-91. doi: 10.1038/nrd2803

Urbánková E, Voltchenko A, Pohl P, Jezek P, Pohl EE. Transport kinetics of uncoupling proteins. Analysis of UCP1 reconstituted in planar lipid bilayers. J Biol Chem. 2003 Aug 29;278(35):32497-500. doi: 10.1074/jbc.M303721200

Urra FA, Muñoz F, Córdova-Delgado M, Ramírez MP, Peña-Ahumada B, Rios M, Cruz P, Ahumada-Castro U, Bustos G, Silva-Pavez E, Pulgar R, Morales D, Varela D, Millas-Vargas JP, Retamal E, Ramírez-Rodríguez O, Pessoa-Mahana H, Pavani M, Ferreira J, Cárdenas C, Araya-Maturana R. FR58P1a; a new uncoupler of OXPHOS that inhibits migration in triple-negative breast cancer cells via Sirt1/AMPK/β1-integrin pathway. Sci Rep. 2018 Sep 4;8(1):13190. doi: 10.1038/s41598-018-31367-9

van Meer G, Voelker DR, Feigenson GW. Membrane lipids: where they are and how they behave. Nat Rev Mol Cell Biol. 2008 Feb;9(2):112-24. doi: 10.1038/nrm2330

Vidal-Puig A, Solanes G, Grujic D, Flier JS, Lowell BB. UCP3: an uncoupling protein homologue expressed preferentially and abundantly in skeletal muscle and brown adipose tissue. Biochem Biophys Res Commun. 1997 Jun 9;235(1):79-82. doi: 10.1006/bbrc.1997.6740

Vozza A, Parisi G, De Leonardis F, Lasorsa FM, Castegna A, Amorese D, Marmo R, Calcagnile VM, Palmieri L, Ricquier D, Paradies E, Scarcia P, Palmieri F, Bouillaud F, Fiermonte G. UCP2 transports C4 metabolites out of mitochondria, regulating glucose and glutamine oxidation. Proc Natl Acad Sci U S A. 2014 Jan 21;111(3):960-5. doi: 10.1073/pnas.1317400111

Wang Y, Tajkhorshid E. Electrostatic funneling of substrate in mitochondrial inner membrane carriers. Proc Natl Acad Sci U S A. 2008 Jul 15;105(28):9598-603. doi: 10.1073/pnas.0801786105.

Wei J, Wang B, Wang H, Meng L, Zhao Q, Li X, Xin Y, Jiang X. Radiation-Induced Normal Tissue Damage: Oxidative Stress and Epigenetic Mechanisms. Oxid Med Cell Longev. 2019 Nov 12;2019:3010342. doi: 10.1155/2019/3010342

Wieckowski MR, Wojtczak L. Involvement of the dicarboxylate carrier in the protonophoric action of long-chain fatty acids in mitochondria. Biochem Biophys Res Commun. 1997 Mar 17;232(2):414-7. doi: 10.1006/bbrc.1997.6298

Williamson JR, Cooper RH. Regulation of the citric acid cycle in mammalian systems. FEBS Lett. 1980 Aug 25;117 Suppl:K73-85. doi: 10.1016/0014-5793(80)80572-2

Wu H, Esteve E, Tremaroli V, Khan MT, Caesar R, Mannerås-Holm L, Ståhlman M, Olsson LM, Serino M, Planas-Fèlix M, Xifra G, Mercader JM, Torrents D, Burcelin R, Ricart W, Perkins R, Fernàndez-Real JM, Bäckhed F. Metformin alters the gut microbiome of individuals with treatment-naive type 2 diabetes, contributing to the therapeutic effects of the drug. Nat Med. 2017 Jul;23(7):850-858. doi: 10.1038/nm.4345.

Xiong G, Zhang K, Ma Y, Song Y, Zhang W, Qi T, Qiu H, Shi J, Kan C, Zhang J, Sun X. BAM15 as a mitochondrial uncoupler: a promising therapeutic agent for diverse diseases. Front Endocrinol (Lausanne). 2023 Oct 11;14:1252141. doi: 10.3389/fendo.2023.1252141

Xu F, Putt DA, Matherly LH, Lash LH. Modulation of expression of rat mitochondrial 2-oxoglutarate carrier in NRK-52E cells alters mitochondrial transport and accumulation of glutathione and susceptibility to chemically induced apoptosis. J Pharmacol Exp Ther. 2006 Mar;316(3):1175-86. doi: 10.1124/jpet.105.094599

Yu XX, Lewin DA, Zhong A, Brush J, Schow PW, Sherwood SW, Pan G, Adams SH. Overexpression of the human 2-oxoglutarate carrier lowers mitochondrial membrane potential in HEK-293 cells: contrast with the unique cold-induced mitochondrial carrier CGI-69. Biochem J. 2001 Jan 15;353(Pt 2):369-75. doi: 10.1042/bj3530369

Zácková M, Krämer R, Jezek P. Interaction of mitochondrial phosphate carrier with fatty acids and hydrophobic phosphate analogs. Int J Biochem Cell Biol. 2000 May;32(5):499-508. doi: 10.1016/s1357-2725(00)00006-6

Zara V, Palmieri F. Inhibition and labelling of the mitochondrial 2-oxoglutarate carrier by eosin-5-maleimide. FEBS Lett. 1988 Aug 29;236(2):493-6. doi: 10.1016/0014-5793(88)80084-x

Zhang CY, Hagen T, Mootha VK, Slieker LJ, Lowell BB. Assessment of uncoupling activity of uncoupling protein 3 using a yeast heterologous expression system. FEBS Lett. 1999 Apr 23;449(2-3):129-34. doi: 10.1016/s0014-5793(99)00441-x

Zhao RZ, Jiang S, Zhang L, Yu ZB. Mitochondrial electron transport chain, ROS generation and uncoupling (Review). Int J Mol Med. 2019 Jul;44(1):3-15. doi: 10.3892/ijmm.2019.4188

Zunica ERM, Axelrod CL, Cho E, Spielmann G, Davuluri G, Alexopoulos SJ, Beretta M, Hoehn KL, Dantas WS, Stadler K, King WT, Pergola K, Irving BA, Langohr IM, Yang S, Hoppel CL, Gilmore LA, Kirwan JP. Breast cancer growth and proliferation is suppressed by the mitochondrial targeted furazano[3,4-b]pyrazine BAM15. Cancer Metab. 2021 Oct 9;9(1):36. doi: 10.1186/s40170-021-00274-5

Žuna K, Jovanović O, Khailova LS, Škulj S, Brkljača Z, Kreiter J, Kotova EA, Vazdar M, Antonenko YN, Pohl EE. Mitochondrial Uncoupling Proteins (UCP1-UCP3) and Adenine Nucleotide Translocase (ANT1) Enhance the Protonophoric Action of 2,4-Dinitrophenol in Mitochondria and Planar Bilayer Membranes. Biomolecules. 2021 Aug 9;11(8):1178. doi: 10.3390/biom11081178

Žuna, K., Tyschuk, T., Beikbaghban, T., Sternberg, F., Kreiter, J., Pohl. E.E. The 2-oxoglutarate/malate carrier extends the family of mitochondrial carriers capable of fatty acid and 2,4-dinitrophenol-activated proton transport. (2024) Acta Physiologica. 2024;00:e14143.